The Dissertation Committee for Myles Winston Gardner Certifies that this is the approved version of the following dissertation:

Development of Chromogenic Cross-Linkers and Selective Gas-Phase Dissociation Methods to Assess Protein Macromolecular Structures by Mass Spectrometry

Committee:

Jennifer S. Brodbelt, Supervisor

Edward M. Marcotte

Jason B. Shear

Scott W. Stevens

Keith J. Stevenson

Development of Chromogenic Cross-Linkers and Selective Gas-Phase Dissociation Methods to Assess Protein Macromolecular Structures by Mass Spectrometry

by

Myles Winston Gardner, B.S.

Dissertation

Presented to the Faculty of the Graduate School of

The University of Texas at Austin

in Partial Fulfillment

of the Requirements

for the Degree of

Doctor of Philosophy

The University of Texas at Austin

December, 2009

For my parents, Win and Rebecca

Acknowledgements

I would first and foremost like to thank my advisor Professor Jennifer Brodbelt, who allowed me the freedom and independence to explore many research avenues of mass spectrometry. I have thoroughly enjoyed my years working in her lab; her patience, guidance, and optimism enhanced my growth, both scientifically and personally. Thanks also to all of the members of the Brodbelt group, past and present, for their assistance, advice, and fruitful discussions.

I would also like to thank all of my collaborators including Dr. Anslyn and Shagufta Shabbir as well as Lisa Vasicek for the synthesis of chemical cross-linkers. I am also grateful to Dr. Jae Schwartz, Dr. George Stafford, Jr., Dr. Joshua Coon and Aaron Ledvina for the opportunity to collaborate with ThermoFisher Scientific in San Jose, California. Thanks to Dr. Na Li and Dr. Andrew Ellington for providing siRNA samples. I would also like to acknowledge Randy Pedder and Paul Jordan for assisting in the design and development of the Q-RIT-TOF mass spectrometer which was briefly alluded to in this dissertation.

In addition, I have to acknowledge my high school organic chemistry teacher, Dr. John Lieberman, who first sparked my interest in analytical chemistry. Without his teaching and mentorship those many years ago, I would have never imagined becoming a chemist.

Finally, I would like to thank my friends and family back on the East coast for their unconditional support during my years “abroad.”

Development of Chromogenic Cross-Linkers and Selective Gas-Phase Dissociation Methods to Assess Protein Macromolecular Structures by Mass Spectrometry

Publication No._____

Myles Winston Gardner, Ph.D.

The University of Texas at Austin, 2009

Supervisor: Jennifer S. Brodbelt

Selective gas-phase dissociation strategies have been developed for the characterization of cross-linked peptides and proteins in quadrupole ion trap mass spectrometers. An infrared chromogenic cross-linker (IRCX) containing a phosphotriester afforded rapid differentiation of cross-linked peptides from unmodified ones in proteolytic digests of cross-linked proteins by selective infrared multiphoton dissociation (IRMPD). Only the cross-linked peptides containing the chromogenic phosphate underwent IRMPD and unmodified peptides were not affected by IR irradiation. IRMPD of IRCX-cross-linked peptides yielded uncross-linked y-ion sequence tags of the constituent peptides due to secondary dissociation of all primary product ions which contained the chromophore, thus allowing successful *de novo* sequencing of the cross-linked peptides.

Peptides cross-linked via a two-step conjugation strategy through the formation of a bis-arylhydrazone (BAH) bond were selectively dissociated by ultraviolet radiation at

355 nm. The BAH-cross-linked peptides could be distinguished from not only unmodified peptides but also dead-end modified peptides based on the selectivity of ultraviolet photodissociation. In a complementary approach, electron transfer dissociation of BAH-cross-linked peptides resulted in preferential cleavage of the hydrazone bond which produced two modified peptides. These modified peptides were subsequently interrogated by CID which allowed for the original site of cross-linking to be pinpointed.

IRMPD was implemented in a dual pressure linear ion trap to demonstrate successful photodissociation of peptides having modest absorptivities. Peptides were observed to efficiently dissociation by IR irradiation exclusively in the low pressure cell whereas no dissociation was observed in the high pressure cell due to extensive collisional cooling. IRMPD provided greater sequence coverage of the peptides than CID and yielded product ion mass spectra which were predominantly composed of singly charged product ions which simplified spectral interpretation. IRMPD was further applied for the sequencing of small-interfering RNA. Complete sequence coverage was obtained and the results were compared to CID.

Table of Contents

Chapter 1

Introduction

1.1 INTRODUCTION

The field of proteomics has greatly expanded in the past decade, in part due to advances in the mass spectrometric analyses of such biological species.[1, 2] Of particular interest is protein structure determination and identification of protein-protein interactions to better understand the roles and functions of proteins.[3] One method that has shown considerable promise in these fields is chemical cross-linking with mass spectrometric analysis. This dissertation focuses on the development and implementation of chemical cross-linking protocols utilizing selective gas-phase dissociation methods including infrared multiphoton dissociation (IRMPD), ultraviolet photodissociation (UVPD), and electron transfer dissociation (ETD) employed on quadrupole ion trap mass spectrometers.

1.2 CHEMICAL CROSS-LINKING

The chemical cross-linking of proteins along with mass spectrometric analysis has become a more widely used method for the determination of low-resolution protein structure and identification of protein-protein interactions and their interfaces.[4, 5] Chemical cross-linking involves reacting proteins or protein-protein complexes with small, organic cross-linking reagents which binds two amino acids residues of the protein (or proteins) that are spatially constrained. By identifying which amino acid residues were cross-linked, one can determine an approximate distance between the two residues or identify the interface of interaction of a protein-protein complex. Chemical cross-

linkers generally consist of two functional groups which are reactive towards a specific amino acid side chain (e.g., *N*-hydroxysuccinimide esters which react with primary amines of Lys; maleimides which react with free sulfhydryl groups of Cys) and are often separated by a carbon spacer chain.

Mass spectrometry (MS) is an ideal method for the analysis of cross-linked proteins. Unlike traditional protein structural determination techniques such as NMR and X-ray crystallography which require on the order of milligrams of pure protein, the MS analysis requires sub-microgram (picomole level) quantities of proteins that can exist as several different species (e.g., protein variants, or proteins with post-translational modifications). The chemical cross-linking experiments and subsequent MS analysis can typically be performed in a few weeks compared to months or years to elucidate protein structures by NMR or X-ray crystallography. Mass spectrometry is also well-suited for the analysis of chemically cross-linked protein-protein complexes which are often not amenable for traditional biological structural analyses. The wide-range of cross-linking reagents available allows one to fine-tune the chemical cross-linking reaction by targeting specific amino acid side chains or functionalities based on the protein or protein-protein complex of interest.[6] By varying the spanner arm length (i.e., the approximate distance the cross-linker can bridge) of the cross-linking reagents one can also obtain more precise spatial distance constraints between the cross-linked residues.[7, 8] The distance constraints obtained from these results in general showed good agreement with measured distances in NMR and X-ray crystallography structures.[7, 9] Chemical cross-linking with mass spectrometric analysis has not only been used to obtain low-resolution three-dimensional structures of proteins[8, 9] and protein complexes[10-13] but has been successfully been applied to determine the fold of a protein,[14] determine sites of interaction of RNA-protein complexes[15, 16] and identify DNA-binding proteins.[17, 18] Kim et al. have probed

conformational changes of proteins upon ligand binding[19] protein activation and inhibition.[20, 21]

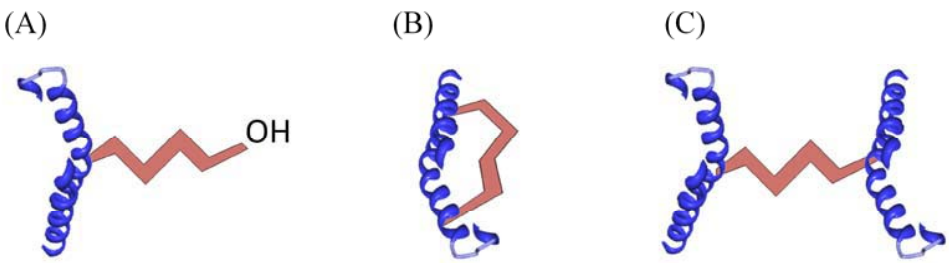

Scheme 1.1 Cross-linked peptide product types. (A) Dead-end modification; (B) intramolecular cross-link; and (C) intermolecular cross-link.

While the chemical cross-linking experimental procedure is well-established, several analytical hurdles in the identification of cross-link locations remain. Cross-linked proteins (or protein-protein complexes) are subjected to proteolytic digestion which produces a complex, heterogeneous mixture of unmodified, dead-end modified, intramolecularly cross-linked, and intermolecularly cross-linked peptides (**Scheme 1.1**). The low stoichiometry of the cross-linked peptides of interest further complicates the analysis and detection of these species. After enzymatic digestion, the peptide mixture is typically analyzed by LC-MS/MS (i.e., tandem mass spectrometry) and the separated peptides are individually interrogated by gas-phase dissociation methods (e.g., collision-induced dissociation) as shown in **Scheme 1.2**. Interpretation of the product ion mass spectra (i.e., fragmentation spectra) of cross-linked peptides, particularly for intermolecularly cross-linked peptides, is complicated by the fact that dissociation can occur along the backbone of either constituent peptide or the cross-linker. While several software tools are available to aid in interpreting product ion mass spectra of cross-linked peptides,[22-25] few are capable of utilizing database search algorithms and none has found widespread use amongst the research community.

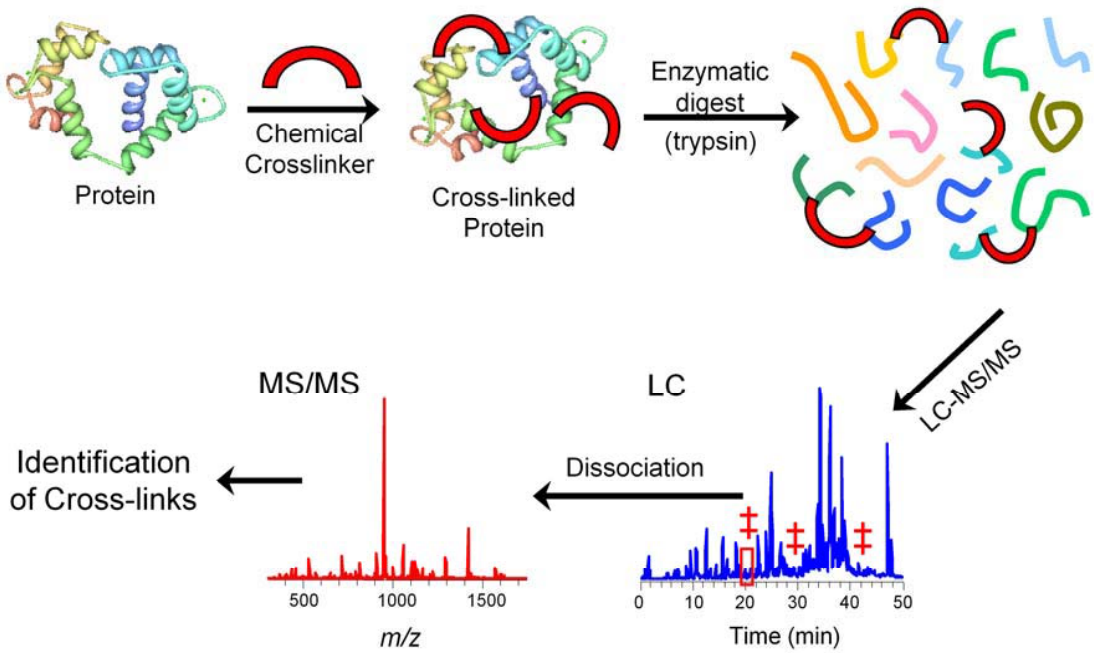

Scheme 1.2 Chemical cross-linking and mass spectrometry experimental and analytical approach.

The first challenge in determining the sites of cross-linking is identification of the cross-linked peptides of interest. Enzymatic digestion of the cross-linked protein yields a heterogeneous mixture that predominantly contains unmodified peptides in addition to products of the cross-linking reaction which include dead-end modification peptides, intramolecularly cross-linked peptides, and intermolecularly cross-linked peptides. These three types of products are shown in **Scheme 1.1**; dead-end modified peptides result from one end of the bifunctional cross-linking reagent reacting with an amino acid side chain of the protein and the other functional group is hydrolyzed. These dead-end modifications generally only provide information as to the surface accessibility of the residue which was modified but no structural information as it relates to distance constraints or protein-protein interfaces. The low abundance of cross-linked peptides in

the enzymatic digest necessitates up-front separation methods or affinity chromatography methods to enrich cross-linked peptides.

The Sinz group has utilized sulfhydryl reactive fluorogenic cross-linkers to distinguish between unmodified and cross-linked peptides during LC separations with online fluorescence detection and MS analysis.[26, 27] While the fluorogenic cross-linkers allow for differentiation, several other groups have developed trifunctional cross-linkers with affinity tags for enrichment of cross-linked peptides.[28-33] The most common approach has been using biotinylated cross-linkers for enrichment on avidin beads.[29, 30] Recently, Yan et al. designed a cross-linker with an acetyl-protected thiol group that upon deprotection selectively reacts with an iodo group on functionalized beads as a non-protein based enrichment strategy.[28]

Isotopically labeled cross-linkers have also been developed to aid in distinguishing cross-linked peptides from unmodified ones in the mass spectra acquired during LC separations. By reacting the protein with the deuterium-labeled (i.e., heavy) and the unlabeled (i.e., light) cross-linkers at a 1:1 ratio, one can readily distinguish cross-linked peptides by mass spectrometric detection by searching for peaks with similar intensities but mass shifts that correspond to the mass difference between the heavy and light labels.[34, 35] Back et al. performed the proteolytic digestion of cross-linked protein complexes in ^{18}O labeled water which results in the incorporation of a two ^{18}O atoms at each C-terminus; linear (i.e., unmodified), dead-end modified, and intramolecularly cross-linked peptides experience a 4 Da mass shift while intermolecularly cross-linked peptides shift 8 Da compared to the unlabeled analogs.[36] Other groups have developed chemical cross-linkers which have incorporated a gas-phase labile bond, such that upon low-energy collisional activation this bond is preferentially cleaved yielding a “reporter” ion to aid in tracking cross-linked peptides.[33, 37, 38]

While these strategies aid in identification of cross-linked peptides from unmodified ones, other research has focused on simplifying the interpretation of the tandem mass spectra of the cross-linked peptides to locate the sites of the cross-link (i.e., the amino acid residues cross-linked). Collision-induced dissociation of chemically cross-linked peptides, specifically those with Lys-Lys cross-linked, yields more complex product ion mass spectra than that of unmodified or linear peptides. Schilling et al. first reported on the gas-phase dissociation trends of cross-linked peptides and noted that single bond cleavage is predominantly observed, originating from one or the other constituent peptides of intermolecularly species.[39] They also observed double cleavage products originating from dissociation of both peptide backbones in lower abundances. While these double cleavage product ions are informative and aid in locating the site of the cross-link, they complicate spectral interpretation and necessitate manual identification and verification of these product ions. Gaucher et al. reported product ions specific to cross-linked species including lysine immonium ions linked to a peptide as well as enhanced cleavage C-terminal to the cross-linked lysine for intramolecularly cross-linked peptides.[40] Work in the Brodbelt group showed that cross-linked peptides which contain Asp or Pro, amino acid residues known to promote site-specific backbone dissociation,[41-44] also greatly influenced the dissociation of cross-linked peptides.[45] In addition, a high abundance of double-cleavage product ions were observed for cross-linked peptides which did not possess a mobile proton.[45]

Given the complexity of the product ion mass spectra of cross-linked peptides, much effort has been devoted to the design of chemical cross-linkers to simplify the fragmentation patterns. The Bruce lab has developed a set of "protein interaction reporters" (PIRs) which possess an affinity tag for enrichment as well as gas-phase labile bonds within the cross-linker.[33, 46] Upon low-energy ion activation, these bonds are

dissociated producing the two constituent peptides each with a unique mass tag. Soderblom et al. incorporated an aspartyl-prolyl bond into the center of their cross-linker which was preferentially dissociated upon CID yielding two modified peptides.[47, 48] These modified peptides were then individually isolated and subjected to another stage of CID for independent sequencing. Their method was also shown to be compatible with database search algorithms for identifying the peptide and site of modification. Recently the Reid group designed an ionic cross-linking reagent with a fixed charge sulfonium ion which directed cleavage of the adjacent C–S bond upon CID to similarly produce the two constituent peptides for subsequent isolation and dissociation by MS^3 experiments.[49] All of these techniques allow for independent sequencing of the constituent peptides for intermolecularly cross-linked peptides, eliminating the influence of the cross-link or the other peptide on the dissociation patterns. All of these methods only addressed one of the two primary challenges in chemical cross-linking experiments with MS analysis – either simplifying interpretation of the product ion mass spectra of cross-linked peptides or aiding in the differentiation and identification of cross-linked peptides of interest from unmodified ones. In this dissertation, the development of chromogenic cross-linkers along with selective photodissociation methods (e.g., IRMPD and UVPD) employed to afford rapid identification of cross-linked peptides and to simplify spectral interpretation are discussed, as well as fundamental studies into the dissociation trends of the biological species of interest.

1.3 TANDEM MASS SPECTROMETRY

Tandem mass spectrometry refers to mass spectrometric experiments in which a specific ion of interest is selected (i.e., isolated) and is then subsequently manipulated. Tandem mass spectrometry is performed in order to gain more information about the

selected precursor ion including structure, energy, and reactivity. Such experiments generally refer to ion activation and dissociation but also include ion-molecule reactions and ion-ion reactions. For structural analysis of analyte ions, dissociation methods are employed and these techniques are widely used for the characterization and sequencing of biological species including peptides, proteins, and oligonucleotides.[50-53]

1.3.1 Collision-Induced Dissociation

The most common and well-established method for dissociating ions in the gas-phase is collision-induced dissociation (CID). Collision-induced dissociation, as employed in the majority of quadrupole ion trap mass spectrometers,[54] involves the application of a supplemental ac waveform with a frequency that matches the secular frequency of the precursor ion.[54, 55] The precursor ion gains kinetic energy through resonance with the applied ac waveform which results in energetic collisions with inert bath gas molecules in the trap and the kinetic energy is converted into internal energy.[56] Once the ion has accumulated enough internal energy through collisional activation, bond dissociation is observed. While CID is the most mature dissociation method in quadrupole ion traps, it is not without its limitations. To effectively perform CID, the rf trapping level (i.e., the amplitude of the rf potential) must be raised to increase the ion kinetic energy. This increase in the rf amplitude results prevents the storage of low mass-to-charge (*m/z*) ions. For most commercial quadrupole ion trap instruments, the lower 28% of the mass range, relative to the precursor ion m/z, is lost and this lower limit is referred to as the low-mass cut-off (LMCO). Another disadvantage of CID is that as resonant dissociation method, only the precursor ion gains internal energy and is fragmented and the lowest energy dissociation pathway may be uninformative, such as dehydration or loss of other small neutral species. These dead-end pathways often

necessitate the use of multiple stages of ion isolation and dissociation (i.e., MS^n experiments) which are time consuming and result in losses in sensitivity. As a collision based method, ion losses due to scattering events can also occur. For these reasons, much effort has been devoted to developing and investigating alternative means to activate and dissociation gas-phase ions, including photodissociation and electron-based dissociation techniques.

1.3.2 Photodissociation

Photon-based dissociation methods have found widespread use on a variety of mass analyzers including quadrupole ion traps,[57-66] time-of-flight mass spectrometers,[67, 68] and Fourier transform ion cyclotron resonance (FT-ICR) instruments.[69-71] Photodissociation is performed by irradiating the ion population with photons at a wavelength at which the ions absorb. Depending on the photon energy, the ion must absorb one or multiple photons to gain enough energy to undergo dissociation. Commonly used infrared (IR) lasers have photon energies on the order of ~0.1 eV (~10 μm) and absorption of IR photons results in vibrational excitation. Tens to hundreds of IR photons must be absorbed to raise the ions internal energy above the critical energy for dissociation. For ultraviolet and visible lasers with photon energies between 3 and 8 eV (~400 to 150 nm), one or two photons provide enough energy to induce dissociation through electronic excitation transitions.

There are several benefits of performing photodissociation as opposed to traditional collisional activation methods. Photodissociation is largely independent of the rf trapping level which allows one to perform photodissociation at a low rf amplitude and thus trap ions of a broader *m/z* range and detect diagnostic low-mass fragment ions.[59, 72, 73] As a non-resonant process, all ions are simultaneously irradiated which results in the

activation and dissociation of not only the precursor ion but also any product ions. Dead-end pathways are circumvented as these primary product ions undergo secondary dissociation and can yield more informative fragment ions. The ion kinetic energy (i.e., translation motion) is not affected by the photon absorption process so ion scattering losses are largely eliminated as well. However, one of the primary advantages of photodissociation is that it allows one to finely tune the energy deposition by varying the irradiation time or number of laser pulses, the photon flux or laser power, and perhaps, most importantly the wavelength of the laser.

Infrared multiphoton dissociation (IRMPD) is typically performed using a CO_2 continuous wave laser at 10.6 μm (~0.12 eV/photon). While IRMPD has shown significant promise as an alternative and complementary dissociation method to CID, it has not found widespread implementation on quadrupole ion traps. Quadrupole ion traps are generally operated at a pressure of ~1 – 5 mTorr of He to collisionally cool the ions to the center of the trap which improves sensitivity and mass resolution;[74] these high pressures are also advantageous for performing CID. However, at these pressures, the rate of collisional cooling (i.e., deactivation) is nearly equivalent to the rate of photon absorption (i.e., activation) for most analyte ions which do not possess a strong chromophore at the laser wavelength (e.g., peptides, proteins).[52, 75] Due to the low probability of photon absorption, the dissociation efficiencies for these analyte ions are low. In recent years, several approaches have been devised to improve IRMPD efficiencies in quadrupole ion traps. The Glish group investigated thermally-assisted IRMPD by heating the bath gas surrounding the ions and Hashimoto et al. collisionally activated the precursor ions during IR irradiation.[76] These methods were aimed at raising the internal energy of the ions to reduce the amount of energy required for dissociation by IR activation at standard trap pressures; however, other groups have focused on reducing

the rate of collisional deactivation by adjusting the pressure of the trap such that gas is introduced during ion accumulation but reduced prior to IR irradiation.[77, 78] Newsome and Glish reported on using a focused CO_2 laser to increase the photon flux and thus reduce the irradiation time necessary to produce high dissociation efficiencies.[65] The Brodbelt group has devoted efforts to developing chemical derivatization schemes to covalently attach chromogenic labels to increase the IR absorption cross-section of ions at 10.6 μm.[38, 73, 79-81]

While a majority of biologically relevant molecules do not exhibit high IRMPD efficiencies, species containing phosphate groups have shown to readily photodissociate upon IR irradiation due to the high IR absorption cross-section of the P–O stretch.[82] Flora and Muddiman initially exploited this feature of phosphate groups to selectively dissociate phosphorylated peptides by IR irradiation in an FT-ICR.[71, 83] Crowe and Brodbelt further utilized this characteristic and were able to rapidly differentiate between unmodified and phosphorylated peptides by IRMPD in a quadrupole ion trap, both by direct infusion electrospray ionization mass spectrometry[84] and in an online LC-IRMPD-MS experiment.[85]

Ultraviolet photodissociation has also been exploited as a screening tool to selectively dissociate species containing specific chromophores. As most biological species, in particular proteins and peptides, do not possess naturally occurring chromophores at commonly used UV laser wavelengths above 200 nm, low UVPD efficiencies are typically observed.[67] These low photodissociation efficiencies have promoted research into utilizing UVPD as a means to selectively dissociate chromogenic species. Tyrosyl-containing peptides have been observed to undergo efficient UVPD at 220 and 262 nm,[63, 86] and peptides with tyrosine or tryptophan residues have dissociated readily by UV irradiation at 266 nm as well.[87] The specific detection of a 107 Da neutral

loss from peptide precursor ions by UVPD at 262 nm indicated that the peptide contained at least a single tyrosyl residue, allowing for screening of these species in database searching.[86] In an effort to improve UVPD efficiencies of biological species without naturally occurring chromophores, the covalent[62, 88, 89] and non-covalent attachment[66, 90] of chromophores through derivatization methods, which have high absorptivities at the appropriate wavelengths, to peptides and proteins has been investigated. Wilson and Brodbelt were able to not only successfully sequence peptides derivatized with chromophores by UVPD at 355 nm, but all primary product ions which retained the chromophore underwent secondary dissociation and were eliminated from the product ion mass spectrum.[62] In this dissertation, the design and application of chromogenic cross-linkers is discussed for rapid screening of cross-linked peptides in complex mixtures.

1.3.3 Electron Transfer Dissociation

Electron-based dissociation methods, such as electron capture dissociation (ECD)[91, 92] and electron transfer dissociation (ETD),[93, 94] have gained widespread use in the past decade. ECD is performed by irradiation of peptide or protein cations with low-energy electrons produced from a conventional heated filament. The electrons are captured at the sites of protonation which induces peptide backbone fragmentation in a non-ergodic manner.[92, 95, 96] However, ECD is not easily implemented on quadrupole ion trap instruments as the thermal electrons are not stabilized and trapped by the rf field due to their low mass. Syka et al. developed ETD, an analogous dissociation method to ECD utilizing radical reagent anions with low electron affinities as the electron source.[93] By simultaneously trapping protonated peptide or protein cations and reacting them with the radical reagent anions, an electron is transferred to the protonated peptide in an exothermic reaction which triggers the migration of a hydrogen radical and initiates

dissociation.[93] One of the primary advantages of ECD and ETD is that as non-ergodic dissociation methods, labile post-translational modifications (PTMs), such as phosphorylation, are retained upon dissociation.[93, 97, 98] In contrast, thermal-based dissociation methods such as CID and IRMPD often result in dominant loss of phosphoric acid from the modified residues in phosphopeptides, negating the ability to unambiguously pinpoint the site of the PTMs.[99] ECD and ETD of peptides and proteins results in nonselective backbone cleavage, however, it was observed early on that disulfide bonds were preferentially dissociated.[100] While this preferential cleavage of disulfide bonds has been further investigated,[101-105] selective dissociation of other chemical functionalities by ECD or ETD has not been reported. In this dissertation preferential cleavage of bis-arylhydrazone cross-linked peptides by ETD is described.

1.3.4 Biomolecular Fragmentation Nomenclature

Ion activation and dissociation of peptides and proteins typically results in cleavage along the peptide backbone. The fragmentation nomenclature of peptides, originally suggested by Roepstorff et al.,[106] is shown graphically in **Scheme 1.3**. For a majority of low-energy, ergodic dissociation methods such as CID and IRMPD, cleavage of the thermally labile amide C–N bond is observed which yields b- and the complementary y-type product ions. Subsequent loss of CO from b-type ions produces a-type fragment ions. Electron-based dissociation methods such as ECD and ETD generally result in cleavage of the N–C_α bond producing c- and the complementary z-type ions. Similarly, dissociation of the C_α–C bond produces a- and x-type ions. If a charge is retained on the N-terminal fragment, a-, b-, and c-ions are produced; similarly, if a charge is retained on the C-terminal fragment, x-, y-, and z-type ions are observed. The numerical subscript refers to the number of N-terminal or C-terminal amino acids

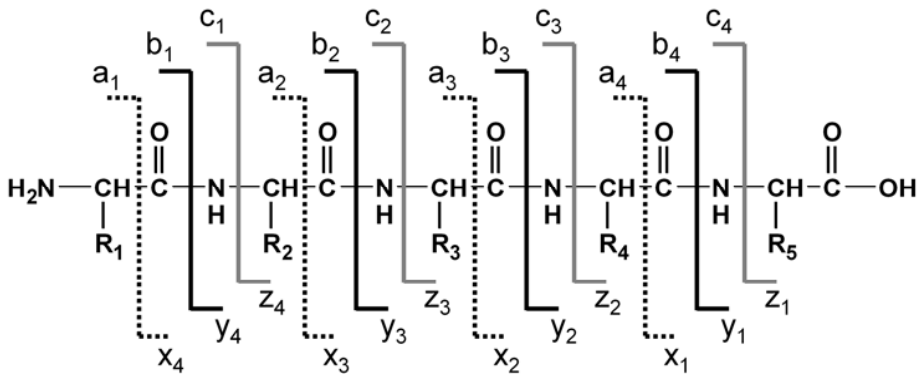

Scheme 1.3 Fragmentation nomenclature of peptides and proteins.

contained in the product ion (e.g., dissociation of the amide bond C-terminal to the second amino acid residue with the charge retained on the N-terminus yields the b_2 ion).

The nomenclature for the dissociation of cross-linked peptides is similar to that for linear peptides. For intramolecularly cross-linked peptides, the nomenclature is identical to that of linear peptides. The nomenclature of the dissociation of intermolecularly cross-linked peptides is based on that proposed by Schilling et al.[39] and Gaucher et al.[40] and is shown in **Scheme 1.4**. The two constituent peptides are termed α and β; dissociation along the backbone of the α-peptide yield e.g., $b_{n\alpha}$ and $y_{n\alpha}$ product ions and dissociation along the backbone of the β-peptide yield e.g., $b_{n\beta}$ and $y_{n\beta}$ ions, where n refers to the number of amino acids contained in the product ion from the N-terminus or C-terminus. Bond dissociation along the cross-linker are labeled as Lαn or Lβn where n is the number of atoms from the C_α atom of the cross-linked amino acid (e.g., lysine residues for the cross-linked peptides discussed in this dissertation) of either the α- or β-peptide. In addition, lysine immonium ions cross-linked to one of the constituent peptides are also observed often in conjunction with a loss of NH_3 (17 Da loss) and these product ions are labeled $K^L\alpha$ and $K^L\alpha$–17 or $K^L\beta$ and $K^L\beta$–17.

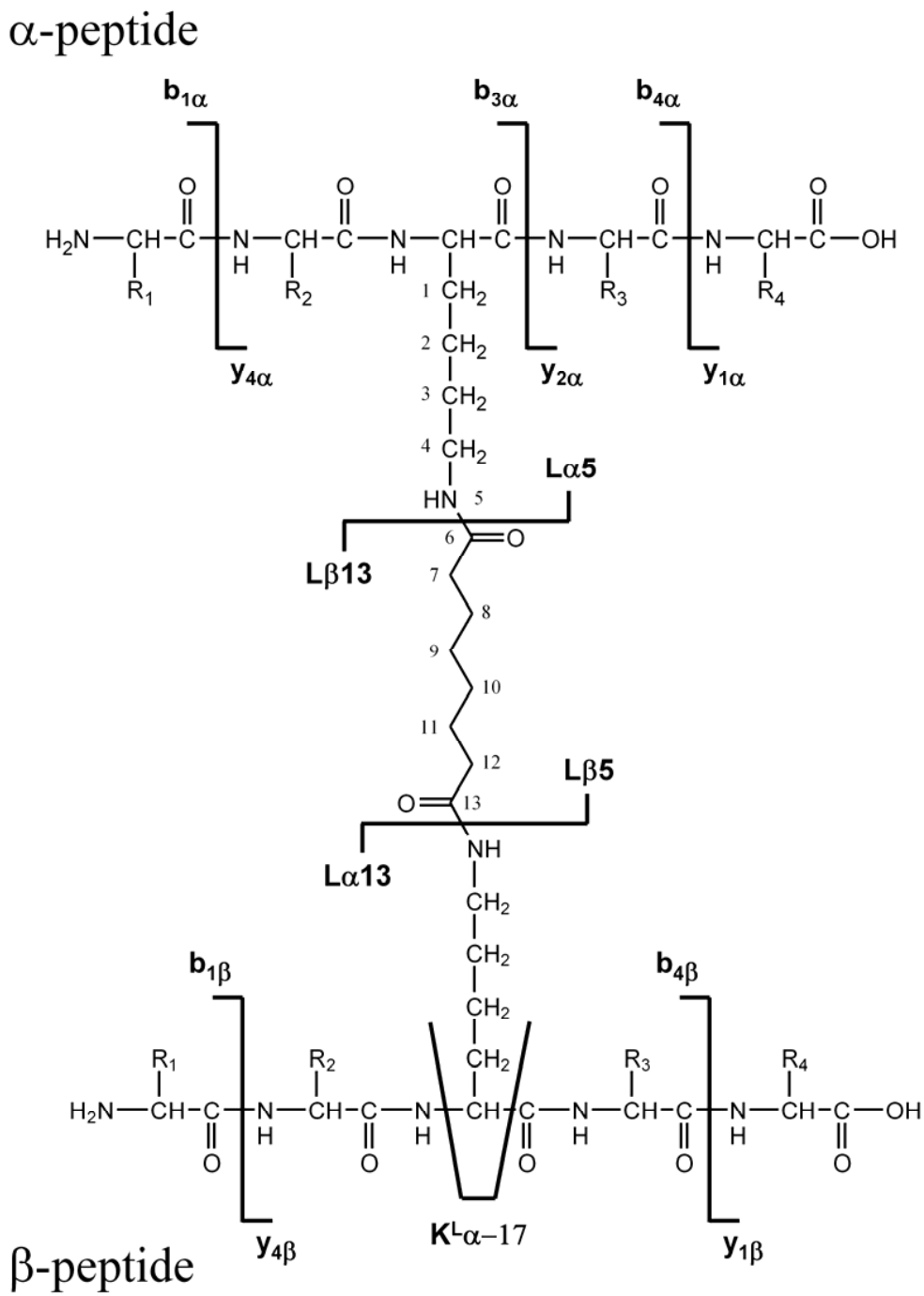

Scheme 1.4 Fragmentation nomenclature for cross-linked peptides.

The dissociation nomenclature for oligonucleotides (e.g., DNA and RNA) used was first proposed by McLuckey et al.[51] as shown in **Scheme 1.5**. Dissociation of DNA generally results in loss of nucleobases which initiates cleavage along the phosphate backbone at the 3' C–O bond yielding [a–Base] and complementary w-type ions. In contrast, dissociation of RNA predominantly results in cleavage of the 5' P–O bond producing c- and the complementary y-type fragment ions.

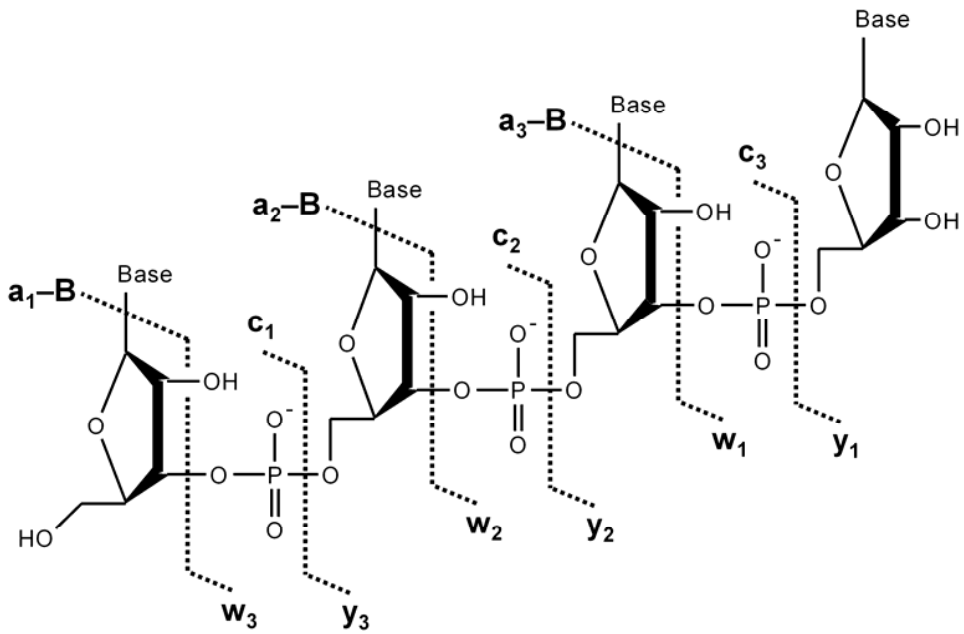

Scheme 1.5 Fragmentation nomenclature of oligoribonucleotides (RNA).

1.4 OVERVIEW OF CHAPTERS

The research presented in this dissertation aims at the development of selective gas-phase dissociation techniques for the characterization of cross-linked or conjugated biological molecules. To understand the typical dissociation pathways of cross-linked peptides, a series of model peptides cross-linked by commercial cross-linkers were investigated by CID (Chapter 3). Aspartic acid and proline residues positioned on either

side of the cross-linked lysine affected the dissociation pathways in a similar manner observed for linear peptides. For cross-linked peptide precursor ions with a mobile proton, cleavage C-terminal to Asp was enhanced, whereas dissociation of the backbone amide bond N-terminal to Pro was enhanced for all charge states of the cross-linked peptides. A high abundance of double cleavage products and internal ion formation was observed for the cross-linked peptides in the low charge states, as well.

An IR chromogenic cross-linker was synthesized to allow for rapid screening of cross-linked peptides in complex mixtures by selective IRMPD (Chapter 4). Only cross-linked peptides which contained the phosphate IR chromophore were observed to undergo efficient IRMPD; un-cross-linked peptides were unaffected by IR irradiation presumably due to a lower rate of photon absorption and thus near equivalent rates of IR photoactivation and collisional cooling. By isolating a wide range of ions and comparing mass spectra acquired with the laser on (IRMPD mass spectra) and with the laser off, the cross-linked peptides were rapidly identified based on the fact that they were the only ones whose abundances decreased. IRMPD of the cross-linked peptides also yielded a series of un-cross-linked y-type ions of both constituent peptides C-terminal to the cross-linked lysines that allowed *de novo* sequencing of the cross-linked peptides due to rapid secondary dissociation of any primary product ion which still retained the chromogenic cross-link. The protein ubiquitin was cross-linked and analyzed by this selective IRMPD strategy in an online LC-MS experiment and a total of four cross-links and two dead-end modifications were identified.

The selective photodissociation based on IRMPD was further developed for peptides conjugated with a UV chromogenic bis-arylhydrazone (BAH) group for UVPD at 355 nm (Chapter 5). Peptides were cross-linked via a two-step conjugation procedure and only upon cross-linking was the chromogenic BAH group formed. This method was

applied to a mock mixture of peptides which was analyzed by online LC-UVPD-MS. Since the unmodified peptides did not contain the UV chromophore, they were not observed to dissociate allowing differentiation between conjugated peptides and both unmodified peptides and uninformative dead-end modified peptides.

The bis-arylhydrazone cross-linked peptides were further investigated by ETD as discussed in Chapter 6. ETD of these cross-linked peptides resulted in preferential dissociation of the hydrazone bond yielding the two constituent peptides – one an odd-electron product, the other an even-electron species – each retaining a unique mass tag at the site of cross-linking. These two tagged peptide product ions were observed at higher abundances than the electron transfer non-dissociative precursor ion and the abundance of all c- and z-type ions. Subsequent CID of the tagged peptide product ions yielded informative sequence ions to identify the constituent peptides independently. The proposed mechanism for this preferential cleavage of the hydrazone bond involved transfer of the electron directly to the protonated hydrazone and subsequent rearrangement and bond dissociation.

To further extend the capabilities of IRMPD for the sequencing of peptides, an IR laser was interfaced to a dual pressure linear ion trap mass spectrometer (Chapter 7). IRMPD of peptides in the high pressure cell did not result in any dissociation, attributed to the high rate of collisional cooling and the low IR absorption cross-section rate of peptides. However, rapid and efficient dissociation of peptides was observed in the low pressure cell; IRMPD of peptide cations conducted in the low pressure cell afforded slightly greater sequence coverage as compared to CID. IRMPD predominantly yielded product ions in the 1+ charge state which simplified spectral interpretation.

In the IRMPD studies conducted on the IR chromogenic cross-linked peptides and in the dual cell LIT, an interesting phenomenon was observed in which the abundances of

unmodified peptide ions actually increased upon IR irradiation. It was hypothesized that this effect was due to IR activation of noise in the mass spectrum consisting of solvated analyte ions of unresolved *m/z*. To investigate this phenomenon, regions of noise in the mass spectra of peptide and protein samples were subjected to supplemental IR activation which resulted in a decrease in the chemical noise and an increase in analyte ion signal (Chapter 8). In fact, when chemical noise regions were isolated and subsequently irradiated, protonated analyte ions were observed in the mass spectrum. The chemical noise was attributed to incomplete desolvation of the electrospray.

Finally, IRMPD of small-interfering RNA (siRNA) single strands and duplexes was explored (Chapter 9). SiRNA was observed to undergo rapid dissociation upon IR irradiation predominantly producing c- and y-type ions as opposed to [a – Base] and w-type ions which are observed for DNA. Full sequence coverage of the siRNAs was obtained by both IRMPD and CID; however, the IRMPD mass spectrum could be tuned to contain predominantly short product ions in the 1+ and 2+ charge states by adjusting the IR irradiation time to simplify spectra interpretation. For future studies, these results suggest that IRMPD will be of great utility for the structural characterization of RNA-protein complexes.

1.6 REFERENCES

(1) Godovac-Zimmermann, J.; Brown, L. R. *Mass Spectrometry Reviews* **2001**, *20*, 1-57.

(2) Aebersold, R.; Mann, M. *Nature* **2003**, *422*, 198-207.

(3) Juan, H.-F.; Liu, H.-L.; Hsu, J.-P. *Current Proteomics* **2004**, *1*, 183-197.

(4) Sinz, A. *Journal of Mass Spectrometry* **2003**, *38*, 1225-1237.

(5) Back, J. W.; De Jong, L.; Muijsers, A. O.; De Koster, C. G. *Journal of Molecular Biology* **2003**, *331*, 303-313.

(6) Hermanson, G. T. *Bioconjugate Techniques*; Academic Press: San Diego, CA, 1996.

(7) Jacobsen, R. B.; Sale, K. L.; Ayson, M. J.; Novak, P.; Hong, J.; Lane, P.; Wood, N. L.; Kruppa, G. H.; Young, M. M.; Schoeniger, J. S. *Protein Science* **2006**, *15*, 1303-1317.

(8) Huang, B. X.; Kim, H.-Y.; Dass, C. *Journal of the American Society for Mass Spectrometry* **2004**, *15*, 1237-1247.

(9) Dihazi, G. H.; Sinz, A. *Rapid Communications in Mass Spectrometry* **2003**, *17*, 2005-2014.

(10) Back, J. W.; Sanz, M. A.; De Jong, L.; De Koning, L. J.; Nijtmans, L. G. J.; De Koster, C. G.; Grivell, L. A.; Van Der Spek, H.; Muijsers, A. O. *Protein Science* **2002**, *11*, 2471-2478.

(11) Schulz, D. M.; Ihling, C.; Clore, G. M.; Sinz, A. *Biochemistry* **2004**, *43*, 4703-4715.

(12) Schulz, D. M.; Kalkhof, S.; Schmidt, A.; Ihling, C.; Stingl, C.; Mechtler, K.; Zschoernig, O.; Sinz, A. *Proteins: Structure, Function, and Bioinformatics* **2007**, *69*, 254-269.

(13) Nechifor, R.; Wilson, K. S. *Journal of Molecular Biology* **2007**, *368*, 1412-1425.

(14) Young, M. M.; Tang, N.; Hempel, J. C.; Oshiro, C. M.; Taylor, E. W.; Kuntz, I. D.; Gibson, B. W.; Dollinger, G. *Proceedings of the National Academy of Sciences of the United States of America* **2000**, *97*, 5802-5806.

(15) Rhode, B. M.; Hartmuth, K.; Urlaub, H.; Luehrmann, R. *RNA* **2003**, *9*, 1542-1551.

(16) Lenz, C.; Kuehn-Hoelsken, E.; Urlaub, H. *Journal of the American Society for Mass Spectrometry* **2007**, *18*, 869-881.

(17) Qiu, H.; Wang, Y. *Journal of Proteome Research* **2009**, *8*, 1983-1991.

(18) Rogacheva, M.; Ishchenko, A.; Saparbaev, M.; Kuznetsova, S.; Ogryzko, V. *Journal of Biological Chemistry* **2006**, *281*, 32353-32365.

(19) Huang, B. X.; Dass, C.; Kim, H.-Y. *Biochemical Journal* **2005**, *387*, 695-702.

(20) Huang, B. X.; Kim, H.-Y. *Molecular and Cellular Proteomics* **2006**, *5*, 1045-1053.

(21) Huang, B. X.; Kim, H.-Y. *Journal of the American Society for Mass Spectrometry* **2009**, *20*, 1504-1513.

(22) Xu, H.; Zhang, L.; Freitas, M. A. *Journal of Proteome Research* **2008**, *7*, 138-144.

(23) Peri, S.; Steen, H.; Pandey, Y. *Trends in Biochemical Sciences* **2001**, *26*, 687-689.

(24) Gao, Q.; Xue, S.; Doneanu, C. E.; Shaffer, S. A.; Goodlett, D. R.; Nelson, S. D. *Analytical Chemistry* **2006**, *78*, 2145-2149.

(25) Singh, P.; Shaffer, S. A.; Scherl, A.; Holman, C.; Pfuetzner, R. A.; Larson Freeman, T. J.; Miller, S. I.; Hernandez, P.; Appel, R. D.; Goodlett, D. R. *Analytical Chemistry* **2008**, *80*, 8799-8806.

(26) Sinz, A.; Wang, K. *Biochemistry* **2001**, *40*, 7903-7913.

(27) Sinz, A.; Wang, K. *Analytical Biochemistry* **2004**, *331*, 27-32.

(28) Yan, F.; Che, F.-Y.; Rykunov, D.; Nieves, E.; Fiser, A.; Weiss, L. M.; Hogue Angeletti, R. *Analytical Chemistry* **2009**, *81*, 7149-7159.

(29) Hurst, G. B.; Lankford, T. K.; Kennel, S. J. *Journal of the American Society for Mass Spectrometry* **2004**, *15*, 832-839.

(30) Sinz, A.; Kalkhof, S.; Ihling, C. *Journal of the American Society for Mass Spectrometry* **2005**, *16*, 1921-1931.

(31) Chu, F.; Mahrus, S.; Craik, C. S.; Burlingame, A. L. *Journal of the American Chemical Society* **2006**, *128*, 10362-10363.

(32) Chowdhury, S. M.; Du, X.; Tolic, N.; Wu, S.; Moore, R. J.; Mayer, M. U.; Smith, R. D.; Adkins, J. N. *Analytical Chemistry* **2009**, *81*, 5524-5532.

(33) Chowdhury, S. M.; Munske, G. R.; Tang, X.; Bruce, J. E. *Analytical Chemistry* **2006**, *78*, 8183-8193.

(34) Mueller, D. R.; Schindler, P.; Towbin, H.; Wirth, U.; Voshol, H.; Hoving, S.; Steinmetz, M. O. *Analytical Chemistry* **2001**, *73*, 1927-1934.

(35) Ihling, C.; Schmidt, A.; Kalkhof, S.; Schulz, D. M.; Stingl, C.; Mechtler, K.; Haack, M.; Beck-Sickinger, A. G.; Cooper, D. M. F.; Sinz, A. *Journal of the American Society for Mass Spectrometry* **2006**, *17*, 1100-1113.

(36) Back, J. W.; Notenboom, V.; de Koning, L. J.; Muijsers, A. O.; Sixma, T. K.; de Koster, C. G.; de Jong, L. *Analytical Chemistry* **2002**, *74*, 4417-4422.

(37) Back, J. W.; Hartog, A. F.; Dekker, H. L.; Muijsers, A. O.; de Koning, L. J.; de Jong, L. *Journal of the American Society for Mass Spectrometry* **2001**, *12*, 222-227.

(38) Gardner, M. W.; Vasicek, L. A.; Shabbir, S.; Anslyn, E. V.; Brodbelt, J. S. *Analytical Chemistry* **2008**, *80*, 4807-4819.

(39) Schilling, B.; Row, R. H.; Gibson, B. W.; Guo, X.; Young, M. M. *Journal of the American Society for Mass Spectrometry* **2003**, *14*, 834-850.

(40) Gaucher, S. P.; Hadi, M. Z.; Young, M. M. *Journal of the American Society for Mass Spectrometry* **2006**, *17*, 395-405.

(41) Dongre, A. R.; Jones, J. L.; Somogyi, A.; Wysocki, V. H. *Journal of the American Chemical Society* **1996**, *118*, 8365-8374.

(42) Tsaprailis, G.; Somogyi, A.; Nikolaev, E. N.; Wysocki, V. H. *International Journal of Mass Spectrometry* **2000**, *195/196*, 467-479.

(43) Vaisar, T.; Urban, J. *Journal of Mass Spectrometry* **1996**, *31*, 1185-1187.

(44) Breci, L. A.; Tabb, D. L.; Yates, J. R., III; Wysocki, V. H. *Analytical Chemistry* **2003**, *75*, 1963-1971.

(45) Gardner, M. W.; Brodbelt, J. S. *Journal of the American Society for Mass Spectrometry* **2008**, *19*, 344-357.

(46) Tang, X.; Munske, G. R.; Siems, W. F.; Bruce, J. E. *Analytical Chemistry* **2005**, *77*, 311-318.

(47) Soderblom, E. J.; Goshe, M. B. *Analytical Chemistry* **2006**, *78*, 8059-8068.

(48) Soderblom, E. J.; Bobay, B. G.; Cavanagh, J.; Goshe, M. B. *Rapid Communications in Mass Spectrometry* **2007**, *21*, 3395-3408.

(49) Lu, Y.; Tanasova, M.; Borhan, B.; Reid, G. E. *Analytical Chemistry* **2008**, *80*, 9279-9287.

(50) Hunt, D. F.; Yates, J. R., III; Shabanowitz, J.; Winston, S.; Hauer, C. R. *Proceedings of the National Academy of Sciences of the United States of America* **1986**, *83*, 6233-6237.

(51) McLuckey, S. A.; Van Berkel, G. J.; Glish, G. L. *Journal of the American Society for Mass Spectrometry* **1992**, *3*, 60-70.

(52) McLuckey, S. A.; Goeringer, D. E. *Journal of Mass Spectrometry* **1997**, *32*, 461-474.

(53) Sleno, L.; Volmer, D. A. *Journal of Mass Spectrometry* **2004**, *39*, 1091-1112.

(54) Louris, J. N.; Cooks, R. G.; Syka, J. E. P.; Kelley, P. E.; Stafford, G. C., Jr.; Todd, J. F. J. *Analytical Chemistry* **1987**, *59*, 1677-1685.

(55) Williams, J. D.; Cooks, R. G.; Syka, J. E. P.; Hemberger, P. H.; Nogar, N. S. *Journal of the American Society for Mass Spectrometry* **1993**, *4*, 792-797.

(56) McLuckey, S. A. *Journal of the American Society for Mass Spectrometry* **1992**, *3*, 599-614.

(57) Brodbelt, J. S.; Wilson, J. J. *Mass Spectrometry Reviews* **2009**, *28*, 390-424.

(58) Stephenson, J. L., Jr.; Booth, M. M.; Shalosky, J. A.; Eyler, J. R.; Yost, R. A. *Journal of the American Society for Mass Spectrometry* **1994**, *5*, 886-893.

(59) Colorado, A.; Shen, J. X.; Brodbelt, J. *Analytical Chemistry* **1996**, *68*, 4033-4043.

(60) Kim, T.-Y.; Thompson, M. S.; Reilly, J. P. *Rapid Communications in Mass Spectrometry* **2005**, *19*, 1657-1665.

(61) Gabelica, V.; Tabarin, T.; Antoine, R.; Rosu, F.; Compagnon, I.; Broyer, M.; De Pauw, E.; Dugourd, P. *Analytical Chemistry* **2006**, *78*, 6564-6572.

(62) Wilson, J. J.; Brodbelt, J. S. *Analytical Chemistry* **2007**, *79*, 7883-7892.

(63) Lemoine, J.; Tabarin, T.; Antoine, R.; Broyer, M.; Dugourd, P. *Rapid Communications in Mass Spectrometry* **2005**, *20*, 507-511.

(64) Kalcic, C. L.; Gunaratne, T. C.; Jones, A. D.; Dantus, M.; Reid, G. E. *Journal of the American Chemical Society* **2009**, *131*, 940-942.

(65) Newsome, G. A.; Glish, G. L. *Journal of the American Society for Mass Spectrometry* **2009**, *20*, 1127-1131.

(66) Yeh, G. K.; Sun, Q.; Meneses, C.; Julian, R. R. *Journal of the American Society for Mass Spectrometry* **2009**, *20*, 385-393.

(67) Reilly, J. P. *Mass Spectrometry Reviews* **2009**, *28*, 425-447.

(68) Moon, J. H.; Yoon, S. H.; Kim, M. S. *Rapid Communications in Mass Spectrometry* **2005**, *19*, 3248-3252.

(69) Hunt, D. F.; Shabanowitz, J.; Yates, J. R., III *Journal of the Chemical Society, Chemical Communications* **1987**, 548-550.

(70) Little, D. P.; Speir, J. P.; Senko, M. W.; O'Connor, P. B.; McLafferty, F. W. *Analytical Chemistry* **1994**, *66*, 2809-2815.

(71) Flora, J. W.; Muddiman, D. C. *Analytical Chemistry* **2001**, *73*, 3305-3311.

(72) Payne, A. H.; Glish, G. L. *Analytical Chemistry* **2001**, *73*, 3542-3548.

(73) Wilson, J. J.; Brodbelt, J. S. *Analytical Chemistry* **2006**, *78*, 6855-6862.

(74) Stafford, G. C., Jr.; Kelley, P. E.; Syka, J. E. P.; Reynolds, W. E.; Todd, J. F. J. *International Journal of Mass Spectrometry and Ion Processes* **1984**, *60*, 85-98.

(75) Black, D. M.; Payne, A. H.; Glish, G. L. *Journal of the American Society for Mass Spectrometry* **2006**, *17*, 932-938.

(76) Hashimoto, Y.; Hasegawa, H.; Yoshinari, K.; Waki, I. *Analytical Chemistry* **2003**, *75*, 420-425.

(77) Boue, S. M.; Stephenson, J. L., Jr.; Yost, R. A. *Rapid Communications in Mass Spectrometry* **2000**, *14*, 1391-1397.

(78) Hashimoto, Y.; Hasegawa, H.; Waki, I. *Rapid Communications in Mass Spectrometry* **2004**, *18*, 2255-2259.

(79) Pikulski, M.; Wilson, J. J.; Aguilar, A.; Brodbelt, J. S. *Analytical Chemistry* **2006**, *78*, 8512-8517.

(80) Pikulski, M.; Hargrove, A.; Shabbir, S. H.; Anslyn, E. V.; Brodbelt, J. S. *Journal of the American Society for Mass Spectrometry* **2007**, *18*, 2094-2106.

(81) Vasicek, L. A.; Wilson, J. J.; Brodbelt, J. S. *Journal of the American Society for Mass Spectrometry* **2009**, *20*, 377-384.

(82) Silverstein, R. M.; Webster, F. X.; Kiemle, D. J. *Spectrometric Identification of Organic Compounds*, 7th ed.; John Wiley & Sons: Hoboken, NJ, 2005.

(83) Flora, J. W.; Muddiman, D. C. *Journal of the American Chemical Society* **2002**, *124*, 6546-6547.

(84) Crowe, M. C.; Brodbelt, J. S. *Journal of the American Society for Mass Spectrometry* **2004**, *15*, 1581-1592.

(85) Crowe, M. C.; Brodbelt, J. S. *Analytical Chemistry* **2005**, *77*, 5726-5734.

(86) Joly, L.; Antoine, R.; Broyer, M.; Dugourd, P.; Lemoine, J. *Journal of Mass Spectrometry* **2007**, *42*, 818-824.

(87) Oh, J. Y.; Moon, J. H.; Kim, M. S. *Journal of Mass Spectrometry* **2005**, *40*, 899-907.

(88) Wilson, J. J.; Brodbelt, J. S. *Analytical Chemistry* **2008**, *80*, 5186-5196.

(89) Oh, J. Y.; Moon, J. H.; Lee, Y. H.; Hyung, S.-W.; Lee, S.-W.; Kim, M. S. *Rapid Communications in Mass Spectrometry* **2005**, *19*, 1283-1288.

(90) Wilson, J. J.; Kirkovits, G. J.; Sessler, J. L.; Brodbelt, J. S. *Journal of the American Society for Mass Spectrometry* **2008**, *19*, 257-260.

(91) Zubarev, R. A.; Kelleher, N. L.; McLafferty, F. W. *Journal of the American Chemical Society* **1998**, *120*, 3265-3266.

(92) Kruger, N. A.; Zubarev, R. A.; Horn, D. M.; McLafferty, F. W. *International Journal of Mass Spectrometry* **1999**, *185/186/187*, 787-793.

(93) Syka, J. E. P.; Coon, J. J.; Schroeder, M. J.; Shabanowitz, J.; Hunt, D. F. *Proceedings of the National Academy of Sciences of the United States of America* **2004**, *101*, 9528-9533.

(94) Coon, J. J.; Shabanowitz, J.; Hunt, D. F.; Syka, J. E. P. *Journal of the American Society for Mass Spectrometry* **2005**, *16*, 880-882.

(95) Zubarev, R. A.; Horn, D. M.; Fridriksson, E. K.; Kelleher, N. L.; Kruger, N. A.; Lewis, M. A.; Carpenter, B. K.; McLafferty, F. W. *Analytical Chemistry* **2000**, *72*, 563-573.

(96) Breuker, K.; Oh, H.; Lin, C.; Carpenter, B. K.; McLafferty, F. W. *Proceedings of the National Academy of Sciences of the United States of America* **2004**, *101*, 14011-14016.

(97) McAlister, G. C.; Berggren, W. T.; Griep-Raming, J.; Horning, S.; Makarov, A.; Phanstiel, D.; Stafford, G.; Swaney, D. L.; Syka, J. E. P.; Zabrouskov, V.; Coon, J. J. *Journal of Proteome Research* **2008**, *7*, 3127-3136.

(98) Shi, S. D. H.; Hemling, M. E.; Carr, S. A.; Horn, D. M.; Lindh, I.; McLafferty, F. W. *Analytical Chemistry* **2001**, *73*, 19-22.

(99) Kapp, E. A.; Schutz, F.; Reid, G. E.; Eddes, J. S.; Moritz, R. L.; O'Hair, R. A.; Speed, T. P.; Simpson, R. J. *Analytical Chemistry* **2003**, *75*, 6251-6264.

(100) Zubarev, R. A.; Kruger, N. A.; Fridriksson, E. K.; Lewis, M. A.; Horn, D. M.; Carpenter, B. K.; McLafferty, F. W. *Journal of the American Chemical Society* **1999**, *121*, 2857-2862.

(101) Fagerquist, C. K.; Hudgins, R. R.; Emmett, M. R.; Hakansson, K.; Marshall, A. G. *Journal of the American Society for Mass Spectrometry* **2003**, *14*, 302-310.

(102) Sawicka, A.; Skurski, P.; Hudgins, R. R.; Simons, J. *Journal of Physical Chemistry B* **2003**, *107*, 13505-13511.

(103) Uggerud, E. *International Journal of Mass Spectrometry* **2004**, *234*, 45-50.

(104) Gunawardena, H. P.; Gorenstein, L.; Erickson, D. E.; Xia, Y.; McLuckey, S. A. *International Journal of Mass Spectrometry* **2007**, *265*, 130-138.

(105) Chrisman, P. A.; Pitteri, S. J.; Hogan, J. M.; McLuckey, S. A. *Journal of the American Society for Mass Spectrometry* **2005**, *16*, 1020-1030.

(106) Roepstorff, P.; Fohlman, J. *Biomedical Mass Spectrometry* **1984**, *11*, 601.

Chapter 2

Experimental

2.1 OVERVIEW

The mass spectrometric methods and procedures used for the experiments described in this dissertation are discussed within this chapter. All mass spectrometry experiments were conducted on quadrupole ion trap mass spectrometers (3D and 2D) using an electrospray ionization (ESI) source. Tandem mass spectrometry techniques such as collisional-induced dissociation (CID), infrared multiphoton dissociation (IRMPD), ultraviolet photodissociation (UVPD), and electron transfer dissociation (ETD) were also employed for structural characterization of the analyte ions. The chemical cross-linking procedures for peptides and proteins, cross-linker syntheses, and sample preparations are included as well.

2.2 MASS SPECTROMETRY

All mass spectrometry experiments were conducted on three-dimensional quadrupole ion trap (QITs) or linear quadrupole ion trap (LITs) mass spectrometers. The instruments used included a ThermoFinnigan LCQ Duo three-dimensional quadrupole ion trap (San Jose, CA), an LCQ Deca XP modified for photodissociation experiments, a ThermoFisher Scientific LTQ XL linear ion trap (San Jose, CA) modified for photodissociation and with electron transfer dissociation capabilities, and a ThermoFisher Scientific LTQ Velos dual pressure linear ion trap mass spectrometer. Each QIT consists of a ring electrode that has a hyperbolic profile to which an rf potential (8500 $V_{pp,max}$, 760 KHz) is applied and two end-cap electrodes, also with hyperbolic profiles, to which

auxiliary ac or broadband waveforms are applied. The rf potential creates a quadrupole electric field which traps the ions. Mass spectra are acquired by ramping the rf amplitude applied to the ring electrode to sequentially destabilize ions and eject them from trap, a mode of operation termed mass selective instability scan.[1] The auxiliary waveforms on the end-cap electrodes provide a means to perform ion isolation and resonant collisional ion activation by matching the applied ac frequency to the secular frequency of the ions. Helium buffer gas is introduced into the ion trap at ~1 mTorr which collisionally cools and focuses the ions to the center of trap, improving mass resolution.[1]

A description of the LTQ linear quadrupole ion trap has been provided elsewhere[2] and is shown schematically in **Figure 2.1a**. Briefly, the linear ion trap consists of a quadrupole with hyperbolic rod profiles physically split into three section and front and back aperture lenses positioned on either side of the trap. An rf potential is applied to the the three-segmented quadrupole of the LTQ linear ion trap (5000 $V_{pp,max}$, 1.2 MHz) in a dipolar fashion (i.e., one phase is applied to the x-rods and the 180° out-of-phase waveform is applied to the y-rods) to radially trap the ions. Independent dc offset potentials can be applied to each section in order to trap the ions in the axial direction. Auxiliary ac and broadband waveforms are applied on top of the rf to one pair of rods of the center section of the LIT in a dipolar fashion (e.g., top y-rod = rf + ac; bottom y-rod = rf – ac) to perform ion isolation and resonant collisional ion activation (**Figure 2.2b**). Front and back aperture lenses are positioned on both sides of the LIT to which dc potentials are applied to gate ions into the trap or to which an auxiliary ac waveform is applied to create a pseudo-quadrupole electric field to allow simultaneous trapping of ions of both polarities in the axial direction. Ions are sequentially ejected from the trap through slits machined into the quadrupole rods by a mass selective instability scan. The LIT is held at approximately 2.5 mTorr with He buffer gas. The dual pressure linear ion

trap mass spectrometer consists of two linear ion traps which are separated by a conductance limiting aperture.[3] The first LIT is held at ~5 × 10^{-3} Torr and the second LIT is held at ~3 × 10^{-4} Torr of He. The two LITs are operated in a similar manner to the LIT described above. Ion isolation and activation can be performed in either cell of the dual pressure LIT; mass analysis was performed in the low pressure cell.

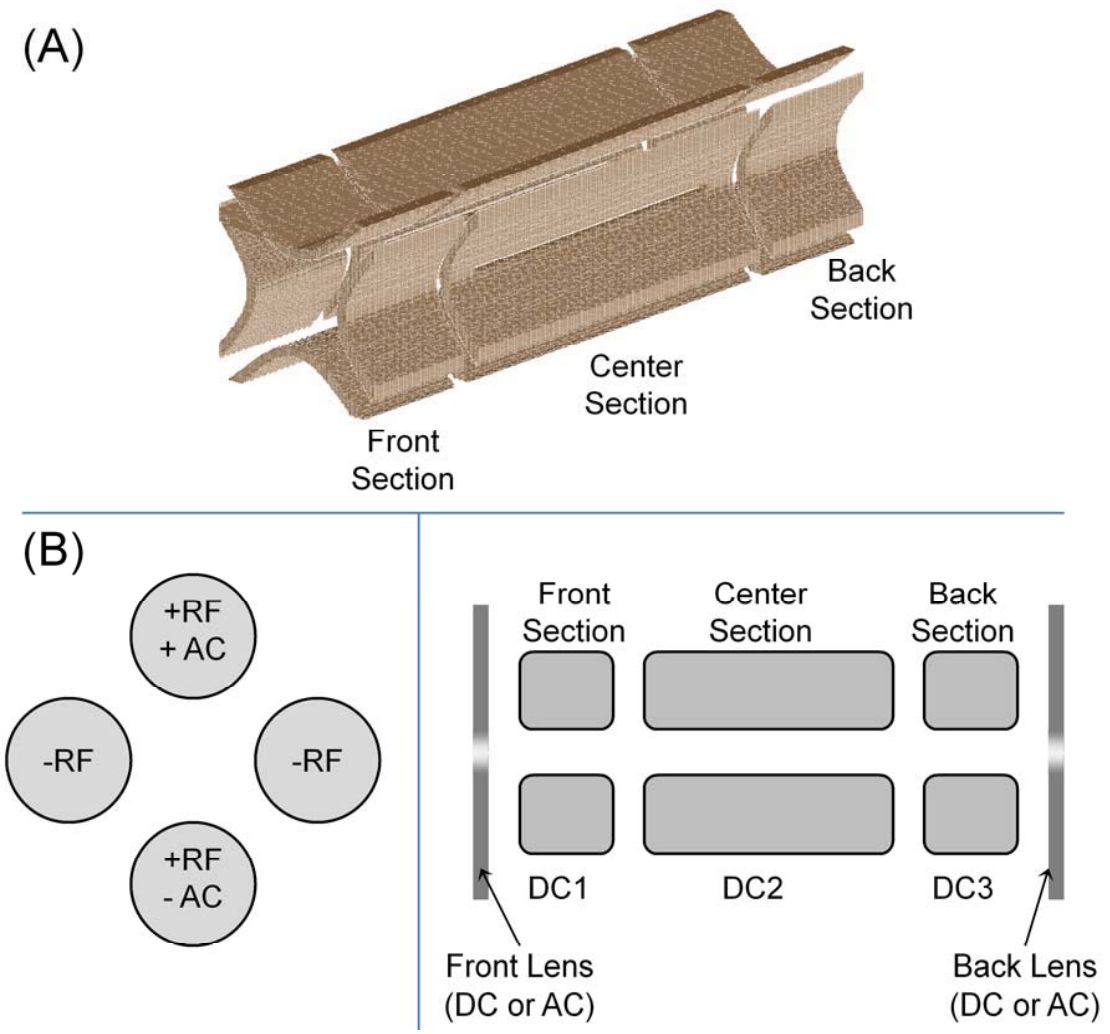

Figure 2.1 (A) Schematic of ThermoFisher Scientific LTQ XL linear quadrupole ion trap and (B) types of waveforms applied for ion trapping and resonant excitation.

Ions are produced by electrospray ionization (ESI) and the standard ESI sources were used on all instruments. ESI is a soft ionization method which allows for a wide variety of biological species, including peptides, proteins, oligonucleotides, and macromolecular complexes, to be analyzed by mass spectrometry.[4] ESI is performed by applying a high potential (~ 4 kV) to a conductive needle or capillary through which the analyte solution is infused. A nebulizing sheath gas flow of nitrogen (~0.3 – 1.0 L/min) is applied co-axial to the spray which aids in desolvation of the charged droplets. Multiply-charged analyte ions are often produced by protonation or deprotonation. To afford efficient ion desolvation, the inlet to the mass spectrometry, a stainless steel capillary, is heated and the temperature was maintained at 180 °C for peptide and protein samples and at 90 °C for siRNA samples. Samples were generally prepared at ~10 μM in 49.5: 49.5: 1 H_2O/MeOH/acetic acid (v/v/v) and infused at 2.5 – 5.0 μL/min using Harvard Apparatus PHD 2000 syringe pump (Holliston, MA). The ESI potential was set to 4.0 – 4.5 kV for positive ion mode analysis and -3.5 to -4.0 kV for negative ion mode. Potentials to the ion optics were tuned for maximum signal. All direct infusion ESI mass spectra are the average of 20 – 100 scans.

Tandem mass spectrometry (MS/MS) experiments are methods in which selected ions of interest are subjected to another or sequential stages of mass spectrometry. Ion activation and dissociation are a subset of MS/MS experiments which involve ion isolation, accomplished by the appropriate application of auxiliary waveforms and ramping of the trapping rf amplitude to eject ions other than the precursor ion, and then ion activation through resonant collisional excitation (CID) or photon absorption (photodissociation). Ion-ion reactions such as ETD are another type of MS/MS experiment in which a precursor ion is first isolated in the trap and then a chemical reagent ion of the opposite polarity is introduced.

2.2.1 Collision-Induced Dissociation (CID)

CID is a resonant excitation technique which is accomplished by applying an auxiliary ac waveform to the end-cap electrodes of a QIT or on top of the rf applied to the LIT with a frequency that matches the secular frequency of the precursor ion. The precursor ion gains kinetic energy and its amplitude of motion increases. As the ion collides with the inert bath gas (He) molecules, the precursor ion gains internal energy which is distributed amongst all degrees of freedom through intramolecular vibrational redistribution. Once the precursor ion has gained enough internal energy through collisional activation (typically hundreds of low-energy collisions), bond dissociation is observed yielding product ions.

CID experiments were performed on all mass spectrometers at an activation q-value of 0.25 for 30 ms. The normalized collision energy (NCE), a ThermoFinnigan parameter which is proportional to the excitation amplitude of the auxiliary ac waveform and normalized for precursor *m/z*, was varied to reduce the precursor ion to less than ~5% relative intensity. Normalized collision energies were converted to excitation voltages using the following formula:

$$V = \frac{NCE(\%)}{30\%} \times \left[\left(m/z \times TickAmpSlope\right) + TickAmpInt\right] \qquad \textbf{Equation 2.1}$$

where V is the excitation voltage, NCE is the normalized collision energy in percent, *m/z* is the precursor ion *m/z* value, and TickAmpSlope and TickAmpInt are instrument calibration factors. In order to compare excitation voltages from one precursor ion to another, the voltages were normalized by degrees of freedom using the following formula:

$$V_{j,corrected} = V_j \times \frac{N_i}{N_j}$$ **Equation 2.2**

where *i* refers to the control precursor ion, *j* the precursor ion for which the excitation voltage is being corrected, and the degrees of freedom $N = 3n - 6$ and *n* is the number of atoms in the precursor ion.[5] Energy-resolved CID experiments were performed by sequentially increasing the NCE and plotting product ion abundances with respect to NCE.

2.2.2 Infrared Multiphoton Dissociation (IRMPD)

Photodissociation is another tandem mass spectrometric method in which ions gain internal energy through photon absorption. IRMPD is an ergodic dissociation method similar to CID in which the more labile bonds are more readily dissociated. Typically, hundreds of IR photons of ~0.12 eV (10.6 μm radiation) must be absorbed by the precursor ion to observe bond dissociation.

IRMPD experiments were performed on the LTQ and the LTQ Velos linear ion trap mass spectrometers. The instrument was modified to permit IRMPD as described in earlier reports.[6] The back flange of the vacuum manifold of the instrument was modified with a CF viewport flange containing a ZnSe window to allow the transmission of 10.6 μm radiation. The unfocused laser beam was aligned on axis with the linear ion trap such that the beam passed through a 1.8 mm aperture mounted to the back flange and then the 2-mm aperture of the exit lens to irradiate the ion cloud. IRMPD was performed using a model 48-5 Synrad 50-W CO_2 continuous wave laser (Mukilteo, WA). The laser was triggered during the activation step in the scan function by a TTL signal from pin 14 of the J1 connector on the digital printed circuit board. All IRMPD experiments were performed at full power (50 W) with irradiation times varying between 0.03 and 250 ms

unless otherwise indicated. The activation q-value was varied between 0.05 and 0.25 to reduce the low-mass cut-off. Wide-range ion isolation and IRMPD mass spectra were acquired by turning off the isolation waveform in the diagnostics panel of the LTQTune instrument software. Isolation mass spectra were acquired by turning off the laser and not performing any form of ion activation. Time-resolved IRMPD experiments were performed by varying the irradiation time and plotting product ion abundances as a function of irradiation time.

2.2.3 Ultraviolet Photodissociation (UVPD)

UVPD experiments were performed on a modified LCQ Deca XP quadrupole ion trap mass spectrometer as previously described.[7] A Spectra-Physics Quanta-Ray GCR-11 Nd:YAG laser with a HG-2 harmonics generator (Mountain View, CA) was used to produce the frequency-tripled harmonic photons at 355 nm (~3.5 eV/photon) for UVPD. Briefly, a CF viewport flange was welded to the vacuum manifold of the mass spectrometer and fitted with a quartz window to allow the transmission of UV radiation. The unfocused laser beam was aligned on-axis with a 5-mm hole drilled through the ring electrode to irradiate the ion cloud. The laser was operated at full power (~65 mJ/pulse), unless otherwise noted, at a repetition rate of 10 Hz in the Q-switched mode which produced ~10 ns pulse widths. The LCQ instrument TTL signal output from pin TP 15-3 Sync_TP was used to trigger a Model 505-2C low-voltage pulse generator (Berkeley Nucleonics Corp., San Rafael, CA) which in turn was used to pulse the laser. Typically, the activation time was set to 1000 ms to produce ten laser pulses unless indicated otherwise. The instrument control files were modified to allow triggering of the laser during LC-MS/MS analyses. Precursor ions were activated at a q_z-value of 0.10. Wide-range ion isolation and UVPD mass spectra were acquired by turning off the second

waveform in the diagnostics panel of the LCQTune instrument software. Isolation mass spectra were acquired by turning off the laser and not performing any form of ion activation. Online liquid chromatography-UVPD-MS was performed by either isolating ions of *m/z* 450 – 1200 without any form of activation or by subjecting all ions of *m/z* 450 – 1200 to ten pulses of UV irradiation at 355 nm.

2.2.4 Electron Transfer Dissociation (ETD)

ETD experiments were performed on the LTQ linear ion trap mass spectrometer. Fluoranthene radical anions were produced by negative chemical ionization and introduced through a mass-resolving quadrupole into the linear ion trap from the opposite side as the electrospray ionization source. The built-in ETD scan function of the LTQTune software was used and is described elsewhere.[8] Briefly, the precursor ion (cation) is first isolated in the ion trap and then transferred to the front section of the LIT by application of appropriate dc potentials to the three sections of the LIT. Fluoranthene radical anions are the introduced to the trap and sequestered in the back section of the LIT in a similar manner. The axial dc trapping potentials are then removed to allow the ion-ion reaction to proceed and mutual storage of cations and anions in the LIT is accomplished by the application of an auxiliary ac waveform to the front and back lenses of the LIT. The fluoranthene radical ions transfer an electron to the peptide or protein cations in an exothermic process which results in non-ergodic dissociation of the precursor ion.[9] The ion-ion reactions varied between 0.03 and 200 ms. The target reagent anion population was set to 1×10^5 ions and the precursor ion population was set to 3×10^4. The activation q-value was such that the low-mass cut-off was reduced to *m/z* 50. Time-resolved ETD experiments were performed by plotting the relative abundances of the observed product ions as a function of the ETD reaction time.

2.3 CHEMICALS AND REAGENTS

The following five peptides were synthesized at the Protein Microanalysis Facility at the University of Texas at Austin and purified by reversed-phase liquid chromatography: Ac-AAAKAAAAR, Ac-AADKAAAAR, Ac-AAAKDAAAR, Ac-AAPKAAAAR, and Ac-AAAKPAAAR. All other peptides were used without further purification. The peptides α-MSH (Ac-SYSMEHFRWGKPV-NH_2), Ac-RFMWMK-NH_2, substance P (RPKPQQFFGLM-NH_2), neurotensin (Pyr-LYENKPRRPYIL), neurotensin 1-6 (Pyr-LYENK), FSWGAEGQR, YGGFLK, ASHLGLAR, and AGCKNFFWKTFTSC (somatostatin-14) were purchased from Bachem (Torrance, CA or King of Prussia, PA). The peptide angiotensin II (DRVYIHPF) was purchased from AnaSpec (San Jose, CA). The peptides fibrinopeptide A (ADSGEGDFLAEGGGVR) and bradykinin (RPPGFSPFR) were purchased from American Peptide Co. (Sunnyvale, CA). The peptides methionine-enkephalin (YGGFM), angiotensin I (DRVYIHPFHL), and melittin (honey bee venom) were purchased from Sigma (St. Louis, MO). Ubiquitin (bovine red blood cells), cytochrome c (horse heart), proteomics grade trypsin, resperine, and the cross-linker disuccinimidyl suberate (DSS) were also obtained from Sigma (St. Louis, MO). *N*-hydroxysuccinimide (NHS), 4-hydroxybenzoic acid, ethyl dichlorophosphate, benzaldehyde, and 2-hydrazinopyridine were from Aldrich (Milwaukee, WI). Imidazole, piperidine, and Amberlite IRN77 were purchased from Sigma-Aldrich (St. Louis, MO). Water (HPLC grade) and acetonitrile (HPLC grade) were from Riedel-de Haën (Seelze, Germany). 1-ethyl-3-(3-dimethylaminopropyl) carbodiimide hydrochloride (EDC), succinimidyl 4-formylbenzoate (SFB), succinimidyl 4-hydrazinonicotinate acetone hydrazone (SANH), and the cross-linker dithiobis (succinimidyl propionate) (DSP) were obtained from Pierce Biotechnology (Rockford,

IL). The cross-linker disuccinimidyl L-tartrate (DST) was purchased from Toronto Research Chemicals (North York, Ontario, Canada). The siRNAs targeting the glyceraldehydes 3-phosphate dehydrogenase (GAPDH) gene and the Lamin A/C gene were purchased from Integrated DNA Technologies (Coralville, IA). The sequences for anti-GAPDH were 5'OH-GUGGAUAUUGUUGCCAUCAdTdT-3'OH (sense strand, 6633.9 Da) and 5'OH-UGAUGGCAACAAUAUCCACdTdT-3'OH (antisense strand, 6644.9 Da). The sequences for anti-Lamin A/C were 5'-biotin-GGAACUGGACUUCCAGAAGAACAUCAU-3'OH (sense strand, 9053.6 Da) and 5'-UAGAUGUUCUUCUGGAAGUCCAGUUCC (antisense strand, 8544.1 Da). All other chemicals and solvents were purchased from Fisher Scientific (Fairlawn, NJ) except for formic acid (EM Science, Gibbstown, NJ).

2.4 CHEMICAL SYNTHESIS

2.4.1 Synthesis of Dibenzoyloxysuccinimidyl Ethyl Phosphate

The synthetic procedure for the IR chromogenic cross-linker, dibenzoyloxysuccinimidyl ethyl phosphate is outlined in **Scheme 2.1** and was prepared by first synthesizing the intermediate *N*-(4-hydroxybenzoyloxy)succinimide. Under an argon atmosphere, dry tetrahydrofuran (THF; 45 mL) and dry dichloromethane (DCM; 45 mL) were added to 5 mmol of 4-hydroxybenzoic acid, 8 mmol of NHS, and 6.5 mmol of EDC. The reaction was stirred under argon at room temperature for 24 hours and then extracted with H_2O (1 × 60 mL), saturated $NaHCO_3$ (1 × 60 mL), and then a saturated brine solution (1 × 60 mL). The final liquid extract was dried over Na_2SO_4, filtered, and dried under vacuum. The intermediate was recrystallized in DCM at 20 °C overnight and filtered.

Dibenzoyloxysuccinimidyl ethyl phosphate was prepared by dissolving 0.5 mmol of *N*-(4-hydroxybenzoyloxy)succinimide in dry THF at 0 °C, and then adding 0.25 mmol of ethyldichlorophosphate dropwise to the solution, followed by 10 mmol of dry triethylamine. The reaction was allowed to warm to room temperature while stirring over 2 hours, then heated to 60 °C and stirred for additional 4 hours. The final solution was dried and concentrated under reduced pressure. The product was washed with cold H_2O, filtered, recrystallized in DCM, and filtered. The cross-linker structure was confirmed by ^{1}H NMR using a 400 MHz Varian instrument and ESI-IRMPD-MS.

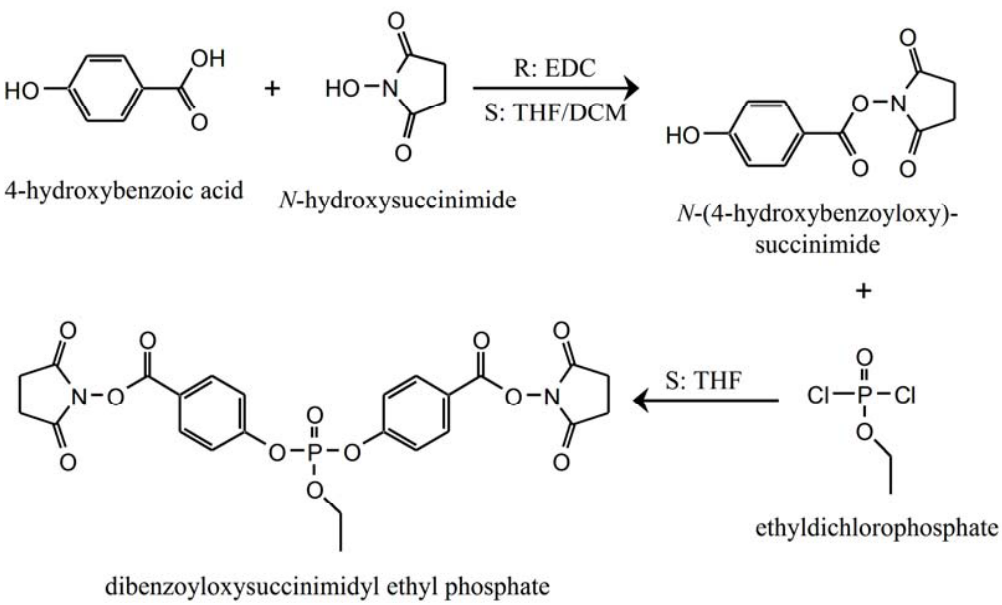

Scheme 2.1 Synthesis of dibenzoyloxysuccinimidyl ethyl phosphate.

2.4.2 Synthesis of Benzaldehyde-2-pyridinylhydrazone and UV-Vis Measurements

The ultra-violet chromophore benzaldehyde-2-pyridinylhydrazone (B2PH) was synthesized by dissolving 1.0 mmol of 2-hydrazinopyridine in 2.0 mL of MeOH and then 102 μL (1.0 mmol) of benzaldehyde was added (**Scheme 2.2**). The solution was heated

to 55 °C and stirred for 16 hours. The reaction mixture was then cooled to room temperature, and the yellow-orange precipitate of B2PH was vacuum filtered. The final product was redissolved in MeOH and then diluted to 50 μM for downstream analysis and characterization by UV-Vis spectroscopy and UVPD-MS. All UV-Vis measurements were obtained on an Agilent 8453 spectrophotometer (Santa Clara, CA).

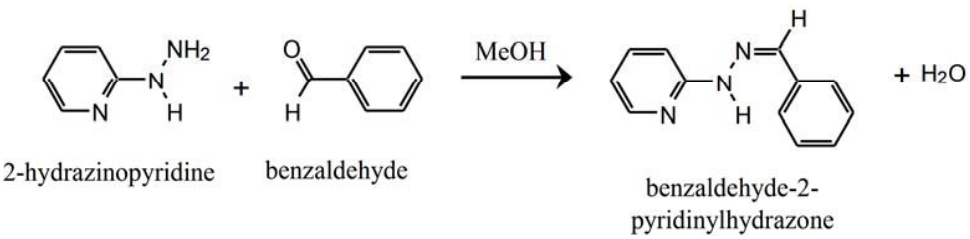

Scheme 2.2 Synthesis of benzaldehyde-2-pyridinylhydrazone.

2.5 CHEMICAL CROSS-LINKING AND CONJUGATION

2.5.1 Peptide Cross-Linking

Stock solutions of the model peptides were prepared at 5.0 mM in H_2O. Cross-linkers were freshly prepared at 20.0 mM in DMSO prior to cross-linking. For intermolecular cross-linking, the two peptides (termed α and β) were cross-linked with at a 4:4:5 molar ratio of α-peptide: β-peptide: cross-linker in 20 mM HEPES, pH 8.0 at a final concentration of ~200 – 500 μM of peptide in ~10 – 50 μL. Intramolecular peptide cross-linking was similarly performed at a 4:5 molar ratio of peptide to cross-linker in the same buffer. All peptide cross-linking reactions were allowed to incubate at room temperature overnight to increase the yield of cross-linked peptides. The reactions were desalted by solid phase extraction using 50 mg tC_{18} Waters (Milford, MA) Sep-Pak cartridges.

2.5.2 Protein Cross-Linking

The cross-linker solution was prepared as described above; stock protein solutions at 200 μM were prepared. The proteins were intramolecularly cross-linked at 1:5, 1:10, 1:25 and 1:50 molar ratios of protein: cross-linker in a 20 mM HEPES buffer, pH 8.0 at a final protein concentration of 10 μM. The reactions were allowed to proceed at room temperature for 30 minutes. The cross-linking was quenched by the addition of NH_4HCO_3 to a final concentration of 10 mM for 15 minutes. The reaction mixtures were desalted against a 5 kDa molecular weight cut-off Ultrafree Biomax membrane (Millipore, Billerica, MA). Aliquots were removed for direct-ESI-MS analysis and the remaining cross-linked protein sample was diluted to 180 μM in 100 mM NH_4HCO_3, pH 8.0 for enzymatic digestion.

2.5.3 Peptide Conjugation

Model peptides were cross-linked together via a two-step conjugation method. All peptides were dissolved to 5.0 mM in H_2O, and the modifying reagents SANH and SFB were each freshly prepared at 20.0 mM in DMSO. Each peptide was individually modified at its primary amines (e.g. free N-termini or lysine residues) by either SANH or SFB in 20 mM HEPES, pH 8.0 buffer at a 1:10 molar ratio of peptide to modifier (200 μM: 2.0 mM). The reactions were allowed to proceed at room temperature overnight to ensure complete modification of the peptides; the product mixture was then desalted using Waters tC_{18} SepPak cartridges (Milford, MA) and peptides were eluted with 100% MeOH. The two modified peptides were then conjugated together at an equimolar ratio (~100 μM) in 99/1 MeOH/HOAc acid at 55 °C overnight forming a bis-aryl hydrazone cross-link. The conjugated peptides were subsequently diluted to ~10 μM in 49.5:49.5:1 H_2O/MeOH/HOAc (v/v/v) for ESI-MS analysis without any further purification.

2.6 ENZYMATIC DIGESTION

Proteins were enzymatically digested in solution with proteomics grade trypsin (Sigma-Aldrich, St. Louis, MO) at a 1:15 enzyme to protein (w/w) ratio. Trypsin (20 μg) was dissolved in 20 μL of 1.0 mM HCl and then added to the protein solution in 100 mM NH_4HCO_3, pH 8.0. Proteins were digested overnight while heating at 37 °C. The digested sample was then desalted by solid-phase extraction using Waters tC_{18} Sep-Pak cartridges (Milford, MA) and diluted to ~10 μM in 50:50 H_2O/MeOH for downstream analysis.

2.7 LIQUID CHROMATOGRAPHY

All high performance liquid chromatography (HPLC) experiments were accomplished using reversed-phase separations using C_{18} columns. A Waters 2695 Separations Module and 486 Tunable Absorbance Detector (Milford, MA), which were both controlled by the Millennium version 3.00 software package, were interfaced to the LCQ Deca XP modified for UVPD experiments. Reversed-phase HPLC was accomplished using a Symmetry300 C_{18} column (2.1 × 50 mm, 3.5 μm packing) using a gradient elution consisting of (A) H_2O with 0.1% formic acid and (B) acetonitrile with 0.1% formic acid at a flow rate of 0.300 mL/min. The mobile phase was held at 95% A for two minutes after sample injection (typically 10 μL of ~10 μM solutions) and then linearly reduced to 60% over 60 minutes. Analytes were detected by UV-Vis absorption spectroscopy at 355 nm as well as by mass spectrometry

A Hitachi L-7000 (Hitachi Ltd.) system including an L-7100 HPLC pump and L-7000 autosampler was interfaced to the LTQ mass spectrometer; the LC system was

controlled using the Hitachi 3DQ software. Reversed-phase HPLC was also accomplished using a Symmetry300 (Waters, Milford, MA) C_{18} column (2.1 × 50 mm, 3.5 μm packing) with a Symmetry300 C_{18} guard column (2.1 × 10 mm, 3.5 μm packing). For analytical separations, a gradient elution of mobile phases consisting of (A) H_2O with 0.1% formic acid and (B) acetonitrile with 0.1% formic acid was used at a flow rate of 0.300 mL/min. After loading the sample (10 – 25 μL injections of 10 μM solutions), the mobile phase was held at 95% A for 2 minutes and then the peptides were eluted using a linear gradient from 95% A to 50% A over 58 minutes.

2.8 siRNA Sample Preparation

Single-strand siRNA samples were desalted by cation exchange using the Amberlite IRN77 resin as described by McLuckey et al.[10] Duplex siRNA was annealed by combining the sense and antisense siRNA strands (30 μM each) in 150 mM NH_4OAc, pH 7.0. The samples were heated at 90 °C for three minutes and then cooled to room temperature overnight. Duplex siRNA solutions were diluted to 10 μM in 25:75 (v/v) methanol/50 mM NH_4OAc in nano-pure H_2O. Solutions of GAPDH single-strand siRNAs were prepared at 10 μM in either 25:75 (v/v) methanol/25 mM NH_4OAc for negative and positive electrospray mass spectrometry (ESI-MS) or 20:80 (v/v) isopropanol/H_2O with 25 mM imidazole and 25 mM piperidine for negative ESI-MS. The Lamin A/C single strand siRNAs were prepared at 10 μM in 25:75 (v/v) methanol/25 mM NH_4OAc for negative and positive ion ESI-MS.

2.9 DATA ANALYSIS

Product ion spectra of cross-linked peptide ions were manually identified aided in part with the software program ProteinXXX, the protein cross-linking function of GPMAW (General Protein Mass Analysis for Windows) version 7.10 (Lighthouse Data, Odense, Denmark) (available at http://www.gpmaw.com) and an in-house program written in National Instruments LabView 8.5. Product ions of siRNA single strands and duplex siRNA were identified using Mongo Oligo Mass Calculator (http://library.med.utah.edu/masspec/mongo.htm) in addition to an oligonucleotide product ion calculator program written in-house using National Instruments LabView 8.5.

Dissociation efficiencies were calculated according to the following formula:

$$Dissociation\ Efficiency = \frac{\sum_i F_i}{\sum_i F_i + P} \times 100\%$$

Equation 2.3

where P is the abundance of the surviving precursor ion after ion activation, and F_i is the abundance of each product ion. The efficiency of the tandem MS experiment (i.e., MS/MS efficiency) is defined below:

$$MS/MS\ Efficiency = \frac{\sum_i F_i}{P_0} \times 100\%$$

Equation 2.4

where P_0 is the abundance of the precursor ion prior to any IR irradiation, collisional activation, or ion-ion reaction, and F_i is the abundance of each product ion. The sum of the product ion abundance (i.e., ΣF_i) was determined by subtracting the abundance of any remaining precursor ion from the total ion abundance for the efficiency calculations. Ion abundances were determined by calculating the peak areas using Origin 7.0.

For the dissociation of cross-linked peptides, the directionality of cleavage bias to the lysine residue was calculated for both the cross-linked peptides and the unmodified species using a method previously suggested by Tabb et al.[11] The C-terminal cleavage bias was determined by taking the ratio of the difference in C-terminal and N-terminal fragment ions, relative to the lysine residue, to the sum of these fragment ion peak areas. For example, the y-ion C-terminal bias was calculated as follows:

$$C_y = \frac{\left(A_{yn\alpha} + A_{yn\beta}\right) - \left(A_{y,n+1,\alpha} + A_{y,n+1,\beta}\right)}{\left(A_{yn\alpha} + A_{yn\beta}\right) + \left(A_{y,n+1,\alpha} + A_{y,n+1,\beta}\right)} \qquad \textbf{Equation 2.5}$$

where A_i is the peak area of the respective y-ions; the y_{n+1} ions are products of cleavage N-terminal to the cross-linked lysine, and the y_n ions are a result of C-terminal cleavage to the cross-linked lysine. The α and β subscripts refer to the α and β peptide of the cross-linked peptide. A positive value indicates a fragmentation bias C-terminally to the lysine residue, whereas a negative value signifies an N-terminal bias. Similarly, for the b-ions, the cleavage bias was calculated using the following formula:

$$C_b = \frac{\left(A_{b,n+1,\alpha} + A_{b,n+1,\beta}\right) - \left(A_{bn\alpha} + A_{bn\beta}\right)}{\left(A_{b,n+1,\alpha} + A_{b,n+1,\beta}\right) + \left(A_{bn\alpha} + A_{bn\beta}\right)} \qquad \textbf{Equation 2.6}$$

where the b_{n+1} ions are the C-terminal cleavage products and the b_n ions are the N-terminal fragments to the cross-linked lysine.

2.10 REFERENCES

(1) Stafford, G. C., Jr.; Kelley, P. E.; Syka, J. E. P.; Reynolds, W. E.; Todd, J. F. J. *International Journal of Mass Spectrometry and Ion Processes* **1984**, *60*, 85-98.

(2) Schwartz, J. C.; Senko, M. W.; Syka, J. E. P. *Journal of the American Society for Mass Spectrometry* **2002**, *13*, 659-669.

(3) Schwartz, J. C.; Syka, J. E. P.; Remes, P. M. *Proceedings of the 56th ASMS Conference on Mass Spectrometry and Allied Topics*. Denver, CO, June 2008.

(4) Fenn, J. B.; Mann, M.; Meng, C. K.; Wong, S. F.; Whitehouse, C. M. *Science* **1989**, *246*, 64-71.

(5) Gabryelski, W.; Li, L. *Rapid Communications in Mass Spectrometry* **2002**, *16*, 1805-1811.

(6) Gardner, M. W.; Vasicek, L. A.; Shabbir, S.; Anslyn, E. V.; Brodbelt, J. S. *Analytical Chemistry* **2008**, *80*, 4807-4819.

(7) Wilson, J. J.; Brodbelt, J. S. *Analytical Chemistry* **2007**, *79*, 7883-7892.

(8) Syka, J. E. P.; Coon, J. J.; Schroeder, M. J.; Shabanowitz, J.; Hunt, D. F. *Proceedings of the National Academy of Sciences of the United States of America* **2004**, *101*, 9528-9533.

(9) Zubarev, R. A.; Kelleher, N. L.; McLafferty, F. W. *Journal of the American Chemical Society* **1998**, *120*, 3265-3266.

(10) Huang, T.; Liu, J.; Liang, X.; Hodges, B. D. M.; McLuckey, S. A. *Analytical Chemistry* **2008**, *80*, 8501-8508.

(11) Tabb, D. L.; Smith, L. L.; Breci, L. A.; Wysocki, V. H.; Lin, D.; Yates, J. R., III *Analytical Chemistry* **2003**, *75*, 1155-1163.

Chapter 3

Impact of Proline and Aspartic Acid Residues on the Dissociation of Intermolecularly Cross-linked Peptides

3.1 OVERVIEW

The dissociation of intermolecularly cross-linked peptides was evaluated for a series of peptides with proline or aspartic acid residues positioned adjacent to the cross-linking sites (lysine residues). The peptides were cross-linked with either disuccinimidyl suberate (DSS) or disuccinimidyl L-tartrate (DST), and the influence of proline and aspartic acid residues on the fragmentation patterns were investigated for precursor ions with and without a mobile proton. Collision-induced dissociation (CID) spectra of aspartic acid-containing cross-linked peptide ions, doubly-charged with both protons sequestered, were dominated by cleavage C-terminal to the Asp residue, similar to that of unmodified peptides. The proline-containing cross-linked peptides exhibited a high degree of internal ion formation, with the resulting product ions having an N-terminal proline residue. Upon dissociation of the doubly-charged cross-linked peptides, twenty to fifty percent of the fragment ion abundance was accounted for by multiple cleavage products. Cross-linked peptides possessing a mobile proton yielded almost a full series of b- and y-type fragment ions, with only proline-directed fragments still observed at high abundances. Interestingly, the cross-linked peptides exhibited a tendency to dissociate at the amide bond C-terminal to the cross-linked lysine residue, relative to the N-terminal side. One could envision updating computer algorithms to include these cross-linker specific product ions – particularly for precursor ions with localized protons – that provide complementary and confirmatory information, to offer more confident identification of both the cross-linked peptides and the location of the cross-link, as well

as affording predictive guidelines for interpretation of the product-ion spectra of cross-linked peptides.

3.2 INTRODUCTION

With tremendous advances in proteomics in the past decade, the interest in understanding protein-protein interactions at a molecular level has expanded as new methods for exploring macromolecules have emerged.[1-3] Chemical cross-linking of proteins coupled with mass spectrometric analysis has become a more widely used method for determining protein-protein interactions in recent years.[4-6] Protein cross-linking is a low resolution, structural analysis technique that allows one to determine distance constraints within single proteins,[7, 8] or protein-ligand complexes.[9-13] Cross-linked proteins are typically subjected to enzymatic digestion to create more easily interpreted peptide segments upon subsequent tandem mass spectrometric analysis. Cross-linking has also been utilized to identify protein folds,[6] conformational changes of proteins upon activation,[14, 15] and RNA-protein interactions.[16] While the chemical cross-linking experiment is often rather straightforward, the technique is restricted by several limitations which must be overcome in order to obtain the desired structural information. First, the cross-linked peptides must be identified from unmodified ones, typically in complex mixtures such as enzymatic digests of the protein or protein-complexes, in which there may only be a few cross-links per protein among an abundance of unmodified peptide fragments. Once distinguished and identified, collision-induced dissociation (CID) experiments on these species are performed in order to sequence the peptide or peptides. Structural assignment of the cross-linked peptides is still not routine despite the emergence of several sequencing algorithms.[17-22] In fact, one of the main pitfalls of mass spectrometric strategies for examination of cross-linked peptides is the

lack of comprehensive rules for interpretation of the product ion spectra. Finally, with the known sequence tags, the site and residue of chemical modification must be pinpointed to estimate distance constraints.

Despite the enormous number of investigations that have elucidated the fragmentation pathways of conventional tryptic peptides, to date only a few studies have focused on mapping the dissociation trends of cross-linked peptides in a systematic fashion.[20, 23, 24] Initial work by Schilling et al. demonstrated that dissociation of intermolecularly cross-linked peptides typically resulted in amide bond cleavage of one peptide, with the cross-link and second peptide acting as a modification.[20] In addition, they observed product ions unique to cross-linked peptides, including two-cleavage fragment ions such as b/b ions, in which two b-type fragment ions were linked together. A more recent study investigating the effects of lysine specific cross-linkers and precursor ion charge observed that without a mobile proton, many of the product ions formed were not of the a-, b-, or y-type.[23] Gaucher et al. also noticed that intramolecularly cross-linked peptides exhibited enhanced dissociation at the peptide amide bonds adjacent to the cross-linked lysine residues.[23]

While many fundamental studies and statistical analyses have examined the influence of amino acid content on the gas-phase dissociation of unmodified peptides,[25-29] no similar work to date has been performed for cross-linked peptides. It has been shown that certain amino acids, including aspartic acid and proline, enhance or promote specific backbone cleavage of peptides.[30-38] The mobile proton model, which proposes that peptide fragmentation is driven by charge-directed cleavages, has shown that higher energies are required to dissociate peptide ions in which the protons are sequestered at basic sites, particularly arginine residues.[26, 30, 38-40] For such peptides which do not possess a mobile proton and have aspartic acid residues, enhanced cleavage at the Asp-

Xxx bond has been observed.[31, 41, 42] Work by the Wysocki group has demonstrated that the acidic side chain of aspartic acid directs fragmentation, site-specifically, at the C-terminal amide bond.[33, 43] Similar dissociation trends were also observed for glutamic acid containing peptides.[33] Proline residues enhance dissociation N-terminally, at the Xxx-Pro amide bond, often yielding intense y-type ions, and has been observed for the dissociation of small, singly-charged peptides as well as multiply-charged proteins.[32, 44] This site-specific cleavage was first attributed to the high gas-phase basicity of the proline residue,[45] but has also been theorized to be due to unfavorable ring strain of a proposed bicyclic structure of the b-type ion that would be formed upon cleavage C-terminal to the proline.[46]

The effects of amino acid content on the gas-phase fragmentation of cross-linked peptides, in particular residues which are known to promote site-specific dissociation along the peptide backbone, have not been analyzed. Knowledge of the dissociation trends of cross-linked peptides, especially with regards to specific amino acids, would be useful for improving computer algorithms to aid in the interpretation of product ion spectra of these ions. In this work, we investigate the influence of aspartic acid and proline on the dissociation of intermolecularly cross-linked peptides. As unmodified peptides tend to exhibit enhanced fragmentation C-terminally to aspartic acid residues for precursor ions with sequestered protons, and N-terminally to prolines, these residues were positioned adjacent to the lysines modified by commonly used primary amine-specific cross-linkers. The impact of these residues on the directionality of cleavage relative to the cross-linked lysine is also reported.

3.3 EXPERIMENTAL

3.3.1 Reagents

The following five peptides were synthesized at the Protein Microanalysis Facility at the University of Texas at Austin and purified by reversed-phase liquid chromatography: Ac-AAAKAAAAR (**AKA**), Ac-AADKAAAAR (**DKA**), Ac-AAAKDAAAR (**AKD**), Ac-AAPKAAAAR (**PKA**), and Ac-AAAKPAAAR (**AKP**). The peptides neurotensin (Pyr-LYENKPRRPYIL) and α-MSH (Ac-SYSMEHFRWGKPV-NH_2) were purchased from Bachem (Torrance, CA). The cross-linker disuccinimidyl suberate (DSS) was purchased from Sigma-Aldrich (St. Louis, MO) and disuccinimidyl L-tartrate (DST) from Toronto Research Chemicals (North York, Ontario, Canada). All other chemicals and solvents were obtained from Fisher Scientific (Fairlawn, NJ) except for extra dry dimethylsulfoxide (DMSO) (Sigma-Aldrich, St. Louis, MO).

3.3.2 Chemical Cross-linking

Stock solutions of each peptide were prepared at 5.0 mM in 20.0 mM sodium phosphate buffer, pH 7.5, and the cross-linkers were freshly prepared at 20.0 mM in DMSO directly before use. The cross-linking reaction was performed by adding 8.0 μL of each peptide to 2.5 μL of cross-linker, for a molar ratio of 4: 4: 5 (α peptide: β peptide: cross-linker). The reaction was allowed to proceed at room temperature for one hour, after which the reaction mixture was desalted by solid-phase extraction using 50 mg tC_{18} Waters (Milford, MA) Sep-Pak cartridges.

3.3.3 Methods and Instrumentation

Samples were diluted to a concentration of 20 μM in 70/30/1 MeOH/H_2O/HOAc (v/v/v) for ESI-MS analysis. Experiments were performed on a ThermoFinnigan LCQ Duo (San Jose, CA) quadrupole ion trap with the standard electrospray source. Solutions were infused into the mass spectrometer at 3 μL/min using a Harvard Apparatus PHD 2000 syringe pump (Holliston, MA). Ionization and ion optic conditions were optimized once for each precursor charge state and were not re-tuned for each individual cross-linked peptide pair. Precursor ions were activated for 30 ms at the typical q_z value of 0.25 for CID and the collision energy was adjusted such that precursor ion abundance was less than 10% of the total ion abundance. Typical CID energies for doubly-charged cross-linked peptide ions ranged from 1.08 to 1.24 V (~30% normalized collision energy), and 0.57 to 0.62 V (~20% normalized collision energy) for the triply-charged species. The precursor ion isolation window was set to 4 *m/z* units in order to retain isotopic profile to aid in determining the charge state of the product ions. For some of the doubly-charged cross-linked peptides, the activation q_z-value was decreased to 0.22 from 0.25 in order to effectively trap the low-mass b_3 fragment ion; the dissociation efficiency and fragment ion abundances were not significantly affected by this change. All collision-induced dissociation experiments were collected in triplicate.

3.3.4 Data Analysis

Relative product ion abundances were calculated by dividing each product ion peak area by the total fragment ion abundance. Fragment ions were grouped into different product ion types: y-ions, b and a-ions, cross-link amide bond cleavage products, lysine immonium ions, internal ions, other double cleavage products (b/b, b/y, and y/y), and specific cross-linker cleavage products (e.g., dissociation of the C7–C8

bond of DST). Peaks were defined as having a minimum relative intensity of 1% and a minimum area of 0.1% of the total area in the spectrum. Water and ammonia losses from each product ion type were included in the corresponding base group (e.g., peak area of a $y_n - NH_3$ ion were included in the y-ion group). Neutral losses including water, ammonia, and CO_2 from the precursor ion were excluded from the total fragment ion abundance for simplicity. To determine the effect of Asp and Pro residues in regards to cleavage at the site of cross-linking, K4, the directionality of cleavage bias to the lysine residue was calculated for both the cross-linked peptides and the unmodified species using a method previously suggested by Tabb et al.[28] The C-terminal cleavage bias was determined by taking the ratio of the difference in C-terminal and N-terminal fragment ions, relative to the lysine residue, to the sum of these fragment ion peak areas. For example, the y-ion C-terminal bias was calculated as follows:

$$C_y = \frac{\left(A_{y5\alpha} + A_{y5\beta}\right) - \left(A_{y6\alpha} + A_{y6\beta}\right)}{\left(A_{y5\alpha} + A_{y5\beta}\right) + \left(A_{y6\alpha} + A_{y6\beta}\right)}$$

Equation 3.1

where A_i is the peak area of the respective y-ions; the y_6 ions are products of cleavage N-terminal to the cross-linked lysine, and the y_5 ions are a result of C-terminal cleavage for the nine-residue peptides analyzed in this study. The α and β subscripts refer to cleavage of the α and β peptides, respectively, and are explained in more detail in the results and discussion. A positive value indicates a fragmentation bias C-terminally to the lysine residue, whereas a negative value signifies an N-terminal bias. Similarly, for the b-ions, the cleavage bias was calculated using the following formula:

$$C_b = \frac{\left(A_{b4\alpha} + A_{b4\beta}\right) - \left(A_{b3\alpha} + A_{b3\beta}\right)}{\left(A_{b4\alpha} + A_{b4\beta}\right) + \left(A_{b3\alpha} + A_{b3\beta}\right)}$$

Equation 3.2

where the b_4 ions are the C-terminal cleavage products and the b_3 ions are the N-terminal fragments.

DSS

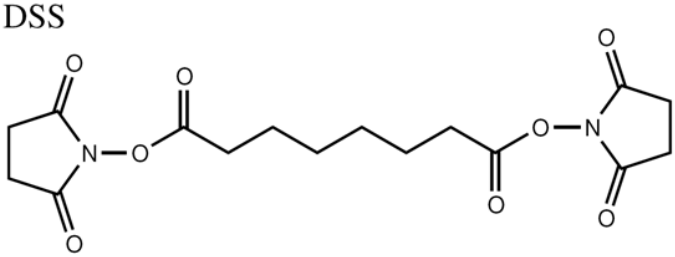

DST

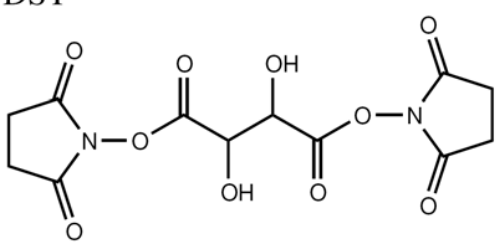

Scheme 1. Chemical Structures of DSS and DST cross-linkers

3.4 RESULTS AND DISCUSSION

The dissociation of cross-linked peptides containing either a proline or an aspartic acid residue was investigated to determine if these species follow similar fragmentation pathways as unmodified peptides. Poly-alanine sequences were used as "filler" residues to minimize competing fragmentation pathways. The peptides were cross-linked with either DSS or DST (**Scheme 3.1**), two widely used cross-linkers which react with primary amines such as free N-termini or the ε-amine of lysine residues. Since the N-termini of these peptides were acetylated, it can be assumed that the site of cross-linking is between K4 of each peptide. A proline or aspartic acid residue was positioned on either the C- or N-terminal side of the cross-linked lysine to determine whether the cross-

link influenced the dissociation trends of the peptides containing either of these two residues. The resulting doubly-charged cross-linked peptides are assumed to have both protons sequestered on the C-terminal arginine residues,[30] whereas the triply-charged species possess a mobile proton. The cross-linked peptides in both the 2+ and 3+ charge states were analyzed by CID to compare the effects of the proline or aspartic acid residues in different charge states. The product ions formed were labeled according to the nomenclature suggested by Schilling et al.[20] and Gaucher et al.[23] In brief, the two intermolecularly cross-linked peptides are labeled α and β, referring to the first and second peptide listed, respectively. Cleavage along the backbone of the α peptide yielding a b-ion is labeled as $b_{n\alpha}$, and similar notation is used other fragment ion types, as well as for the β peptide. Product ions of both peptides cross-linked together are labeled with the fragmentation nomenclature for each cleavage (e.g., $b_{4\alpha}y_{7\beta}$). Lysine immonium ions which maintain the cross-link to the other peptide are labeled as $K^{L\alpha}$, where L represents the cross-linker molecules (e.g., DSS or DST) and α is the other peptide. Due to the repeating alanine sequences of the peptides studied, certain fragment ions cannot be specifically identified as either cleavage of the α peptide or the β peptide as the products are isobars, and are labeled with subscript α/β to represent such cases.

3.4.1 Dissociation of DSS-Cross-linked Peptides

Representative CID spectra of the homo-intermolecularly DSS-cross-linked peptides are shown in Figure 1. For the control cross-linked peptide, [Ac-AAAKAAAAR + DSS + Ac-AAAKAAAAR + 2H]$^{2+}$, a series of singly charged non-cross-linked y-ions were observed in increasing abundance as the site of cleavage moves closer to the cross-linked lysine residue (i.e., $y_{5\alpha} > y_{4\alpha} > y_{3\alpha}$) (**Figure 3.1a**). Similar to this y-ion series, the abundances of singly charged cross-linked b-ions increased as the

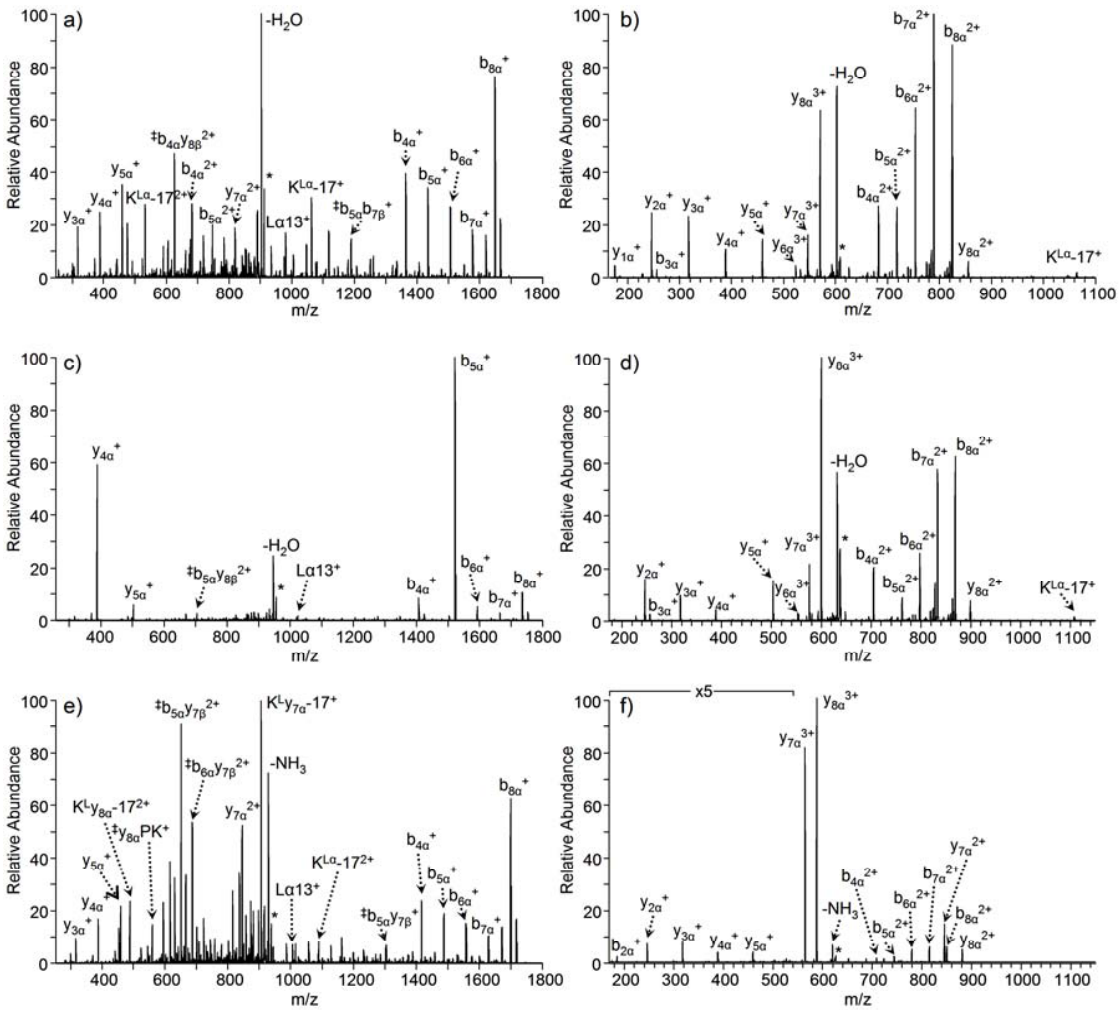

Figure 3.1 CID spectra of DSS intermolecularly cross-linked peptides. Precursor ions were (a) [**AKA** + **AKA** + DSS + 2H]$^{2+}$, (b) [**AKA** + **AKA** + DSS + 3H]$^{3+}$, (c) [**AKD** + **AKD** + DSS + 2H]$^{2+}$, (d) [**AKD** + **AKD** + DSS + 3H]$^{3+}$, (e) [**PKA** + **PKA** + DSS + 2H]$^{2+}$, and (f) [**PKA** + **PKA** + DSS + 3H]$^{3+}$. An asterisk (*) is used to signify the precursor ion. Several double cleavage product ions could not be uniquely identified due to isobars inherent to the peptide sequences and are labeled with one possible identity preceded by ‡.

amide bond cleavage site moved towards K4, with the exception of the $b_{8\alpha}$ fragment ion which was observed as the most abundant b-ion. Without the mobile proton several double cleavage products, such as $b_{4\alpha}y_{8\beta}$ and $b_{5\alpha}b_{7\beta}$, were also formed at similar abundances to the single cleavage fragment ions. Cross-linked lysine immonium ions

were detected after the loss of neutral ammonia, as had previously been observed by Gaucher et al.,[23] and cleavage of the cross-link amide also occurred, yielding the Lα13 ion of *m/z* 980.5. Dissociation of the triply-charged species yielded a more easily interpretable product ion spectrum in which greater than 95% of the fragment ions were single cleavage b- and y-type ions (**Figure 3.1b**). A full series of y-ions and b-ions were observed, both modified ($y_{6\alpha}$ – $y_{8\alpha}$ and $b_{4\alpha}$ – $b_{8\alpha}$) and non-cross-linked ($y_{1\alpha}$ – $y_{5\alpha}$ and $b_{2\alpha}$ – $b_{3\alpha}$), but the relative abundances of these fragment ions did not follow any strict trend. Triply-charged cross-linked y-ions were observed and the cross-linked b-ions were also detected in the higher, 2+, charge state when compared to the dissociation of the analogous doubly-charged precursor ions. In general, for both the b- and y-ions, as the cleavage site moved further away from the cross-link, the fragment ion abundance increased. At a much lower abundance, the $K^{L\alpha}$-17 product ion was also detected.

CID of the homo-intermolecularly DSS-cross-linked Ac-AAAKDAAAR peptide yielded very few sequence ions for the doubly-protonated precursor ion, as shown in **Figure 3.1c**. With both protons sequestered on the C-terminal arginine residues, aspartic acid directed fragmentation dominates and the two products of cleavage C-terminal to D5 are observed at a high abundance – $y_{4\alpha}$ and $b_{5\alpha}$. The other three cross-linked b-ions are also detected, but at a much lower abundance. Only one other y-ion is observed in the product ion spectrum. Cleavage N-terminally to the aspartic acid residue yielded the product ions $y_{5\alpha}$ and $b_{4\alpha}$, but at a much lower abundance. The triply-charged precursor ion possesses a mobile proton, and dissociation of this species is not dominated by a single pathway; rather, a full series of b- and y-ions were seen limited only by the low-mass cut-off inherent to resonant excitation in ion traps (**Figure 3.1d**). Unlike the CID spectrum for the Ac-AAAKAAAAR cross-linked peptide, no distinct trends were observed regarding fragment ion abundances. Upon CID, the cross-linked [Ac-

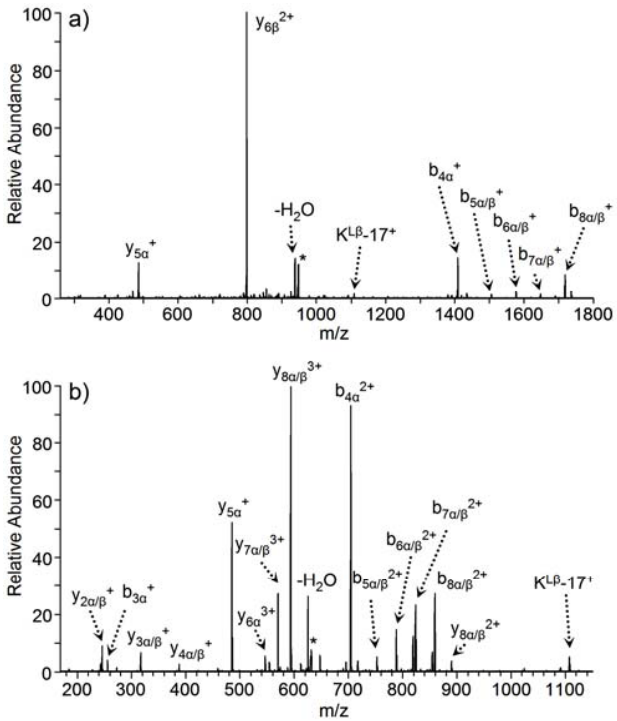

Figure 3.2 CID spectra of hetero-DSS-intermolecularly cross-linked peptide **AKP** + DSS + **DKA** in the (**a**) 2+ charge state and (**b**) 3+ charge state. **AKP** is referred to as the α peptide and **DKA** as the β peptide; α/β nomenclature is used to signify that cleavage could have occurred on either peptide, as the two possible fragment ions are isobaric. An asterisk (*) is used to signify the precursor ion.

AAPKAAAAR + DSS + Ac-AAPKAAAAR + 2H]$^{2+}$ peptide yielded an abundance of double cleavage products as evident in **Figure 3.1e**. Cleavage of the amide bond N-terminal to the proline residue, P3, dominated the dissociation of this ion producing cross-linked internal ions ($y_{7\alpha}$PKA), lysine immonium ions linked to the $y_{7\alpha}$ ion ($K^{L}y_{7\alpha}$ – 17), and a series of $b_{n\alpha}y_{7\beta}$ fragment ions. Most of these fragment ions are redundant as they do not provide additional information to identify the location of the cross-link nor sequence the constituent peptides. Dissociation of the triply-charged species was similarly dominated by cleavage N-terminal to the proline residue yielding the $y_{7\alpha}$ fragment; in addition a high abundance of the $y_{8\alpha}$ product was observed as shown in

Figure 3.1f. No cleavage between P3 and K4 was detected for the DSS cross-linked Ac-AAPKAAAAR, regardless of precursor ion charge state.

The hetero-cross-linked peptides containing one proline and a single aspartic acid residue exhibited dissociation that followed both Asp- and Pro-directed pathways. CID mass spectra of these doubly-charged DSS-cross-linked species were typically dominated by fragmentation C-terminal to the aspartic acid residue and to a lesser degree, N-terminal to the proline. A representative CID spectrum is shown in **Figure 3.2a** for [Ac-AAAKPAAAR + DSS + Ac-AADKAAAAR + 2H]$^{2+}$. Cleavage of the amide bond between D3 and K4 of the β peptide (Ac-AADKAAAAR), thus resulting in the $y_{6\beta}^{2+}$ ion, is the most abundant pathway with the two proline-directed fragments being the next two most abundant ions, $y_{5\alpha}^{+}$ and $b_{4\alpha}^{+}$. Also present, but to a much lesser degree, are the other cross-linked b-ions as well as a lysine immonium fragment cross-linked to Ac-AADKAAAAR. It should be noted that due to the alanine sequences present in both peptides which create isobaric species, certain fragment ions could not be identified conclusively as to whether the bond cleavage occurred within the α or the β peptide (e.g.., $b_{5\alpha}$ has the same mass as the $b_{5\beta}$ fragment and as such is labeled as $b_{5\alpha/\beta}$ in **Figure 3.2a**). Dissociation of the triply-charged DSS cross-linked peptide results in an almost complete series of b- and y-type fragment ions, as evident in **Figure 3.2a**. With the addition of the mobile proton, dissociation of the β peptide C-terminal to the Asp residue does not dominate the spectrum, and is in fact one of few sequence fragment ions not observed. Proline-directed fragmentation still yields two of the most abundant product ions, $b_{4\alpha}^{2+}$ and $y_{5\alpha}^{+}$. This data suggests that in order to obtain fragmentation information essential to locate the site of cross-linking as well as to sequence the two linked peptides, dissociation of more highly charged cross-linked peptides would be beneficial.

3.4.2 Dissociation of DST-Cross-linked Peptides

The DST-cross-linked peptides exhibited similar dissociation pathways as the DSS-linked species, as shown in **Figure 3.3**, with one notable exception in that cleavage of the C7–C8 bond of the DST cross-linker was observed for the doubly charged precursor ions (described later in this section). The doubly-charged DST homo-intermolecularly cross-linked Ac-AADKAAAAR peptide predominantly dissociated via Asp-directed fragmentation, C-terminal to D3, as seen in **Figure 3.3a**, yielding the $y_{6\alpha}^{2+}$ ion. At much lower abundances, double cleavage products, including ones involving cleavage C-terminal to the aspartic residues of both peptides ($y_{6\alpha}y_{6\beta}$) and cross-linked b-ions were observed. CID of the triply charged species, presumed to have a mobile proton, yielded a full series of b- and y-type fragment ions, again only limited by the low-mass cut-off (**Figure 3.3b**). With the mobile proton, the Asp-directed fragmentation which dominated the CID mass spectrum of the doubly charged cross-linked peptide was circumvented. Fragment ions unique to cross-linked peptides, including products from the dissociation of the cross-link amide bond (Lα9 and Lα5), and cross-linked lysine immonium ions ($K^{L\alpha}$ and $K^{L\alpha}$-17) were also detected. For all of the DST-cross-linked peptides analyzed, fragmentation of the C7–C8 bond of the DST cross-linker occurred, as illustrated in **Scheme 3.2**. Dissociation of this bond yields product ions corresponding to +56 and +58 Da adducts of the unmodified peptides, and they are labeled as Lα7 and Lβ7 ions in **Figure 3.3**. (It should be noted that there is a 1 *m/z* unit difference between the precursor ion and Lα7 fragment ions in **Figures 3.3a – 3.3d**.) For the second proline-containing peptide analyzed in this study, Ac-AAAKPAAAR, dissociation of the doubly-charged DST-cross-linked peptide predominantly produced three fragment ions, Lα7 and the two fragments corresponding to proline directed dissociation, $y_{5\alpha}$ and $b_{4\alpha}$ (**Figure 3.3c**). The triply-charged Ac-AAAKPAAAAR + DST + Ac-AAAKPAAAR ion also

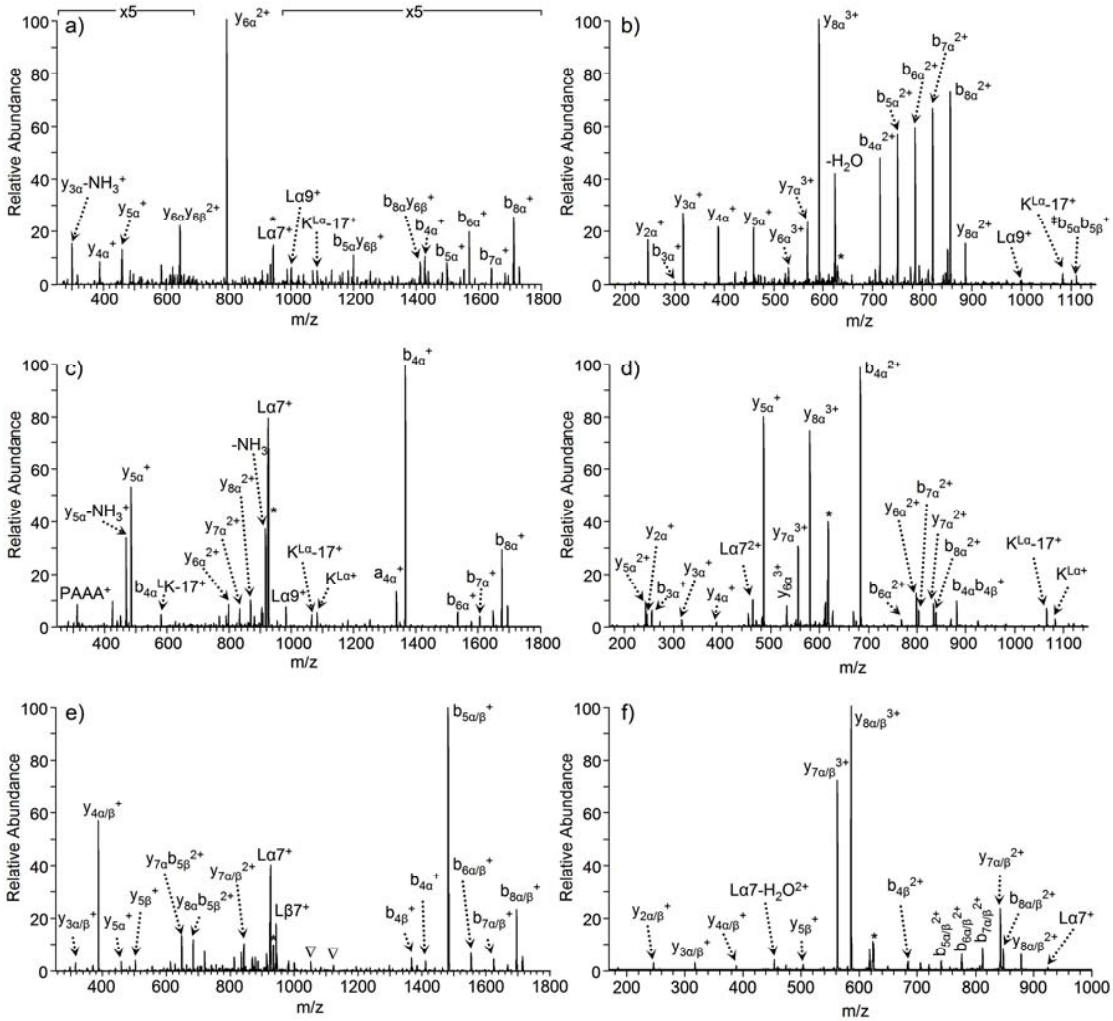

Figure 3.3 CID spectra of DST intermolecularly cross-linked peptides. Precursor ions were (a) [**DKA** + **DKA** + DST + 2H]$^{2+}$, (b) [**DKA** + **DKA** + DST + 3H]$^{3+}$, (c) [**AKP** + **AKP** + DST + 2H]$^{2+}$, (d) [**AKP** + **AKP** + DST + 3H]$^{3+}$, (e) [**PKA** + **AKD** + DST + 2H]$^{2+}$, and (f) [**PKA** + **AKD** + DST + 3H]$^{3+}$. The first peptide listed is referred to as the α peptide and the second peptide as β; α/β nomenclature is used to signify that cleavage could have occurred on either peptide. Internal ions that could not be conclusively identified due to isobaric species are labeled with ∇. An asterisk (*) is used to signify the precursor ion.

showed preferential cleavage between K4 and P5, while the other b- and y-type ions had abundances similar to that observed for the 2+ charged precursor (**Figure 3.3d**).

Regardless of the charge state, proline-directed fragmentation dominates the CID spectrum of the Ac-AAAKPAAAR cross-linked peptides.

Collisional-induced dissociation of [Ac-AAPKAAAAR + DST + Ac-AAAKDAAAR + 2H]$^{2+}$ more clearly shows fragmentation of the C7–C8 bond of DST, producing the corresponding Lα7 and Lβ7 ions, as shown in **Figure 3.3e**. Aspartic acid-directed fragmentation dominates the product ion spectrum yielding $y_{4\alpha/\beta}^{+}$ and $b_{5\alpha/\beta}^{+}$, and numerous proline-directed fragments were detected between *m/z* 600 and 1300, including internal ions of the form PKA_n cross-linked to $b_{n\beta}$ ions (labeled with ∇) and $y_{7\alpha}$ containing fragments. The influences of both Asp and Pro were observed by the formation of certain product ions, including $y_{7\alpha}b_{5\beta}^{2+}$, analogous to those observed for the DSS-cross-linked species. The triply-charged DST hetero-cross-linked peptide yielded a series of doubly-charged cross-linked b-ions, a series of cross-linked y-ions, and a series of uncross-linked y-ions for both peptides, as evident in **Figure 3.3f**. The aspartic acid effects were not observed when the precursor ion had a mobile proton, but fragment ions with N-terminal prolines were detected at high abundances, in particular $y_{7\alpha/\beta}$. The DST specific cleavage of the C7–C8 bond was also observed, but at lower abundances compared to that observed for the analogous doubly-charged precursor ion. Dissociation of the amide bond N-terminal to the cross-linked lysine for either constituent peptide, Ac-AAPKAAAAR or Ac-AAAKDAAAR, to yield the expected $y_{6\alpha}$ or $y_{6\beta}$ fragments did not occur, suggesting a cleavage bias due to the cross-link.

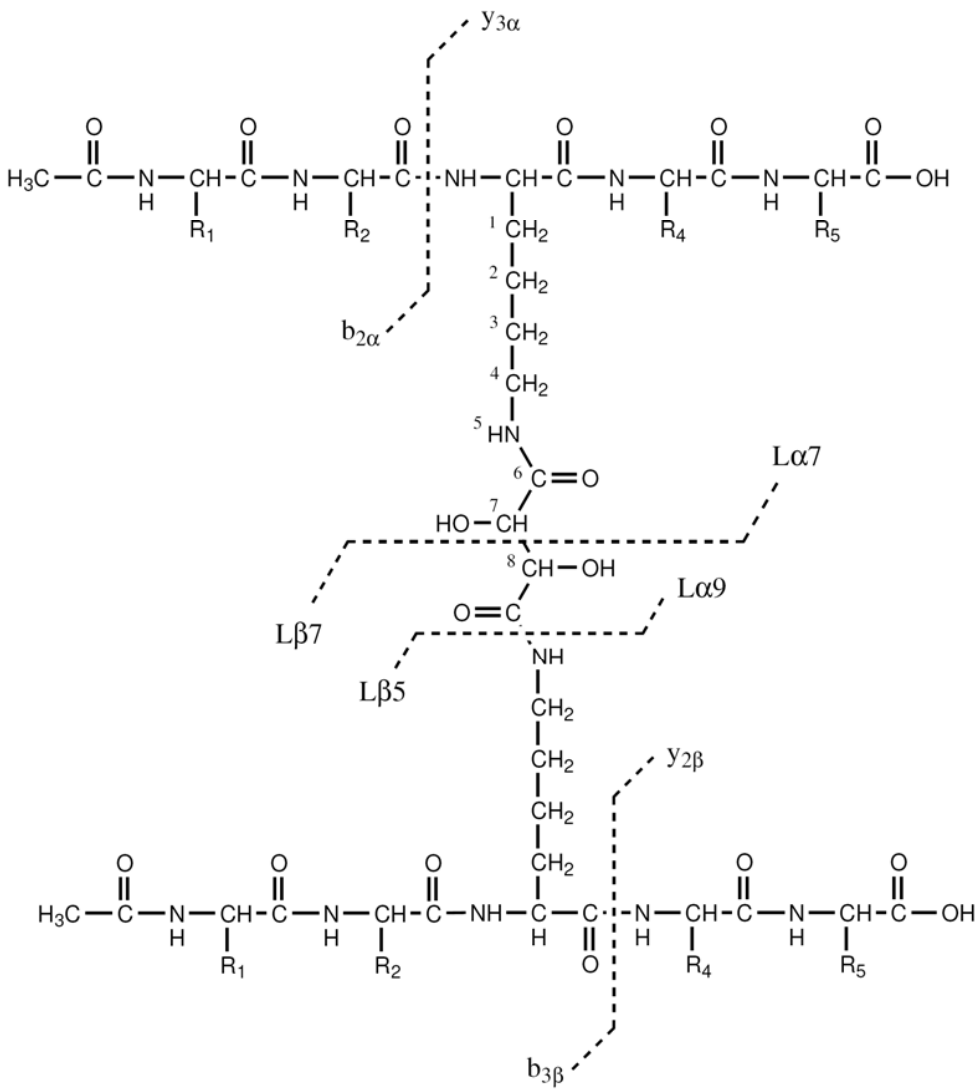

Scheme 3.2 Diagram of observed bond cleavages of DST-cross-linked peptides.

3.4.3 Fragment Ion Type Abundances

The relative abundance of each fragment ion type was calculated in order to shed light on the general trends of the dissociation of these proline- and aspartic acid-containing cross-linked peptides. As shown in **Figure 3.4a** for the doubly-charged DSS-cross-linked peptides, a-, b-, and y-type fragment ions, on average, accounted for

approximately 75% of the total product ion abundance. For aspartic acid-containing cross-linked peptides, this abundance increased to over 85% as Asp-directed fragmentation of these doubly-charged precursor ions, in which both protons are sequestered, produced predominantly single cleavage b- and y-type ions. Multiple cleavage fragments, including internal ions, b/b, b/y, y/y, and linked lysine immonium ions, accounted for 19% of all the fragment ions. For the doubly charged DSS-cross-linked peptides, two types of fragment ions unique to cross-linked peptides, those involving cleavage of the cross-link amide bond and cross-linked lysine immonium ions, accounted for 2.5% and approximately 6% of the product ion abundance, respectively. Cross-linked peptides containing Ac-AAPKAAAAR yielded a high abundance of internal ions; approximately 11% of all the fragments observed were internal ions, compared to 2% for the non-Ac-AAPKAAAAR cross-linked peptides. A majority of these internal ions had the proline residue at the N-terminus. Dissociation of the various triply-charged DSS-linked peptides, all of which possess a mobile proton, yielded a much higher abundance of single-cleavage a-, b-, and y-type fragment ions – on average greater than 95% relative abundance, as shown in **Figure 3.4b**. The total abundance of the cross-linked lysine immonium ions was less than 1%, and cleavage of the cross-link amide bond was observed at less than 0.1% abundance. For the triply-charged aspartic acid- or the proline-containing cross-linked peptides, there were no major differences in fragment ion abundances except that y-ions were observed at over 76% relative abundance for the Ac-AAPKAAAAR cross-linked species, due to preferential cleavage N-terminal to the proline residue yielding an unusually high abundance of $y_{7\alpha}$ fragments. No significant differences in the multiple cleavage products were detected between the various cross-linked peptides.

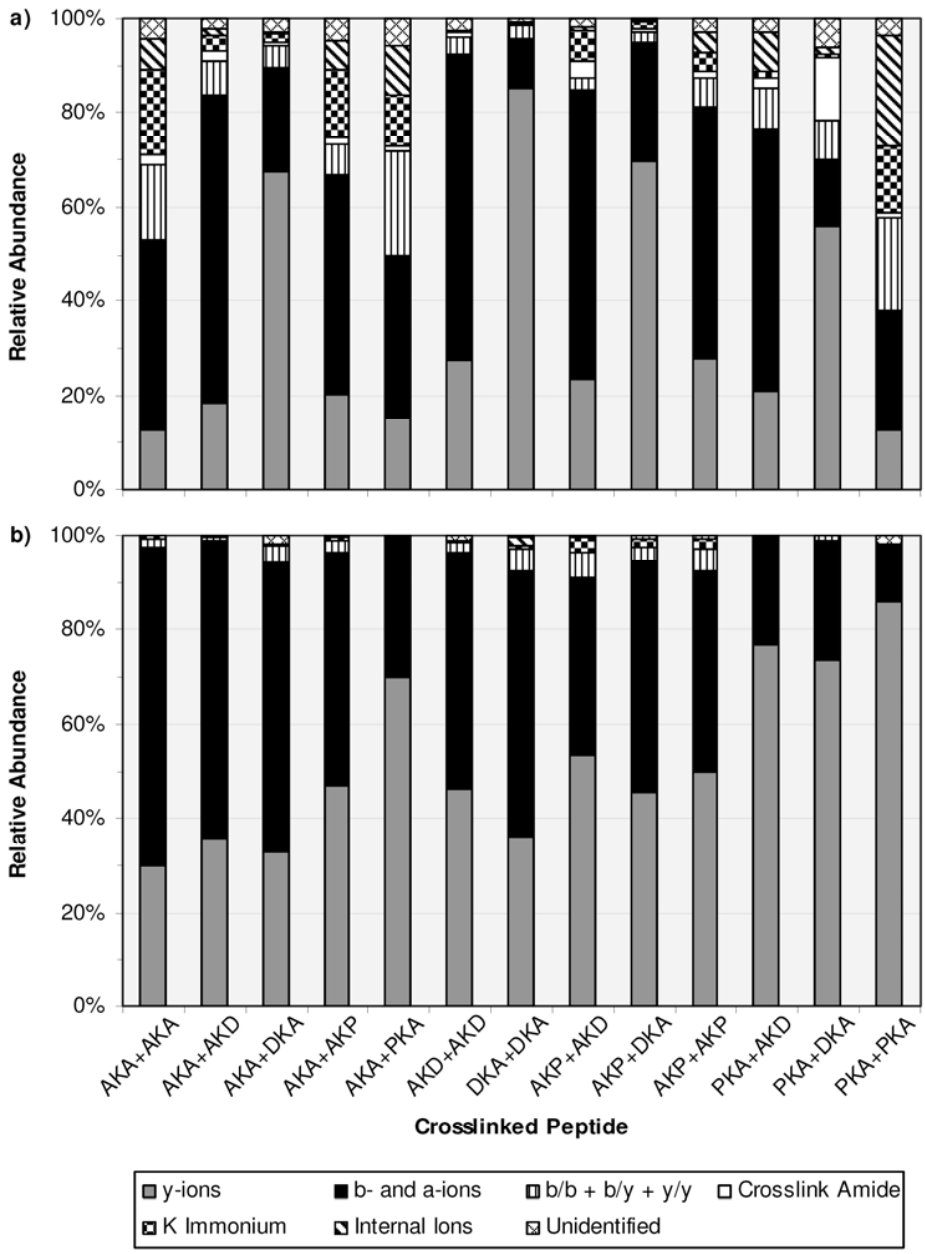

Figure 3.4 Relative fragment ion abundance for the DSS cross-linked peptides in the (a) 2+ charge state and (b) 3+ charge state. Each category represents the abundance of that product ion type relative to the total fragment ion abundance minus neutral losses from the precursor ion. Errors are less than 0.5% relative abundance.

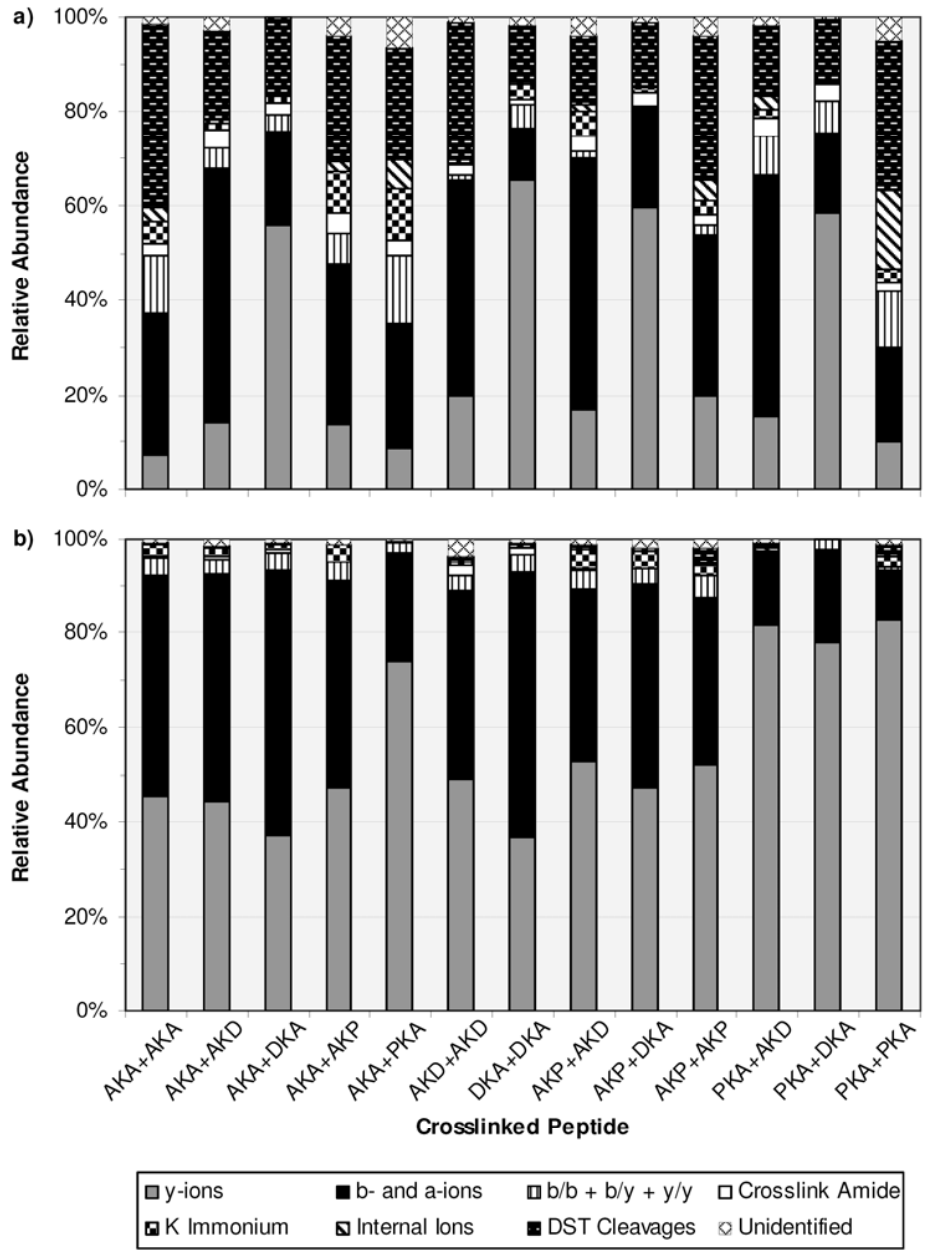

Figure 3.5 Relative fragment ion abundance for the DST cross-linked peptides in the (a) 2+ charge state and (b) 3+ charge state. Each category represents the abundance of that product ion type relative to the total fragment ion abundance minus neutral losses from the precursor ion. Errors are less than 0.5% relative abundance.

The DST-cross-linked peptides, particularly for species without a mobile proton, as noted earlier, exhibited far more unique dissociation pathways compared to the DSS-linked peptides. Fragmentation of the C7–C8 bond of the DST cross-linker occurred for all of these cross-linked peptides in the 2+ charge state, accounting for over 21% of the total fragment ion abundance, as shown in **Figure 3.5a**, and these fragments do not provide any diagnostic information for determining the cross-link location or sequencing the peptide. Similar to the DSS-cross-linked peptides, doubly-charged DST-linked species yielded on average 60% single cleavage b, y, and a-ions, with the remainder accounted for by multiple cleavage products and cross-linker specific product ions. The latter product ions, excluding ones stemming from dissociation of the DST linker at the C7–C8 bond, were observed at approximately 15% relative abundance, similar to that for the DSS-cross-linked species. Various internal ions were also observed at similar abundances for the DST-linked peptides than for the DSS-cross-linked products – 3% relative abundance compared to approximately 5%, respectively. The DST-cross-linked products containing the Ac-AAPKAAAAR peptide did exhibit a higher degree of internal ion formation than the other peptides studied, but the difference was not as pronounced as that for the DSS-cross-linked products. Dissociation of the triply-charged DST-cross-linked peptides, as summarized in **Figure 3.5b**, yielded similar results as the analogous DSS-linked species. Across the series, over 92% of the fragment ion abundance consisted of single bond cleavage a, b, and y-ions. Fragment ions due to cleavage of the DST cross-linker at the C7–C8 bond totaled less than 1% relative abundance, suggesting that this fragmentation pathway is preferred only for precursor ions without a mobile proton. The only modest difference between the fragmentation patterns of the triply charged DSS- and DST-linked peptides was an increased abundance of double cleavage products and cross-linked lysine immonium ions, from 3% to 6%.

The addition of the mobile proton to these DSS- and DST-cross-linked peptides increased the abundance of useful sequence ions, ones which are easily interpretable. Also, aspartic acid-directed fragmentation of the triply-charged ions did not occur, thus yielding a wider array of single cleavage products. Proline-directed fragmentation still dominated the CID spectra of the triply charged cross-linked peptides, however, a full series of b- and y-ions were still observed, with the exception of cleavage C-terminal to proline residues. The degree of multiple-cleavage products, particularly the abundance of internal ions for the proline containing peptides, was greatly reduced for dissociation of the more highly charged cross-linked peptide ions.

3.4.4 Effect of Cross-linkers on Cleavage Bias Adjacent to the Modified Lysine

As evident from the dissociation of the intermolecularly cross-linked peptides, the aspartic acid or proline residue tends to direct peptide fragmentation. One earlier study indicated a qualitative enhancement of cleavage of the amide bond adjacent to the cross-linked lysine for intramolecularly cross-linked peptides, so we aimed to investigate a possible preference for intermolecularly cross-linked species.[23] The directionality bias of cleavage to the cross-linked lysine was determined for both the non-modified peptides (1+ and 2+) and the homo-intermolecularly cross-linked peptides (2+ and 3+) as shown in **Figure 3.6**. A positive C-terminal cleavage bias value indicates that more fragment ions were formed from cleavage of the amide bond C-terminal to the cross-linked lysine, whereas a negative value indicates a bias towards forming product ions from dissociation of the N-terminal amide bond. For species without a mobile proton (e.g., 1+ charge state for unmodified peptides, 2+ charge state for cross-linked peptides), the influences of proline and aspartic acid on y-ion formation were not greatly affected upon cross-linking (**Figure 3.6a**). The y-ion C-terminal bias was only enhanced for the Ac-AAAKPAAAR

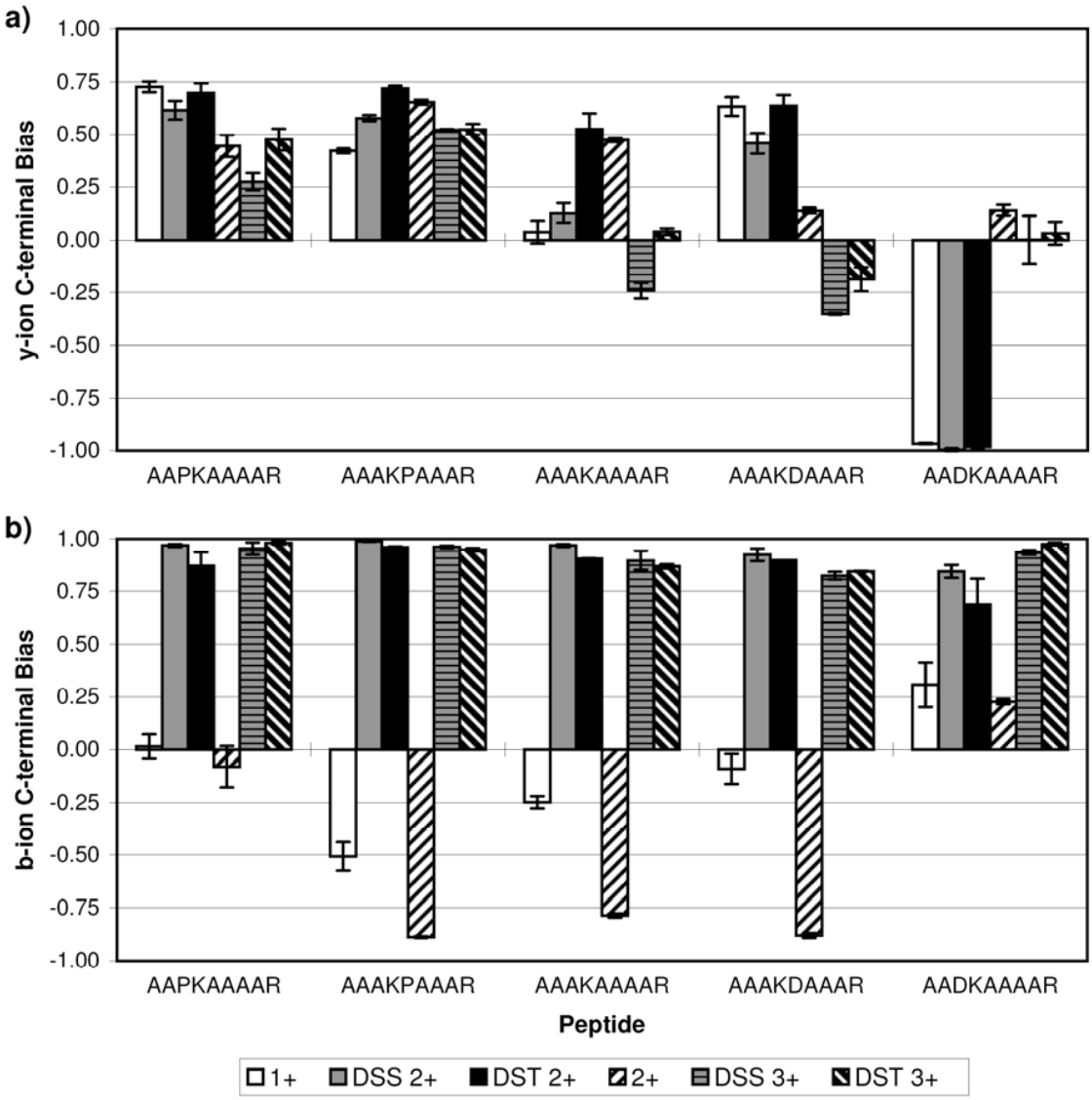

Figure 3.6 The C-terminal cleavage bias relative to the lysine residue, for both the unmodified peptides in the 1+ and 2+ charge state and the homo-intermolecularly cross-linked peptides in the 2+ and 3+ charge state, for (a) y-ions and (b) b-ions.

and Ac-AAAKAAAAR peptides after cross-linking. All of the doubly-charged cross-linked peptides preferentially dissociated via cleavage of the C-terminal amide bond to the lysine residue, except for the homo-intermolecularly cross-linked Ac-AADKAAAAR

peptide; these species fragmented via Asp-direction dissociation C-terminal to D3, or N-terminally to the modified lysine residue. With the addition of a mobile proton, the Asp-containing cross-linked peptides did not exhibit any significant cleavage bias towards the formation of y-ions. The cross-linked peptides with proline residues still displayed signs of a C-terminal fragmentation bias in the 3+ charge state; however, these results can be explained by preferential cleavage N-terminally to proline residues. With the proline residue positioned N-terminally to the lysine (e.g., Ac-AAPKAAAAR), cleavage of the bond between P3 and K4 is suppressed, thus decreasing the $y_{6\alpha}$ product ion abundance relative to $y_{5\alpha}$ fragment ions. For the other proline containing peptide, Ac-AAAKPAAAR, formation of the $y_{5\alpha}$ ion is enhanced relative to $y_{6\alpha}$ due to Pro-directed dissociation between K4 and P5.

Analysis of the b-ions detected showed that the unmodified peptides all preferentially dissociated N-terminally to K4 yielding b_3 ions, as shown in **Figure 3.6b**, except for $[\text{Ac-AADKAAAAR} + \text{H}]^+$ in which no b_3 or b_4 ions were detected (i.e., peak abundance was below the peak threshold). For the doubly-charged unmodified peptides, the N-terminal cleavage bias increased over the singly-charged peptides, with the Ac-AADKAAAAR peptide as the lone exception. This particular unmodified peptide exhibited similar cleavage biases for both b and y-ions. Interestingly, analysis of the b-ions suggests there is a significant C-terminal cleavage bias for all of the cross-linked peptides. The doubly-charged cross-linked peptides have both protons localized on the C-terminal arginines, so one would not expect to detect b_3 ions which do not contain the cross-link or a charge. Cleavage C-terminal to the lysine residue yields a $b_{4\alpha}$ ion which contains the cross-linker as well as the β peptide with the sequestered proton at its C-terminal arginine. A high C-terminal cleavage bias for the formation of b-ions also was observed for all of the triply-charged cross-linked peptides. Even with the additional

mobile proton, $b_{3\alpha}$ ions were not detected at high abundances in the CID spectra. Having a proline residue N-terminal to the lysine reduces the abundance of N-terminal fragment ions (e.g., b_3), while a proline C-terminal enhances the formation of b_4 ions. In the 3+ charge state, the aspartic acid effect does not dominate the peptide fragmentation pathways, and any cleavage bias due to the aspartic acid residues is eliminated. However, the high C-terminal b-ion abundance relative to N-terminal fragments for the Asp-containing cross-linked peptides, as well as the Ac-AAAKAAAAR peptide, suggests that the presence of the cross-link affects the dissociation of the amide bonds adjacent to the modified lysine.

The observed C-terminal cleavage bias could be due to the composition and position of the amino acids residues chosen for this study. Cleavage C-terminal to the cross-linked lysine yields the $y_{5\alpha}$ fragment ion (XAAAR) and a $b_{4\alpha}$ fragment ion (Ac-AAXK + cross-linker + β peptide), while N-terminal cleavage produces the $b_{3\alpha}$ fragment (Ac-AAX) and the corresponding $y_{6\alpha}$ fragment (KXAAAR + cross-linker + β peptide). The b_3 fragment is unlikely to carry a charge without a basic residue present and thus would not be observed. The $b_{4\alpha}$, $y_{6\alpha}$, and $y_{5\alpha}$ fragments would all be detected as ions due to the presence of at least one C-terminal arginine residue. The location of the arginines may explain the greater C-terminal cleavage bias observed for the b-ions compared to y-ion formation, particularly for the triply-charged precursor ions without a proline residue. However, in most protein cross-linking experiments, cross-linked peptides with C-terminal arginines will be produced after enzymatic digestions with trypsin, and the trends observed in this study should be considered in sequence identification software.

For the unmodified peptides, the mobile proton is assumed to be located on the second most basic site, the ε-amine group of the lysine residue. This proton, when mobilized upon ion activation, could easily promote charge-directed fragmentation at

either amide bond adjacent to the lysine residue. However, after the cross-linking reaction which produces an amide bond involving the amino group of the lysine side chain, the third proton of the cross-linked peptide is likely not as localized as that of the mobile proton for the unmodified peptides. Ongoing work in our lab examining infrared multiphoton dissociation of cross-linked peptides has shown enhanced photodissociation efficiencies for the triply-charged cross-linked peptides compared to the doubly-charged unmodified peptides, suggesting a lower activation energy for the less basic cross-linked species. The gas-phase basicity differences and probable localization of protons between cross-linked and non-cross-linked peptides may help explain this enhanced C-terminal cleavage bias to the linked lysine residues.

3.4.5 Dissociation of Other Cross-linked Peptides

The peptides α-MSH (Ac-SYSMEHFRWGKPV-NH_2, α peptide) and neurotensin (Pyr-LYENKPRRPYIL, β peptide) were cross-linked by either DSS or DST to determine whether the same dissociation trends are observed for cross-linked peptides with more random sequences. Since the two cross-linkers react with primary amines, it was assumed that the cross-link was formed between K11 of α-MSH and K6 of neurotensin, and the product ion spectra of the DST- cross-linked species support this assumption (**Figure 3.7**). Dissociation of the triply-charged precursor ion was dominated by cleavage C-terminal to the acidic residues, E5 of α-MSH and E4 of neurotensin, yielding $y_{8\alpha}^{3+}$ (*m/z* 937.8) and $y_{9\beta}^{3+}$ (*m/z* 978.7) as the three protons are localized by the three total arginine residues present in the two peptides (**Figure 3.7a**). To a lesser degree proline-directed cleavages were observed, producing $b_{11\alpha}^{3+}$ (*m/z* 1080.0) and $b_{9\beta}^{3+}$ (*m/z* 982.7) Without a mobile proton, dissociation of the C7–C8 bond of the DST cross-link was observed producing $L\beta7^{2+}$ and the corresponding $L\alpha7^{+}$ product ions of *m/z* 865.6 and

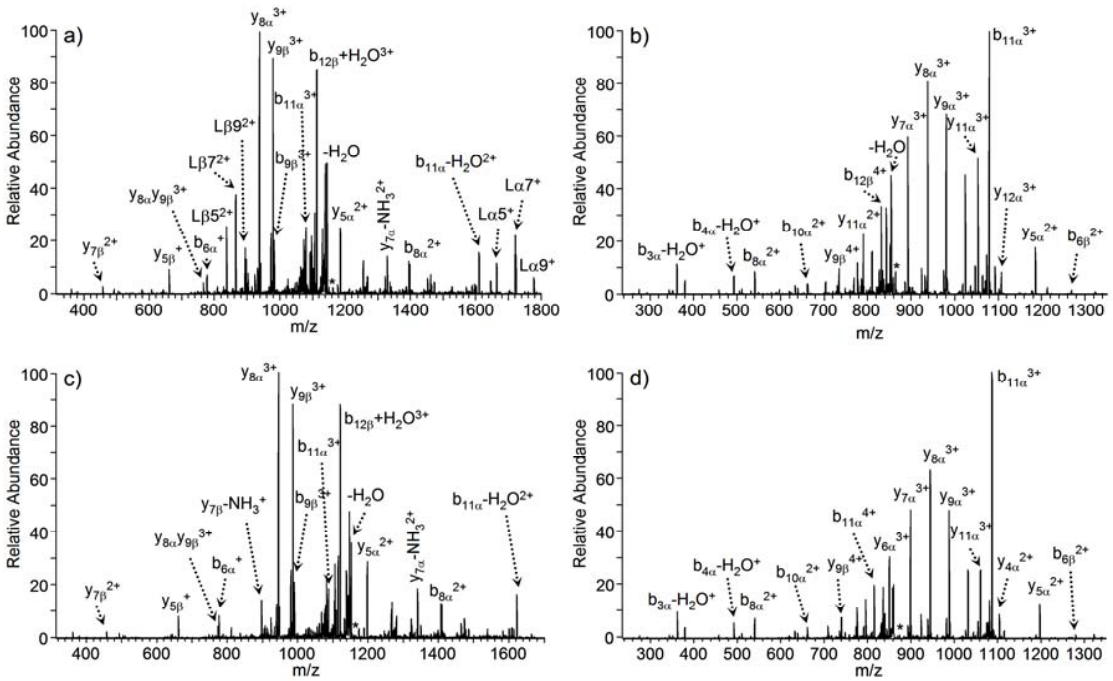

Figure 3.7 CID spectra of α-MSH cross-linked to neurotensin by DST in the (a) 3+ charge state and (b) 4+ charge state. Product ion spectra of α-MSH cross-linked to neurotensin by DSS in the (c) 3+ charge state and (d) 4+ charge state. α-MSH (Ac-SYSMEHFRWGKPV-NH_2) is referred to as the α peptide and neurotensin (Pyr-LYENKPRRPYIL) as the β peptide; the cross-link is between K11 of α-MSH and K6 of neurotensin. An asterisk (*) is used to signify the precursor ion.

1721.9, respectively. Other cross-linker specific fragment ions were detected including cleavage of the cross-link amide bond yielding the unmodified constituent peptides ($L\beta5^{2+}$ and $L\alpha5^{+}$), and the constituent peptides modified by the DST cross-linker ($L\beta9^{2+}$ and $L\alpha9^{+}$). Interestingly, cross-linked lysine immonium ions were observed at less than 0.5% relative abundance for the triply-charged precursor ion, compared to approximately 5% for the model cross-linked peptide species without a mobile proton. CID of the quadruply-charged precursor ion $[\alpha\text{-MSH} + \text{DST} + \text{neurotensin} + 4H]^{4+}$ yielded a full series of cross-linked y_α ions ($y_{3\alpha} - y_{12\alpha}$), and a full series of uncross-linked b_α-ions ($b_{2\alpha}$

– $b_{10\alpha}$), as shown in **Figure 3.7b**. With an additional mobile proton, fragment ions stemming from the cleavage of amide bonds C-terminal to acidic residues were not observed. Proline-directed fragmentation yielded the most abundant product ion $b_{11\alpha}^{3+}$. Similar to the CID results of the model cross-linked peptides, cross-linker specific product ions were not observed at any significant abundance; instead b- and y-type fragment ions dominated the entire CID spectrum. Most of the product ions were a result of backbone cleavage along α-MSH, and not neurotensin, with the exception of amino acid specific fragmentation.

The DSS-cross-linked species in the 3+ charge state produced similar fragment ions as the DST-cross-linked analog (**Figure 3.7c**). Ions resulting from cleavage C-terminal to the two glutamic acid residues dominated the CID spectrum ($y_{8\alpha}^{3+}$ and $y_{9\beta}^{3+}$), and proline-directed products were also abundant ($b_{11\alpha}^{3+}$ and $b_{9\beta}^{3+}$). Cross-linker specific product ions were not observed for the DSS-cross-linked peptide at similar high abundances as the DST-cross-linked species without a mobile proton. Such product ions accounted for less than 1% of the total fragment ion abundance. Collision-induced dissociation of the quadruply-charged DSS-cross-linked peptide yielded higher sequence coverage, specifically a series of y-ions of the α-MSH peptide cross-linked to intact neurotensin (**Figure 3.7d**). Acidic residue directed cleavages were not observed for the precursor ion possessing a mobile proton; dissociation N-terminal to proline was still dominant yielding the $b_{11\alpha}$ ions. No cross-linker specific product ions, including cross-linked lysine immonium ions, or fragments from the cleavage of the cross-link amide bonds were observed for this cross-linked peptide ion.

3.5 CONCLUSIONS

Intermolecularly cross-linked peptides, in general, dissociate via similar pathways to that of unmodified peptides. For DSS- and DST-cross-linked peptide ions in which the protons were sequestered, aspartic acid-directed fragmentation dominated the product ion spectra, more so than fragmentation N-terminally to proline residues among the two linked peptides. These doubly-charged cross-linked peptides yielded a high abundance of multiple cleavage products, including b/b, b/y, y/y, cross-linked lysine immonium ions, and internal ions, which complicated the interpretation of the CID spectra, but provided complementary sequence information. In particular, for cross-linked peptides with a proline N-terminal to the linked lysine residue (i.e., a PK sequence), a high degree of cross-linked internal ions were formed. The DST-cross-linked peptide ions without a mobile proton dissociated in a unique manner compared to the analogous DSS species, in which cleavage of the C7–C8 bond of the DST linker molecule was observed regardless of amino acid content.

Dissociation of the cross-linked peptides possessing a mobile proton resulted in almost full sequence coverage (b- and y-type ions) of both peptides, allowing one to determine the site of cross-linking, as cleavage C-terminal to Asp residues was observed to a much lesser degree. Dissociation N-terminal to the proline residues was still prevalent for the more highly charged cross-linked peptides. Products unique to cross-linked peptides, such as cross-linked lysine immonium ions, multiple cleavage fragments, and cleavage of the cross-linkers, including both the cross-linker amide bond and within the DST linker, accounted for less than 10% of the fragment ion abundance for the triply-charged species, compared to upwards of 50% of the fragment ions for precursor ion without a mobile proton. In addition, the cross-linked peptides exhibited a tendency to preferentially cleave C-terminally to the modified lysine residue, particularly in the

formation of b-ions, compared to the unmodified peptides. Unless an aspartic acid residue is positioned N-terminally to the cross-linked lysine and the precursor ion does not have a mobile proton, this C-terminal cleavage bias was observed for all of the cross-linked peptides regardless of the position of proline and aspartic acid residues.

By incorporating these dissociation trends noted for cross-linked peptides into computer algorithms, one would expect the confidence in the assignment of product ions and subsequent peptide identification to increase. In the presence of a mobile proton the intermolecularly cross-linked peptide tends to behave as two individual peptides, each modified at the lysine residue by the cross-linker and the other peptide. However, as evident in dissociation of the cross-linked model peptides without a mobile proton, several unique types of fragment ions were identified. Many commercial cross-linkers are primary amine specific, and after cross-linking, in which an amide bond is formed, the overall gas-phase basicity of the peptide or protein is reduced, thus decreasing the ionization efficiency of more highly-charged cross-linked peptides. Particularly for tryptic peptides in which basic residues are not conserved, cross-linked peptides without a mobile proton dissociate via several pathways yielding multiple cleavage product ions (e.g., $b_{\alpha}y_{\beta}$), cross-linked lysine immonium ions, and fragments from the dissociation of the cross-link amide bond or of the cross-linker (e.g., Lα7 and Lβ7 fragments of DST cross-linked peptides), as well as the typical b- and y-type product ions. Computer algorithms which do not currently account for these product ion types may lead to incorrect peptide and protein identifications. Also, these cross-linker specific product ion types can provide not only complementary but also confirmatory sequence information which can aid in identifying the location of the chemical cross-link.

3.6 REFERENCES

(1) Heck, A. J. R.; van den Heuvel, R. H. H. *Mass Spectrometry Reviews* **2004**, *23*, 368-389.

(2) Juan, H.-F.; Liu, H.-L.; Hsu, J.-P. *Current Proteomics* **2004**, *1*, 183-197.

(3) Borch, J.; Jorgensen, T. J. D.; Roepstorff, P. *Current Opinion in Chemical Biology* **2005**, *9*, 509-516.

(4) Sinz, A. *Journal of Mass Spectrometry* **2003**, *38*, 1225-1237.

(5) Back, J. W.; De Jong, L.; Muijsers, A. O.; De Koster, C. G. *Journal of Molecular Biology* **2003**, *331*, 303-313.

(6) Young, M. M.; Tang, N.; Hempel, J. C.; Oshiro, C. M.; Taylor, E. W.; Kuntz, I. D.; Gibson, B. W.; Dollinger, G. *Proceedings of the National Academy of Sciences of the United States of America* **2000**, *97*, 5802-5806.

(7) Huang, B. X.; Kim, H.-Y.; Dass, C. *Journal of the American Society for Mass Spectrometry* **2004**, *15*, 1237-1247.

(8) Pearson, K. M.; Pannell, L. K.; Fales, H. M. *Rapid Communications in Mass Spectrometry* **2002**, *16*, 149-159.

(9) Lanman, J.; Lam, T. T.; Barnes, S.; Sakalian, M.; Emmett, M. R.; Marshall, A. G.; Prevelige, P. E. *Journal of Molecular Biology* **2003**, *325*, 759-772.

(10) Back, J. W.; Sanz, M. A.; De Jong, L.; De Koning, L. J.; Nijtmans, L. G. J.; De Koster, C. G.; Grivell, L. A.; Van Der Spek, H.; Muijsers, A. O. *Protein Science* **2002**, *11*, 2471-2478.

(11) Chu, F.; Shan, S.-o.; Moustakas, D. T.; Alber, F.; Egea, P. F.; Stroud, R. M.; Walter, P.; Burlingame, A. L. *Proceedings of the National Academy of Sciences of the United States of America* **2004**, *101*, 16454-16459.

(12) Kalkhof, S.; Ihling, C.; Mechtler, K.; Sinz, A. *Analytical Chemistry* **2005**, *77*, 495-503.

(13) Ahrends, R.; Kosinski, J.; Kirsch, D.; Manelyte, L.; Giron-Monzon, L.; Hummerich, L.; Schulz, O.; Spengler, B.; Friedhoff, P. *Nucleic Acids Research* **2006**, *34*, 3169-3180.

(14) Huang, B. X.; Dass, C.; Kim, H.-Y. *Biochemical Journal* **2005**, *387*, 695-702.

(15) Huang, B. X.; Kim, H.-Y. *Molecular and Cellular Proteomics* **2006**, *5*, 1045-1053.

(16) Urlaub, H.; Hartmuth, K.; Kostka, S.; Grelle, G.; Luhrmann, R. *Journal of Biological Chemistry* **2000**, *275*, 41458-41468.

(17) Chen, T.; Jaffe, J. D.; Church, G. M. *Journal of Computational Biology* **2001**, *8*, 571-583.

(18) de Koning, L. J.; Kasper, P. T.; Back, J. W.; Nessen, M. A.; Vanrobaeys, F.; Van Beeumen, J.; Gherardi, E.; de Koster, C. G.; de Jong, L. *FEBS Journal* **2006**, *273*, 281-291.

(19) Gao, Q.; Xue, S.; Doneanu, C. E.; Shaffer, S. A.; Goodlett, D. R.; Nelson, S. D. *Analytical Chemistry* **2006**, *78*, 2145-2149.

(20) Schilling, B.; Row, R. H.; Gibson, B. W.; Guo, X.; Young, M. M. *Journal of the American Society for Mass Spectrometry* **2003**, *14*, 834-850.

(21) Seebacher, J.; Mallick, P.; Zhang, N.; Eddes, J. S.; Aebersold, R.; Gelb, M. H. *Journal of Proteome Research* **2006**, *5*, 2270-2282.

(22) Tang, Y.; Chen, Y.; Lichti, C. F.; Hall, R. A.; Raney, K. D.; Jennings, S. F. *BMC Bioinformatics* **2005**, *6*, S9.

(23) Gaucher, S. P.; Hadi, M. Z.; Young, M. M. *Journal of the American Society for Mass Spectrometry* **2006**, *17*, 395-405.

(24) Raftery, M. J.; Geczy, C. L. *Journal of the American Society for Mass Spectrometry* **2002**, *13*, 709-718.

(25) Hunt, D. F.; Yates, J. R., III; Shabanowitz, J.; Winston, S.; Hauer, C. R. *Proceedings of the National Academy of Sciences of the United States of America* **1986**, *83*, 6233-6237.

(26) Biemann, K.; Martin, S. A. *Mass Spectrometry Reviews* **1987**, *6*, 1-76.

(27) Huang, Y.; Triscari, J. M.; Tseng, G. C.; Pasa-Tolic, L.; Lipton, M. S.; Smith, R. D.; Wysocki, V. H. *Analytical Chemistry* **2005**, *77*, 5800-5813.

(28) Tabb, D. L.; Smith, L. L.; Breci, L. A.; Wysocki, V. H.; Lin, D.; Yates, J. R., III *Analytical Chemistry* **2003**, *75*, 1155-1163.

(29) Kapp, E. A.; Schutz, F.; Reid, G. E.; Eddes, J. S.; Moritz, R. L.; O'Hair, R. A.; Speed, T. P.; Simpson, R. J. *Analytical Chemistry* **2003**, *75*, 6251-6264.

(30) Dongre, A. R.; Jones, J. L.; Somogyi, A.; Wysocki, V. H. *Journal of the American Chemical Society* **1996**, *118*, 8365-8374.

(31) Tsaprailis, G.; Nair, H.; Somogyi, A.; Wysocki, V. H.; Zhong, W.; Futrell, J. H.; Summerfield, S. G.; Gaskell, S. J. *Journal of the American Chemical Society* **1999**, *121*, 5142-5154.

(32) Loo, J. A.; Edmonds, C. G.; Smith, R. D. *Analytical Chemistry* **1993**, *65*, 425-438.

(33) Tsaprailis, G.; Somogyi, A.; Nikolaev, E. N.; Wysocki, V. H. *International Journal of Mass Spectrometry* **2000**, *195/196*, 467-479.

(34) Papayannopoulos, I. A. *Mass Spectrometry Reviews* **1995**, *14*, 49-73.

(35) Reid, G. E.; Wu, J.; Chrisman, P. A.; Wells, J. M.; McLuckey, S. A. *Analytical Chemistry* **2001**, *73*, 3274-3281.

(36) Reid, G. E.; Stephenson, J. L., Jr.; McLuckey, S. A. *Analytical Chemistry* **2002**, *74*, 577-583.

(37) Sullivan, A. G.; Brancia, F. L.; Tyldesley, R.; Bateman, R.; Sidhu, K.; Hubbard, S. J.; Oliver, S. G.; Gaskell, S. J. *International Journal of Mass Spectrometry* **2001**, *210/211*, 665-676.

(38) Wysocki, V. H.; Tsaprailis, G.; Smith, L. L.; Breci, L. A. *Journal of Mass Spectrometry* **2000**, *35*, 1399-1406.

(39) Burlet, O.; Orkiszewski, R. S.; Ballard, K. D.; Gaskell, S. J. *Rapid Communications in Mass Spectrometry* **1992**, *6*, 658-662.

(40) Summerfield, S. G.; Gaskell, S. J. *International Journal of Mass Spectrometry and Ion Processes* **1997**, *165/166*, 509-521.

(41) Harrison, A. G.; Tn, Y.-P. *Journal of Mass Spectrometry* **1998**, *33*, 532-542.

(42) Yu, W.; Vath, J. E.; Huberty, M. C.; Martin, S. A. *Analytical Chemistry* **1993**, *65*, 3015-3023.

(43) Gu, C.; Tsaprailis, G.; Breci, L.; Wysocki, V. H. *Analytical Chemistry* **2000**, *72*, 5804-5813.

(44) Loo, J. A.; Edmonds, C. G.; Smith, R. D. *Science* **1990**, *248*, 201-204.

(45) Schwartz, B. L.; Bursey, M. M. *Biological Mass Spectrometry* **1992**, *21*, 92-96.

(46) Vaisar, T.; Urban, J. *Journal of Mass Spectrometry* **1996**, *31*, 1185-1187.

Chapter 4

Chromogenic Cross-linker for the Characterization of Protein Structure by Infrared Multiphoton Dissociation Mass Spectrometry

4.1 OVERVIEW

A new IR chromogenic cross-linker (IRCX) has been developed to aid in rapidly distinguishing cross-linked peptides from unmodified species in complex mixtures. By incorporating a phosphate functional group into the cross-linker, one can take advantage of its unique IR absorption properties, affording selective infrared multiphoton dissociation (IRMPD) of the cross-linked peptides. In a mock mixture of unmodified peptides and IRCX-cross-linked peptides (intramolecularly and intermolecularly cross-linked), only the peptides containing the IRCX modification were shown to dissociate upon exposure to 50 ms of 10.6 μm radiation. LC-IRMPD-MS proved to be an effective method to distinguish the cross-linked peptides in a tryptic digest of IRCX-cross-linked ubiquitin. A total of four intermolecular cross-links and two dead-end modifications were identified using IRCX and LC-IRMPD-MS. IRMPD of these cross-linked peptides resulted in secondary dissociation of all primary fragment ions containing the chromophore, producing a series of unmodified b- or y-type ions that allowed the cross-linked peptides to be sequenced without the need for collision-induced dissociation (CID).

4.2 INTRODUCTION

As the field of proteomics continues to rapidly expand, there has been a growing interest in determining the three-dimensional structure of proteins as well as the

interfaces of protein-protein complexes.[1, 2] Chemical cross-linking of proteins with mass spectrometric analysis has proven to be a useful method to determine low-resolution protein structural information and protein-protein interactions.[3-6] Compared to X-ray crystallography and NMR spectroscopy, chemical cross-linking requires relatively low amounts of protein to probe distance constraints within a single protein[7] or protein-ligand complexes.[8-10] While the experimental procedure for chemically cross-linking proteins is well established, there are several analytical challenges that remain in the identification of the cross-linked peptides by mass spectrometric means. The two main difficulties in this technique have been the differentiation of cross-linked peptides from unmodified ones in enzymatic digests of cross-linked proteins and the ability to identify the specific location of the cross-link using tandem MS.

To circumvent these limitations, much work has been dedicated to developing new cross-linkers to simplify identification by mass spectrometric methods. For example, several cross-linkers that incorporate isotope labels have been designed to create doublet peaks within the mass spectra,[11-14] thus allowing facile pinpointing of the cross-linked products. Other cross-linkers incorporate fluorophores to facilitate distinction of modified proteins[15] and peptides from the unmodified ones during LC-MS analyses,[16, 17] while others introduce chemically cleavable functionalities.[18-20] Affinity tags such as biotin labels have also shown promise as a means to enrich the cross-linked peptides from complex mixtures prior to mass spectrometry.[20-22] Cross-linkers have also been designed with gas-phase labile bonds such that traceable fragment ions unique to cross-linked peptides are formed upon low energy activation during MS/MS analysis.[20, 23-25]

Interpretation of the cross-linked peptide product ion spectra, which typically contain diagnostic fragment ions both to locate the cross-link and sequence the peptides,

remains a difficult challenge even with available software. Several algorithms have been written to aid in the identification of intact cross-linked peptides based on product ion spectra of these species, but they do not take into account all of the possible product ions specific to cross-linked peptides.[26-31] Initial work by Schilling et al. demonstrated that dissociation of cross-linked peptides typically resulted in cleavage of an amide bond of one peptide, yielding one unmodified fragment and the corresponding fragment linked to the other peptide.[26] A systematic study by Gardner et al. (Chapter 3) indicated that intermolecularly cross-linked peptides without a mobile proton yielded a high degree of internal ions, as well as other double cleavage products which make interpretation of the product ion spectra difficult.[32] Thus, developing new chemical cross-linkers to reduce the complexity of the product ion spectra is still an ongoing area of interest. Recent work by Soderblom et al. reported the design of a cross-linker in which a gas-phase labile bond was inserted in the chemical cross-linker, thus cleaving upon low-energy collisions to yield the two constituent peptides.[33, 34] Bruce and coworkers developed a similar strategy using cross-linkers with two labile bonds that upon dissociation produce the two peptides in addition to a diagnostic reporter fragment ion.[24, 25] After cleavage of the labile bond of these cross-linkers, the two modified peptides are then further interrogated via MS^3 to sequence each peptide.

The aim is to develop a chemical cross-linking technique in conjunction with photodissociation methods to eliminate the need for MS^n experiments and streamline the analysis of cross-linked peptides. Infrared multiphoton dissociation (IRMPD) has shown promise as an alternative means to activate and dissociate biomolecules in the gas phase[35, 36] and has been shown to be an effective means to selectively dissociate phosphopeptides in both FTICR[37, 38] and quadrupole ion trap (QIT) mass spectrometers.[39, 40] Previous work in the Brodbelt group[39] and by Flora and Muddiman[37,

[38, 41] have shown that the phosphate group has a high absorption at the wavelength of a continuous wave (cw) CO_2 laser, 10.6 μm. Because of the large differences in absorption efficiency of phosphopeptides and unmodified peptides, phosphopeptides dissociate upon IR irradiation far more readily than unmodified peptides.

IRMPD in QITs offers other advantages over conventional collisional activation methods.[36, 42-47] IRMPD is a non-resonant activation process whose efficiency is independent of the rf trapping voltage, thus allowing a much broader *m/z* trapping range than conventional CID. This feature is particularly important for detection of key terminal sequence ions in the low *m/z* range. Ion losses due to collisions or unstable trajectories are eliminated as the photodissociation process does not affect the translational motion of ions. The non-resonant nature of photodissociation methods also yields secondary and higher order product ions that might only be obtained by MS^n approaches using CID.

In this chapter, the development and application a novel IR-chromogenic cross-linker which incorporates a phosphate chromophore that allows the identification of cross-linked peptides and facilitates the interpretation of the product ion spectra of the constituent peptides is reported. Infrared multiphoton dissociation (IRMPD) in a linear quadrupole ion trap is used to selectively dissociate the cross-linked peptides, allowing for these peptides to be easily distinguished from unmodified peptides (i.e., ones that do not afford any protein contact information). The resulting IRMPD spectra of intermolecularly cross-linked peptides are dominated by b- and y-type product ions of each constituent peptide. Online liquid chromatography (LC)-IRMPD-MS has been applied for the screening of complex peptide mixtures, including tryptic digests of chemically cross-linked proteins.

4.3 EXPERIMENTAL

4.3.1 Chemicals and Reagents

The peptides α-MSH (Ac-SYSMEHFRWGKPV-NH_2), Ac-RFMWMK-NH_2, substance P (RPKPQQFFGLM-NH_2), and neurotensin 1-6 (Pyr-LYENK) were purchased from Bachem (Torrance, CA). The peptide angiotensin II (DRVYIHPF) was purchased from AnaSpec (San Jose, CA). Ubiquitin from bovine red blood cells, proteomics grade trypsin, bradykinin (RPPGFSPFR), methionine-enkephalin (YGGFM), melittin and the cross-linker disuccinimidyl suberate (DSS) were obtained from Sigma (St. Louis, MO). N-hydroxysuccinimide, 4-hydroxybenzoic acid, and ethyl dichlorophosphate were from Aldrich (Milwaukee, WI). Water (HPLC grade) and acetonitrile (HPLC grade) were from Riedel-de Haën (Seelze, Germany). 1-ethyl-3-(3-dimethylaminopropyl) carbodiimide hydrochloride was obtained from Pierce Biotechnology (Rockford, IL). All other chemicals and solvents were purchased from Fisher Scientific (Fairlawn, NJ) except for formic acid (EM Science, Gibbstown, NJ).

4.3.2 Synthesis of Dibenzoyloxysuccinimidyl Ethyl Phosphate

The IR chromogenic cross-linker (IRCX, **Figure 4.1a**), dibenzoyloxysuccinimidyl ethyl phosphate, was synthesized by first preparing the intermediate *N*-(4-hydroxybenzoyloxy)succinimide. Under an argon atmosphere, dry tetrahydrofuran (THF) (45 mL) and dry dichloromethane (DCM) (45 mL) were added to 5 mmol of 4-hydroxybenzoic acid, 8 mmol of *N*-hydroxysuccinimide, and 6.5 mmol of 1-ethyl-3-(3-dimethylaminopropyl)carbodiimide hydrochloride. The reaction was stirred under argon at room temperature for 24 hours and then extracted with H_2O (1 × 60 mL), saturated

$NaHCO_3$ (1 × 60 mL), and then a saturated brine solution (1 × 60 mL). The final liquid extract was dried over Na_2SO_4, filtered, and dried under vacuum. The intermediate was recrystallized in DCM at 20 °C overnight and filtered.

Dibenzoyloxysuccinimidyl ethyl phosphate was prepared by dissolving 0.5 mmol of *N*-(4-hydroxybenzoyloxy)succinimide in dry THF at 0 °C, and then adding 0.25 mmol of ethyldichlorophosphate dropwise to the solution, followed by 10 mmol of dry triethylamine. The reaction was allowed to warm to room temperature while stirring over 2 hours, then heated to 60 °C and stirred for additional 4 hours. The final solution was dried and concentrated under reduced pressure. The product was washed with cold H_2O, filtered, recrystallized in DCM, and filtered. The cross-linker structure was confirmed by ^{1}H NMR using a 400 MHz Varian instrument. ^{1}H NMR at 400 MHz in $CDCl_3$ yielded: 8.29 ppm (d, 4H), 7.39 ppm (d, 4H), 4.20 ppm (m, 2H), 2.94 (s, 8H), 1.71 (br, 3H); these findings are consistent with the proposed structure. ESI-IRMPD-MS of protonated IRCX (*m/z* 561) using 2.0 ms of irradiation yielded an abundant product ion corresponding to the loss of succinimide (*m/z* 464), and a less abundant ion of *m/z* 446 (loss of N-hydroxysuccinimide) (data not shown).

4.3.3 Chemical Cross-linking of Model Peptides

Stock solutions of the model peptides were prepared at 5.0 mM in H_2O. IRCX and DSS were freshly prepared at 20.0 mM in DMSO prior to cross-linking. The peptides α-MSH and Ac-RFMWMK-NH_2 were intermolecularly cross-linked with IRCX at a 4:4:5 molar ratio of peptide: peptide: cross-linker in 20 mM HEPES, pH 8.0 to produce a final concentration of 1.7 mM in a total volume of 12 μL. Substance P was similarly intramolecularly cross-linked by IRCX or DSS at a 4:5 molar ratio in the same buffer. All peptide cross-linking reactions were allowed to incubate at room temperature

overnight to increase the yield of cross-linked peptides. The reactions were desalted by solid phase extraction using 50 mg tC_{18} Waters (Milford, MA) Sep-Pak cartridges.

4.3.4 Chemical Cross-linking and Enzymatic Digestion of Ubiquitin

The protein ubiquitin was intramolecularly cross-linked by IRCX at 1:5, 1:10, 1:25 and 1:50 molar ratios of protein: cross-linker in a 20 mM HEPES buffer, pH 8.0 at a final protein concentration of 10 μM. The reactions were allowed to proceed at room temperature for 30 minutes. The cross-linking was quenched by the addition of NH_4HCO_3 to a final concentration of 10 mM for 15 minutes. The reaction mixtures were desalted against a 5 kDa molecular weight cut-off Ultrafree Biomax membrane (Millipore, Billerica, MA). Aliquots were removed for direct-ESI-MS analysis and the remaining cross-linked ubiquitin sample was diluted to 180 μM in 100 mM NH_4HCO_3, pH 8.0. Cross-linked ubiquitin was enzymatically digested with trypsin at a 1:10 ratio enzyme-to-protein (w/w) overnight at 37 °C. The digested sample was then desalted by solid-phase extraction as described above and diluted to ~10 μM in 50:50 H_2O/MeOH.

4.3.5 Mass Spectrometry

All mass spectrometry experiments were performed on a modified ThermoFisher Scientific LTQ XL linear ion trap mass spectrometer using the XCalibur version 2.2 software package and the standard ESI source. For direct infusion experiments the ESI voltage was set to 4.5 kV and solutions were infused at 2.5 μL/min. Solutions were prepared at ~10 μM in 49.5:49.5:1 H_2O/MeOH/HOAc (v/v/v) for ESI-MS analysis. For CID experiments, the precursor ions were activated for 30 ms at the default q-value of 0.25. Energy-variable CID experiments were performed by incrementally raising the

CID voltage, and the CID voltage necessary to reduce the precursor ion abundance to 50% was determined. For energy-variable CID, normalized collision energies (NCE) were converted to CID voltages to account for the differences in *m/z* of the precursor ions based on the calibration settings of the instrument. The CID voltages for the IRCX-cross-linked peptides were then corrected for their greater degrees of freedom compared to the DSS-cross-linked analogs using the following formula:

$$V_{50\%,corrected} = V_{50\%} \times \frac{N_{DSS}}{N_{IRCX}} \qquad \textbf{Equation 4.1}$$

where the degrees of freedom $N = 3n - 6$ and n is the number of atoms in the peptide cross-linked by either DSS or IRCX.[48] All energy-variable CID experiments were performed in triplicate; the drifts in the CID voltages were determined to be less than 0.08 mV.

4.3.6 Infrared Multiphoton Dissociation

IRMPD was performed using a model 48-5 Synrad 50-W CO_2 continuous wave laser (Mukilteo, WA). The back flange of the vacuum manifold of the instrument was modified with a CF viewport flange with a ZnSe window to allow the transmission of 10.6 μm radiation. The unfocused laser beam was aligned on axis with the linear ion trap such that the beam passed through the 2-mm aperture of the exit lens to irradiate the ion cloud. The laser was triggered during the activation step in the scan function by a TTL signal from pin 14 of the J1 connector on the digital printed circuit board. All IRMPD experiments were performed at full power (50 W) with irradiation times varying between 5 and 100 ms unless otherwise indicated. The q-value of the precursor was set between 0.1 and 0.15 to reduce the low-mass cut-off (LMCO) value to less than *m/z* 150. The

pressure in the analyzer region was nominally 9.0×10^{-6} Torr and no changes to the He bath gas pressure were made.

4.3.7 Analytical High-Performance Liquid Chromatography and Tandem Mass Spectrometry

Liquid chromatography was performed using a Hitachi L-7000 (Hitachi Ltd.) system including an L-7100 HPLC pump and L-7000 autosampler; the LC system was controlled using the Hitachi 3DQ software. Reversed-phase HPLC was accomplished using a Symmetry300 (Waters, Milford, MA) C_{18} column (2.1 × 50 mm, 3.5 μm packing) with a Symmetry300 C_{18} guard column (2.1 × 10 mm, 3.5 μm packing). For analytical separations, a gradient elution of mobile phases consisting of (A) H_2O with 0.1% formic acid and (B) acetonitrile with 0.1% formic acid was used at a flow rate of 0.300 mL/min. After loading the sample (10 – 25 μL injections of 10 μM solutions), the mobile phase was held at 95% A for 2 minutes and then the peptides were eluted using a linear gradient from 95% A to 50% A over 58 minutes.

Two types of online LC-IRMPD-MS experiments were performed. The first data-acquisition sequence employed collecting a full mass spectrum of *m/z* 300 – 2000, then an isolation spectrum of *m/z* 450 – 2000 in which all ions of m/z in this range were isolated for 50 ms but not subjected to any form of activation, and then an IRMPD spectrum of all ions of *m/z* 450 – 2000 with an irradiation time of 50 ms. For the isolation and IRMPD spectra, the q-value was set to 0.18 for ions of *m/z* 450, thus establishing the lower *m/z* limit as 90. The second LC-IRMPD-MS experiment employed data-dependent MS/MS in which IRMPD and CID spectra were acquired for the two most abundant ions observed in the full mass spectrum. IRMPD was performed for 30 ms with the q-value of the precursor ion set to 0.1 (lower *m/z* limit ranged from 50 to 175

depending on the precursor ion) and CID was performed for 30 ms at a normalized collision energy of 45% using a precursor ion q-value of 0.25 (lower *m/z* limit 115 – 455).

4.3.8 Identification of Cross-linked Peptides

Product ion spectra of peptide ions exhibiting high IRMPD efficiency were manually identified aided in part with the software program ProteinXXX, the protein cross-linking function of GPMAW (General Protein Mass Analysis for Windows) version 7.10 (Lighthouse Data, Odense, Denmark) (available at http://www.gpmaw.com). This program was used to provide a list of intact masses of possible cross-linked tryptic peptides allowing for cleavage C-terminal to only arginine and unmodified lysine residues (i.e., no cleavage C-terminal to cross-linked or dead-end modified lysine residues). The intact mass of the eluting species were matched to the list potential candidates and then the identity of the precursor ion was confirmed manually by IRMPD; all product ions were also identified manually.

4.4 RESULTS AND DISCUSSION

4.4.1 Cross-linker Design and Characterization

It has previously been demonstrated that phosphorylated peptides can be selectively dissociated via IRMPD in quadrupole ion trap.[39, 40] The cross-linker (**Figure 4.1a**) incorporated a phosphate chromophore due to its greater IR absorption efficiency at 10.6 μm.[37-39, 41] The chromophore was placed in the center of the cross-linker, thus creating a phosphate tri-ester to avoid the neutral loss of phosphoric acid which is commonly observed upon ion activation of phosphorylated peptides.[49-52] The cross-

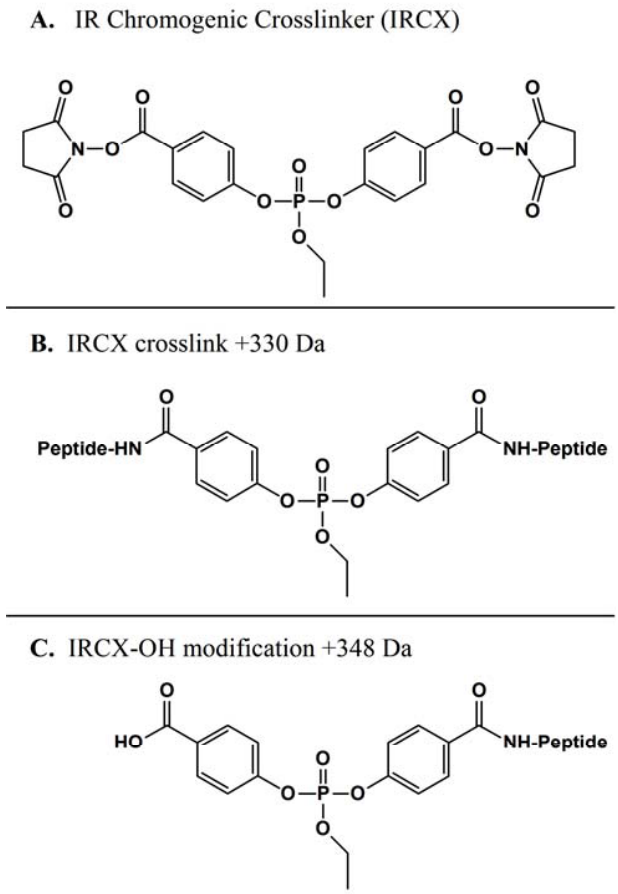

Figure 4.1 Structures of IRCX (A), an IRCX cross-link (B), and an IRCX-OH modification (C).

linker was designed as a homobifunctional reagent with two terminal NHS-esters that react with primary amines (e.g., ε-amine of lysine residues or free N-terminus) similar to most common commercial cross-linkers. IRCX has a spanner arm-length of ~16 Å and could span a distance up to ~28 Å between α-carbons of two lysine residues in proteins. Upon reaction of each NHS-ester with a primary amine, stable amide bonds are formed, yielding a cross-link corresponding to a mass addition of 330 Da (**Figure 4.1b**). If one NHS-ester does not react with the protein or peptide and is hydrolyzed, a dead-end modification is produced, termed IRCX-OH as shown in **Figure 4.1c**, with a mass

addition of 348 Da. Product ions formed upon dissociation of the cross-linked peptides were labeled according to previously suggested nomenclature.[26, 53] Briefly, for intermolecularly cross-linked peptides, the two constituent peptides are labeled α and β, referring to the first and second peptide, respectively. Cleavage along the backbone of the α peptide yields products ions such as $y_{n\alpha}$ or $b_{n\alpha}$, and similar nomenclature is used for the β peptide and other product ion types. For intramolecularly cross-linked peptides, the nomenclature is identical to that of unmodified peptides. In addition, lysine immonium ions which are linked to the other peptide are labeled $K^{L}\alpha$, where L represents the cross-linker and α is the other peptide. Similar nomenclature is used for referring to internal ions of one peptide linked to the second peptide, or a fragment ion of the second peptide (e.g., $b_{4\alpha}{}^{L}y_{7\beta}$).

4.4.2 IRMPD Analysis of IRCX Cross-linked Peptides

The peptides α-MSH (α peptide) and Ac-RFMWMK-NH_2 (β peptide) were incubated with IRCX yielding all three possible intermolecularly cross-linked products (α ⊗ α, β ⊗ β, α ⊗ β). The two constituent peptides each have only a single reactive site for the cross-linking reaction, Lys-11 of α-MSH and Lys-6 of Ac-RFMWMK-NH_2 as the N-termini of each of these peptides are acetylated, allowing for the site of the cross-link to be known with certainty for these initial studies. It was possible to readily screen for the cross-linked peptides in the product mixture by acquiring an isolation spectrum in which ions of *m/z* 400 – 2000 were isolated for 30 ms without activation by toggling off the isolation waveform, and subsequently acquiring an IRMPD mass spectrum of ions in the same *m/z* range by triggering the CO_2 laser for those 30 ms (**Figure 4.2**). Upon IR irradiation, only the peptide ions containing an IRCX cross-link or an IRCX-OH

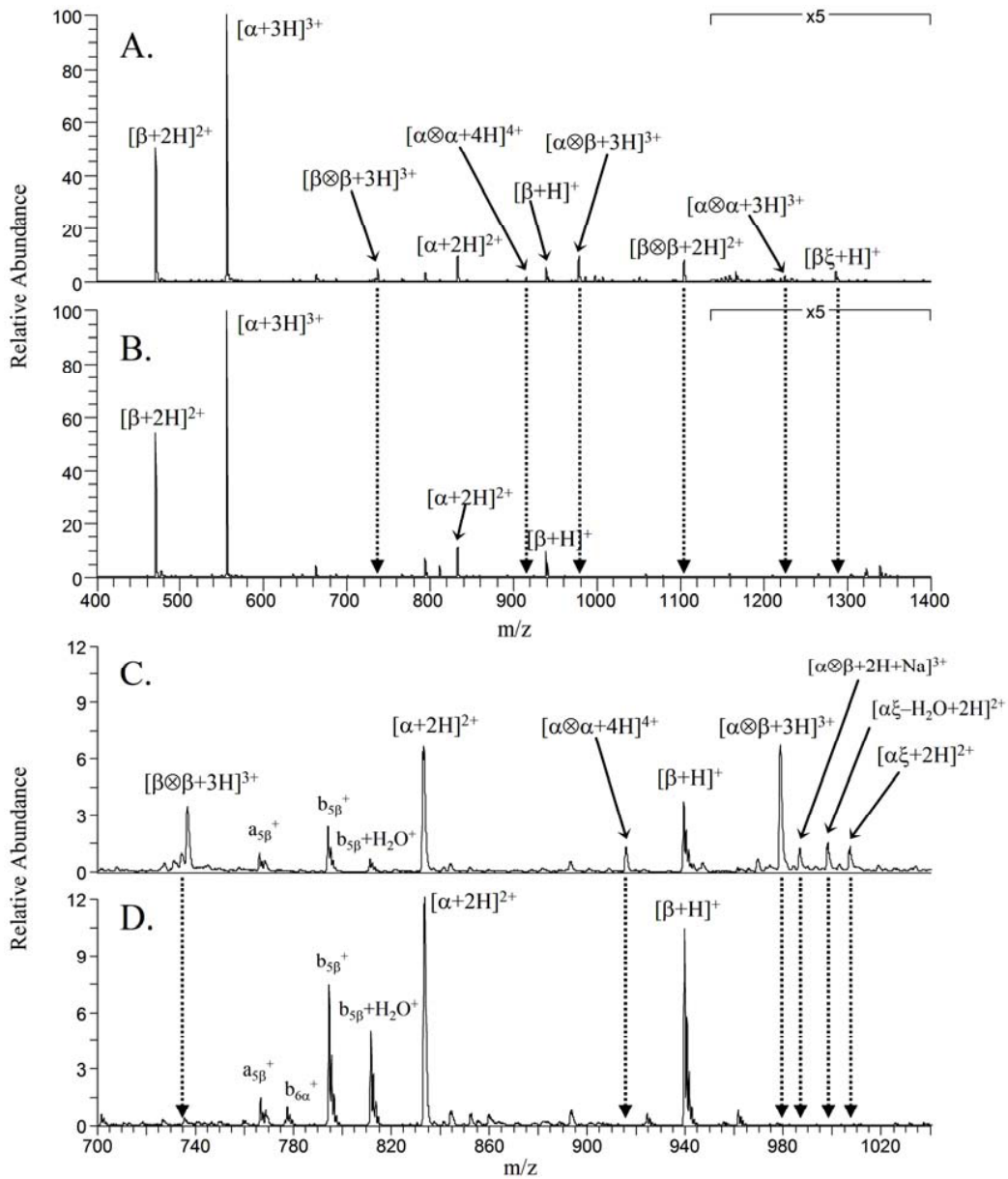

Figure 4.2 Isolation (A and C) and IRMPD (B and D) mass spectra of IRCX cross-linking product mixture of α-MSH (α peptide) and Ac-RFMWMK-NH_2 (β peptide). IRCX cross-links are represented by ⊗ and IRCX-OH dead-end modifications by ξ. Ions were either isolated with the laser off (a and c) or irradiated for 30 ms at 50 W (B and D). Zoomed in region of *m/z* 700 – 1040 shown in C and D.

modification decreased in ion abundance, allowing rapid screening of the IRCX containing ions of interest. All of the cross-linked peptide ions, regardless of charge state, reduced in ion abundance by greater than 95%, as well as the peptide ions with a dead-end IRCX-OH modification. The unmodified peptides did not undergo photodissociation and no decrease in their ion abundances was observed. After pinpointing the IRCX-cross-linked peptide ions, they can be more closely interrogated by IRMPD, CID, or both. For example, the intermolecularly cross-linked peptide [α-MSH ⊗ IRCX ⊗ Ac-RFMWMK-NH_2 + 3H]$^{3+}$ was analyzed by IRMPD to determine the location of the cross-link. As shown in **Figure 4.3a**, the IRCX-cross-linked peptide underwent very efficient dissociation upon 12 ms of irradiation, and broad sequence coverage of each constituent peptide was observed. CID of the same ion produced similar sequence coverage of each peptide; however, in contrast the triply and doubly charged $b_{11\alpha}$ product ions of *m/z* 907.5 and 1360.4 dominated the spectrum. Previous work as discussed in Chapter 3 has shown that a proline residue positioned N-terminal to the cross-linked lysine enhances dissociation of the amide bond between the lysine and proline, in this case producing the $b_{11\alpha}$ fragment.[32] Most of the product ions observed in the CID spectrum had relative abundances of less than 1%, making it difficult to distinguish these peaks from noise. In addition, due to the limited *m/z* storage range during CID, the diagnostic $y_{2\alpha}$ product ion of *m/z* 214.0 cannot be trapped and detected.

Upon closer examination of the IRMPD spectrum in **Figure 4.3a**, there is a distinct difference between the relative abundances of the product ions containing the IRCX cross-link and those without the modification (e.g., $b_{n\alpha}^{+}$ and $b_{n\beta}^{+}$ ions). Fragment ions which contain the IRCX cross-link still retain the phosphate chromophore and thus can undergo IR photon absorption and secondary dissociation. CID predominantly yielded product ions which retained the cross-link (e.g., series of $y_{n\alpha}^{2+}$ ions) whereas

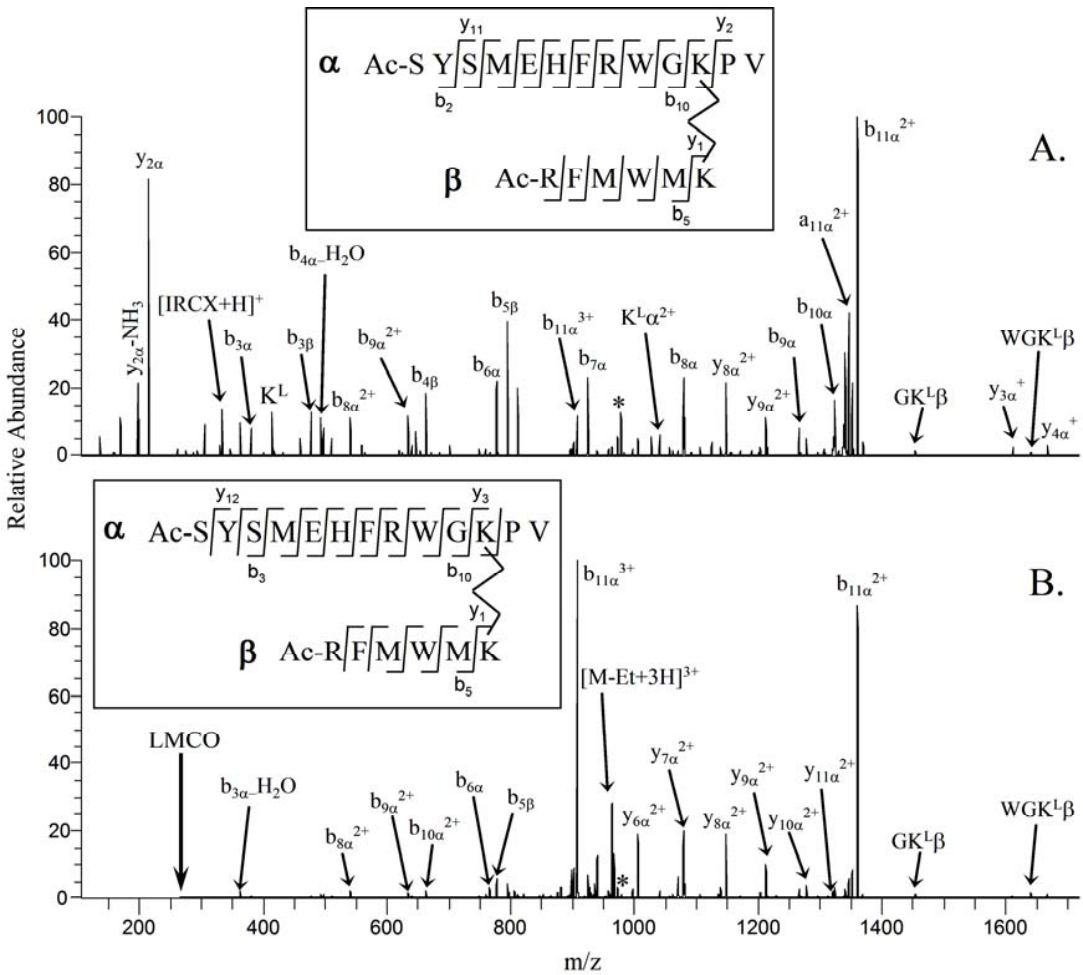

Figure 4.3 Product ion mass spectra of [α-MSH ⊗ IRCX ⊗ Ac-RFMWMK-NH_2 + 3H]$^{3+}$ (A) IRMPD of *m/z* 978.5 (q=0.1, 12 ms, 50 W) and (B) CID of *m/z* 978.5 (q=0.25, 30 ms, 34.1 mV). α-MSH is referred to as the α peptide and Ac-RFMWMK-NH_2 as the β peptide. The precursor ion is represented by an asterisk (*).

these fragment ions were less abundant in the IRMPD spectrum. Time-resolved IRMPD was performed in order to investigate the relative abundances of the product ion types observed by varying the irradiation time from 0 ms to 100 ms. For each IRMPD spectrum acquired the peak areas of the various product ion types – those containing or not containing the IRCX cross-link – were measured and summed as a function of

irradiation time. The time-resolved IRMPD plot in **Figure 4.4** indicates that for irradiation times less than 10 ms the most abundant product ions observed were IRCX-cross-linked fragments. With longer irradiation times these product ions decreased in relative abundance, forming unmodified b- and y-type ions, and after ~30 ms of irradiation virtually no IRCX-containing product ions survived. Using IRMPD one can thus circumvent many dead-end dissociation pathways such as dehydration because the primary IRCX-containing fragment ions undergo secondary dissociation to produce more informative fragment ions.

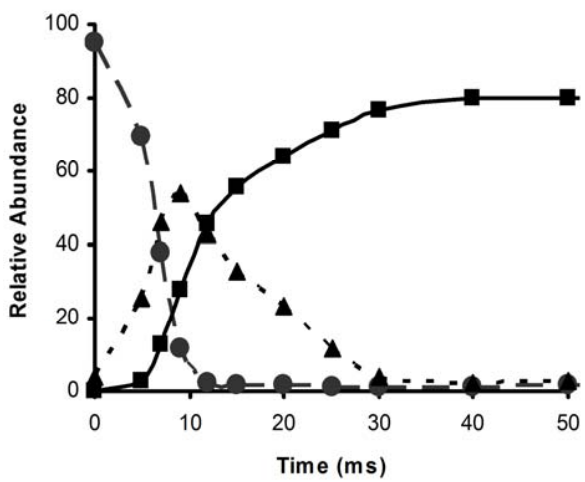

Figure 4.4 Time-resolved IRMPD (50 W) of [α-MSH ⊗ IRCX ⊗ Ac-RFMWMK-NH_2 + 3H]$^{3+}$ displaying the relative abundances of the precursor ion (●), non-IRCX containing product ions (■), and IRCX containing product ions (▲). Ion abundances are all relative to the total ion abundance of the spectrum acquired with 0 ms of irradiation.

Upon reaction with IRCX, the peptide substance P was intramolecularly cross-linked between the free N-terminus and Lys-3. The doubly-protonated IRCX-cross-linked substance P underwent efficient photodissociation using 50 ms of irradiation at only 35 W (**Figure 4.5a**). This result, in conjunction with those described above, indicates that both intramolecularly and intermolecularly IRCX-cross-linked peptides can

be readily photodissociated. A series of singly charged b-ions were observed along with the dominant y_8 ion, a result of cleavage C-terminal to the intramolecular cross-link which has previously been noted as a site of enhanced dissociation.[53] Collision-induced dissociation of [substance P ⊗ IRCX + 2H]$^{2+}$, as shown in **Figure 4.5b**, yielded similar sequence coverage as IRMPD, suggesting that either method is suitable for identifying the site of the cross-link. However, in the CID mass spectrum the b-ions retaining the IRCX cross-link were observed in both the 1+ and 2+ charge state (e.g., b_8^{2+}, b_9^{2+}, and b_{10}^{2+}), cluttering the product ion mass spectrum, and fragment ions of low *m/z* had much lower relative abundances than in the IRMPD mass spectrum. Upon IR irradiation, the more highly charged IRCX-containing b-ions apparently undergo secondary dissociation at a faster rate than the singly-charged ions due to the presence of a mobile proton. In addition, the expanded *m/z* storage range possible during IRMPD allowed the detection of the low-mass y_1 ion which was not observed by CID. For precursor ions of higher *m/z*, the low-mass cut-off inherent to CID would be alleviated by utilizing IRMPD, thus allowing other product ions to be observed that would otherwise be undetectable by CID.

The CID voltages determined from energy-variable CID experiments performed on both DSS- and IRCX-cross-linked peptides indicate the IRCX-cross-linked species have higher dissociation energies than the DSS-cross-linked analogs. For example, for the intermolecularly cross-linked α-MSH and Ac-RFMWMK-NH_2 in the 3+ charge state, the IRCX species had a higher CID voltage than the DSS analog by 3.7 mV (32.8 mV versus 29.1 mV). Likewise, the doubly protonated IRCX-intramolecularly cross-linked substance P required a CID voltage of 1.8 mV greater than that of the analogous DSS-peptide (24.9 mV versus 23.1 mV). Moreover, the IRCX-containing peptides dissociated readily upon less than 30 ms of irradiation, whereas the DSS-cross-linked peptides did not undergo efficient IRMPD upon irradiation for 250 ms, indicating that the presence of

the phosphate chromophore results in a much greater IR absorption at 10.6 μm (data not shown). These collective results confirm that the successful and selective IRMPD of the IRCX-containing peptides is due to their high IR absorption efficiencies, not due to lower dissociation energies.

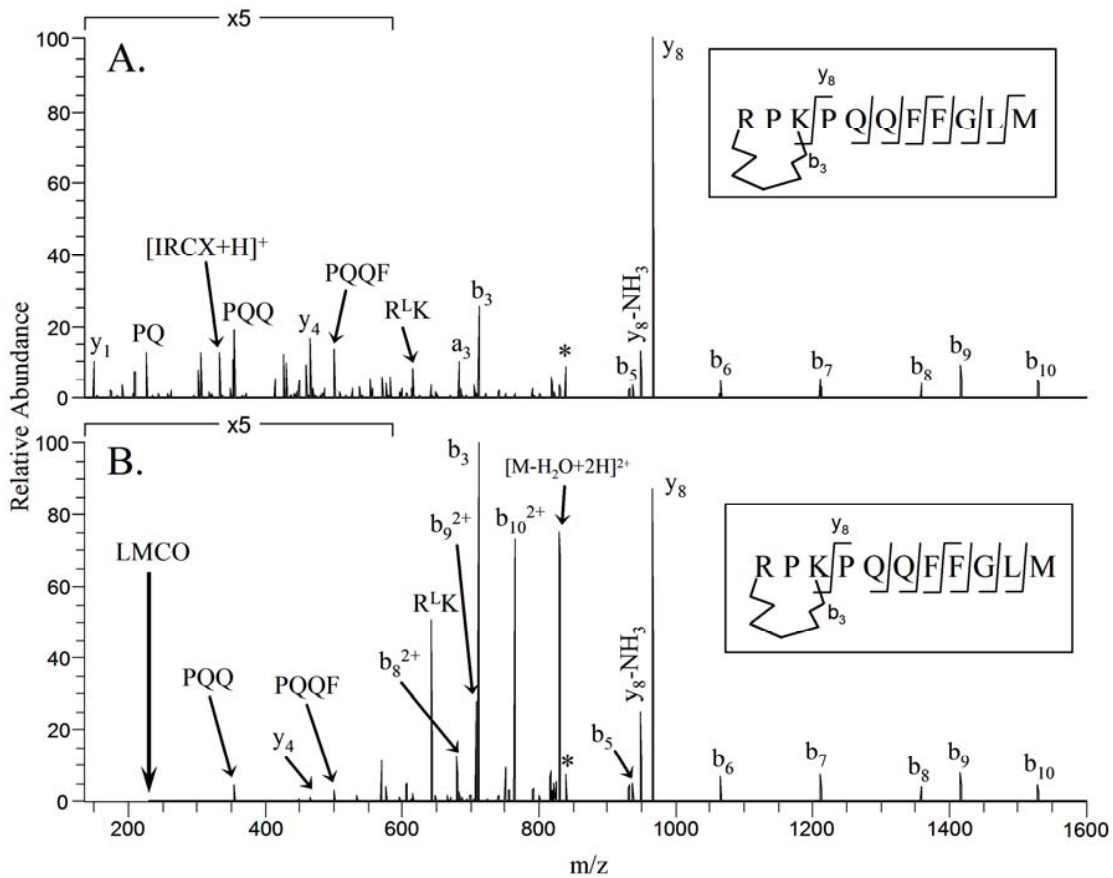

Figure 4.5 Product ion spectra of [substance P ⊗ IRCX + 2H]$^{2+}$ (A) IRMPD of *m/z* 839.3 (q=0.15, 50 ms, 35 W) and (B) CID of *m/z* 839.3 (q=0.25, 30 ms, 26.7 mV). The precursor ion is represented by an asterisk (*).

4.4.3 Screening of IRCX-Cross-linked Peptides in a Mock Mixture by IRMPD

IRMPD analysis was performed on a mock mixture of peptides to demonstrate selective dissociation of IRCX-cross-linked peptides. The peptide mixture contained an equimolar amount (10 μM) of (**1**) Pyr-LYENK, (**2**) YGGFM, (**3**) bradykinin, (**4**)

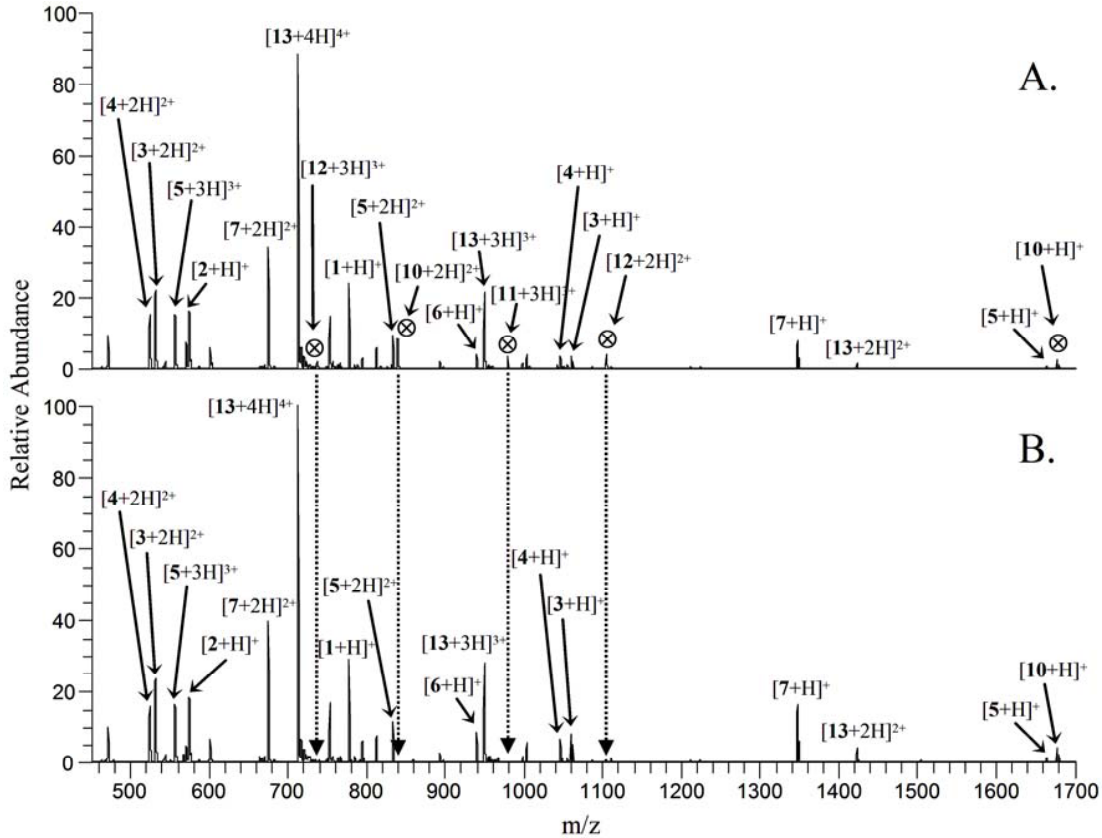

Figure 4.6 Direct-infusion (A) isolation (25 ms) and (B) IRMPD (25 ms, 50 W) spectra of a mock mixture of peptides. The identities of the peptides are listed in **Table 4.1**. IRCX cross-linked peptide ions are labeled with ⊗.

angiotensin II, (**5**) α-MSH, (**6**) Ac-RFMWMK-NH_2, (**7**) substance P, and (**13**) melittin. Also present were equimolar amounts (10 μM) of the IRCX intermolecular cross-linked product mixture of α-MSH with Ac-RFMWMK-NH_2 and the intramolecular cross-linked product mixture of substance P. Products observed in the ESI mass spectrum included (**8**) α-MSH + IRCX-OH, (**9**) α-MSH ⊗ IRCX ⊗ α-MSH, (**10**) substance P ⊗ IRCX, (**11**) α-MSH ⊗ IRCX ⊗ Ac-RFMWMK-NH_2, and (**12**) Ac-RFMWMK-NH_2 ⊗ IRCX ⊗ Ac-RFMWMK-NH_2. Using direct infusion ESI-MS, the mixture was rapidly screened by comparing the abundances of ions of *m/z* 450 – 2000 in the isolation mass spectrum

Table 4.1 Relative ion abundance decreases upon IR irradiation (25 ms, 50 W) for a mock mixture of peptides using direct infusion ESI-IRMPD-MS. Ion abundances are relative to the total ion abundance in either the isolation or IRMPD spectrum. All measurements were in triplicate.

Label	Species	*m/z*	Average Relative Abundances		Average Percent Abundance Decrease	Std. Dev.
			Isolation	IRMPD		
1	$[Pyr\text{-}LYENK + H]^{+}$	777.4	3.64	4	-9.8	3.7
2	$[YGGFM + H]^{+}$	574.2	3.97	4.08	-2.8	3.5
3	$[bradykinin + 2H]^{2+}$	530.7	6.09	6.13	-0.7	3.5
3	$[bradykinin + H]^{+}$	1060.5	0.42	0.9	-113	7.6
4	$[angiotensin\ II + 2H]^{2+}$	523.8	4.35	4.37	-0.4	3.6
4	$[angiotensin\ II + H]^{+}$	1046.5	0.48	0.67	-39.2	3
5	$[\alpha\text{-MSH} + 3H]^{3+}$	555.6	4.35	4.37	-0.4	3.2
5	$[\alpha\text{-MSH} + 2H]^{2+}$	832.9	2.17	2.34	-7.8	2.6
5	$[\alpha\text{-MSH} + H]^{+}$	1664.8	0.08	0.11	-40	19
6	$[Ac\text{-}RFMWMK\text{-}NH_2 + 2H]^{2+}$	470.2	2.99	3.07	-2.7	1.9
6	$[Ac\text{-}RFMWMK\text{-}NH_2 + H]^{+}$	939.5	0.58	1.15	-98.4	5.3
7	$[substance\ P + 2H]^{2+}$	674.4	9.02	9.35	-3.6	3.6
7	$[substance\ P + H]^{+}$	1347.7	1.19	2.31	-95	15
8	**$[\alpha\text{-MSH} + IRCX\text{-}OH + 2H]^{2+}$**	**1006.9**	**0.22**	**0.03**	**86.3**	**1.7**
9	**$[\alpha\text{-MSH} \otimes IRCX \otimes \alpha\text{-MSH} + 4H]^{4+}$**	**915.4**	**0.07**	**0.01**	**84.6**	**3.5**
10	**$[substance\ P \otimes IRCX + 2H]^{2+}$**	**839.4**	**2.13**	**0.03**	**98.6**	**0.2**
10	**$[substance\ P \otimes IRCX + H]^{+}$**	**1677.7**	**0.39**	**0.51**	**-29.4**	**1.8**
11	**$[\alpha\text{-MSH} \otimes IRCX \otimes Ac\text{-}RFMWMK\text{-}NH_2 + 3H]^{3+}$**	**978.4**	**0.84**	**0.03**	**95.9**	**0.7**
12	**$[2(Ac\text{-}RFMWMK\text{-}NH_2) \otimes IRCX + 3H]^{3+}$**	**736.6**	**0.55**	**0.09**	**84.1**	**3.7**
12	**$[2(Ac\text{-}RFMWMK\text{-}NH_2) \otimes IRCX + 2H]^{2+}$**	**1104.5**	**0.89**	**0.09**	**89.8**	**1.1**
13	$[melittin + 5H]^{5+}$	570.1	1.89	1.14	39.8	2
13	$[melittin + 4H]^{4+}$	712.4	17.2	17.3	-0.5	4
13	$[melittin + 3H]^{3+}$	949.6	4.69	5.65	-20.5	6.7
13	$[melittin + 2H]^{3+}$	1423.9	0.18	0.56	-224	42

(**Figure 4.6a**) to the IRMPD mass spectrum obtained using 25 ms of irradiation at 50 W (**Figure 4.6b**). The abundances of the unmodified peptide ions are unaffected by IR irradiation, whereas the IRCX-cross-linked peptide ions readily photodissociate with reductions in ion abundance of ~90% with the exception of the singly-protonated intramolecularly cross-linked substance P ion (**Table 4.1**). While the doubly-charged analog undergoes efficient IRMPD, the singly-protonated species which does not have a mobile proton actually increased in abundance upon IR irradiation in this experiment (relative abundance increased from 0.39% to 0.51%). This charge-state dependence on IRMPD efficiencies provides a means to distinguish between intra- and inter-molecularly IRCX cross-linked peptides, in which the inter-molecularly cross-linked peptides of all charge-states exhibit high photodissociation efficiencies. Most intramolecularly cross-linked tryptic peptides will possess a free N-terminus and either an unmodified Lys or Arg at the C-terminus and thus will predominantly be observed as doubly-charged ions, leading to efficient IRMPD. No discernable decrease in the ion abundances of the unmodified peptides was observed using irradiation times of greater than 250 ms; this indicates that the laser irradiation time and power has an ample range of usability to differentiate between IRCX-cross-linked peptides and unmodified ones.

For more complex mixtures such as those expected for peptides with isobaric *m/z* values, an HPLC separation is required prior to IRMPD screening, as demonstrated for the same mock mixture. As detailed in the experimental section, the scan sequence to accomplish this task includes acquisition of a full mass spectrum, then an isolation mass spectrum from *m/z* 450 – 2000, and then an IRMPD mass spectrum of all isolated ions. Selected ion chromatograms (SICs) for each of the species in the mixture were extracted and then plotted together to form a reconstructed ion chromatogram (RIC). The reconstructed ion chromatograms for the isolation and IRMPD spectra are shown in

Figure 4.7, and the changes in ion abundances are summarized in **Table 4.2**. The difference between the RICs for the isolation and IRMPD mass spectra is striking. Upon IR irradiation, the unmodified peptide ions did not exhibit any decrease in ion abundance with the exception of $[\text{melittin} + 5\text{H}]^{5+}$ which decreased in abundance by ~20% (based on peak areas in the SICs). In contrast, the IRCX-cross-linked and modified peptide ions are reduced on the order of 60 – 100% in abundance after irradiation. All of the species which eluted between 37 and 44 minutes contained either an IRCX cross-link or IRCX-OH modification, and upon 25 ms of IR irradiation, the intact peptide ions containing the IRCX chromophore were no longer detected.

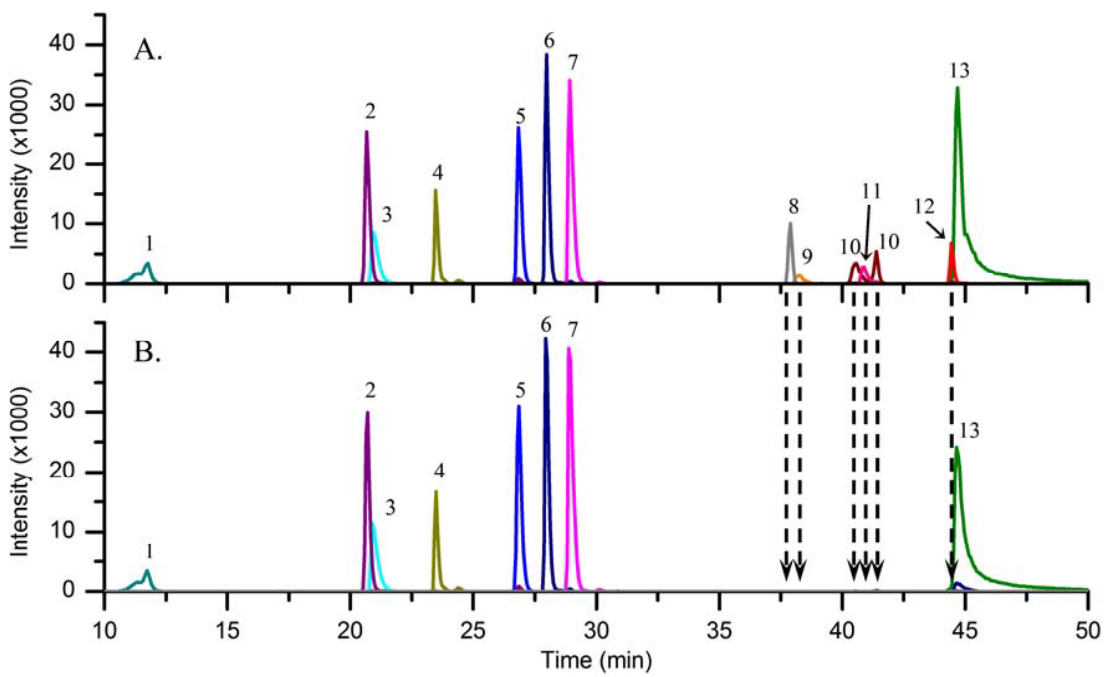

Figure 4.7 Reconstructed ion chromatograms of (A) isolation (25 ms) and (B) IRMPD (25 ms, 50 W) spectra from LC-IRMPD-MS of a mock mixture of peptides. The identities of the eluting species are listed in **Table 4.2**. Ion chromatogram intensities of $[\alpha\text{-MSH} + \text{IRCX-OH} + 2\text{H}]^{2+}$ (**8**) and $[\alpha\text{-MSH} \otimes \text{IRCX} \otimes \alpha\text{-MSH} + 4\text{H}]^{4+}$ (**9**) were zoomed in 10× in both (A) and (B).

Table 4.2 Ion abundance decreases upon IR irradiation from LC-IRMPD-MS reconstructed ion chromatograms of a mock mixture of peptides. Percent abundance decreases calculated from the decrease of the peak areas of the SICs from the isolation and IRMPD spectra.

Label	Elution (min)	Species	*m/z*	Peak Area Isolation	Peak Area IRMPD	Percent Abundance Decrease
1	11.8	[Pyr-LYENK + H]$^{+}$	777.4	2072.76	1853.8	10.6
2	20.7	[YGGFM + H]$^{+}$	574.2	5402.8	6251.49	-15.7
3	20.9	[bradykinin + 2H]$^{2+}$	530.7	2942.05	3595.3	-22.2
	20.9	[bradykinin + H]$^{+}$	1060.5	49.78	53.84	-8.2
4	23.5	[angiotensin II + 2H]$^{2+}$	523.8	2806.8	3087.37	-10
	23.5	[angiotensin II + H]$^{+}$	1046.5	131.89	122.36	7.2
5	26.8	[α-MSH + 3H]$^{3+}$	555.6	5863.15	6994.73	-19.3
	26.8	[α-MSH + 2H]$^{2+}$	832.9	1533.24	1717.75	-12
	26.8	[α-MSH + H]$^{+}$	1664.8	5.28	7.12	-35
6	28	[Ac-RFMWMK-NH_2 + 2H]$^{2+}$	470.2	7154.23	8144.27	-13.8
	28	[Ac-RFMWMK-NH_2 + H]$^{+}$	939.5	181.8	168.69	7.2
7	28.9	[substance P + 2H]$^{2+}$	674.4	7937.77	9496.41	-19.6
	28.9	[substance P + H]$^{+}$	1347.7	179.17	189.83	-5.9
8	**37.9**	**[α-MSH + IRCX-OH + 2H]$^{2+}$**	**1006.9**	**190.39**	**0**	**100**
9	**38.3**	**[α-MSH ⊗ IRCX ⊗ α-MSH + 4H]$^{4+}$**	**915.4**	**53.83**	**0**	**100**
	28.3	**[α-MSH ⊗ IRCX ⊗ α-MSH + 3H]$^{3+}$**	**1220.2**	**7.89**	**0.06**	**99.2**
10	**40.6, 41.4**	**[substance P ⊗ IRCX + 2H]$^{2+}$**	**839.4**	**2459.99**	**0.06**	**100**
	40.6, 41.4	**[substance P ⊗ IRCX + H]$^{+}$**	**1677.7**	**77.85**	**31.29**	**59.8**
11	**40.9**	**[α-MSH ⊗ IRCX ⊗ Ac-RFMWMK-NH_2 + 3H]$^{3+}$**	**978.4**	**894.07**	**0**	**100**
	40.9	**[α-MSH ⊗ IRCX ⊗ Ac-RFMWMK-NH_2 + 2H]$^{2+}$**	**1467.1**	**69.18**	**12.89**	**81.4**
	44.4	**[2(Ac-RFMWMK-NH_2) ⊗ IRCX + 3H]$^{3+}$**	**736.6**	**218.9**	**11.68**	**94.7**
12	**44.4**	**[2(Ac-RFMWMK-NH_2) ⊗ IRCX + 2H]$^{2+}$**	**1104.5**	**1165.07**	**12.79**	**98.9**
13	44.7	[melittin + 5H]$^{5+}$	570.1	19847.59	16037.27	19.2
	44.7	[melittin + 4H]$^{4+}$	712.4	18792.54	19778.43	-5.2
	44.7	[melittin + 3H]$^{3+}$	949.6	4885.16	5050.55	-3.4

4.4.4 LC-IRMPD-MS of IRCX Cross-linked Ubiquitin

To test the utility of LC-IRMPD-MS for screening and identifying IRCX-cross-linked peptides, a trypsin digest of IRCX-cross-linked ubiquitin was analyzed as a model cross-linked protein. Upon incubation with IRCX, ESI-MS analysis indicated that ubiquitin was modified to different degrees. For the lowest molar ratio of cross-linker to protein (5:1), the most abundant species present was unmodified ubiquitin; also observed at approximately the same abundance in the ESI mass spectrum was ubiquitin with a single dead-end modification as well as singly-cross-linked ubiquitin. At a 25:1 molar ratio, upwards of two modifications were observed but the singly-cross-linked species was the most abundant. Unmodified ubiquitin was still detected as the least abundant species. The most abundant species observed in the full mass spectrum of 50:1 IRCX-cross-linked ubiquitin corresponded to the introduction of a single cross-link and a single dead-end modification (**Figure 4.8**). Also observed, but to lesser degrees, was ubiquitin with two IRCX cross-links, as well as ubiquitin possessing three total modifications (combination of two cross-links and one dead-end modification or one cross-link and two dead-end modifications). All LC-IRMPD-MS analyses were performed on the product mixture of the 50:1 molar ratio of IRCX to ubiquitin to eliminate any unmodified ubiquitin from the sample. No separation of the different IRCX cross-linked and modified ubiquitin products was performed, and all products were subjected simultaneously to trypsin digestion. After digestion, the tryptic peptides were separated and analyzed by LC-IRMPD-MS in a similar manner to the mock mixture described above, acquiring isolation and IRMPD spectra of ions of *m/z* 450 – 2000. The RICs for the isolation spectra and IRMPD spectra are shown in **Figure 4.9**, and the eluting species are summarized in **Table 4.3**. The differences between the two chromatograms are dramatic – only the IRCX-cross-linked or modified peptides (species labeled 7 – 13)

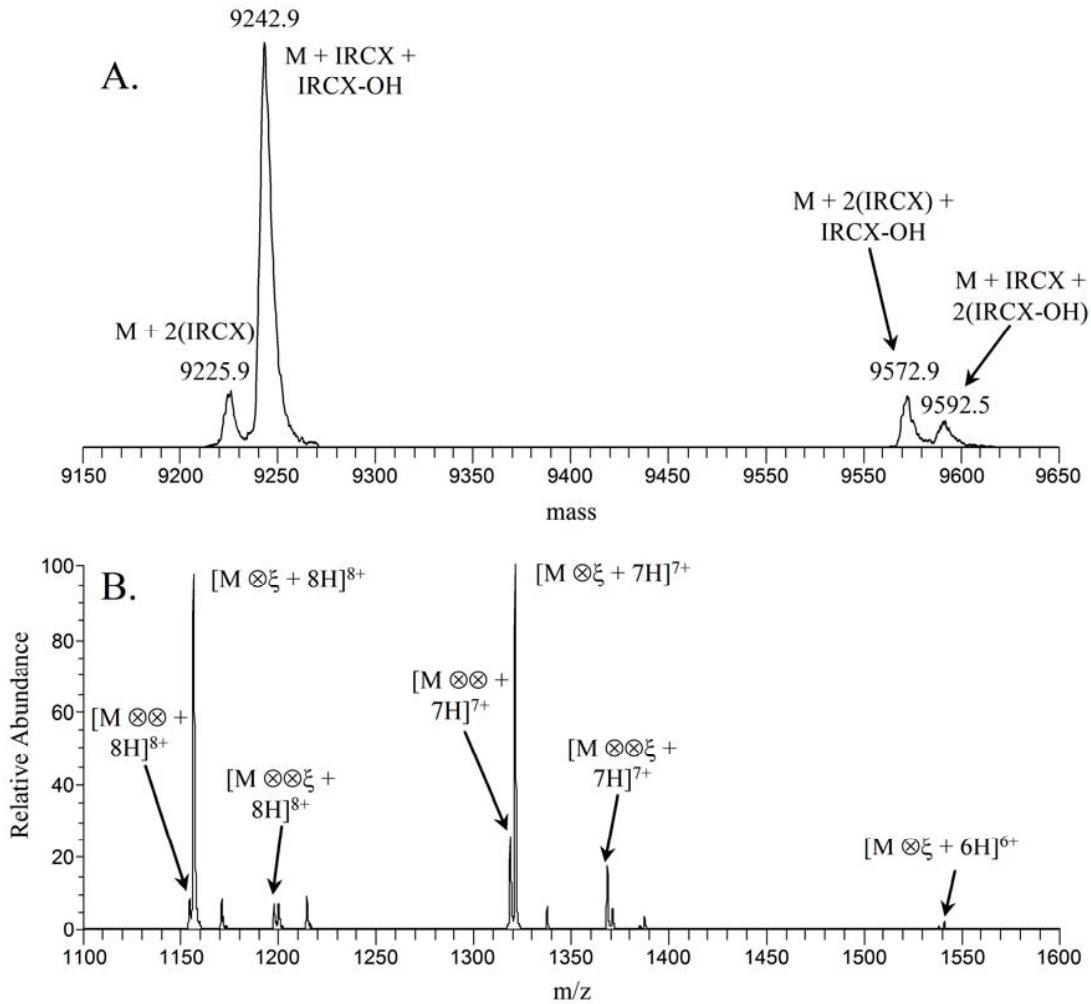

Figure 4.8 Deconvoluted full mass spectrum of IRCX cross-linked ubiquitin (A) and ESI mass spectrum (B) from the 50:1 molar ratio (IRCX to ubiquitin) reaction. IRCX cross-links and IRCX-OH dead-end modifications are represented by ⊗ and ξ, respectively. Ubiquitin is represented by M.

exhibit IRMPD, and upon 50 ms of irradiation decrease in ion abundance to below the detection limit. On average, the unmodified peptide ions exhibited an increase in ion abundance of about 20%, which is attributed to fluctuations in ion trapping during the isolation and IRMPD steps, as well as to differences in the number of ions being injected into the trap between the two scans, despite using the automatic gain control (AGC)

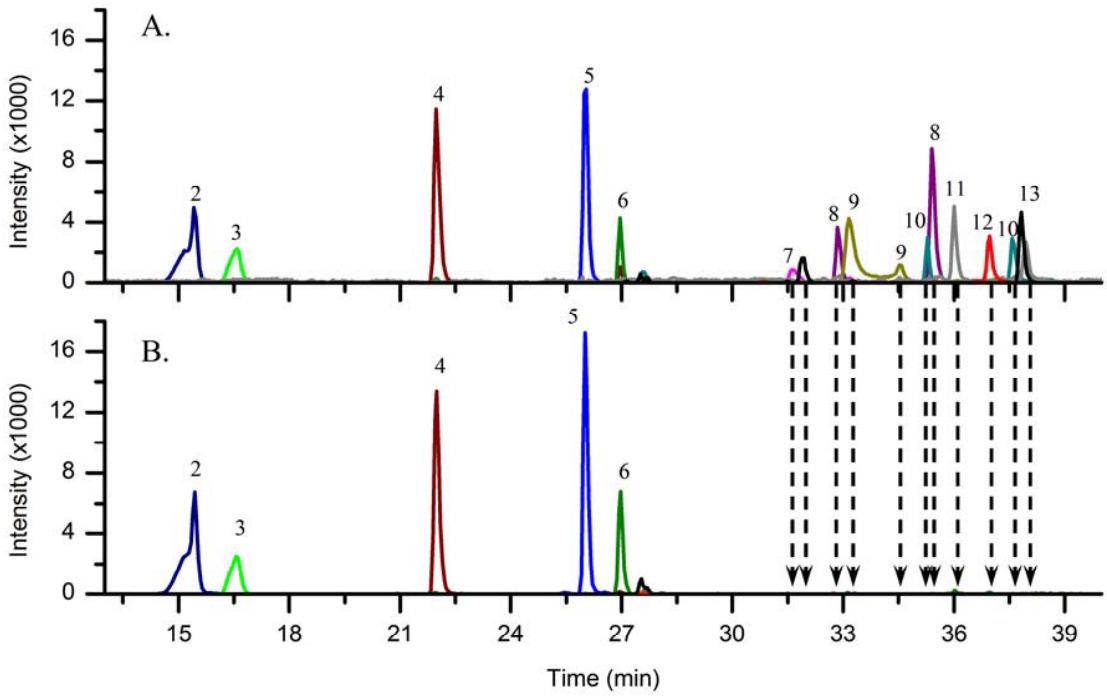

Figure 4.9 Reconstructed ion chromatograms of (A) isolation (50 ms) and (B) IRMPD (50 ms, 50 W) spectra from LC-IRMPD-MS of a tryptic digest of ubiquitin cross-linked by IRCX. See **Table 4.3** for identities of eluting species. Ion chromatogram intensities of $[43\text{-}48]^{+}$ (**3**), $[55\text{-}72]^{3+}$ (**6**), $[30\text{-}42 \otimes \text{IRCX} \otimes 7\text{-}27]^{4+}$ (**7**), $[55\text{-}72 \otimes \text{IRCX} \otimes 30\text{-}42]^{5+}$ (**9**), $[1\text{-}11 + \text{IRCX-OH}]^{2+}$ (**10**), $[55\text{-}72 + \text{IRCX-OH}]^{3+}$ (**11**), and $[55\text{-}72 \otimes \text{IRCX} \otimes 1\text{-}11]^{5+}$ (**13**) were zoomed in by 10× in both (A) and (B).

feature of the ion trap. The IRCX-cross-linked peptides decreased by ~100%, with the exception of $[T^{55}LSDYNIQ\mathbf{K}^{63}ESTLHLVLR^{72} \otimes \text{IRCX} \otimes L^{43}IFAGI\mathbf{K}^{48}QLEDGR^{54} + 4H]^{4+}$, which was reduced in abundance by 92%. The abundance of this quadruply-charged cross-linked peptide likely did not decrease by 100% due to an isobar with the $y_{10\beta}\text{-}17^{3+}$ product ion, corresponding to cleavage C-terminal to the cross-linked Lys-48 of $L^{43}IFAG\mathbf{K}^{48}QLEDGR^{54}$ and incomplete secondary dissociation of this fragment ion. Even with this isobaric overlap, there is a consistent difference in IRMPD efficiencies that allows the IRCX-cross-linked peptides to be readily distinguished.

Table 4.3 Ion abundance decreases upon IR irradiation from LC-IRMPD-MS reconstructed ion chromatograms of a tryptic digest of ubiquitin cross-linked by IRCX. Percent abundance decreases calculated from the decrease of the peak areas of the SICs from the isolation and IRMPD spectra.

Label	Elution (min)	Species	*m/z*	Primary Sequence[a]	Average Percent Abundance Decrease[b]	Std. Dev.[b]
1	0.6	$[30\text{-}42]^{3+}$	509.0	IQDKEGIPPDQQR	31	14
2	15.5	$[55\text{-}63]^{2+}$	541.3	TLSDYNIQK	-28	4
3	16.6	$[43\text{-}48]^{+}$	648.3	LIFAGK	-4	5
4	22	$[64\text{-}72]^{2+}$	534.6	ESTLHLVLR	-28	17
5	26	$[12\text{-}27]^{2+}$	894.6	TITLEVEPSDTIENVK	-37	15
6	27	$[55\text{-}72]^{3+}$	710.8	TLSDYNIQKESTLHLVLR	-66	24
7	**31.6, 33.2**	**[30-42 ⊗ IRCX ⊗ 7-27]$^{4+}$**	**1036.1**	**IQDK*EGIPPDQQR ⊗ IRCX ⊗ TLTGK*TITLEVEPSDTIENVK**	**100**	**0**
8	**32.8. 35.4**	**[43-54 + IRCX-OH]$^{2+}$**	**848.0**	**LIFAGK*QLEDGR + IRCX-OH**	**100**	**0**
9	**33.1**	**[55-72 ⊗ IRCX + 30-42]$^{5+}$**	**797.8**	**TLSDYNIQK*ESTLHLVLR + IRCX + IQDK*EGIPPDQQR**	**100**	**0**
	33.1	**[55-72 ⊗ IRCX ⊗ 30-42]$^{4+}$**	**996.6**	**TLSDYNIQK*ESTLHLVLR ⊗ IRCX ⊗ IQDK*EGIPPDQQR**	**100**	**0**
10	**35.3, 37.6**	**[1-11 + IRCX-OH]$^{2+}$**	**807.0**	**MQIFVK*TLTGK + IRCX-OH**	**99**	**1**
11	**36.0, 37.9**	**[55-72 + IRCX-OH]$^{3+}$**	**826.8**	**TLSDYNIQK*ESTLHLVLR + IRCX-OH**	**100**	**0**
12	**37**	**[55-72 ⊗ IRCX ⊗ 43-54]$^{5+}$**	**762.9**	**TLSDYNIQK*ESTLHLVLR ⊗ IRCX ⊗ LIFAGK*QLEDGR**	**100**	**0**
	37	**[55-72 ⊗ IRCX ⊗ 43-54]$^{4+}$**	**952.8**	**TLSDYNIQK*ESTLHLVLR ⊗ IRCX ⊗ LIFAGK*QLEDGR**	**92**	**5**
	37	**[55-72 ⊗ IRCX ⊗ 43-54]$^{3+}$**	**1269.6**	**TLSDYNIQK*ESTLHLVLR ⊗ IRCX ⊗ LIFAGK*QLEDGR**	**99.4**	**0.8**
13	**37.8**	**[55-72 ⊗ IRCX ⊗ 1-11]$^{5+}$**	**746.9**	**TLSDYNIQK*ESTLHLVLR ⊗ IRCX ⊗ MQIFVK*TLTGK**	**100**	**0**
	37.8	**[55-72 ⊗ IRCX ⊗ 1-11]$^{4+}$**	**932.7**	**TLSDYNIQK*ESTLHLVLR ⊗ IRCX ⊗ MQIFVK*TLTGK**	**99.9**	**0.1**

[a] Site of modification or cross-link represented by *. [b] Percent abundance decreases calculated from the decrease in the peak areas of the SICs from the isolation and the IRMPD mass spectra. Results obtained in triplicate.

While comparing isolation and IRMPD spectra to determine which peptide ions undergo photodissociation upon IR irradiation allows rapid pinpointing of the IRCX-cross-linked peptides, one cannot directly use these IRMPD spectra to locate the site of cross-linking because all ions of *m/z* 450 – 2000 are irradiated simultaneously in the screening step, creating complicated, overlapping dissociation patterns of all IRCX-cross-linked peptides. In order to obtain product ion information of individual cross-linked peptides, data-dependent MS/MS was utilized to isolate and subsequently perform IRMPD on the most abundant ions.

None of the unmodified tryptic peptides of ubiquitin underwent IRMPD, again allowing for them to be distinguished from the IRCX-cross-linked peptides. An example of an IRMPD mass spectrum of an unmodified peptide is shown in **Figure 4.10a** in which doubly-protonated T^{12}ITLEVEPSDTIENVK^{27} does not photodissociate upon 30 ms of IR irradiation; the precursor ion remains the only ion observed in the spectrum. In contrast, IRMPD spectra acquired during the data-dependent LC-IRMPD-MS method for three IRCX-cross-linked peptides are shown in **Figure 4.11**, and in all cases the precursor ions readily photodissociate. For example, the second cross-linked peptide to elute contains T^{55}LSDYNIQ**K**^{63}ESTLHLVLR^{72} (α peptide) linked to I^{30}QD**K**^{33}EGIPPDQQR^{42} (β peptide) through Lys-63 and Lys-33. IRMPD of this cross-linked peptide ion provided ten unique sequence ions (**Figure 4.11a**). No product ions containing the IRCX cross-link were observed, most likely a result of secondary dissociation of these fragment ions. Almost a full series of y_α ions without the IRCX cross-link (e.g., y_α ions C-terminal of the cross-linked Lys-63) were detected, providing a sequence tag for identifying one of the two constituent peptides. The highly abundant y_6 ions, result of cleavage N-terminal to Pro-37, provide information necessary to determine that the β peptide contains P^{37}PDQQR^{42}. However, the corresponding $b_{7\beta}$

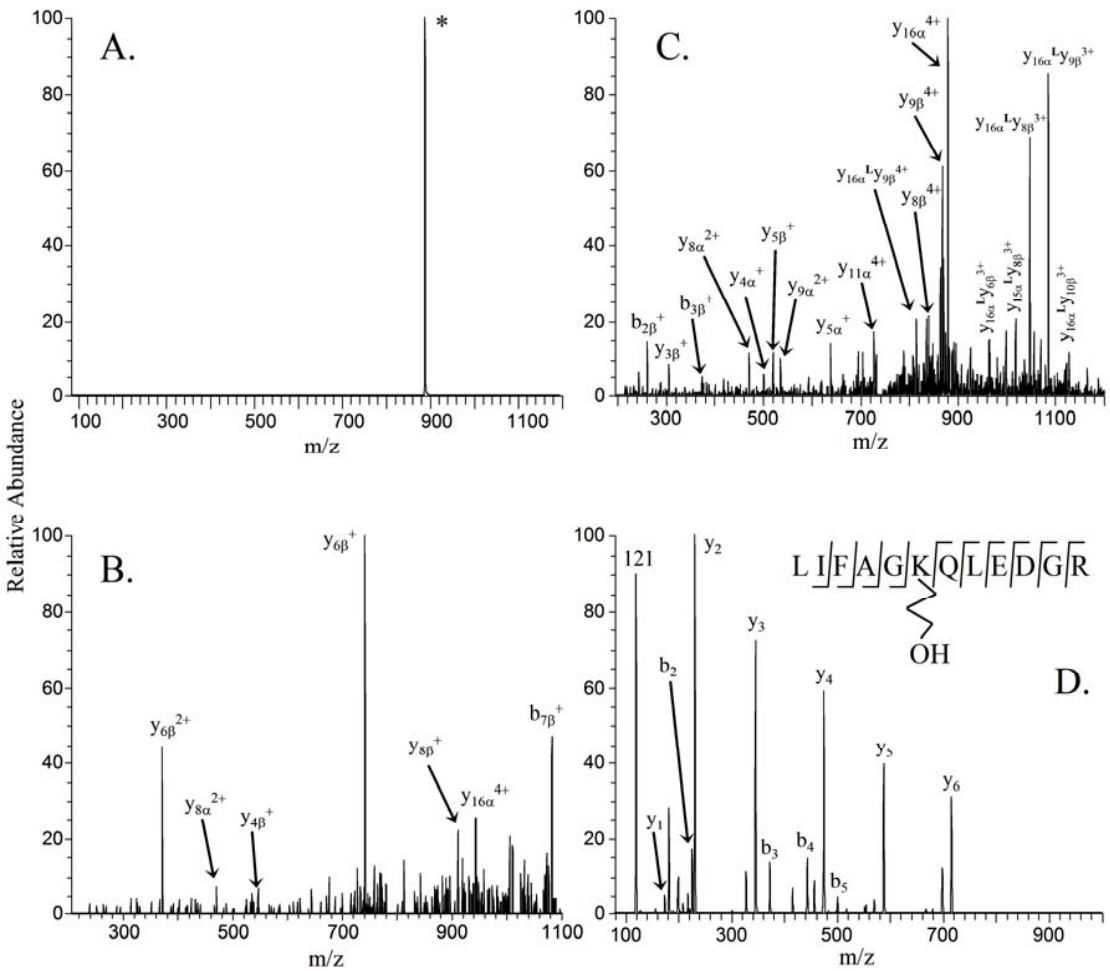

Figure 4.10 Product ion mass spectra of peptides observed in data-dependent LC-IRMPD-MS analysis of tryptic digest of IRCX-cross-linked ubiquitin. (A) IRMPD of $[T^{12}ITLEVEPSDTIENVK^{27} + 2H]^{2+}$ of *m/z* 894.6 (residues 12-27). (B) CID of $[T^{55}LSDYNIQ\mathbf{K}^{63}ESTLHLVLR^{72} \otimes IRCX \otimes I^{30}QD\mathbf{K}^{33}EGIPPDQQR^{42} + 5H]^{5+}$ of *m/z* 797.8. (C) CID of $[T^{55}LSDYNIQ\mathbf{K}^{63}ESTLHLVLR^{72} \otimes IRCX \otimes M^{1}QIFV\mathbf{K}^{6}TLTGK^{11} + 5H]^{5+}$ of *m/z* 746.1. (D) IRMPD of $[L^{43}IFAGI\mathbf{K}^{48}QLEDGR^{54} + IRCX\text{-}OH + 2H]^{2+}$ of *m/z* 848.0. For IRMPD, the precursor ion was irradiated for 30 ms, 50 W, at a q-value of 0.10. For CID, the precursor ion was activated for 30 ms, at 45% normalized collision energy at a q-value of 0.25. The lysine residues in bold font indicate the location of the cross-link or modification. The first peptide listed is the α peptide; the second peptide is referred to as the β peptide. Precursor ions, if observed, are labeled with an asterisk (*).

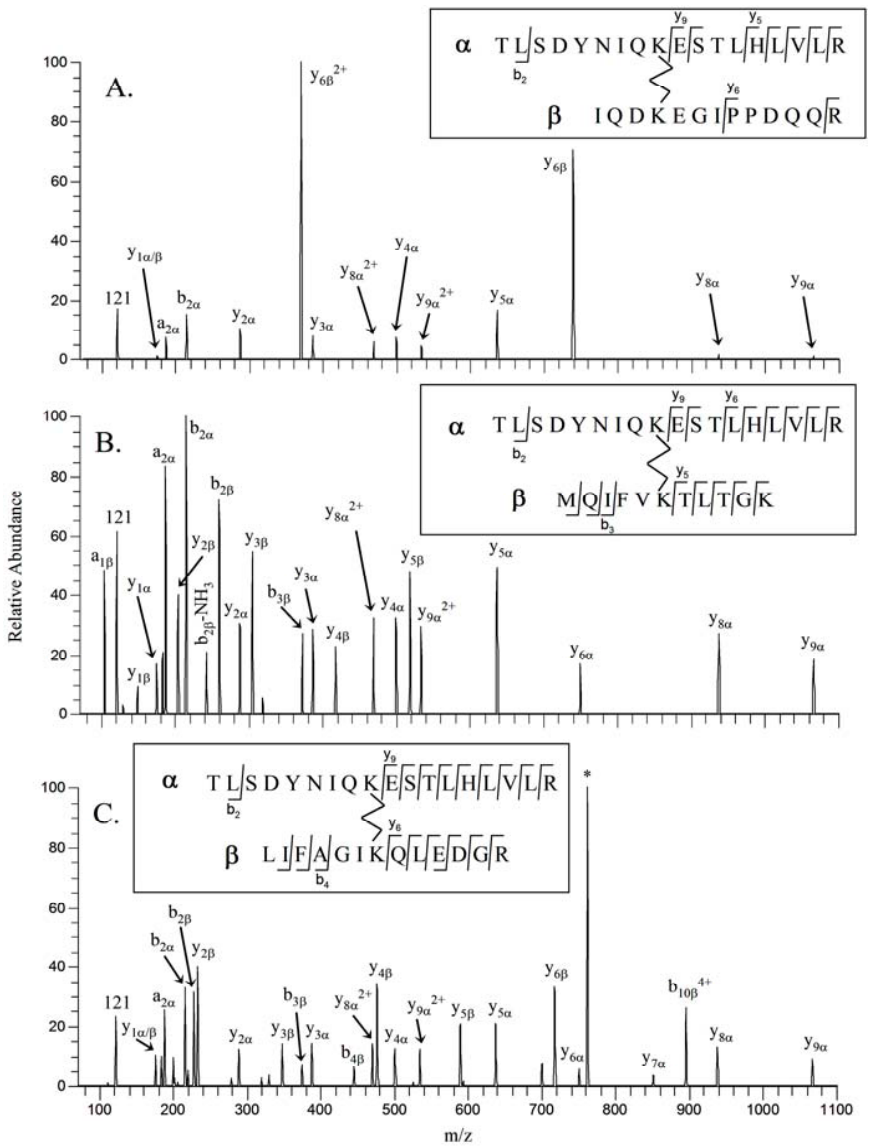

Figure 4.11 IRMPD spectra (30 ms, 50 W, q=0.1) of tryptic peptides of ubiquitin cross-linked by IRCX acquired during data-dependent LC-IRMPD-MS experiment: (A) $[T^{55}LSDYNIQ\mathbf{K}^{63}ESTLHLVLR^{72} \otimes IRCX \otimes I^{30}QD\mathbf{K}^{33}EGIPPDQQR^{42} + 5H]^{5+}$ of *m/z* 797.8, (B) $[T^{55}LSDYNIQ\mathbf{K}^{63}ESTLHLVLR^{72} \otimes IRCX \otimes M^{1}QIFV\mathbf{K}^{6}TLTGK^{11} + 5H]^{5+}$ of *m/z* 746.1, and (C) $[T^{55}LSDYNIQ\mathbf{K}^{63}ESTLHLVLR^{72} \otimes IRCX \otimes L^{43}IFAGI\mathbf{K}^{48}QLEDGR^{54} + 5H]^{5+}$ of *m/z* 762.4. The first peptide listed is the α peptide; the second peptide is referred to as the β peptide. Precursor ions, if observed, are labeled with an asterisk (*).

product ion which contains the chromophore and the α peptide can undergo secondary dissociation to yield additional diagnostic fragment ions. Along with the identity of the α peptide and the intact mass of the cross-linked peptide, one can deduce the identity of the second peptide and finally the location of the cross-link, between Lys-63 and Lys-33. In contrast, CID of the 5+ charge state of this cross-linked peptide yielded only seven identifiable product ions ($y_{6\beta}^{2+}$, $y_{6\beta}^{+}$, $y_{8\alpha}^{2+}$, $y_{4\beta}^{+}$, $y_{8\beta}^{+}$, $y_{16\alpha}^{4+}$, and $b_{7\beta}^{3+}$), three of which correspond to cleavage N-terminal to Pro-37 (**Figure 4.10b**). No sequential series of product ions was observed using CID, and most of the ions observed could not be identified as typical a-, b-, or y-type ions (including double-cleavage products). The IRCX-cross-linked peptide containing T^{55}LSDYNIQ**K**^{63}ESTLHLVLR^{72} (α peptide) and M^{1}QIFV**K**^{6}TLTGK^{11} (β peptide) readily photodissociated upon IR irradiation, yielding only fragment ions without the IRCX chromophore (**Figure 4.11b**). Thirteen of the 14 amide bonds C-terminal to the cross-linked lysines were cleaved by IRMPD, providing a sequence tag for both constituent peptides. CID of this cross-linked peptide yielded a variety of product ions including both b- and y-type fragment ions with and without the cross-link (**Figure 4.10c**). In addition several double-cleavage product ions were observed including a series of $y_{16\alpha}{}^{L}y_{n\beta}$ ions (i.e., $y_{16\alpha}$ fragment linked to a y-ion of the β peptide) which complicate interpretation of the CID mass spectrum. IRMPD alone provides far more diagnostic product ions allowing for the cross-linked peptide to be identified. For the cross-linked peptide ion [T^{55}LSDYNIQ**K**^{63}ESTLHLVLR^{72} ⊗ IRCX ⊗ L^{43}IFAG**K**^{48}QLEDGR^{54} + 5H]$^{5+}$, all of y-ions C-terminal to the two cross-linked lysine residues were detected using IRMPD (**Figure 4.11c**). Using these y-ions, one could easily sequence the C-terminal ends of the two constituent peptides via a de novo approach. In addition, three $b_{n\beta}$ product ions were detected providing confirmation of the identity of the β peptide, L^{43}IFAGI**K**^{48}QLEDGR^{54}. Two dead-end modifications, at Lys-

48 and Lys-6, could also be identified. The IRMPD mass spectrum for the species containing $L^{43}IFAGI\mathbf{K}^{48}QLEDGR^{54}$ modified by IRCX-OH at Lys-48 is shown in **Figure 4.10d**. Cleavage of all backbone amide bonds occurred, yielding a series of b-ions N-terminal to the modified lysine and a series of y-ions C-terminal to the modified lysine, all without the IRCX chromophore.

A majority of the product ions observed upon IRMPD were y-ions without the IRCX cross-link, as opposed to b-ions. Earlier work as discussed in Chapter 3 suggested that there is a preference for cleavage C-terminal to the cross-linked lysine for intermolecularly cross-linked peptides, possibly due to charge localization on the C-terminal arginine residues.[32] Dissociation at this amide bond of the α peptide would result in a y_α-ion with a protonated C-terminal arginine and a b_α-ion retaining the IRCX cross-link and the β peptide. This b_α-ion would likely undergo secondary and higher order dissociation since it contains the phosphate chromophore, possibly producing an uncross-linked y_β-ion. Any secondary product ion still retaining the chromophore may continue to absorb photons and dissociate, resulting in small fragments that are not observed (e.g., neutral fragments, *m/z* below the low-mass cut-off, etc.). However, if a charge is retained on the N-terminus, uncross-linked b-ions would also be detected.

In all of the IRMPD mass spectra of the IRCX-cross-linked and IRCX-OH modified peptides, a product ion of *m/z* 121 was detected This fragment ion, observed only after significant secondary dissociation, corresponds in mass to a double-cleavage product – cleavage of the cross-link amide bond and between the P–O bond nearest the cleaved amide bond. The formation of this diagnostic product ion, which is not isobaric with any immonium ions of the amino acids, provides another means of distinguishing IRCX-cross-linked peptides from unmodified ones. Using traditional CID, one would not observe this reporter ion as it has an *m/z* value below the low-mass cut-off.

Moreover, as a higher-order product ion, it is only observed after significant secondary dissociation afforded by IRMPD, not CID.

In total, four cross-links and two dead-end modifications were identified using the IRCX and LC-IRMPD-MS strategy, as summarized in **Table 4.4**. IRCX has a spacer-arm length of ~16 Å and given the flexibility of lysine side chains, distances of ~28 Å between α-carbons of lysines could be spanned. For all four of the observed cross-links, the distance between the α-carbons was less than 20 Å based on the x-ray crystal structure (PDB: 1AAR). The two phenyl groups of IRCX create a more rigid cross-linker that may not be able to easily span short distances, as evident by the fact that no cross-links spanning a distance of less than 13 Å were observed. The rigidity of IRCX would not promote the formation of short cross-links as the one observed between Lys-6 and Lys-11 (Δx = 5.8 Å) in a previous study using DSS.[54] Three of the four cross-links identified in the present study involved Lys-63, which is located on the surface of ubiquitin. Upon creation of an amide bond between IRCX and Lys-63, the other NHS-ester of IRCX could react with other surface-accessible lysines within 20 Å, including Lys-48, Lys-33, and Lys-6, yielding a mixture of cross-linked products, as observed. While other lysines are potential sites of cross-linking, Lys-63 is likely more reactive resulting in limited structural information. Recently, a partial acetylation technique has been used to enhance the diversity of cross-linking reactions by blocking the more reactive lysine residues to provide more comprehensive distance constraints.[55] Using such an approach may yield more informative cross-links between other lysine pairs. The two dead-end modifications were located at Lys-48 and Lys-6, two other surface-accessible primary amines that were also observed to be cross-linked.

Table 4.4 Summary of cross-links and modifications of ubiquitin identified using IRCX and LC-IRMPD-MS.

Tryptic Fragment	Peptide Sequence(s)[a]	Complex Mass Measured[b]	Complex Mass Calculated[b]	Charge States Observed	Cross-linked /Modified Site(s)	Distance (Å)[c]
30-42	IQDK*EGIPPDQQR	4140.4	4140	4+	Lys-33	13.3
7-27	TLTGK*TITLEVEPSD TIENVK				Lys-11	
55-72	TLSDYNIQK*ESTLHL VLR	3982.8	3982	5+, 4+	Lys-63	19.6
30-42	IQDK*EGIPPDQQR				Lys-33	
55-72	TLSDYNIQK*ESTLHL VLR	3805.7	3804.9	5+, 4+, 3+	Lys-63	18.4
43-54	LIFAGIK*QLEDGR				Lys-48	
55-72	TLSDYNIQK*ESTLHL VLR	3724.9	3723.9	5+, 4+	Lys-63	15.1
1-11	MQIFVK*TLTGK				Lys-6	
43-54	LIFAGIK*QLEDGR	1693.8	1694.8	2+	Lys-48	n/a
1-11	MQIFVK*TLTGK	1613.3	1613.8	2+	Lys-6	n/a

[a] Site of modification or cross-link represented by *. [b] Neutral monoisotopic mass in Da. [c] Distance between α-carbons of lysine residues calculated from X-ray crystal structure of ubiquitin (PDB: 1AAR).

4.5 CONCLUSIONS

By incorporating a phosphate chromophore into the chemical cross-linker IRCX, it has been shown that both intra- and intermolecularly cross-linked peptides can be rapidly distinguished from unmodified peptides using IRMPD-MS. Using 50 ms of irradiation, only the IRCX cross-linked or dead-end modified peptides underwent efficient photodissociation, thus allowing the identification of these key species by simply comparing ion abundances before and after exposure to IR irradiation. This technique has been successfully applied to both direct-infusion ESI-IRMPD-MS and online LC-IRMPD-MS using data-dependent MS/MS experiments for a mock mixture of peptides and a tryptic digest of IRCX-cross-linked ubiquitin. For the cross-linked ubiquitin sample, a total of four cross-links and two dead-end modifications were

observed, and the locations of the cross-links were unambiguously identified. IRMPD of the intermolecularly cross-linked peptides yielded a series of y-ions C-terminal to the cross-linked lysines without the IRCX cross-link due to secondary dissociation of fragment ions containing the chromophore. These product ions could then be used to sequence each of the two constituent peptides in a de novo manner, potentially providing a ready means to identify not only the cross-linked peptides but also the proteins in an intracellular chemical cross-linking experiment.

4.6 REFERENCES

(1) Borch, J.; Jorgensen, T. J. D.; Roepstorff, P. *Current Opinion in Chemical Biology* **2005**, *9*, 509-516.

(2) Heck, A. J. R.; van den Heuvel, R. H. H. *Mass Spectrometry Reviews* **2004**, *23*, 368-389.

(3) Back, J. W.; De Jong, L.; Muijsers, A. O.; De Koster, C. G. *Journal of Molecular Biology* **2003**, *331*, 303-313.

(4) Sinz, A. *Mass Spectrometry Reviews* **2006**, *25*, 663-682.

(5) Sinz, A. *Journal of Mass Spectrometry* **2003**, *38*, 1225-1237.

(6) Young, M. M.; Tang, N.; Hempel, J. C.; Oshiro, C. M.; Taylor, E. W.; Kuntz, I. D.; Gibson, B. W.; Dollinger, G. *Proceedings of the National Academy of Sciences of the United States of America* **2000**, *97*, 5802-5806.

(7) Huang, B. X.; Kim, H.-Y.; Dass, C. *Journal of the American Society for Mass Spectrometry* **2004**, *15*, 1237-1247.

(8) Carlsohn, E.; Angstrom, J.; Emmett, M. R.; Marshall, A. G.; Nilsson, C. L. *International Journal of Mass Spectrometry* **2004**, *234*, 137-144.

(9) Lanman, J.; Lam, T. T.; Barnes, S.; Sakalian, M.; Emmett, M. R.; Marshall, A. G.; Prevelige, P. E. *Journal of Molecular Biology* **2003**, *325*, 759-772.

(10) Back, J. W.; Sanz, M. A.; De Jong, L.; De Koning, L. J.; Nijtmans, L. G. J.; De Koster, C. G.; Grivell, L. A.; Van Der Spek, H.; Muijsers, A. O. *Protein Science* **2002**, *11*, 2471-2478.

(11) Mueller, D. R.; Schindler, P.; Towbin, H.; Wirth, U.; Voshol, H.; Hoving, S.; Steinmetz, M. O. *Analytical Chemistry* **2001**, *73*, 1927-1934.

(12) Back, J. W.; Notenboom, V.; de Koning, L. J.; Muijsers, A. O.; Sixma, T. K.; de Koster, C. G.; de Jong, L. *Analytical Chemistry* **2002**, *74*, 4417-4422.

(13) Chu, F.; Mahrus, S.; Craik, C. S.; Burlingame, A. L. *Journal of the American Chemical Society* **2006**, *128*, 10362-10363.

(14) Ihling, C.; Schmidt, A.; Kalkhof, S.; Schulz, D. M.; Stingl, C.; Mechtler, K.; Haack, M.; Beck-Sickinger, A. G.; Cooper, D. M. F.; Sinz, A. *Journal of the American Society for Mass Spectrometry* **2006**, *17*, 1100-1113.

(15) Wine, R. N.; Dial, J. M.; Tomer, K. B.; Borchers, C. H. *Analytical Chemistry* **2002**, *74*, 1939-1945.

(16) Sinz, A.; Wang, K. *Biochemistry* **2001**, *40*, 7903-7913.

(17) Sinz, A.; Wang, K. *Analytical Biochemistry* **2004**, *331*, 27-32.

(18) Bennett, K. L.; Kussmann, M.; Bjork, P.; Godzwon, M.; Mikkelsen, M.; Sorensen, P.; Roepstorff, P. *Protein Science* **2000**, *9*, 1503-1518.

(19) Petrotchenko, E. V.; Olkhovik, V. K.; Borchers, C. H. *Molecular and Cellular Proteomics* **2005**, *4*, 1167-1179.

(20) Trester-Zedlitz, M.; Kamada, K.; Burley, S. K.; Fenyoe, D.; Chait, B. T.; Muir, T. W. *Journal of the American Chemical Society* **2003**, *125*, 2416-2425.

(21) Hurst, G. B.; Lankford, T. K.; Kennel, S. J. *Journal of the American Society for Mass Spectrometry* **2004**, *15*, 832-839.

(22) Sinz, A.; Kalkhof, S.; Ihling, C. *Journal of the American Society for Mass Spectrometry* **2005**, *16*, 1921-1931.

(23) Back, J. W.; Hartog, A. F.; Dekker, H. L.; Muijsers, A. O.; de Koning, L. J.; de Jong, L. *Journal of the American Society for Mass Spectrometry* **2001**, *12*, 222-227.

(24) Tang, X.; Munske, G. R.; Siems, W. F.; Bruce, J. E. *Analytical Chemistry* **2005**, *77*, 311-318.

(25) Chowdhury, S. M.; Munske, G. R.; Tang, X.; Bruce, J. E. *Analytical Chemistry* **2006**, *78*, 8183-8193.

(26) Schilling, B.; Row, R. H.; Gibson, B. W.; Guo, X.; Young, M. M. *Journal of the American Society for Mass Spectrometry* **2003**, *14*, 834-850.

(27) Gao, Q.; Xue, S.; Doneanu, C. E.; Shaffer, S. A.; Goodlett, D. R.; Nelson, S. D. *Analytical Chemistry* **2006**, *78*, 2145-2149.

(28) Chen, T.; Jaffe, J. D.; Church, G. M. *Journal of Computational Biology* **2001**, *8*, 571-583.

(29) Tang, Y.; Chen, Y.; Lichti, C. F.; Hall, R. A.; Raney, K. D.; Jennings, S. F. *BMC Bioinformatics* **2005**, *6*, S9.

(30) de Koning, L. J.; Kasper, P. T.; Back, J. W.; Nessen, M. A.; Vanrobaeys, F.; Van Beeumen, J.; Gherardi, E.; de Koster, C. G.; de Jong, L. *FEBS Journal* **2006**, *273*, 281-291.

(31) Seebacher, J.; Mallick, P.; Zhang, N.; Eddes, J. S.; Aebersold, R.; Gelb, M. H. *Journal of Proteome Research* **2006**, *5*, 2270-2282.

(32) Gardner, M. W.; Brodbelt, J. S. *Journal of the American Society for Mass Spectrometry* **2008**, *19*, 344-357.

(33) Soderblom, E. J.; Goshe, M. B. *Analytical Chemistry* **2006**, *78*, 8059-8068.

(34) Soderblom, E. J.; Bobay, B. G.; Cavanagh, J.; Goshe, M. B. *Rapid Communications in Mass Spectrometry* **2007**, *21*, 3395-3408.

(35) Little, D. P.; Speir, J. P.; Senko, M. W.; O'Connor, P. B.; McLafferty, F. W. *Analytical Chemistry* **1994**, *66*, 2809-2815.

(36) Payne, A. H.; Glish, G. L. *Analytical Chemistry* **2001**, *73*, 3542-3548.

(37) Flora, J. W.; Muddiman, D. C. *Analytical Chemistry* **2001**, *73*, 3305-3311.

(38) Flora, J. W.; Muddiman, D. C. *Journal of the American Chemical Society* **2002**, *124*, 6546-6547.

(39) Crowe, M. C.; Brodbelt, J. S. *Journal of the American Society for Mass Spectrometry* **2004**, *15*, 1581-1592.

(40) Crowe, M. C.; Brodbelt, J. S. *Analytical Chemistry* **2005**, *77*, 5726-5734.

(41) Flora, J. W.; Muddiman, D. C. *Journal of the American Society for Mass Spectrometry* **2004**, *15*, 121-127.

(42) Colorado, A.; Shen, J. X.; Brodbelt, J. *Analytical Chemistry* **1996**, *68*, 4033-4043.

(43) Gabryelski, W.; Li, L. *Rapid Communications in Mass Spectrometry* **2002**, *16*, 1805-1811.

(44) Goolsby, B. J.; Brodbelt, J. S. *Analytical Chemistry* **2001**, *73*, 1270-1276.

(45) Hashimoto, Y.; Hasegawa, H.; Waki, I. *Rapid Communications in Mass Spectrometry* **2004**, *18*, 2255-2259.

(46) Stephenson, J. L., Jr.; Booth, M. M.; Shalosky, J. A.; Eyler, J. R.; Yost, R. A. *Journal of the American Society for Mass Spectrometry* **1994**, *5*, 886-893.

(47) Wilson, J. J.; Brodbelt, J. S. *Analytical Chemistry* **2006**, *78*, 6855-6862.

(48) Jones, J. L.; Dongre, A. R.; Somogyi, A.; Wysocki, V. H. *Journal of the American Chemical Society* **1994**, *116*, 8368-8369.

(49) Huddleston, M. J.; Annan, R. S.; Bean, M. F.; Carr, S. A. *Journal of the American Society for Mass Spectrometry* **1993**, *4*, 710-717.

(50) Carr, S. A.; Huddleston, M. J.; Annan, R. S. *Analytical Biochemistry* **1996**, *239*, 180-192.

(51) DeGnore, J. P.; Qin, J. *Journal of the American Society for Mass Spectrometry* **1998**, *9*, 1175-1188.

(52) Szczepanowska, J.; Zhang, X.; Herring, C. J.; Qin, J.; Korn, E. D.; Brzeska, H. *Proceedings of the National Academy of Sciences of the United States of America* **1997**, *94*, 8503-8508.

(53) Gaucher, S. P.; Hadi, M. Z.; Young, M. M. *Journal of the American Society for Mass Spectrometry* **2006**, *17*, 395-405.

(54) Kruppa, G. H.; Schoeniger, J.; Young, M. M. *Rapid Communications in Mass Spectrometry* **2003**, *17*, 155-162.

(55) Guo, X.; Bandyopadhyay, P.; Schilling, B.; Young, M. M.; Fujii, N.; Aynechi, T.; Guy, R. K.; Kuntz, I. D.; Gibson, B. W. *Analytical Chemistry* **2008**, *80*, 951-960.

Chapter 5

Ultraviolet Photodissociation Mass Spectrometry of Bis-aryl Hydrazone Conjugated Peptides

5.1 OVERVIEW

Ultraviolet photodissociation (UVPD) at 355 nm was used to rapidly identify peptides which had been chemically conjugated through bis-aryl hydrazone (BAH) moieties. The two biomolecules of interest were separately tagged to introduce either an aldehyde or a hydrazine and then were conjugated together through these functional groups to form the UV-chromogenic BAH-group. In a mock mixture of peptides, UVPD was used to screen for the BAH-conjugated peptides in direct infusion ESI-UVPD-MS and online LC-UVPD-MS methods by comparing the abundances of the ions with the laser off and with the laser on. Only the BAH-conjugated peptides were observed to photodissociate upon exposure to UV irradiation, thus affording excellent selectivity for the pinpointing the relevant conjugated peptides in a complex mixture of non-conjugated peptides. UVPD analysis of conjugated model peptides indicated that the UVPD efficiencies of these species were charge state dependent. BAH-conjugated peptides that had a mobile proton which could protonate the basic BAH-moiety underwent more efficient photodissociation than the peptide ions with sequestered protons. Ultraviolet photodissociation of BAH-cross-linked peptides also yielded more diagnostic sequence ions than CID to unambiguously locate the site of conjugation.

5.2 INTRODUCTION

In the past decade the conjugation of proteins and peptides to other biomolecules has gained widespread attention as a means to couple the independent functionalities and properties of each individual component. One area of particular interest has been in utilizing peptides or small proteins which can pass through biological membranes as delivery vehicles for peptides, proteins, drugs, oligonucleotides, or other therapeutic agents.[1] Cell penetrating peptides or protein transduction domains have shown promise as an effective means for direct transcellular delivery without extensive degradation.[2, 3] One common method to conjugate biological species is a two-step protocol in which first each biomolecule is separately labeled to introduce either aldehyde or hydrazine moieties. The aldehyde-modified peptide is then linked to the hydrazide-modified ligand (or vice versa) forming a UV chromogenic bis-aryl hydrazone (BAH) bond, which absorbs well at 354 nm.[4] The coupling of aldehyde functionalities to hydrazides has been used to create many protein-peptide conjugates including a follicle-stimulating hormone mutant protein-occludin peptide complex,[5] immunogenic poly-glutamic acid-protein conjugates to anthrax,[6] insulin-transferrin complexes,[7] as well as oxylipid-protein,[8] small molecule-peptide,[9] and many oligonucleotide-protein complexes.[10-12] Analysis of these bioconjugates is typically performed using gel electrophoresis or spectrophotometric methods, but these methods do not provide specific information about the location of the cross-link. LC-MS/MS methods are commonly used for more detailed structural analysis of bioconjugates, usually in conjunction with enzymatic digestion to convert large macromolecules into smaller constituents.[7, 8, 13] Although creating more manageable components, the enzymatic digestion step also results in more complex mixtures containing many species that offer no direct information about the conjugation sites.

As the interest in using protein and peptide conjugates for therapeutic applications continues to expand, there are several ongoing analytical challenges related to characterization of the conjugates, especially in the context of the LC-MS/MS methods mentioned above that are used to analyzed the complex digests and decipher the conjugation sites. Two of the most significant challenges include the ability to rapidly distinguish the conjugated peptides of interest from the uninformative peptides (e.g. dead-end modified or unmodified peptides) and interpretation of the product ion (MS/MS) spectra of the cross-linked peptide-peptide complexes to identify the site of conjugation. Several mass spectrometric strategies have been developed to aid in the identification of cross-linked peptides, with much work devoted to the design and synthesis of novel cross-linkers. Some methods have focused on distinguishing conjugated peptides from unmodified ones by incorporating affinity tags into the linkers to enrich the peptides of interest in complex mixtures,[14-17] or using isotopically labeled cross-linking reagents to pinpoint conjugated peptide ions in the mass spectra,[15, 18, 19] introducing a reporter ion which is observed upon low-energy collision-induced dissociation (CID),[20] or utilizing fluorogenic cross-linkers to differentiate between conjugated and unmodified peptides during a front-end LC separation.[21-23] Other groups have aimed at simplifying interpretation of the product ion spectra of intermolecularly cross-linked peptides by incorporating gas-phase labile bonds which can be cleaved upon low energy CID, thus yielding two modified peptides that can then be individually sequenced by a second stage of CID.[14, 24-26]

Each of these techniques, however, only focuses on one of the two challenges mentioned above – either distinguishing cross-linked peptides from uninformative ones in mixtures or sequencing the cross-linked peptides of interest. As discussed previously in Chapter 4, an IR chromogenic cross-linker which contained a phosphate chromophore

promoted the selective infrared multiphoton dissociation (IRMPD) of cross-linked peptides for differentiation of cross-linked peptides from unmodified ones.[27] IRMPD of these cross-linked peptides also yielded a series of y-type fragment ions C-terminal to the cross-linked lysine residues which allowed the two constituent peptides to be sequenced without the need for MS^n methods. However, this technique, as well as those described above, suffered in distinguishing between cross-linked peptides of interest and dead-end modified peptides (e.g. peptides that have reacted with the cross-linker but the other reactive site of the cross-linker has been hydrolyzed) which generally are not structurally informative. In addition, phosphorylated peptides could be initially falsely classified as IRCX-cross-linked peptides as they also contain the same phosphate chromophore and thus would efficiently dissociate upon IR irradiation.[28]

In this chapter, ultraviolet photodissociation at 355 nm in a quadrupole ion trap mass spectrometer is used to selectively photodissociate only the chromogenic bis-aryl hydrazone conjugated peptides. In recent years, UVPD has been utilized as an alternative to CID as an ion activation technique for peptides.[29-32] Compared to CID, UVPD in ion traps affords several advantages such as secondary dissociation of primary product ions and a potential reduction in ion losses due to scattering since photodissociation does not alter ion trajectories. Moreover, as a non-resonant process, UVPD can be performed at a lower rf trapping voltage than CID which facilitates the detection of diagnostic low-mass product ions. Photodissociation methods have also been used as a screening tool to selectively dissociate specific chromogenic species, such as phosphorylated peptides using IRMPD at 10.6 μm,[28, 33, 34] disulfide bonds at 157 nm,[35] and tyrosyl-containing peptides at 220 and 262 nm.[36, 37] UVPD is used as a selective dissociation method to screen the chromogenic BAH-conjugated peptides in complex mixtures, as demonstrated for a mixture of peptides, using both direct infusion ESI-MS and online LC-UVPD-MS

techniques. Upon UV irradiation at 355 nm, only the BAH-conjugated peptides are shown to undergo photodissociation. In contrast, the non-conjugated aldehyde- and hydrazine-modified peptides or other non-BAH peptides do not absorb at 355 nm and thus do not photodissociate, offering a high degree of selectivity for the rapid identification of the conjugated peptides of interest.

5.3 EXPERIMENTAL

5.3.1 Chemicals and Reagents

The peptides Ac-RFMWMK-NH_2, α-MSH (Ac-SYSMEHFRWGKPV-NH_2), neurotensin (Pyr-LYENKPRRPYIL), and substance P were purchased from Bachem (Torrance, CA). The peptide angiotensin II was obtained from AnaSpec (San Jose, CA). The peptides bradykinin, YGGFM, and disuccinimidyl suberate (DSS) were purchased from Sigma (St. Louis, MO). The peptides Ac-AAAKAAAAR and Ac-AAAKPAAAR were synthesized at the Protein Microanalysis Facility at the University of Texas at Austin and purified by reversed-phase HPLC. Benzaldehyde and 2-hydrazinopyridine were obtained from Aldrich (Milwaukee, WI). Succinimidyl 4-hydrazinonicotinate acetone hydrazone (SANH) and succinimidyl 4-formylbenzoate (SFB) were from Pierce Biotechnology (Rockford, IL). All other chemical and solvents (HPLC grade) were purchases from Fisher Scientific (Fairlawn, NJ).

5.3.2 Synthesis of Benzaldehyde-2-pyridinylhydrazone and UV-Vis Measurements

The ultra-violet chromophore benzaldehyde-2-pyridinylhydrazone (B2PH) was synthesized by dissolving 1.0 mmol of 2-hydrazinopyridine in 2.0 mL of MeOH and then 102 μL (1.0 mmol) of benzaldehyde was added. The solution was heated to 55 °C and

stirred for 16 hours. The reaction mixture was then cooled to room temperature, and the yellow-orange precipitate of B2PH was vacuum filtered. The final product was redissolved in MeOH and then diluted to 50 μM for downstream analysis. All UV-Vis measurements were obtained on an Agilent 8453 spectrophotometer (Santa Clara, CA).

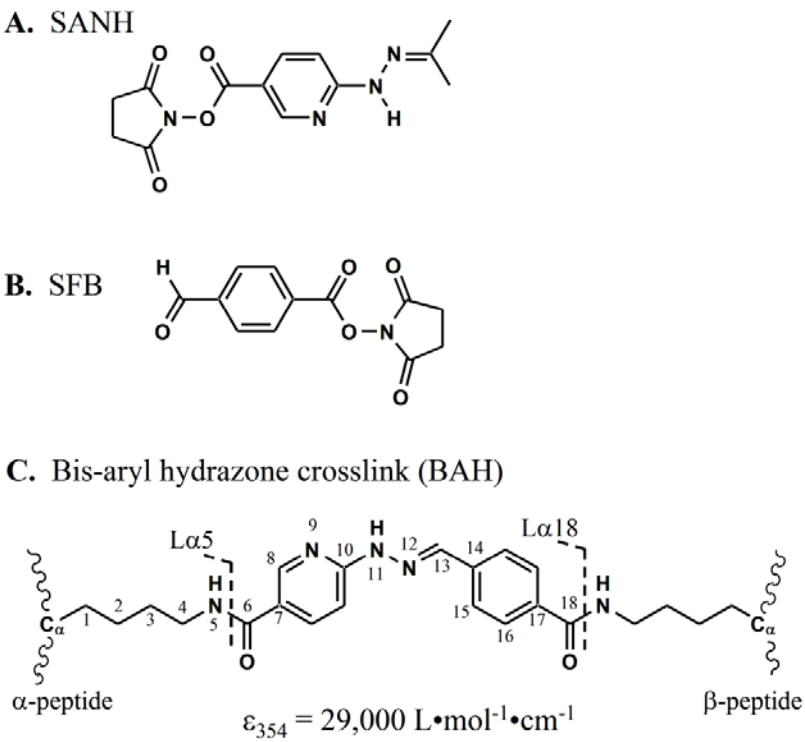

Figure 5.1 Structures of the modifying reagents (A) succinimidyl 4-hydrazinonicotinate acetone hydrazone (SANH), and (B) succinimidyl 4-formylbenzoate (SFB), as well as the (C) bis-aryl hydrazone cross-link and observed bond cleavages. The solution-phase molar absorptivity of the BAH-cross-link is reported.[4] Numbering scheme in (C) refers to the number of atoms away from the C_α atom of the peptide backbone in the α-peptide.[38]

5.3.3 Chemical Cross-linking of Model Peptides.

Model peptides were cross-linked together via a two-step conjugation method. All peptides were dissolved to 5.0 mM in H_2O, and the modifying reagents SANH and SFB (**Figure 5.1a and 5.1b**) were each freshly prepared at 20.0 mM in DMSO. Each

peptide was individually modified at its primary amines (e.g. free N-termini or lysine residues) by either SANH or SFB in 20 mM HEPES, pH 8.0 buffer at a 1:10 molar ratio of peptide to modifier (200 μM: 2.0 mM). The reactions were allowed to proceed at room temperature overnight to ensure complete modification of the peptides; the product mixture was then desalted using Waters tC_{18} SepPak cartridges (Milford, MA) and peptides were eluted with 100% MeOH. The two modified peptides were then conjugated together at an equimolar ratio (~100 μM) in 99/1 MeOH/HOAc acid at 55 °C overnight forming a bis-aryl hydrazone cross-link (**Figure 5.1c**). The conjugated peptides were subsequently diluted to ~10 μM in 49.5:49.5:1 H_2O/MeOH/HOAc (v/v/v) for ESI-MS analysis without any further purification.

5.3.4 Analytical High-Performance Liquid Chromatography

Liquid chromatography was performed with a Waters 2695 Separations Module and 486 Tunable Absorbance Detector (Milford, MA), which were both controlled by the Millennium version 3.00 software package. Reversed-phase HPLC was accomplished using a Symmetry300 C_{18} column (2.1 × 50 mm, 3.5 μm packing) using a gradient elution consisting of (A) H_2O with 0.1% formic acid and (B) acetonitrile with 0.1% formic acid at a flow rate of 0.300 mL/min. The mobile phase was held at 95% A for two minutes after sample injection (typically 10 μL of ~10 μM solutions) and then linearly reduced to 60% over 60 minutes. Analytes were detected by UV-Vis absorption spectroscopy at 355 nm as well as by mass spectrometry.

5.3.5 Mass Spectrometry and Ultraviolet Photodissociation

Mass spectrometry experiments were performed on a modified ThermoFinnigan LCQ Deca XP quadrupole ion trap mass spectrometer (San Jose, CA) using the XCalibur version 1.3 software package as previously described.[30] For all direct infusion experiments the solutions were infused at 2.5 μL/min using an ESI voltage of 4.5 kV. Ultraviolet photodissociation (UVPD) was performed with a Spectra-Physics Quanta-Ray GCR-11 Nd:YAG laser with a HG-2 harmonics generator (Mountain View, CA) to produce the tripled harmonic photons at 355 nm. Briefly, a CF viewport flange was welded to the vacuum manifold of the LCQ Deca XP instrument and fitted with a quartz window to allow the transmission of UV radiation. The unfocused laser beam was aligned on-axis with a 5-mm hole drilled through the ring electrode to irradiate the ion cloud. For all direct infusion UVPD-MS experiments, the laser was operated at full power (~65 mJ/pulse), unless otherwise noted, at a repetition rate of 10 Hz in the Q-switched mode. The LCQ instrument TTL signal output from pin TP 15-3 Sync_TP was used to trigger a Model 505-2C low-voltage pulse generator (Berkeley Nucleonics Corp., San Rafael, CA) which in turn was used to pulse the laser. Typically, the activation time was set to 1000 ms to produce ten laser pulses unless indicated otherwise. The instrument control files were modified to allow triggering of the laser during LC-MS/MS analyses. Precursor ions were activated at a q_z-value of 0.25 for CID and 0.10 for UVPD. Energy-variable CID experiments were performed by stepping-up the CID voltage to determine the voltage necessary to dissociate the precursor ion to 50% relative abundance as previously described.[27] Online LC-UVPD-MS was performed by either isolating ions of *m/z* 450 – 1200 without any form of activation or by subjecting all ions of *m/z* 450 – 1200 to ten pulses of UV irradiation at 355 nm. In order to acquire an isolation spectrum, a precursor ion of interest was selected for activation at a normalized collision energy of

0.0% and the isolation waveform was turned off, allowing ions to be effectively isolated and detected.

5.4 RESULTS AND DISCUSSION

5.4.1 Bis-aryl Hydrazone Chromophore and UVPD Screening Strategy

The conjugation strategy employs a two-step conjugation method in which the two biomolecules of interest are first tagged by either SANH that introduces a hydrazine group or by SFB which incorporates an aromatic aldehyde (**Scheme 5.1**). The two modified biomolecules are then cross-linked together through a specific reaction between the hydrazine and aldehyde to form a bis-aryl hydrazone. As shown in this study, the two-stage conjugation reaction affords a high degree of UVPD selectivity when analyzing mixtures containing unmodified, dead-end modified, and conjugated peptides. Ultraviolet photodissociation can be used to rapidly screen for BAH-conjugated peptides in which only the peptide ions that readily absorb radiation at 355 nm dissociate. Unmodified peptides, as well as those with dead-end SFB- or SANH-modifications, will not photodissociate as they do not contain the critical BAH-chromophore. The selective photodissociation of all BAH-cross-linked peptides allows ready differentiation between diagnostic conjugated peptides and unmodified ones as well as uninformative dead-end modified species.

Prior to conducting peptide conjugation experiments with the SANH and SFB reagents, the chromophore of the bis-aryl hydrazone cross-link was duplicated in a model compound by synthesis of benzaldehyde-2-pyridinylhydrazone (B2PH, **Figure 5.2b**) and characterized by UV-Vis spectroscopy and UVPD-MS. The UV-Vis absorbance spectrum of this molecule at 50 μM in MeOH did not reveal an absorption band around

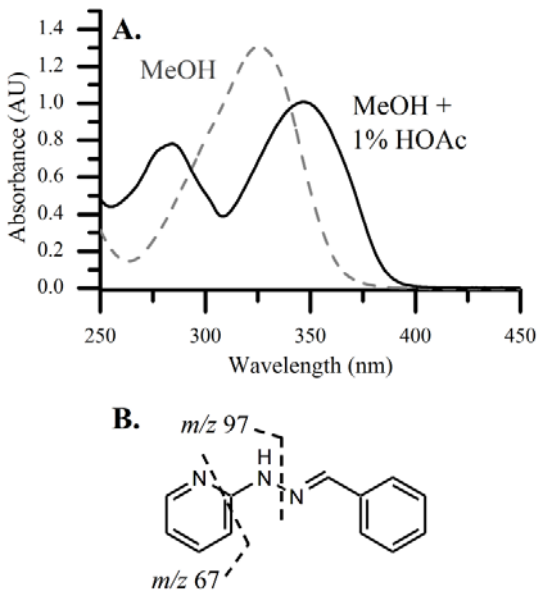

Figure 5.2 (A) UV-Vis spectra of 50 μM benzaldehyde-2-pyridinylhydrazone in MeOH (dashed gray line) and in 99/1 MeOH/HOAc (v/v) (solid black line). (B) Structure of benzaldehyde-2-pyridinylhyrazone and product ions observed by UVPD-MS.

355 nm, the wavelength of a tripled Nd:YAG laser, as shown in **Figure 5.2a**. To convert B2PH to its protonated form, acetic acid (1% v/v) was added to the solution and a red-shift in the absorption profile was observed. In fact, the maximum peak absorption shifted from 325 nm to 347 nm, and the molar absorptivity at 355 nm (the wavelength that corresponds to the tripled harmonic of a Nd:YAG laser) increased from 6600 L mol^{-1} cm^{-1} to 19000 L mol^{-1} cm^{-1}. Neither of the two reagents, SANH nor SFB, exhibited high absorbance near 355 nm, suggesting that peptides containing these modifications would not undergo efficient UVPD. Although the UV absorption profiles of B2PH in solution are not expected to perfectly mirror the UV absorption profiles in the gas phase, these initial results do suggest that the bis-aryl hydrazone moiety exhibits a strong dependence on whether it is protonated or not, and the high absorptivity at 355 nm in solution shows

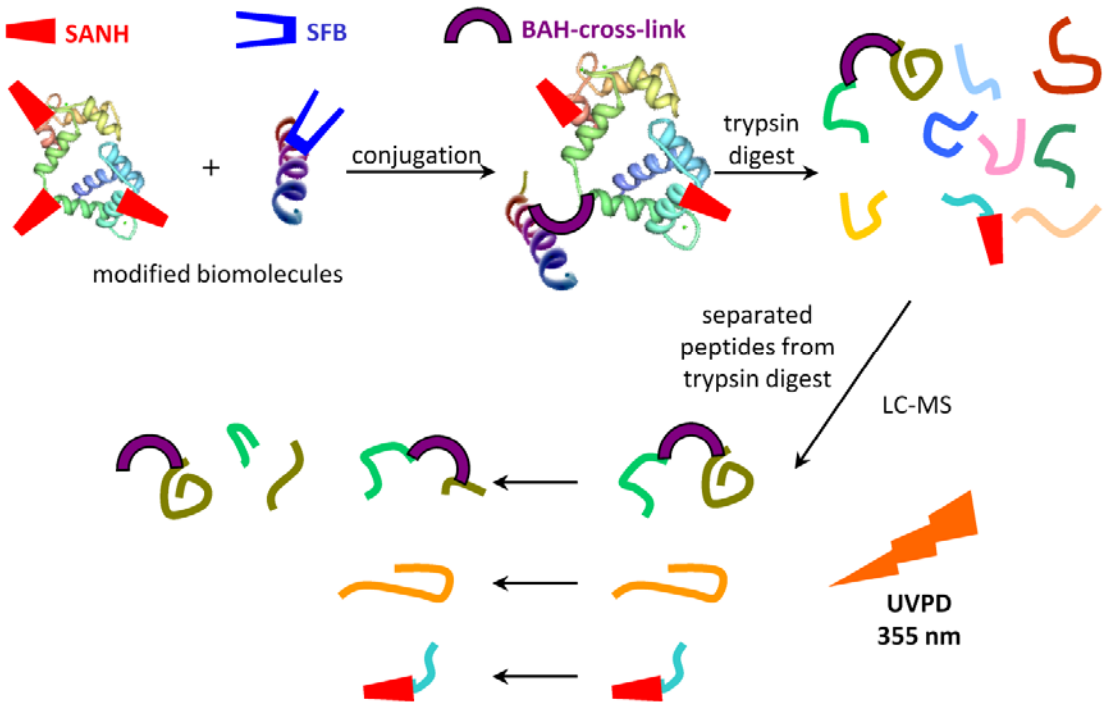

Scheme 5.1 Two-step conjugation and UVPD screening strategy

remarkable agreement with our gas-phase UVPD results. ESI-MS of B2PH yielded a single peak of *m/z* 198.1 corresponding to the protonated molecule. Benzaldehyde-2-pyridinylhydrazone was subjected to UVPD-MS, and upon two pulses of 355 nm radiation at ~18 mJ/pulse (~28% power), the abundance of the precursor ion decreased by 60% and two abundant product ions were observed of *m/z* 94 and of *m/z* 67 (**Figure 5.2b**). The efficient UV photodissociation of B2PH at low laser powers suggested that bis-aryl hydrazone cross-linked peptides should also undergo UVPD.

For the spectra discussed in this report, all product ions of the conjugated or cross-linked peptides were labeled according to previously suggested nomenclature.[38, 39] Briefly, the two constituent peptides are labeled α and β, and dissociation along the backbone of the α-peptide yields product ions such as $y_{n\alpha}$ or $b_{n\alpha}$. Lysine immonium ions

linked to the other peptide are labeled as $K^{L}\alpha$ where L refers to the linker, and fragment ions due to dissociation of the linker moiety are labeled as Lαn referring to cleavage *n* bonds away from the C_α atom of the α-peptide (see **Figure 5.1c** for observed bond cleavages and numbering scheme). Similar nomenclature is used for product ions of the β-peptide.

5.4.2 UVPD-MS of BAH-Conjugated Model Peptides

The peptides Ac-AAAKAAAAR (α-peptide) and neurotensin (β-peptide) were chosen as model peptides to evaluate the feasibility of the UVPD strategy, and each were modified by SFB or SANH, respectively, and then cross-linked together. The mass spectrum (with a wide isolation range of *m/z* 600 – 1200) of the conjugated product mixture is shown in **Figure 5.3a** in which each of the two modified peptides were detected, corresponding to a mass addition of 132 Da for SFB and 135 Da of SANH (after deprotection of the acetone moiety), as well as the conjugated peptide-peptide complex in the 3+ and 4+ charge states with the BAH-linker adding 249 Da. In addition, unmodified neurotensin (2+), and fragment ions of the α-peptide conjugated to neurotensin were observed. (These latter ions are attributed to in-source dissociation due to the high tube lens voltage necessary to effectively transmit ions within the isolated *m/z* range of 600 to 1200 and were not observed when trapping the entire range from *m/z* 300 to 2000 as shown in **Figure 5.4**; no ions were observed above *m/z* 1400. The necessity of using a high tube lens voltage is an artifact of the limited flexibility of the LCQ software when implementing a simultaneous broad trapping and activation experiment as opposed to conventional CID in which a selected precursor ion is isolated and activated.) The cross-link was formed between Lys-4 of Ac-AAAKAAAAR and Lys-6 of neurotensin as each peptide only has a single primary amine that can react with the SANH and SFB

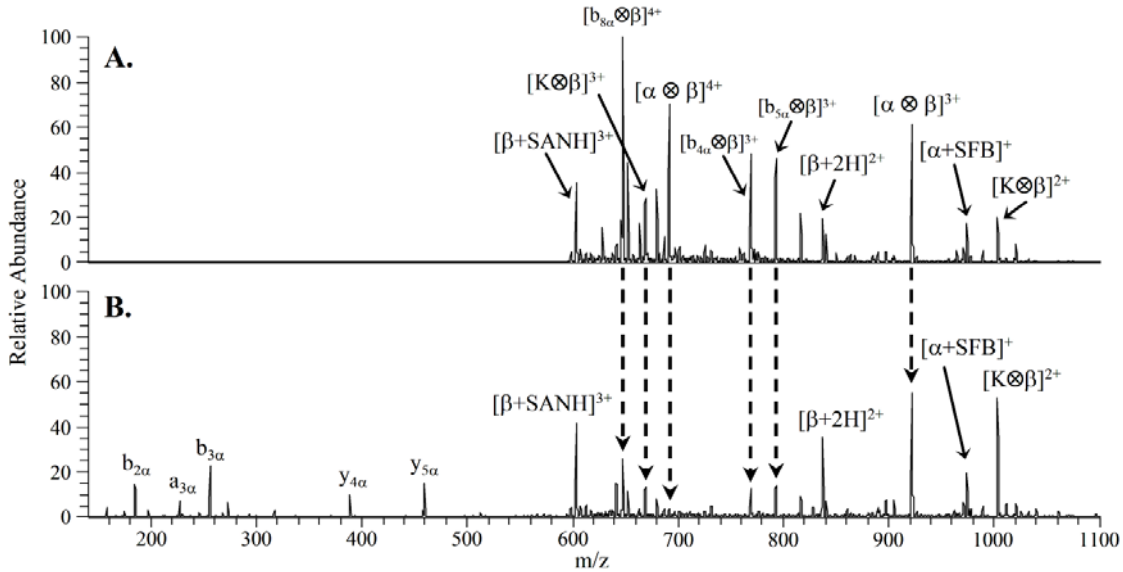

Figure 5.3 (A) Wide *m/z* isolation and (B) UVPD mass spectra (10 pulses) of *m/z* 600 - 1100 of the reaction mixture of Ac-AAAKAAAAR + SFB/SANH + neurotensin. The first peptide listed is referred to as α and the second peptide as β. BAH-cross-links are represented by ⊗.

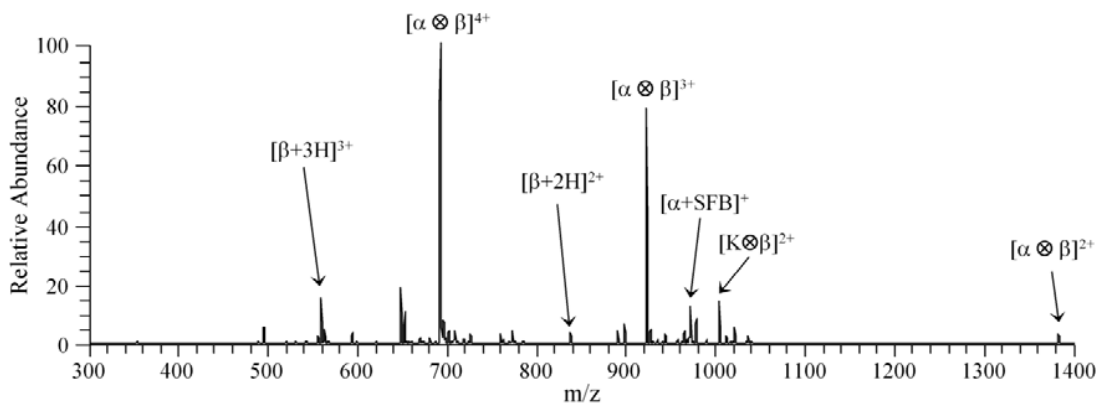

Figure 5.4 ESI mass spectrum of the product mixture of Ac-AAAKAAAAR + SFB/SANH + neurotensin. The first peptide listed is referred to as α and the second peptide as β. BAH-cross-links are represented by ⊗.

reagents. Upon ten pulses of UV irradiation of all ions of *m/z* 600 – 1200, only the ions which contained the BAH-linker underwent photodissociation and were reduced in abundance (**Figure 5.3b**). By comparing the relative abundances of each ion in the two

spectra, one can rapidly determine which ions correspond to BAH-conjugated peptides. The unmodified doubly-charged neurotensin ion actually increased in ion abundance upon UV irradiation, most likely due to dissociation of the conjugated peptide-peptide complexes yielding the neurotensin peptide ion as a product ion. Of particular importance is that the dead-end modified peptides, $[\beta + SANH + 3H]^{3+}$ of *m/z* 603.5 and $[\alpha + SFB + H]^{+}$ of *m/z* 974.5 did not decrease in abundance. As reported in Chapter 4, an IR chromogenic cross-linker and IRMPD were utilized to selectively dissociate cross-linked peptides, but the uninformative dead-end modified peptides also contained the phosphate chromophore and would photodissociate as well, thus preventing the distinction of cross-linked peptides from dead-end modified peptides.[27] Since the BAH-chromophore is formed only upon specific conjugation of SFB- and SANH-modified peptides, the dead-end modified peptides do not efficiently photodissociate at 355 nm. Both SANH- and SFB-modified peptides were individually examined by UVPD-MS to determine if these ions would photodissociate. Neurotensin modified by SANH was examined in the 2+ and 3+ charge states, and both doubly-charged SFB-modified neurotensin and α-MSH were analyzed (**Figure 5.5**). For all four of these species, the intact surviving precursor ion is the only ion of significant abundance observed after 10 pulses of UV irradiation at full power, confirming their lack of UV absorptivity which confers selectivity to the UVPD strategy.

After demonstration that UVPD can be used to rapidly screen BAH-conjugated peptides in simple peptide mixtures, UVPD was then compared to CID to determine its utility for sequencing the two constituent peptides and locating the site of conjugation. UVPD of $[\alpha\text{-MSH} \otimes BAH \otimes \text{Ac-RFMWMK-NH}_2 + 4H]^{4+}$ (*m/z* 714.3) yielded a full series of conventional b-ions of the β-peptide (Ac-RFMWMK-NH_2), as well as several product ions due to dissociation of the backbone of the α-peptide (α-MSH) (**Figure**

5.6a). In addition, the cross-linker specific fragment ions of $K^{L}\alpha$ and Lα18 were observed. The presence of the $b_{10\alpha}$ ion without the BAH-linker and the adjacent $b_{11\alpha}$ ion retaining the cross-link allows one to locate the site of conjugation to Lys-11 of the α-peptide. Similarly the $b_{5\beta}$ and $y_{1\beta}$ ions can be used to pinpoint the cross-link to Lys-6 of the β-peptide. Unambiguous determination of the cross-link location is necessary even

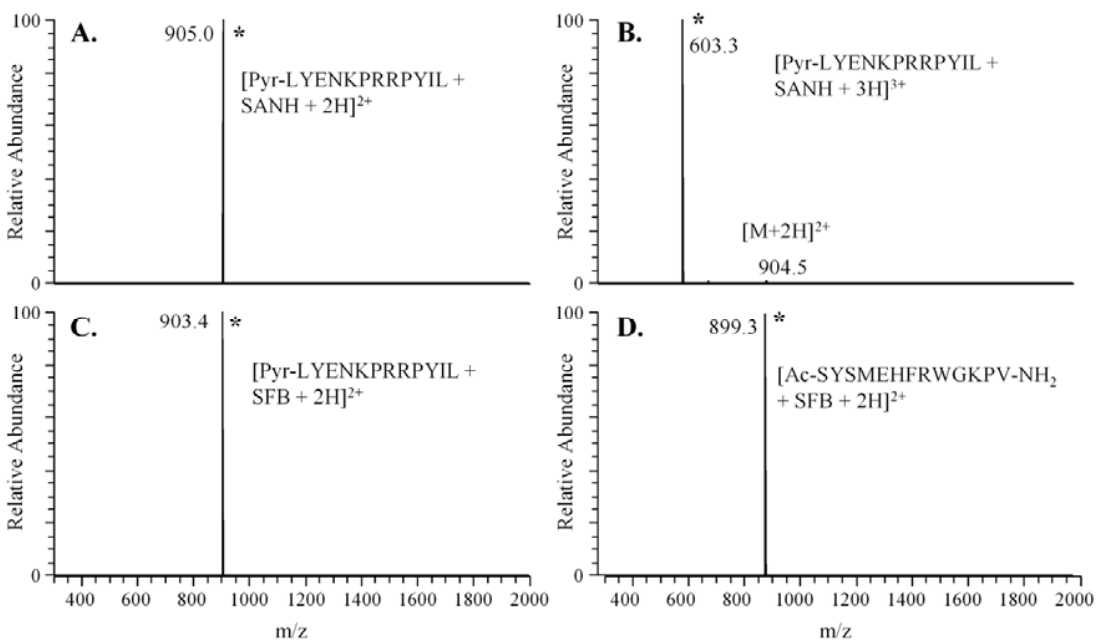

Figure 5.5 UVPD mass spectra (10 pulses) of (A) [neurotensin + SANH + 2H]$^{2+}$ of *m/z* 905.0, (B) [neurotensin + SANH + 3H]$^{3+}$ of *m/z* 603.3, (C) [neurotensin + SFB + 2H]$^{2+}$ of *m/z* 903.4, and (D) [α-MSH + SFB + 2H]$^{2+}$ of *m/z* 899.3. No photodissociation was observed.

with a priori knowledge of the peptide sequence, as recent work has identified that NHS-esters not only react with lysine residues and free primary amines but also with tyrosines, serines, and threonines.[40] CID of this conjugated peptide ion ([α-MSH ⊗ BAH ⊗ Ac-RFMWMK-NH_2 + 4H]$^{4+}$ of *m/z* 714.3) did not produce as many informative sequence fragment ions – the most dominant pathway was dehydration (**Figure 5.6b**). Only a total

of three product ions were detected, and while the $b_{5\beta}$ and $y_{1\beta}$ ions can be used to unambiguously assign the location of conjugation to Lys-6 of the β-peptide, the other fragment $K^{L}\alpha$ does not provide any sequence information. For this conjugated peptide-peptide complex, UVPD clearly yields a more informative product ion spectrum with diagnostic fragment ions that can be used to pinpoint the cross-link location on both constituent peptides, whereas this peptide predominantly dissociated through a dead-end neutral loss pathway by CID.

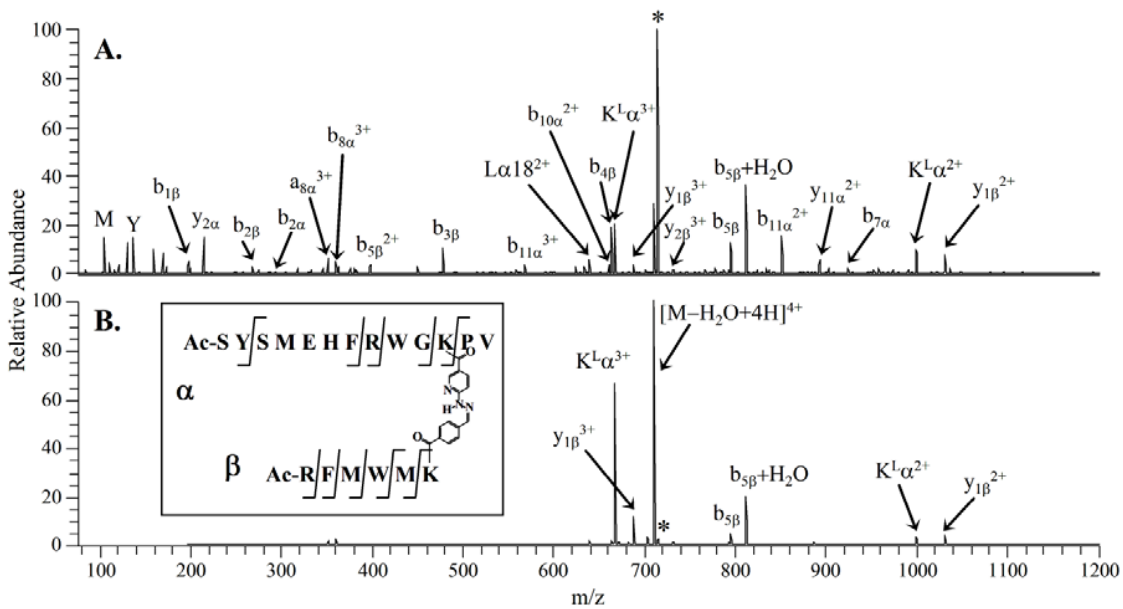

Figure 5.6 (A) UVPD (10 pulses) and (B) CID (0.344 V) mass spectra of [α-MSH ⊗ BAH ⊗ Ac-RFMWMK-NH_2 + 4H]$^{4+}$ of *m/z* 714.3. The first peptide listed is referred to as α and the second peptide as β. Precursor ions are signified with an asterisk (*). Schematic of bond cleavages refers to product ions observed in UVPD mass spectrum.

5.4.3 Screening of BAH-Conjugated Peptides in Mock Mixtures

To demonstrate the selective UVPD of BAH-conjugated peptides in a more complex mixture, a mock mixture of peptides was analyzed. The mock mixture contained an equimolar amount (~10 μM) of bradykinin, angiotensin II, neurotensin, substance P, YGGFM, and the cross-linking product mixtures of Ac-AAAKAAAAR + SFB/SANH + Ac-AAAKPAAAR, Ac-AAAKAAAAR + SFB/SANH + neurotensin, and α-MSH + SANH/SFB + Ac-RFMWMK-NH_2. This mock mixture of peptides was rapidly screened via direct infusion ESI-UVPD-MS by comparison of a wide *m/z* range isolation spectrum and the UVPD mass spectrum (**Figure 5.7**). Ions without the BAH-chromophore were unaffected by UV irradiation and were observed in both the isolation and UVPD mass spectra. The more highly-charged BAH-conjugated peptide-peptide complexes exhibited high UVPD efficiency and their abundances substantially decreased in the UVPD mass spectra (**Figure 5.7b**). The abundances of these highly-protonated BAH-conjugated peptides diminished on average by ~70%, whereas the abundances of the lower-charged conjugated peptide ions decreased by only ~20 – 30% (**Table 5.1**). The SFB-, SANH-, and unmodified peptides did not exhibit any significant decrease in abundance upon exposure to UV irradiation at 355 nm. The differences in ion abundances of these various species between the wide *m/z* isolation and UVPD mass spectra could be discerned with as few as 5 pulses of UV irradiation and up to 20 pulses, thus indicating a wide usable range of experimental conditions for distinguishing between BAH-conjugated peptides and uninformative species.

To demonstrate the utility of UVPD to screen BAH-conjugated peptides in more complex samples, the same mock mixture was also analyzed by online LC-UVPD-MS. In this method, a wide *m/z* isolation mass spectrum and then a UVPD mass spectrum

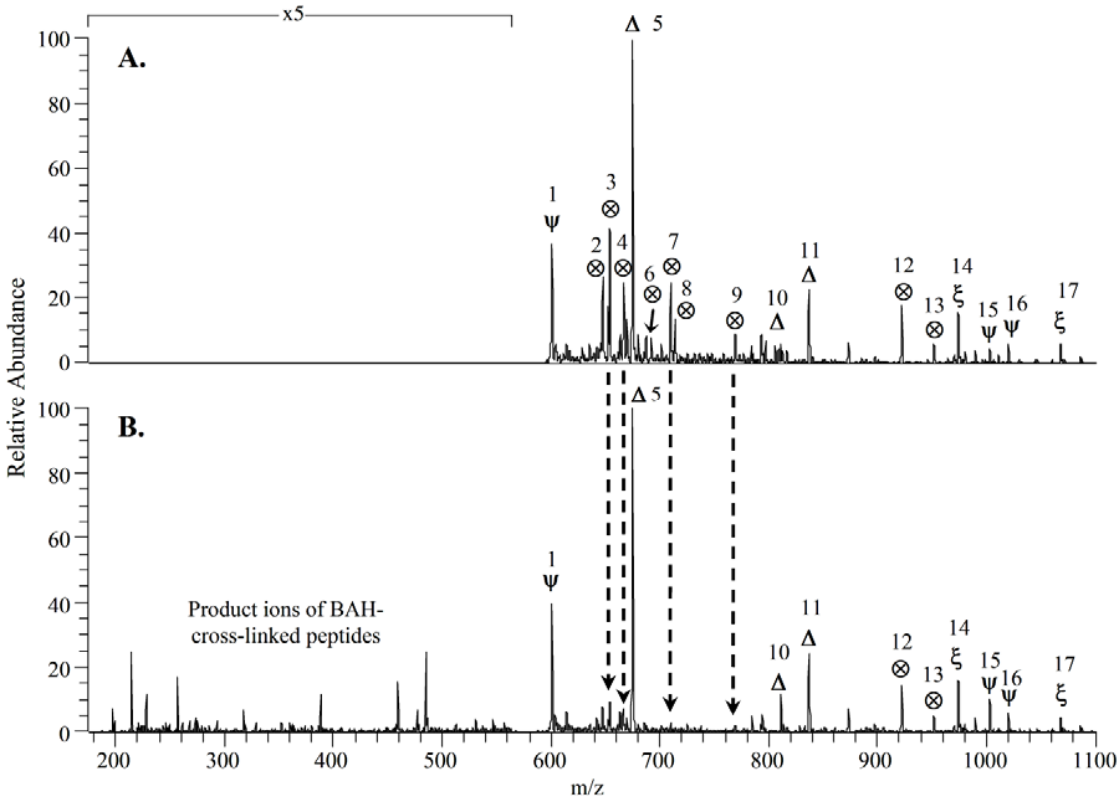

Figure 5.7 (A) Wide *m/z* range isolation and (B) UVPD (10 pulses) mass spectra of *m/z* 600 – 1100 of a mock mixture of BAH-cross-linked (⊗), SFB- (ξ), SANH- (ψ), and un-modified peptides (Δ). Ion identities are listed in **Table 5.1**.

were acquired in an alternating fashion throughout the LC separation. Selected ion chromatograms (SICs) of the eluting species were extracted from the total ion chromatograms of the isolation and UVPD mass spectra. These SICs were then re-plotted on the same time axis to create reconstructed ion chromatograms (RIC) as shown in **Figure 5.8**. The peak areas of each component in the mixture were measured in the isolation and UVPD SICs to calculate the decreases in ion abundance upon UV irradiation (given as percentages) (**Table 5.2**). Comparison of the two RICs allow ready determination of which ions possess the BAH-chromophore as these species decreased in abundance by an average of 73%. If the BAH-containing peptide ions are further

Table 5.1 Changes in relative ion abundances upon UV irradiation (10 pulses) for a mixture of peptides analyzed by direct infusion ESI-MS/MS.

label	species	*m/z*	peak area isolation[a]	peak area UVPD[a]	peak area percent change[a]	std. dev.[b]
1	[α-MSH + SANH + 3H]$^{3+}$	600.5	3.41E+05	3.25E+05	-4.8	0.9
2	[Ac-AAAKAAAA ⊗ BAH ⊗ neurotensin + 4H]$^{4+}$ [c]	647.4	2.36E+05	7.06E+04	-70.1	0.6
3	[Ac-AAAKAAAAR ⊗ BAH ⊗ Ac-AAAKPAAAR + 3H]$^{3+}$	654.1	4.68E+05	1.24E+05	-74	2
4	[α-MSH ⊗ BAH ⊗ K + 3H]$^{3+}$	666.6	2.45E+05	7.87E+04	-68	2
5	[substance P + 2H]$^{2+}$	674.4	8.00E+05	7.71E+05	-4	3
	[Ac-AAAKAAAAR ⊗ BAH ⊗ neurotensin - H_2O + 4H]$^{4+}$	687.5	7.81E+04	1.70E+04	-78	8
6	[Ac-AAAKAAAAR ⊗ BAH ⊗ neurotensin + 4H]$^{4+}$	692.0	7.03E+04	1.19E+04	-83	6
7	[α-MSH ⊗ BAH ⊗ Ac-RFMWMK-NH_2 - H_2O + 4H]$^{4+}$	710.1	2.08E+05	2.21E+04	-89	4
8	[α-MSH ⊗ BAH ⊗ Ac-RFMWMK-NH_2 + 4H]$^{4+}$	714.3	1.06E+05	1.46E+04	-86	1
9	[Ac-AAAK ⊗ BAH ⊗ neurotensin + 3H]$^{3+}$ [c]	769.5	8.73E+04	2.05E+04	-77	2
10	[Ac-RFMWM + H_2O + H]$^{+}$ [c]	811.3	6.50E+04	9.38E+04	44	9
11	[neurotensin + 2H]$^{2+}$	836.9	2.11E+05	2.27E+05	8	3
12	[Ac-AAAKAAAAR ⊗ BAH ⊗ neurotensin + 3H]$^{3+}$	922.0	1.55E+05	1.29E+05	-17	4
13	[α-MSH ⊗ BAH ⊗ Ac-RFMWMK-NH_2 + 3H]$^{3+}$	951.5	6.19E+04	4.99E+04	-19	2
14	[Ac-AAAKAAAAR + SFB + H]$^{+}$	974.3	1.21E+05	1.17E+05	-3	4
	[Ac-AAAKAAAAR ⊗ BAH ⊗ Ac-AAAKPAAAR + 2H]$^{2+}$	980.3	3.29E+04	2.34E+04	-29	4
15	[Ac-AAAKPAAAR + SANH + H]$^{+}$	1003.3	5.02E+04	8.43E+04	68	13
16	[Ac-AAAKPAAAR + SANH + H_2O + H]$^{+}$	1020.2	4.29E+04	4.33E+04	1	5
	[angiotensin II + H]$^{+}$	1046.3	9.24E+03	8.96E+03	-3	4
	[bradykinin + H]$^{+}$	1060.3	9.22E+03	1.05E+04	13.8	0.5
17	[Ac-RFMWMK-NH_2 + SFB + H]$^{+}$	1068.2	4.41E+04	4.41E+04	0	7
	[Ac-RFMWMK-NH_2 + SFB + H_2O + H]$^{+}$	1086.2	1.81E+04	1.87E+04	3	8
	[substance P + H]$^{+}$	1347.3	6.62E+03	6.80E+03	2.8	0.7

[a] Values are the average of data obtained in triplicate. [b] Standard deviation of the percent abundance changes. [c] Ion is isobaric with a product ion of a cross-linked peptide

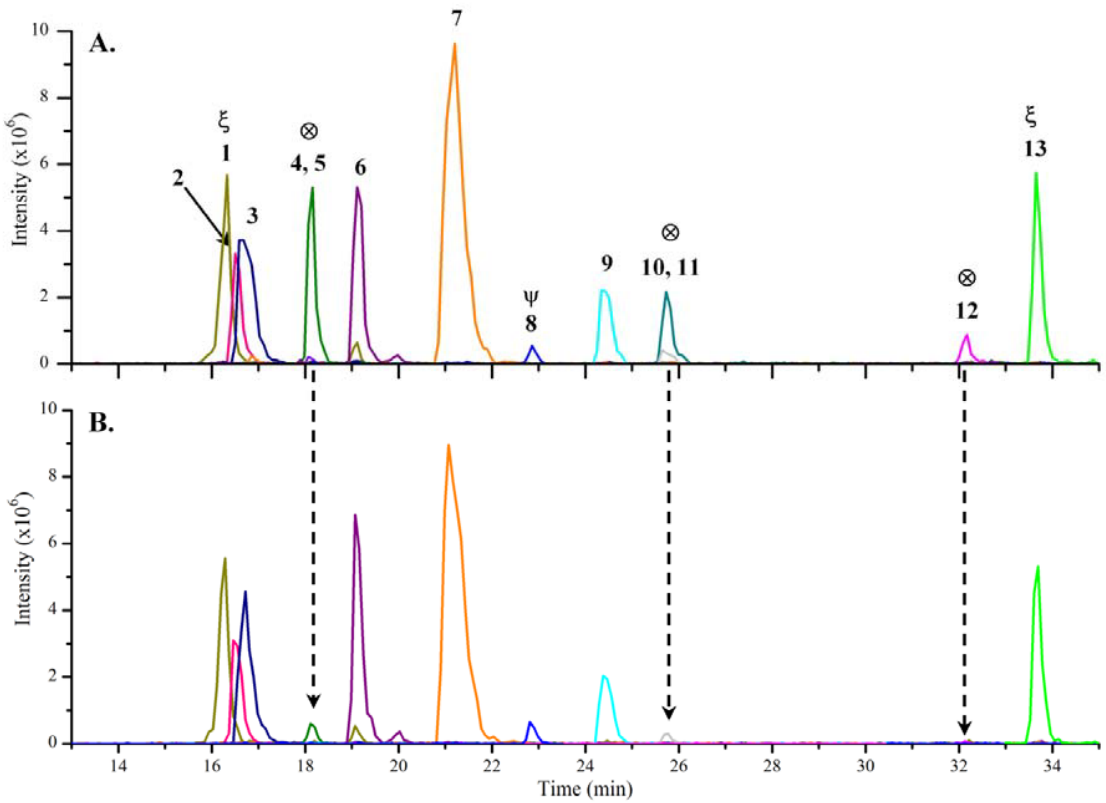

Figure 5.8 Reconstructed total ion chromatograms from (A) wide *m/z* range isolation and (B) UVPD (10 pulses) spectra of LC-MS/MS analysis of a mixture of peptides. Ions of *m/z* 475 – 1100 were either isolated or UV irradiated. BAH-conjugated peptides are labeled with ⊗, SFB-modified with ξ, and SANH-modified with ψ. Ion identities are listed in **Table 5.2**.

categorized by charge state, the more highly-charged species reduce in abundance by ~94 ± 4% and the species in the corresponding lower charge states (i.e. without a mobile proton) decrease by ~43 ± 25%. The non-chromogenic peptide ions exhibited an average decrease in peak area of only 0.7%.

UV-Vis absorption measurements at 355 nm of the eluting peptides also provided another means to aid in distinguishing the BAH-conjugated peptides from unmodified peptides and dead-end-modified peptides. All of the peptides with a BAH-cross-link had

an absorbance of at least 0.029; unmodified, SFB-modified, and SANH-modified peptides showed no absorbance at 355 nm (**Table 5.2**). However, for co-eluting species in which one peptide is conjugated and the other is not, the UV-Vis measurements in combination with a standard mass spectrum would not provide enough information to determine which of the two species contains the BAH-chromophore. Only by utilizing UVPD can one differentiate between two or more co-eluting species that absorbed well at 355 nm.

It should be noted that another type of dead-end modified peptides were observed in some of the UVPD-MS experiments corresponding to a reaction between free SANH (in which the NHS-ester was hydrolyzed) with SFB-modified peptides or vice versa creating a chromogenic dead-end modified peptide, termed BAH-OH (+267 Da mass shift). These peptides exhibited high UVPD efficiencies but lower than that of the BAH-conjugated peptides. A UVPD mass spectrum of $[\alpha\text{-MSH} + \text{BAH-OH} + 3\text{H}]^{3+}$ is shown in **Figure 5.9** and several informative product ions were observed allowing identification of the precursor as a BAH-OH modified peptide. In fact, one product ion observed was the unmodified peptide, $[\alpha\text{-MSH} + 2\text{H}]^{2+}$, of *m/z* 833.5 which corresponds to the loss of the BAH-OH modification. Since these species do undergo relatively efficient photodissociation, they could yield false positives in the isolation/UVPD screening process. However, these dead-end modified peptides can be reduced to a minimum through rigorous sample clean-up to remove any excess free SANH or SFB from the reaction mixtures prior to MS analysis; in addition, these species were observed to increase in concentration in the samples over time and thus it is recommended that the samples be analyzed by ESI-UVPD-MS as soon as possible after the reactions are complete.

Table 5.2 Changes in ion abundance upon UV irradiation from LC-UVPD-MS reconstructed ion chromatograms of a mixture of peptides.

label	elution (min)	species	*m/z*	absorbance (355 nm)[a, b]	peak area isolation[a]	peak area UVPD[a]	percent change in peak area[a]	std. dev.[c]
1	16.3	[Ac-AAAKAAAAR + SFB + H]$^{+}$	488.5	n/d	1.59E+06	1.45E+06	-8	10
2	16.5	[YGGFM + H]$^{+}$	574.8	0.0002	8.27E+05	8.63E+05	+5	9
3	16.7	[bradykinin + 2H]$^{2+}$	531.3	n/d	1.68E+06	1.54E+06	-8	1
4	18.1	[Ac-AAAKAAAAR ⊗ BAH ⊗ Ac-AAAKPAAAR + 3H]$^{3+}$	653.9	0.0372	1.11E+06	1.07E+05	-90	3
5	18.1	[Ac-AAAKAAAAR ⊗ BAH ⊗ Ac-AAAKPAAAR + 2H]$^{2+}$	980.7		3.49E+04	1.15E+04	-67	14
6	19.1	[angiotensin II + 2H]$^{2+}$	524.1	0.0007	1.61E+06	1.60E+06	-0.2	12
7	21.1	[neurotensin + 3H]$^{3+}$	558.4	0.0019	4.44E+06	4.38E+06	-1	3
	21.1	[neurotensin + 2H]$^{2+}$	837.3		1.63E+05	1.75E+05	+8	10
8	22.8	[α-MSH + SANH + 3H]$^{3+}$	600.6	n/d	9.73E+04	9.52E+04	-5	21
9	24.3	[substance P + 2H]$^{2+}$	674.6	n/d	6.77E+05	6.65E+05	-0.4	13
10	25.6	[Ac-AAAKAAAAR ⊗ BAH ⊗ neurotensin + 4H]$^{4+}$	691.8	0.0488	3.84E+05	2.91E+03	-99.4	0.6
11	25.6	[Ac-AAAKAAAAR ⊗ BAH ⊗ neurotensin + 3H]$^{3+}$	922.2		1.04E+05	7.44E+04	-23	23
12	32.1	[α-MSH ⊗ BAH ⊗ Ac-RFMWMK-NH_2 + 4H]$^{4+}$	714.6	0.0298	2.48E+05	1.36E+04	-94.5	0.7
	32.1	[α-MSH ⊗ BAH ⊗ Ac-RFMWMK-NH_2 + 3H]$^{3+}$	951.4		2.49E+04	1.89E+04	-21	16
13	33.6	[Ac-RFMWMK-NH_2 + SFB + 2H]$^{2+}$	536.2	n/d	1.10E+06	1.11E+06	+0.1	7

[a] Percent change calculated from the difference in the peak areas of the SICs from the isolation and UVPD spectra relative to the isolation peak area; values are the average of data obtained in triplicate. [b] n/d = no peak detected. [c] Standard deviation of the percent abundance changes.

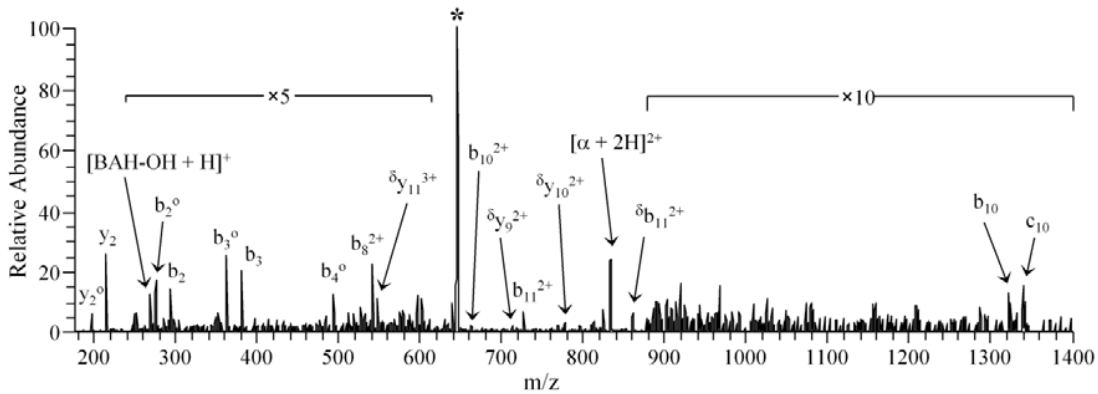

Figure 5.9 UVPD mass spectrum of $[\alpha\text{-MSH} + \text{BAH-OH} + 3H]^{3+}$ of *m/z* 645.5 using 10 laser pulses at 355 nm. The precursor ion is indicated with an asterisk (*) and the peptide is referred to as α. Product ions which retain the BAH-OH modification are indicated with superscript δ and water (H_2O) loss is indicated by superscript ^{o}.

5.4.4 Charge state dependence of UVPD

Upon closer examination of the decreases in ion abundances when comparing the wide *m/z* isolation mass spectra to the UVPD mass spectra in the direct infusion ESI-MS and LC-UVPD-MS experiments, it is clear that the more highly-charged BAH-conjugated peptide ions underwent more efficient photodissociation than those in lower charge states. The quadruply protonated BAH-conjugated peptide complex of *m/z* 692.0 in **Figure 5.3** corresponding to $[\text{Ac-AAAKAAAAR} \otimes \text{BAH} \otimes \text{neurotensin} + 4H]^{4+}$ decreased in relative abundance by ~90% whereas the triply-charged analog was reduced by only ~20%. This phenomenon was further investigated by conjugating the model peptides Ac-AAAKAAAAR + SFB with Ac-AAAKPAAAR + SANH and individually analyzing the doubly- and triply-charged cross-linked products by UVPD-MS. Ultraviolet photodissociation of the resulting conjugated peptide in the 3+ charge state yielded a wide array of product ions as evident in **Figure 5.10a**. Cross-linked b- and y-

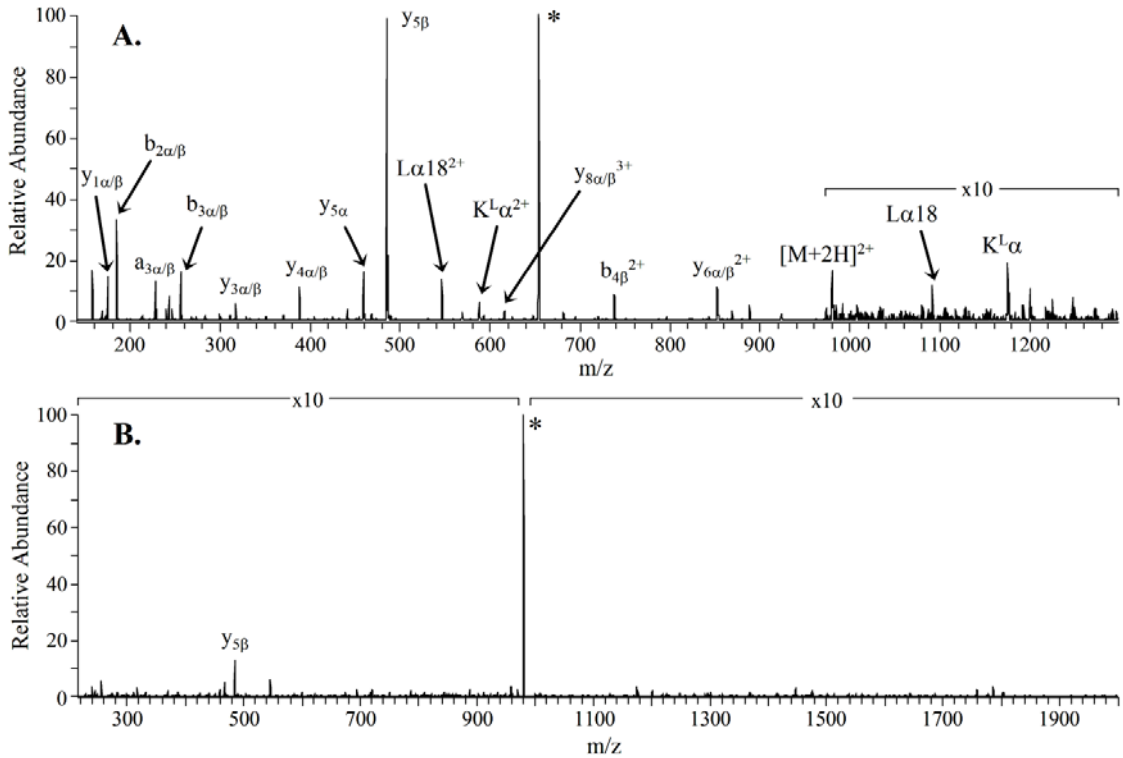

Figure 5.10 UVPD mass spectra of Ac-AAAKAAAAR ⊗ BAH ⊗ Ac-AAAKPAAAR in the (A) 3+ (*m/z* 653.7) and (B) 2+ (*m/z* 980.0) charge states using 7 and 15 pulses of UV irradiation, respectively. The first peptide listed is referred to as α and the second peptide as β; α/β nomenclature is used for product ions which could have resulted from cleavage of either peptide. Precursor ions are signified with an asterisk (*).

type ions as well as specific cross-linked fragment ions such as lysine immonium ions linked to one peptide (e.g. $K^L\alpha$) and those arising from cleavage of the linker amide bond (e.g. Lα18) were observed. In addition a full series of conventional b- and y-type ions were also detected for each constituent peptide. However, UVPD of the analogous doubly-protonated conjugated peptide resulted in minimal product ion formation (**Figure 5.10b**). Only a single identifiable fragment ion was observed ($y_{5\beta}$) at a relative abundance of less than 1.5%. It is believed that this charge-dependent UVPD efficiency is due to the protonation state of the bis-aryl hydrazone moiety. The doubly-protonated

conjugated peptide of Ac-AAAKAAAAR ⊗ BAH ⊗ Ac-AAAKPAAAR is assumed to have both protons sequestered at the two C-terminal arginine residues. However, the triply-protonated species has one additional mobile proton, presumably partially localized at the basic BAH-chromophore, thus protonating N12 (see **Figure 5.1** for numbering scheme).

It is speculated that the additional mobile proton alters the resulting gas-phase absorption profile of the BAH-conjugated peptide, in this case increasing the UVPD efficiency at 355 nm. This effect parallels the solution-phase absorption properties of B2PH as indicated in the UV-Vis spectra of this molecule in neutral and acid-spiked solutions (**Figure 5.2a**). The difference in UVPD efficiencies cannot simply be explained by a decrease in the energy necessary to dissociate the 3+ versus 2+ precursor ions because peptides cross-linked by the non-chromogenic DSS molecule did not exhibit any UVPD in any charge state (data not shown). In addition, lower CID voltages were required to dissociate these DSS-cross-linked analogs than the BAH-cross-linked peptides as determined by energy-variable CID in which the abundances of the selected precursor peptide ions were monitored as the CID voltage was raised. The triply-charged BAH-conjugated peptide needed a 25% greater CID voltage than the DSS-cross-linked species to reach the 50% dissociation level (0.326 V vs. 0.259 V). Preliminary studies of pulse-resolved UVPD, in which fragment ion abundances were measured as a function of the number of UVPD pulses, suggest that the primary product ions also exhibit this charge-dependent photodissociation efficiency (e.g. primary product ions with a mobile proton undergo absorption and photodissociation upon subsequent pulses of UV irradiation whereas product ions with protons sequestered at arginine residues do not undergo efficient secondary dissociation).

5.5 CONCLUSIONS

Using a two-step conjugation method in which the chromogenic bis-aryl hydrazone functionality was formed upon reaction of two modified biomolecules, we have been able to rapidly distinguish cross-linked peptides from dead-end and unmodified peptides by UVPD-MS. Ultraviolet photodissociation of the cross-linked peptides provided more diagnostic sequence ion information than CID, allowing one to readily identify the cross-linked residues of the constituent peptides. The UVPD efficiencies were also observed to be charge-dependent as protonation of the hydrazone bond was necessary for rapid photodissociation, mirroring the solution-phase UV-Vis absorption profile of the BAH-chromophore in neutral and acidic solutions. Only BAH-conjugated peptides were observed to undergo efficient UV photodissociation at 355 nm allowing for facile and selective identification of these ions of interest. Unmodified peptides, as well as SFB- and SANH-modified peptides, do not contain the BAH-chromophore and thus were not observed to photodissociate under any conditions. Online LC-UVPD-MS and direct-infusion ESI-UVPD-MS techniques were successfully applied to a mock mixture of peptides. By using a laser with a higher repetition rate and/or a higher peak power, it would be possible to increase the duty cycle of this method in order to perform on the fly data-dependent UVPD of eluting ions in an LC-MS analysis.

5.6 REFERENCES

(1) Torchilin, V. P. *Annual Review of Biomedical Engineering* **2006**, *8*, 343-375.

(2) El-Andaloussi, S.; Holm, T.; Langel, U. *Current Pharmaceutical Design* **2005**, *11*, 3597-3611.

(3) Zatsepin, T. S.; Turner, J. J.; Oretskaya, T. S.; Gait, M. J. *Current Pharmaceutical Design* **2005**, *11*, 3639-3654.

(4) Jagannadham, M. V.; Nagaraj, R. *Journal of Peptide Research* **2005**, *66*, 94-100.

(5) Wong, C.-H.; Mruk, D. D.; Lee, W. M.; Cheng, C. Y. *FASEB Journal* **2007**, *21*, 438-448.

(6) Kubler-Kielb, J.; Liu, T.-Y.; Mocca, C.; Majadly, F.; Robbins, J. B.; Schneerson, R. *Infection and Immunity* **2006**, *74*, 4744-4749.

(7) Kavimandan, N. J.; Losi, E.; Wilson, J. J.; Brodbelt, J. S.; Peppas, N. A. *Bioconjugate Chemistry* **2006**, *17*, 1376-1384.

(8) Han, B.; Stevens, J. F.; Maier, C. S. *Analytical Chemistry* **2007**, *79*, 3342-3354.

(9) Miranda-Olvera, A. D.; Ferro-Flores, G.; Pedraza-Lopez, M.; Arteaga de Murphy, C.; De Leon-Rodriguez, L. M. *Bioconjugate Chemistry* **2007**, *18*, 1560-1567.

(10) Bailey, R. C.; Kwong, G. A.; Radu, C. G.; Witte, O. N.; Heath, J. R. *Journal of the American Chemical Society* **2007**, *129*, 1959-1967.

(11) Kozlov, I. A.; Melnyk, P. C.; Stromsborg, K. E.; Chee, M. S.; Barker, D. L.; Zhao, C. *Biopolymers* **2004**, *73*, 621-630.

(12) Jarvius, M.; Paulsson, J.; Weibrecht, I.; Leuchowius, K.-J.; Andersson, A.-C.; Waehlby, C.; Gullberg, M.; Botling, J.; Sjoeblom, T.; Markova, B.; Oestman, A.; Landegren, U.; Soederberg, O. *Molecular and Cellular Proteomics* **2007**, *6*, 1500-1509.

(13) Negishi, J.; Shirahama, T.; Nagaoka, Y.; Takemoto, Y.; Uesato, S. *Yakugaku Zasshi* **2008**, *128*, 1317-1323.

(14) Chowdhury, S. M.; Munske, G. R.; Tang, X.; Bruce, J. E. *Analytical Chemistry* **2006**, *78*, 8183-8193.

(15) Chu, F.; Mahrus, S.; Craik, C. S.; Burlingame, A. L. *Journal of the American Chemical Society* **2006**, *128*, 10362-10363.

(16) Sinz, A.; Kalkhof, S.; Ihling, C. *Journal of the American Society for Mass Spectrometry* **2005**, *16*, 1921-1931.

(17) Hurst, G. B.; Lankford, T. K.; Kennel, S. J. *Journal of the American Society for Mass Spectrometry* **2004**, *15*, 832-839.

(18) Mueller, D. R.; Schindler, P.; Towbin, H.; Wirth, U.; Voshol, H.; Hoving, S.; Steinmetz, M. O. *Analytical Chemistry* **2001**, *73*, 1927-1934.

(19) Ihling, C.; Schmidt, A.; Kalkhof, S.; Schulz, D. M.; Stingl, C.; Mechtler, K.; Haack, M.; Beck-Sickinger, A. G.; Cooper, D. M. F.; Sinz, A. *Journal of the American Society for Mass Spectrometry* **2006**, *17*, 1100-1113.

(20) Back, J. W.; Hartog, A. F.; Dekker, H. L.; Muijsers, A. O.; de Koning, L. J.; de Jong, L. *Journal of the American Society for Mass Spectrometry* **2001**, *12*, 222-227.

(21) Sinz, A.; Wang, K. *Biochemistry* **2001**, *40*, 7903-7913.

(22) Sinz, A.; Wang, K. *Analytical Biochemistry* **2004**, *331*, 27-32.

(23) Wine, R. N.; Dial, J. M.; Tomer, K. B.; Borchers, C. H. *Analytical Chemistry* **2002**, *74*, 1939-1945.

(24) Soderblom, E. J.; Goshe, M. B. *Analytical Chemistry* **2006**, *78*, 8059-8068.

(25) Tang, X.; Munske, G. R.; Siems, W. F.; Bruce, J. E. *Analytical Chemistry* **2005**, *77*, 311-318.

(26) Lu, Y.; Tanasova, M.; Borhan, B.; Reid, G. E. *Analytical Chemistry* **2008**, *80*, 9279-9287.

(27) Gardner, M. W.; Vasicek, L. A.; Shabbir, S.; Anslyn, E. V.; Brodbelt, J. S. *Analytical Chemistry* **2008**, *80*, 4807-4819.

(28) Crowe, M. C.; Brodbelt, J. S. *Analytical Chemistry* **2005**, *77*, 5726-5734.

(29) Reilly, J. P. *Mass Spectrometry Reviews* **2009**, *28*, 425-447.

(30) Wilson, J. J.; Brodbelt, J. S. *Analytical Chemistry* **2007**, *79*, 7883-7892.

(31) Thompson, M. S.; Cui, W.; Reilly, J. P. *Journal of the American Society for Mass Spectrometry* **2007**, *18*, 1439-1452.

(32) Oh, J. Y.; Moon, J. H.; Lee, Y. H.; Hyung, S.-W.; Lee, S.-W.; Kim, M. S. *Rapid Communications in Mass Spectrometry* **2005**, *19*, 1283-1288.

(33) Crowe, M. C.; Brodbelt, J. S. *Journal of the American Society for Mass Spectrometry* **2004**, *15*, 1581-1592.

(34) Flora, J. W.; Muddiman, D. C. *Analytical Chemistry* **2001**, *73*, 3305-3311.

(35) Fung, Y. M. E.; Kjeldsen, F.; Silivra, O. A.; Chan, T. W. D.; Zubarev, R. A. *Angewandte Chemie, International Edition* **2005**, *44*, 6399-6403.

(36) Lemoine, J.; Tabarin, T.; Antoine, R.; Broyer, M.; Dugourd, P. *Rapid Communications in Mass Spectrometry* **2005**, *20*, 507-511.

(37) Joly, L.; Antoine, R.; Broyer, M.; Dugourd, P.; Lemoine, J. *Journal of Mass Spectrometry* **2007**, *42*, 818-824.

(38) Schilling, B.; Row, R. H.; Gibson, B. W.; Guo, X.; Young, M. M. *Journal of the American Society for Mass Spectrometry* **2003**, *14*, 834-850.

(39) Gaucher, S. P.; Hadi, M. Z.; Young, M. M. *Journal of the American Society for Mass Spectrometry* **2006**, *17*, 395-405.

(40) Kalkhof, S.; Sinz, A. *Analytical and Bioanalytical Chemistry* **2008**, *392*, 305-312.

Chapter 6

Sequencing of Bis-arylhydrazone Cross-Linked Peptides by Electron Transfer Dissociation to Assess Protein-Protein Interactions

6.1 OVERVIEW

Electron transfer dissociation (ETD) was used to sequence bis-aryl hydrazone (BAH) cross-linked peptides through preferential cleavage of the hydrazone bond. Between 50% and 80% of the observed ETD fragment ion abundance was accounted for by product ions due to cleavage of the N12–N13 hydrazone, yielding the two constituent peptides – one an even-electron product ion termed Lα12, the other an odd-electron radical ion termed Lβ11$^{\bullet}$ – which allowed each peptide to be individually sequenced by MS/MS methods and the site of cross-linking to be identified. The proposed pathway for the dissociation of the hydrazone bond involves transfer of the electron directly to the protonated hydrazone functionality and subsequent rearrangement to yield the Lα12 and Lβ11$^{\bullet}$ products. Collision induced dissociation (CID) of the even-electron Lα12 product yielded a series of b- and y-type ions; CID of the odd-electron Lβ11$^{\bullet}$ product resulted in a wide range of fragment ions including a-, b-, c-, y-, and z-type ions.

6.2 INTRODUCTION

As the field of proteomics advances, there is a growing need to more clearly understand the relationship between protein structure and protein function. To this end it is vital to not only identify but map protein-protein interactions.[1-3] Traditional protein structure determination methods such as X-ray crystallography and NMR spectroscopy are time-consuming and require relatively large amounts of protein. In an effort to

overcome these disadvantages, chemical cross-linking with mass spectrometric analysis has become a more widespread technique that provides low-resolution structural information about proteins and protein-protein complexes.[4-6] Chemical cross-linking generally involves covalently connecting pairs of amino acid residues that are spatially constrained within a single protein (intramolecular cross-linking) or between two proteins (intermolecular cross-linking) to determine relative distances between residues or identify interacting interfaces in protein complexes. In recent years, cross-linking with mass spectrometry (MS) analysis has been used to determine the fold of a single protein,[7] the quaternary structure of protein-ligand complexes,[8-11] elucidate conformational changes in protein structure upon activation,[12] as well as ligand modulation of protein-protein interactions.[13]

While chemical cross-linking has shown significant promise as an alternative means to map protein interactions, there are several persistent analytical hurdles associated with this method. The rapid and accurate identification of cross-linked peptides in complex mixtures arising from the proteolytic digestion of cross-linked proteins and the interpretation of product ion (MS/MS) spectra of cross-linked peptides remain two of the greatest challenges. To facilitate identification of cross-linked peptides in complex mixtures – containing not only the cross-linked species of interest but also unmodified and dead-end cross-linked peptides – several mass spectrometric methods have been developed with a focus on the synthesis of novel cross-linkers that allow the selective capture or identification of cross-linked peptides. Affinity tags such as biotin have been incorporated into cross-linkers to enrich cross-linked species,[14-17] isotopically labeled cross-linking reagents as well as ^{18}O labeling have been used to identify cross-linked peptide ions in the mass spectra by their unique isotopic signatures,[15, 18-20] and fluorogenic cross-linkers and online fluorescent detection during a front-end LC

separation have been utilized as well.[21-23] Yan et al. recently designed a novel tri-functional photocleavable cross-linker with an acetyl protected thiol group that upon deprotection selectively reacts with a free iodo group on functionalized magnetic beads, allowing capture and enrichment of cross-linked peptides.[24]

Recently an IR chromogenic cross-linked was designed and synthesized which contained a phosphate chromophore that promoted selective infrared multiphoton dissociation (IRMPD) of cross-linked peptides allowing facile differentiation of these species of interest from unmodified peptides (Chapter 4).[25] In addition, IRMPD of these cross-linked peptides yielded a series of y-type product ions C-terminal to the cross-linked residues which allowed for each constituent peptide to be sequenced without the need for MS^n methods. Other groups have focused on developing cross-linkers that display characteristic fragmentation patterns upon collision-induced dissociation (CID) by including gas-phase labile bonds. The first method to employ cleavable bonds utilized them to produce "reporter" ions upon low energy CID to readily identify and screen for cross-linked peptides.[26, 27] Chowdhury and co-workers designed a tri-functional cross-linker with an affinity group for enrichment and an NO_2 tag which was observed as a neutral loss upon CID.[28] In a second strategy, these gas-phase labile bonds were incorporated into the cross-link itself such that the cross-link is cleaved upon CID, yielding each constituent peptide with a characteristic modification.[14, 27, 29-32] Soderblom and Goshe incorporated an aspartyl-prolyl bond in the center of their cross-linker,[29] while the Reid group used a fixed-charged cross-linker containing a sulfonium ion which induced dissociation on either side of the sulfur atom.[31] These approaches required an additional stage of CID to sequence either the cross-linked peptide for the "reporter" ion technique or the modified constituent peptides for the latter method.

The gas-phase cleavable cross-linking reagents developed to date all use ergodic dissociation methods (e.g. IRMPD and CID) in which selective dissociation or bond-cleavage may not be observed for all cross-linked peptides. Cross-linked peptides have been shown to exhibit dissociation trends similar to that of unmodified peptides in which fragmentation is not only dependent on amino acid composition and sequence but also charge state.[33, 34] For peptides with labile post-translational modifications (PTMs) such as phosphorylation, the losses of these modifications are often the preferred the dissociation pathways that may be favored over cleavage of the labile bond located within the cross-linker.

While preferential cleavage of the most labile bonds is often observed upon CID of peptides, electron capture dissociation (ECD)[35] or electron transfer dissociation (ETD),[36] two non-ergodic dissociation methods, promote alternative fragmentation pathways. For peptide cations, one of the proposed mechanisms as shown in **Scheme 6.1** involves electron capture at the protonation sites (e.g., amines of lysines or N-termini or guanidino group of arginines) which results in the ejection and transfer of a hydrogen atom to a carbonyl oxygen.[37] Subsequent dissociation of the N–C_α bond of the peptide backbone is observed which produces the characteristic c- and $z^\bullet$-type ions observed by ECD and ETD. However, preferential cleavage of disulfide bonds was observed in early top-down dissociation studies of proteins by ECD.[38] This high propensity of S–S bond dissociation is attributed to the high affinity of this bond for the hydrogen atom ($H^\bullet$). While cleavage of disulfide bonds was favored for the specific protein studied, in the ECD product ion mass spectra almost complete sequence coverage of the protein was also obtained due to backbone cleavages of the N–C_α bonds.[37] The McLuckey group analyzed disulfide-bonded peptides by ETD, and for most of triply charged peptide cations studied, cleavage of the disulfide bond accounted for ~70% – 80% of the ETD

product ions.[39] For quadruply charged peptide cations, lower yields (~33%) of the observed product ions arose from disulfide bond dissociation.

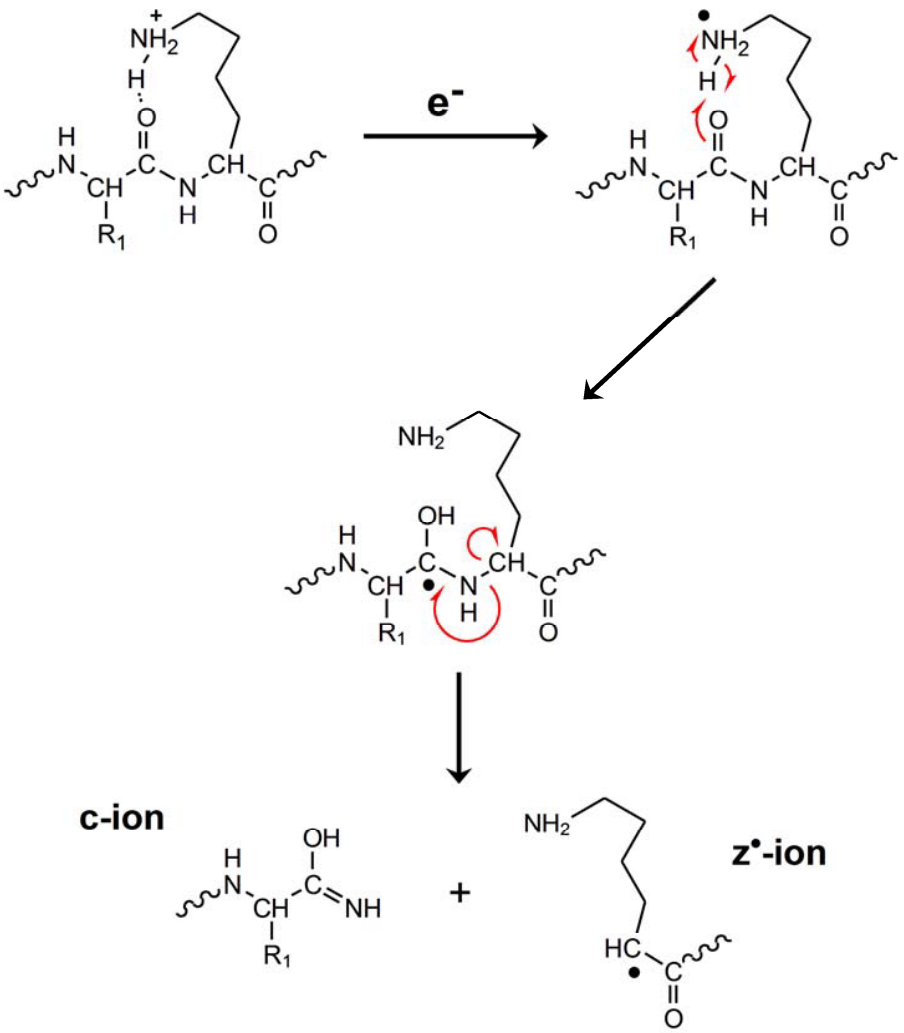

Scheme 6.1 Electron capture dissociation (ECD) mechanism yielding c- and z-type ions.

In this chapter, electron transfer dissociation of bis-arylhydrazone cross-linked peptides is explored in a linear ion trap mass spectrometer. Earlier studies as discussed in Chapter 5 showed that BAH-cross-linked peptides could be selectively dissociated by ultraviolet photodissociation as a means to rapidly screen for these species in complex

mixtures.[40] In the present study, upon reaction with fluoranthene radical anions, the BAH-cross-linked peptides were observed to undergo ETD with preferential cleavage of the N–N hydrazone bond. Dissociation of the hydrazone bond yielded the two constituent peptides each with a unique mass tag at the cross-linking site, one an even electron species and the other an odd electron product. The propensity for cleavage of the hydrazone bond by ETD is compared to the preferential dissociation of the disulfide bond of peptides cross-linked with dithiobis (succinimidyl propionate). A mechanism for the preferential cleavage of the hydrazone bond is proposed and discussed. Collision-induced dissociation of the primary product ions due to cleavage of the hydrazone bond yield diagnostic sequence ions which allow the site of cross-linking to be unambiguously identified.

6.3 EXPERIMENTAL

6.3.1 Chemicals and Reagents

The peptides α-MSH (Ac-SYSMEHFRWKGPV-NH_2), neurotensin (Pyr-LYENKPRRPYIL) and Ac-RFMWMK-NH_2 were obtained from Bachem (Torrance, CA) and used without further purification. The peptides Ac-AAAKAAAAR and Ac-AAAKPAAAR were synthesized at the Protein Microanalysis Facility at the University of Texas at Austin and purified by reversed-phase HPLC. Succinimidyl 4-formylbenzoate (SFB), succinimidyl 4-hydrazinonicotinate acetone hydrazone (SANH), and dithiobis (succinimidyl propionate) (DSP) were obtained from Pierce Biotechnology (Rockford, IL). All other reagents and chemicals were from Fisher Scientific (Fairlawn, NJ).

6.3.2 Peptide Chemical Conjugation and Cross-Linking

Peptides were cross-linked together as previously described and is shown in **Scheme 6.2**.[40] Briefly, peptides were first modified by either SANH or SFB at a 1:10 molar ratio of peptide to derivatizing reagent (200 μM: 2.0 mM) in a 20 mM HEPES, pH 8.0 buffer. After reacting overnight, the solutions were desalted via C_{18} solid-phase extraction using Waters tC_{18} SepPak cartridges (Milford, MA). The modified peptides were conjugated together in 99:1 MeOH/acetic acid (v/v) at an equimolar ratio (100 μM) at 55 °C overnight. Model peptides were also cross-linked with DSP. A fresh solution of DSP was prepared at 20 mM in DMSO and an aliquot was added to a solution containing the peptides to be cross-linked at a molar ratio of 3: 2: 2 (300 μM cross-linker: 200 μM α-peptide: 200 μM β-peptide) 20 mM HEPES, pH 8.0 buffer. The percent volume of DMSO in the cross-linking solution was 5%. The peptides were cross-linked overnight and then desalted by C_{18} solid-phase extraction. All conjugated and cross-linked peptides were diluted to ~10 μM in 49.5: 49.5: 1 H_2O/MeOH/acetic acid (v/v/v) for ESI-MS/MS analysis. Samples were infused at a flow rate of 3.0 μL/min using an ESI voltage of 4.0 kV.

6.3.3 Mass Spectrometry

All mass spectrometry analyses were conducted on a ThermoFisher Scientific LTQ XL linear quadrupole ion trap mass spectrometer (San Jose, CA) equipped with the standard ESI source operated at 4.0 kV and ETD capabilities allowing for the chemical ionization and injection of fluoranthene radical anions. The mass spectrometer was controlled with the XCalibur 2.0.7 software package. Collision-induced dissociation

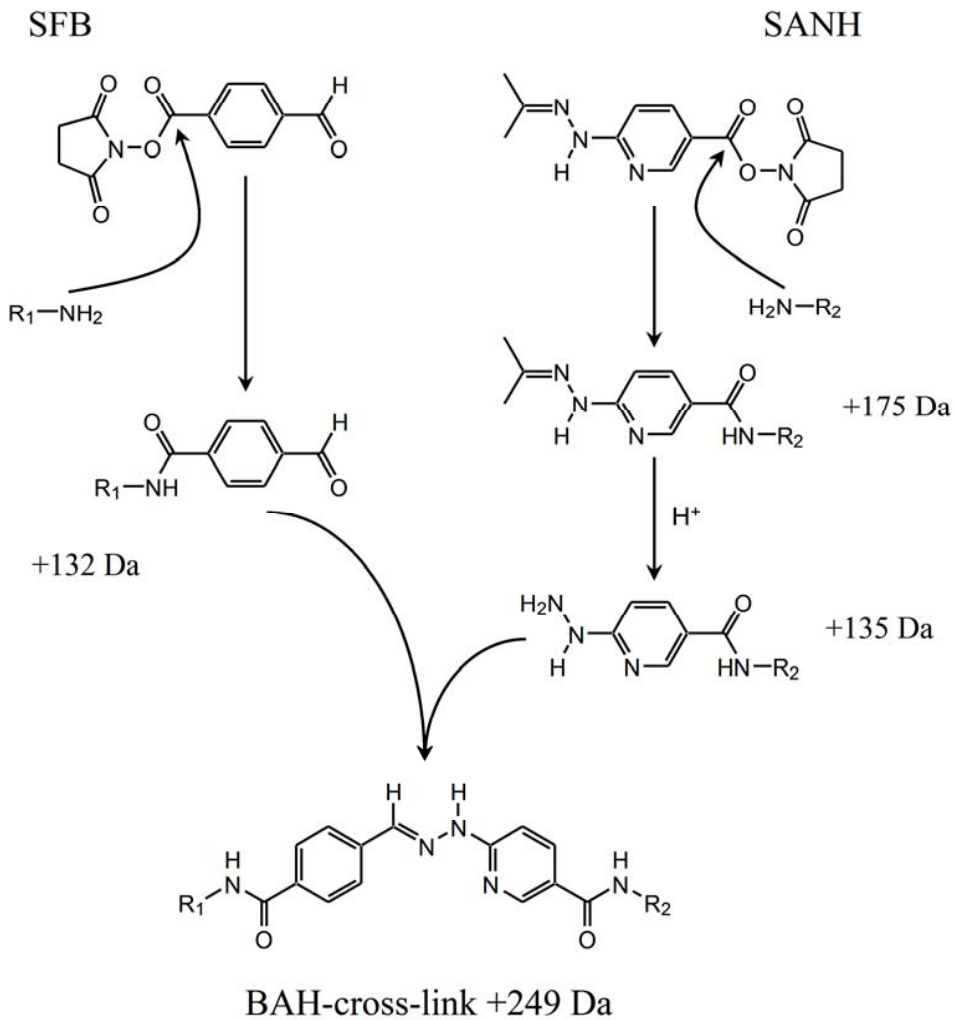

Scheme 6.2 Two step BAH-conjugation procedure via SFB- and SANH-modification..

experiments were performed by activating the precursor ions for 30 ms at a q-value of 0.25. Electron transfer dissociation was performed by injecting 1×10^5 reagent anions into the trap and the reaction time was varied between 0.03 and 100 ms. The precursor ion population for CID and ETD was set to 1×10^4 ions. Time-resolved ETD experiments were performed by plotting the relative abundances of the observed product ions as a function of the ETD reaction time.

6.3.4 Identification of Cross-Linked Peptides

The ETD spectra of these cross-linked peptides were manually identified, as were the MS^3 CID spectra. Product ion spectra of cross-linked peptides were labeled according to the proposed nomenclature.[41] Briefly, the two constituent peptides are labeled as α and β, and for the purposes of this chapter, the α-peptide is designated as the one which was modified by SFB and the β-peptide by SANH and bis-arylhydrazone cross-linked peptides are referred to as α + BAH + β (i.e., BAH = SFB/SANH). Dissociation of the peptide backbone of the α-peptide would yield e.g. $b_{n\alpha}$, $c_{n\alpha}$, $y_{n\alpha}$, and $z_{n\alpha}$ product ions. Similar notation is used for dissociation of the β-peptide. Lysine immonium ions cross-linked to either peptide are labeled as $K^L\alpha$ or $K^L\beta$. Product ions due to dissociation along the cross-linker are labeled based on the number of atoms away from the alpha-carbon of the cross-linked lysine of the peptide which retains the charge as shown in **Scheme 6.3** with the numbering beginning from the α-peptide; similar numbering is used beginning from the β-peptide.

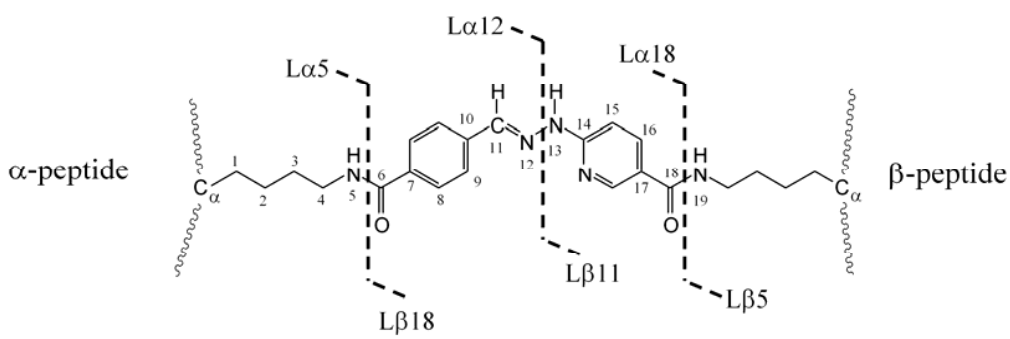

Scheme 6.3 Fragmentation nomenclature for BAH-cross-linked peptides.

6.4 RESULTS AND DISCUSSION

6.4.1 Electron Transfer Dissociation of Bis-arylhydrazone Cross-Linked Peptides

Bis-arylhydrazone cross-linked peptides were analyzed by CID and ETD to assess the ability to sequence the constituent peptides and locate the sites of the cross-links. For example, the peptide Ac-AAAKAAAAR (α-peptide) was cross-linked to neurotensin (Pyr-LYENKPRRPYIL, β-peptide) through SFB/SANH conjugation. Collision-induced dissociation of this cross-linked peptide in the 4+ charge state, as shown in **Figure 6.1a**,

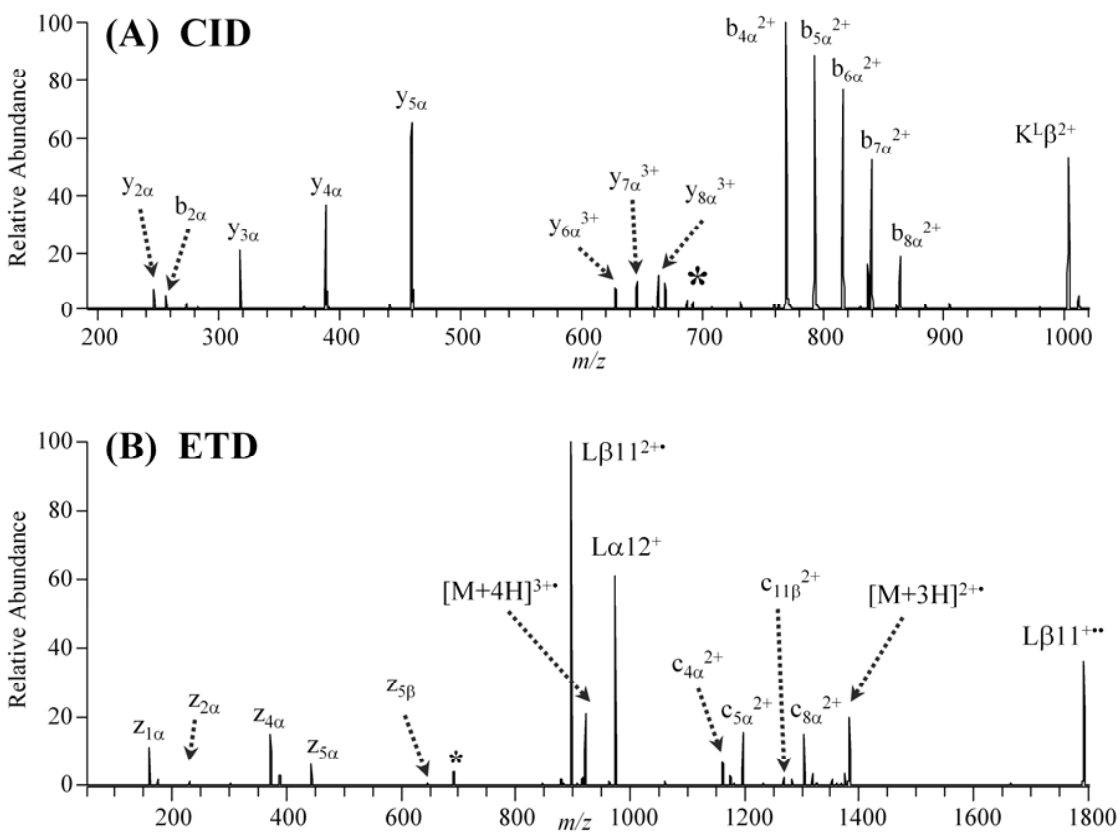

Figure 6.1 (A) CID and (B) ETD (100 ms) product ion mass spectra of [Ac-AAAKAAAAR + BAH + neurotensin + 4H]$^{4+}$ of *m/z* 692.3. The first peptide listed is referred to as α and the second peptide as β. The precursor ion is represented by an asterisk (*).

predominantly resulted in cleavage of backbone amide bonds of the α-peptide (Ac-AAAKAAAAR), yielding a series of $y_{n\alpha}$ ($y_{2\alpha} - y_{5\alpha}$) and complementary cross-linked $b_{n\alpha}$ ions (b_n ion of the α-peptide cross-linked to intact neurotensin) . One lysine immonium ion (from the α-peptide) cross-linked to neurotensin was also detected ($K^L\beta^{2+}$ ion). However, no product ions stemming from cleavage of the peptide backbone of neurotensin were observed in the CID mass spectrum, meaning that no diagnostic β-peptide ions were formed. In contrast, ETD of the same cross-linked peptide yielded three abundant product ions of *m/z* 896.9, 973.4, and 1793.7 (**Figure 6.1b**) which arose from dissociation of the N12–N13 bond of the bis-aryl hydrazone cross-link (atom labeling shown in **Scheme 6.3**). This yielded the two constituent peptides each with a unique mass tag at the cross-linked lysines, designated as the Lα12 ion (α-peptide + 131 Da, SFB tag, *m/z* 896.9^{2+}) and the complementary Lβ11 ion (β-peptide + 119 Da, SANH tag, *m/z* 973.4). The third most abundant product ion of *m/z* 1793.7 is the singly charged (i.e., charge reduced) analog of the Lα12 product.

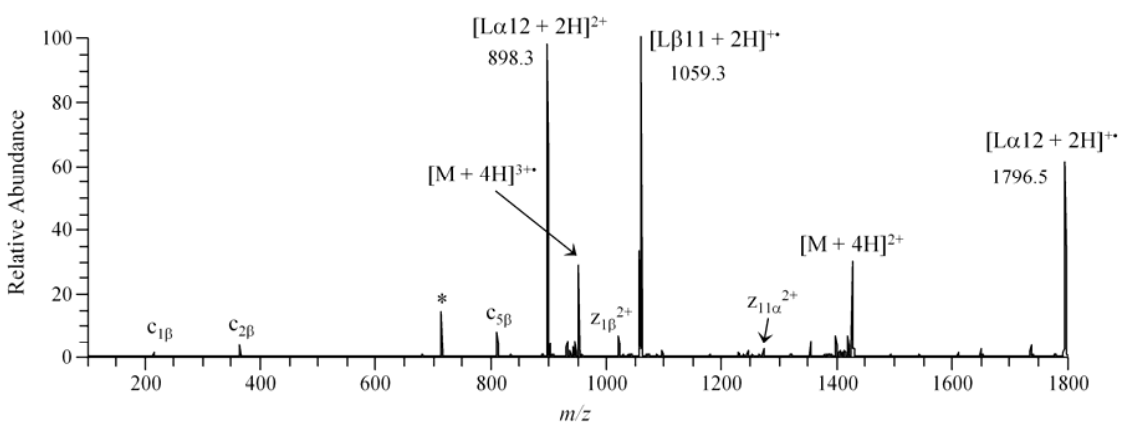

Figure 6.2 ETD mass spectra of $[\alpha\text{-MSH} + \text{BAH} + \text{Ac-RFMWMK-NH}_2 + 4\text{H}]^{4+}$ of *m/z* 714.1 (40 ms reaction time). The first peptide listed is referred to as α and the second peptide as β. The precursor ion is represented by an asterisk (*).

A second BAH-cross-linked peptide contained α-MSH as the α-peptide and Ac-RFMWMK-NH_2 as the β-peptide. Upon ETD, the [α-MSH + BAH + Ac-RFMWMK-NH + 4H]$^{4+}$ ion of *m/z* 713.6 yielded three dominant product ions of *m/z* 898.4, 1059.3 and 1796.5, as shown in **Figure 6.2**. Cleavage of the N12–N13 hydrazone bond produces the Lα12 ion (α-peptide + 131 Da, SFB tag, *m/z* 898.4^{2+}) and the complementary Lβ11 ion (β-peptide + 119 Da, SANH tag, *m/z* 1059.3). The product ion of *m/z* 1796.7 is the charge reduced Lα12 species.

Upon ETD of each of these cross-linked peptides, the abundance of the Lα12 and Lβ11 product ions is greater than that of the charge reduced precursor ions (i.e., [M+4H]$^{3+\bullet}$) or any conventional c- or z$^{\bullet}$-type sequence ions typically formed by ETD. The ability to preferentially cleave a bond within a cross-linker to yield the two constituent ions is of particular interest as it simplifies data analysis and allows one to utilize well-established database search algorithms such as SEQUEST[42] and Mascot[43] to identify the cross-linked peptides. In our study, the formation of the complementary and highly diagnostic Lα12 and Lβ11 ions is observed upon ETD of all cross-linked peptides, a significant feature of the present strategy.

A proposed route for the preferential dissociation of the hydrazone bond is shown in **Scheme 6.4**. Previous studies of hydrazone-containing molecules, as discussed in Chapter 5, indicate the UV absorption profile shifts in both the gas-phase and solution-phase upon protonation of the hydrazone functionality, which is presumed to be due to its high gas-phase basicity. Assuming that the N12 atom of the bis-arylhydrazone cross-link is protonated, the electron could likely be transferred to this functionality, resulting in a hypervalent species in which the extra electron would initially be localized at the C11 atom of the charge reduced species. Upon rearrangement, the N12–N13 bond is cleaved producing the complementary Lα12 and Lβ11$^{\bullet}$ product ions. While the radical is

displayed as localized on the amine group of the final Lβ11$^{\bullet}$ product ion in **Scheme 6.4**, the radical can be resonance stabilized by the adjacent pyridinyl ring. The mass shifts observed for these two product ions are consistent with the proposed pathway in which the Lα12 species is an even-electron product (+131 Da, SFB tag) and Lβ11 (+119 Da, SANH tag) possesses the extra electron. There may be a high propensity for cleavage of the hydrazone bond by ETD because the mechanism does not require the migration of a hydrogen atom (H$^{\bullet}$) to initiate dissociation as is necessary to produce conventional c- and z$^{\bullet}$-type ions (see **Scheme 6.1**).

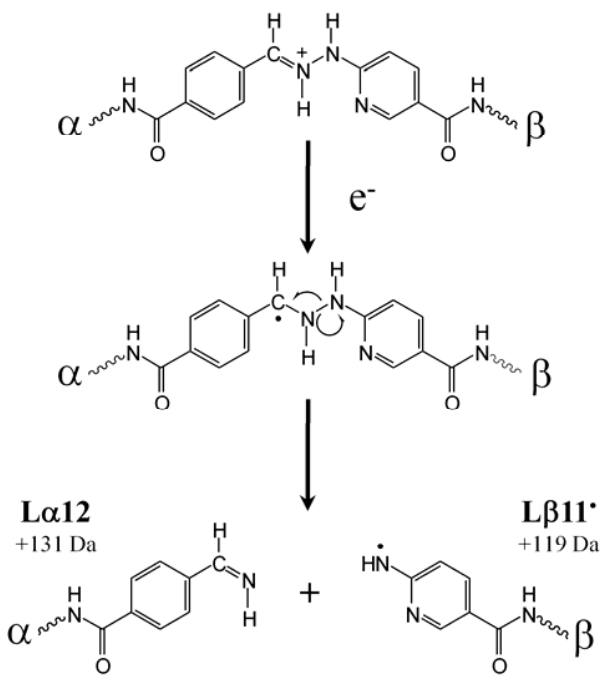

Scheme 6.4 Proposed mechanism for the dissociation of the hydrazone bond.

6.4.2 Preferential Cleavage of Hydrazone by ETD

Preferential cleavage of the hydrazone bond was observed for the cross-linked peptides described above as well as for other model cross-linked peptides (data not shown). In addition, pairs of peptides were also reversed with respect to the orientation of conjugation (i.e., the α-peptide and β-peptide were reversed). For example, the α-MSH and Ac-RFMWMK-NH_2 peptides were conjugated to create [α-MSH + BAH + Ac-RFMWMK-NH_2] and [Ac-RFMWMK-NH_2 + BAH + α-MSH] products. Time-resolved ETD experiments were performed to determine the appropriate reaction conditions to produce the greatest abundance of the diagnostic Lα12 and Lβ11$^{\bullet}$ ions. The relative abundances of the various types of product ions observed in the ETD mass spectra were plotted as a function of ETD reaction time for α-MSH + BAH + Ac-RFMWMK-NH_2 as well as the same cross-linked peptides conjugated in the reverse orientation, Ac-RFMWMK-NH_2 + BAH + α-MSH, in the 3+ and 4+ charge states (**Figure 6.3**). For the cross-linked peptides in the 4+ charge state, the Lα12 and Lβ11$^{\bullet}$ product ions were observed to be the most abundant ions in the ETD mass spectra, in fact greater in abundance than the charge reduced precursor ions when the ETD reaction time was greater than 25 ms (**Figure 6.3a and 6.3c**). Greater than 70% of the total ion current was comprised of these key Lα12 and Lβ11$^{\bullet}$ ions in the ETD mass spectra of the 4+ charged cross-linked peptides. In the ETD mass spectra of the triply charged cross-linked peptides, the Lα12 and Lβ11$^{\bullet}$ ions are the most abundant *fragment ions* (i.e., products of the ion-ion reaction that are due to bond cleavage), but not the most abundant *product ions*. The most abundant product ions arise from electron transfer that yields the charge reduced precursor ($[M+3H]^{2+\bullet}$) and proton transfer from the precursor to the reagent anion that yields $[M+2H]^{2+}$ (**Figure 6.3b and 6.3d**). The relative abundance of the hydrazone cleavage products, Lα12 and Lβ11$^{\bullet}$, was ~25% maximum upon ETD of the

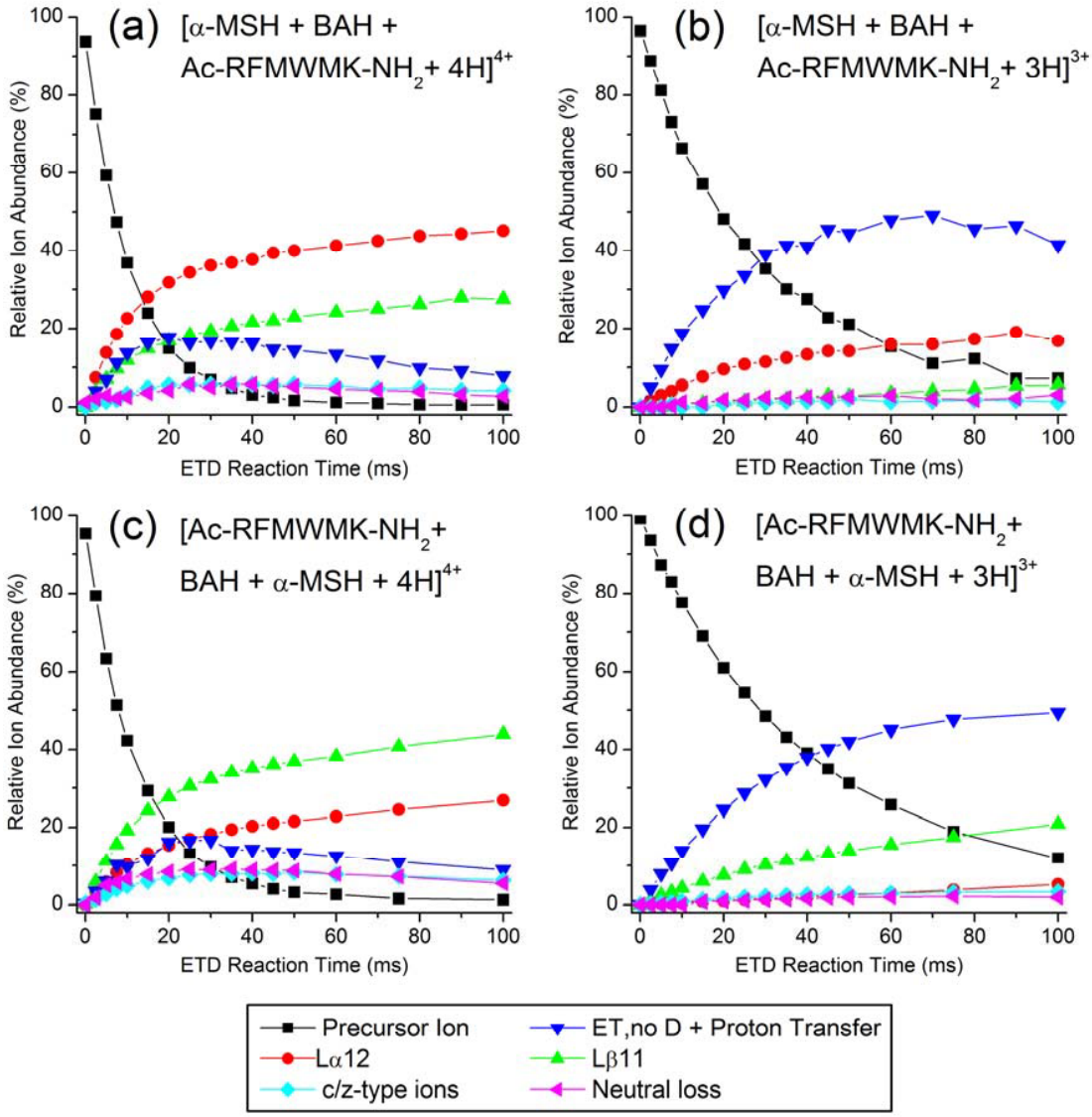

Figure 6.3 Relative ion abundances plotted as a function of ETD reaction time for α-MSH + BAH + Ac-RFMWMK-NH_2 in the (A) 4+ and (B) 3+ charge states. and for Ac-RFMWMK-NH_2 + BAH + α-MSH in the (C) 4+ and (D) 3+ charge states. The first peptide listed is referred to as α and the second peptide as β. Ion abundances are relative to the total ion current in each ETD product ion spectra.

triply charged precursors. Uninformative neutral loss products (e.g., side chains losses from Arg residues including loss of NH_3) and c/z$^{\bullet}$-type ions accounted for a maximum of

~6% of the total ion abundance in the ETD mass spectra of the 4+ charged cross-linked peptide ions and only 2% - 3% each in the mass spectra of the 3+ charged precursors. Charge reduction due to electron attachment without dissociation accounted for almost 50% of the ion abundance in the ETD mass spectra of the 3+ charged precursors.

We speculate that the differences in the relative abundances of the hydrazone cleavage products (Lα12 and Lβ11$^{\bullet}$ ions) for the 4+ and 3+ charge states of the cross-linked peptides (i.e., such as for the α-MSH/AcRFMWMK-NH_2 pair) correlate with whether the hydrazone functionality is protonated. For the 4+ charge state, the hydrazone functionality is likely protonated, thus facilitating the pathway outline in **Scheme 6.4**. In contrast, for the triply charged cross-linked peptides, it is likely that the two Arg residues are protonated, and then the third proton is localized at either the hydrazone functionality or His-6 of α-MSH (Ac-SYSMEHFRWGKPV-NH_2), with the latter likely leading to c/z$^{\bullet}$-type ion production or charge reduction.

The only noticeable difference upon ETD of the two reverse orientation cross-linked peptides, [α-MSH + BAH + Ac-RFMWMK-NH_2] and [Ac-RFMWMK-NH_2 + BAH + α-MSH], is that the abundance of the hydrazone cleavage product containing the α-MSH peptide (Lα12 in **Figure 6.3a and 6.3b**, Lβ11$^{\bullet}$ in **Figure 6.3c and 6.3d**) was always 1.5 to 2 times greater than the complementary product containing the Ac-RFMWMK-NH_2 peptide (Lβ11$^{\bullet}$ in **Figure 6.3a and 6.3b**, Lα12 in **Figure 6.3c and 6.3d**). This phenomenon was further investigated by measuring the ratio of Lα12 to Lβ11$^{\bullet}$ product ions for other charge states of the cross-linked α-MSH/Ac-RFMWMK-NH_2 and Ac-RFMWMK-NH_2/α-MSH peptides, and the results are summarized in **Table 6.1**. The product ion comprised of the α-MSH peptide consistently had a 1.7 to 7 times greater abundance than its Ac-RFMWMK-NH_2 counterpart. This asymmetric partitioning between complementary product ions was initially presumed to be due to

Table 6.1 Ratio of abundance (peak areas) of Lα12: Lβ11• product ions by ETD of BAH-cross-linked peptides. The first peptide listed is the α-peptide and the second peptide is the β-peptide.

Peptide	Charge State	Lα12/Lβ11• Ratio					
		25 ms	50 ms	80 ms	100 ms	Average	Std. Dev.
Ac-AAAKAAAAR + BAH + Ac-AAAKAAAAR	3+	1.54	1.52	1.46	1.46	1.50	0.04
Ac-AAAKAAAAR + BAH + Ac-AAAKPAAAR	3+	1.539	1.552	1.573	1.580	1.56	0.02
α-MSH + BAH + Ac-RFMWMK-NH_2	4+	1.878	1.743	1.668	1.634	1.73	0.11
α-MSH + BAH + Ac-RFMWMK-NH_2	3+	7.180	4.958	3.778	2.982	4.7	1.8
Ac-RFMWMK-NH_2 + BAH + α-MSH	4+	0.548	0.554	0.565	0.586	0.56	0.02
Ac-RFMWMK-NH_2 + BAH + α-MSH	3+	0.075	0.147	0.178	0.175	0.14	0.05

differences in the gas-phase basicities of the two peptides as the α-MSH (Ac-SYSMEHFRWGKPV-NH_2) peptide contains two basic residues, His-6 and Arg-8, compared to Ac-RFMWMK-NH_2 which possesses a single unmodified basic residue, Arg-1. (Since each peptide only has a single primary amine, the lysines are presumed to be the cross-link sites. Upon modification of the lysines with SFB or SANH, these basic primary amines are converted to amide groups.) To remove the influence of the peptide sequence on the asymmetric partitioning, ETD of the cross-linked peptide Ac-AAAKAAAAR + BAH + Ac-AAAKAAAAR was examined. On average, the abundance of the $L\alpha 12^+$ product ion was 1.5 times greater than the $L\beta 11^{+\bullet}$ product ion which indicates that there is a difference in the inherent reactivities or stabilities of these two product ions. The lower abundance of the odd-electron Lβ11• product ion may be

due to its greater reactivity as the radical may initiate secondary dissociation, yielding smaller fragment ions; this issue is under further study.

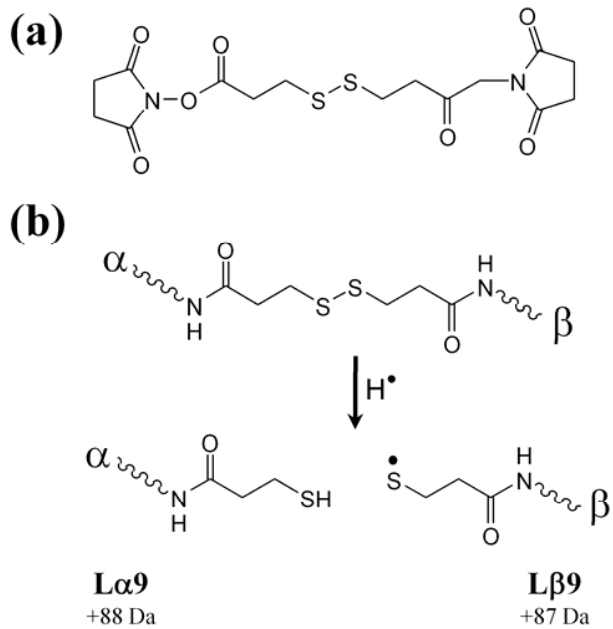

Scheme 6.5 (a) DSP cross-linker and (b) dissociation of disulfide bond upon ETD.

The preferential cleavage of the hydrazone bond was compared to the propensity for disulfide bond cleavage for peptides cross-linked through disulfide bonds. For these comparative experiments, peptides were cross-linked by DSP which contains a disulfide bond at the center of the cross-linking reagent (**Scheme 6.5a**). ETD mass spectra of α-MSH + DSP + Ac-RFMWMK-NH_2 in the 4+ and 3+ charge states are shown in **Figure 6.4**. ETD of the cross-linked peptide in the 4+ charge state predominantly resulted in cleavage of the disulfide bond, producing the complementary Lα9 and Lβ9 ions (**Figure 6.4a**). Cleavage of the S–S bond is shown schematically based on the proposed mechanism for dissociation of disulfide-containing peptides (**Scheme 6.5b**).[38] A high abundance of the charge reduced precursor was also observed upon ETD of the DSP-

cross-linked peptides (4+). Upon ETD of the triply charged cross-linked peptide, charge reduction via electron attachment without subsequent dissociation was the dominant pathway, with only minor production of the Lα9 product ion stemming from cleavage of the disulfide bond (**Figure 6.4b**). The complementary Lβ9 fragment ion was not detected.

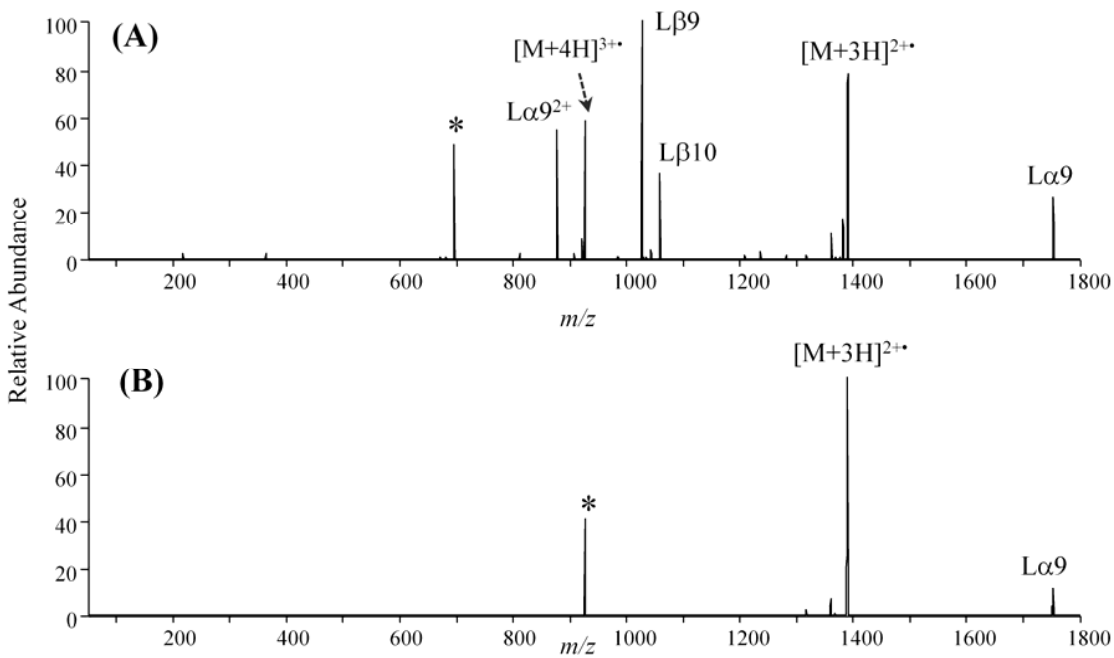

Figure 6.4 ETD product ion mass spectra of α-MSH + DSP + Ac-RFMWMK-NH_2 in the (A) 4+ and (B) 3+ charge states. The ETD reaction times were 50 ms and 75 ms, respectively. The first peptide listed is referred to as α and the second peptide as β. The precursor ion is represented by an asterisk (*).

The propensity for cleavage of the N12–N13 bond of BAH-cross-linked peptides relative to the cleavage of the S–S bond of DSP-cross-linked peptides is summarized in **Table 6.2**. Upon ETD of the BAH-cross-linked peptides in the 4+ charge state (i.e., in which the hydrazone functionality is presumed to be protonated), between 65% and 70% of the product ions were due to cleavage of the N12–N13 bond, leading to the diagnostic

Table 6.2 Product partitioning between ETD, electron transfer without dissociation (ETnoD), proton transfer (PT), and hydrazone (N–N) or disulfide bond cleavage (S–S) of BAH- or DSP-cross-linked peptides, respectively. The ion-ion reaction time was 80 ms.

Cross-Linked Peptide	Charge State	% ETD	% ETnoD + % PT	% N-N or S-S / % (ETD + ETnoD + PT)
Ac-AAAKAAAAR + BAH + Ac-AAAKAAAAR	3+	95.54	4.46	64.86
Ac-AAAKAAAAR + BAH + Ac-AAAKPAAAR	3+	96.07	3.93	69.63
α-MSH + BAH + Ac-RFMWMK-NH_2	4+	90.10	9.90	70.65
α-MSH + BAH + Ac-RFMWMK-NH_2	3+	48.00	52.00	24.88
Ac-RFMWMK-NH_2 + BAH + α-MSH	4+	92.75	7.25	66.21
Ac-RFMWMK-NH_2 + BAH + α-MSH	3+	42.15	57.85	20.01
Ac-RFMWMK-NH_2 + DSP + α-MSH	4+	62.05	37.95	42.89
Ac-RFMWMK-NH_2 + DSP + α-MSH	3+	12.20	87.80	5.97

Lα12/Lβ11$^{\bullet}$ products Upon ETD of the DSP-cross-linked peptides in the 4+ charge state, only 43% of the product ions were due to disulfide bond cleavage. For the 3+ charge state, the value dropped to approximately 20% to 25% for the BAH-cross-linked peptides and 6% for the DSP-cross-linked peptides. These results indicate that there is a clear preference for the dissociation of the hydrazone bond by ETD.

6.4.3 Sequencing of Cross-Linked Peptides by ETD-CID MS^n Methods

The high propensity for the hydrazone bond cleavage upon ETD provides a means to individually sequence the two constituent peptides of intermolecularly BAH-cross-

linked peptides through an MS^3 strategy as shown in **Scheme 6.6**. After conjugation of the two peptides of interest, ETD of the cross-linked species yields the two peptides with each containing a unique mass tag based on its original conjugation reagent – 131 Da for the peptide covalently modified by SFB (Lα12), or 119 Da for the peptide modified by SANH (Lβ11$^{\bullet}$). These key primary product ions, Lα12 and Lβ11$^{\bullet}$, formed upon ETD are excellent candidates for subsequent CID in order to sequence each constituent peptide individually. Subsequent CID (MS^3) of each modified peptide produces diagnostic fragment ions that allow sequencing of each peptide and location of the site of cross-linking. Although **Scheme 6.6** for simplicity shows the conjugation of peptides, the strategy is geared for more compelling protein applications, in which the conjugation of proteins is followed by enzymatic digestion to produce cross-linked peptides that can be used to track and identify the conjugation pattern of the targeted proteins.

The sequence coverage obtained by the ETD-CID method was compared to CID alone for the cross-linked complex containing α-MSH (Ac-SYSMEHFRWGKPV-NH_2) and Ac-RFMWMK-NH_2, first with α-MSH as the α-peptide and Ac-RFMWMK-NH_2 as the β-peptide, then reversed. The CID mass spectra of these crosslinked peptides are shown in **Figure 6.5**. CID predominantly results in cleavage of amide bonds near the cross-linked lysines, yielding cross-linker-containing fragment ions such as lysine immonium ions linked to the other peptide (e.g. $K^{L}\alpha$ or $K^{L}\beta$) or ions due to cleavage of the cross-link amide bond (e.g. Lα18 or Lβ18; see **Scheme 6.3**). Only a single abundant peptide sequence ion was observed, the b_5 ion of Ac-RFMWMK-NH_2 ($b_{5\beta}$), and no fragment ions of α-MSH were detected. The CID results did not provide sufficient diagnostic sequence information to identify the peptides nor locate the sites of the cross-links.

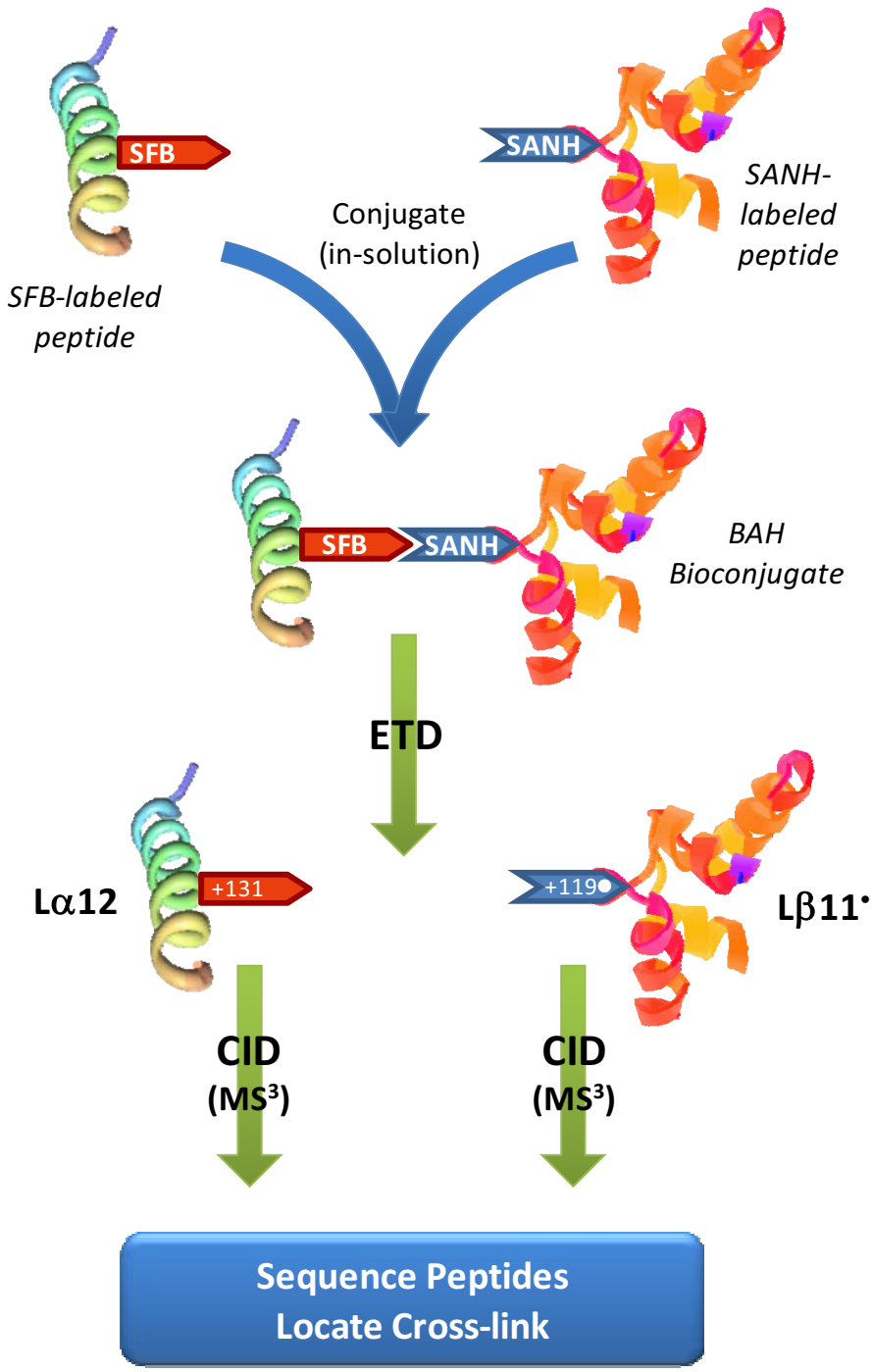

Scheme 6.6 Conjugation and ETD-CID-MS strategy for sequencing BAH-cross-linked peptides.

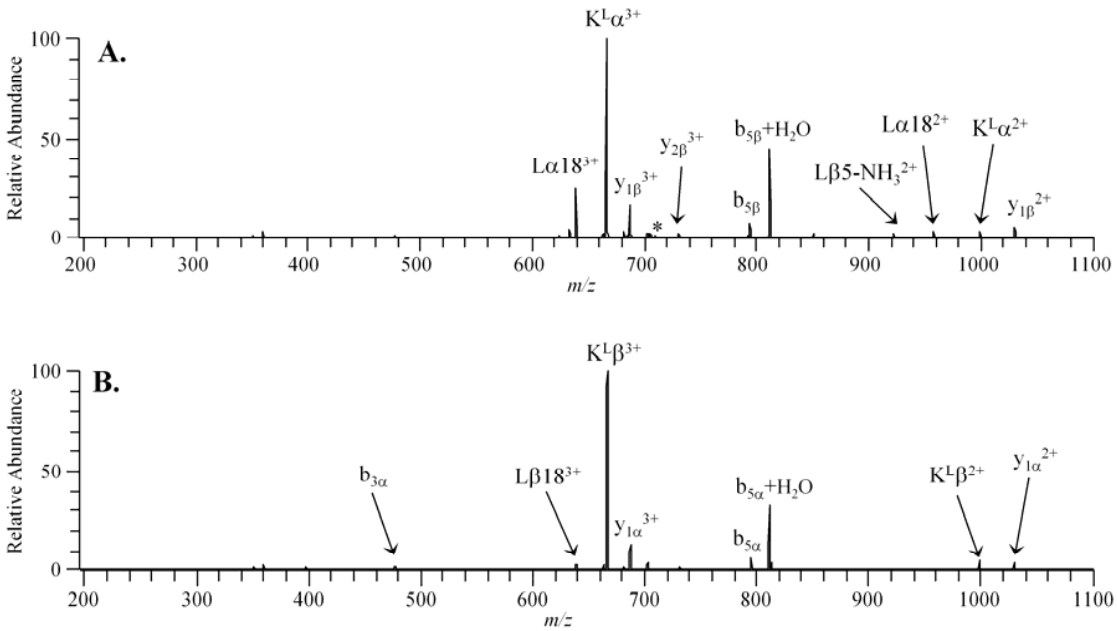

Figure 6.5 (A) CID mass spectrum of $[\alpha\text{-MSH} + \text{BAH} + \text{Ac-RFMWMK-NH}_2 + 4\text{H}]^{4+}$ of *m/z* 714.1 (11% NCE). (B) CID mass spectrum of $[\text{Ac-RFMWMK-NH}_2 + \text{BAH} + \alpha\text{-MSH} + 4\text{H}]^{4+}$ of *m/z* 714.1 (11% NCE). The first peptide listed is referred to as α and the second peptide as β. The precursor ion is represented by an asterisk (*).

The ETD-CID results are shown in Figure 6.7. In this case, the $[L\alpha12 + H]^+$ and $[L\beta11 + 2H]^{2+\bullet}$ produced upon ETD of the (Ac-RFMWMK-NH_2 + BAH + α-MSH) complexes were selected for CID. CID of the even-electron Lα12 ion (Ac-RFMWMK-NH_2 + 131 Da) yielded a variety of a-, b-, and y-ions, the types of product ions which are typically observed upon CID of peptides (**Figure 6.6a**). Full sequence coverage (as defined as number of observed backbone cleavages divided by the number of backbone bonds) of the Ac-RFMWMK-NH_2 peptide was obtained, and the cross-link site was confirmed at Lys-6 through the observation of the unmodified b_5 ion and the y_2 ion which contains the 131 Da mass tag. In fact, all of the y-ions contained the cross-linker mass tag. Likewise, there were no ions arising from cleavage of the amide bond connecting

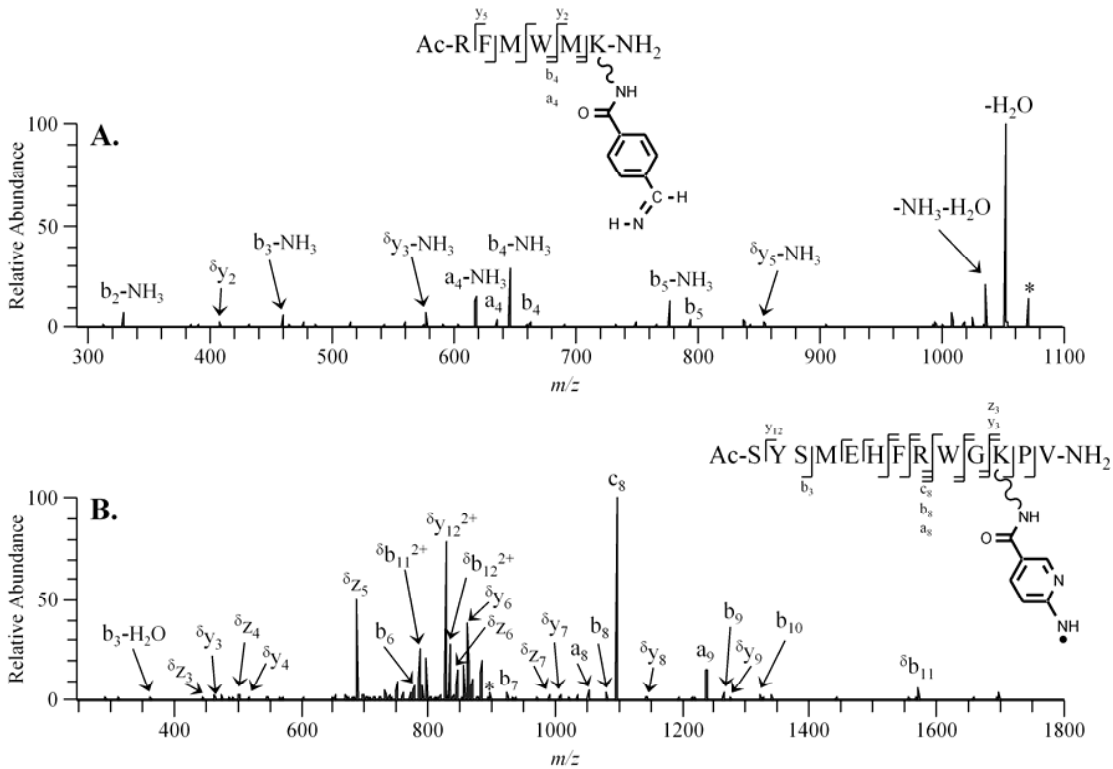

Figure 6.6 CID mass spectra (MS^3) of product ions from ETD of [Ac-RFMWMK-NH_2 + BAH + α-MSH + 4H]$^{4+}$ of *m/z* 714.1 (30 ms reaction time). The first peptide listed is referred to as α and the second peptide as β. (A) MS^3 CID mass spectrum of [Lα12 + H]$^+$ of *m/z* 1070.2 (17% NCE). (B) MS^3 CID mass spectrum of [Lβ11 + 2H]$^{2+\bullet}$ of *m/z* 892.6 (15% NCE). Product ions which retain the modification are labeled with δ. The precursor ion is represented by an asterisk (*).

the SFB moiety and the lysine side chain. CID of the odd-electron Lβ11$^\bullet$ ion (α-MSH + 119 Da) yielded a-, b-, c-, y- and z-type ions – a mixture of product ions which are generally observed upon CID (a-, b-, and y-ions) and ETD (c/z$^\bullet$-ions) of conventional peptides (**Figure 6.6b**). The c- and z-type ions are most likely produced by radical-driven backbone cleavages in which the radical is mobilized upon collisional activation. Since the radical can also be stabilized by delocalization within the pyridinyl ring, dissociation of backbone amide bonds also occurs, yielding the b- and y-ions which are

conventional charge-directed fragment ions. While spectral interpretation can be more difficult when a greater array of types of fragment ion are produced, in this case near complete sequence coverage (91.7%) of the β-peptide was obtained. The 119 Da (SANH) mass tag was retained upon CID of this Lβ11$^{\bullet}$ peptide, thus allowing the cross-linking site to be pinpointed to the Lys-11 site based on the detection of the unmodified b_{10} and modified b_{11} ions.

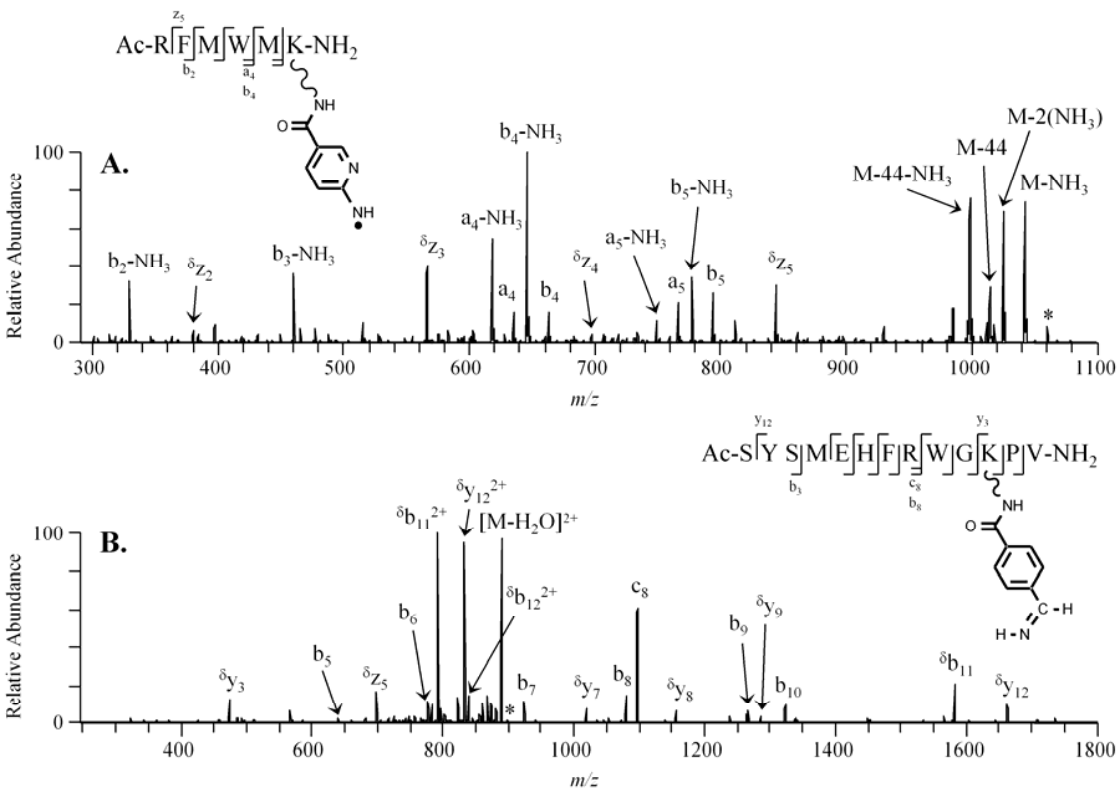

Figure 6.7 CID mass spectra of product ions from ETD of [α-MSH + BAH + Ac-RFMWMK-NH_2 + 4H]$^{4+}$ of *m/z* 714.1 (30 ms reaction time). The first peptide listed is referred to as α and the second peptide as β. (**A**) MS^3 CID mass spectrum of [Lβ11 + H]$^{+\bullet}$ of *m/z* 1059.3 (18% NCE). (**B**) MS^3 CID mass spectrum of [Lα12 + 2H]$^{2+}$ of *m/z* 898.2 (14.5% NCE). Product ions which retain the modification are labeled with δ. The precursor ion is represented by an asterisk (*).

CID of the Lβ11$^{\bullet}$ and Lα12 ions formed upon ETD of the same peptide cross-linked in the opposite orientation, (α-MSH + BAH + Ac-RFMWMK-NH_2), also provided near complete sequence coverage of the two peptides (**Figure 6.7**). For the Lβ11$^{\bullet}$ ion (Ac-RFMWMK + 119 Da, SANH tag), radical-induced cleavages (z-ions) and traditional charge-directed fragments (a-, b-, and y-type ions) were observed upon CID (**Figure 6.7a**), similar to the types of products observed for the other Lβ11$^{\bullet}$ ion described above. CID of the Lα12 ion (α-MSH + 131 Da, SFB tag), as shown in **Figure 6.7b,** predominantly yielded b- and y-type ions along with one c- and one z-type fragment ion. The observation of an unmodified b_{10} ion along with a b_{11} ion containing the 131 Da SFB tag pinpoints the cross-link to Lys-11 of α-MSH. Full sequence coverage of the α-peptide (Ac-RFMWMK-NH_2) was observed by the ETD-CID method, and all but one backbone bond was cleaved of the β-peptide (α-MSH; 91.7% sequence coverage).

For both the Lβ11$^{\bullet}$ and Lα12 ions created upon ETD of the cross-linked peptides, the SFB and SANH mass tags were retained upon collisional activation, allowing conclusive identification of the site of the cross-link. It is critical that the cross-linker mass tags are retained upon ion activation; if the cross-link amide bonds are cleaved upon CID, then all tracking information about the unique location of the site of cross-linking is lost. These key amide bonds are in fact cleaved upon CID of the cross-linked peptides, and thus the sites of cross-linking cannot be determined for the constituent peptides by direct CID. Another advantage of the ETD-CID strategy as opposed to direct CID is that double-cleavage cross-linked product ions are not observed. CID of cross-linked peptides often yields product ions which are due to cleavage of multiple backbone amide bonds as discussed in Chapter 3, such as combined dissociation of an amide bond of the α-peptide and an amide bond of the β-peptide, producing fragment ions of the form $b_{n\alpha}{}^{L}y_{n\beta}$. While these types of product ions can be informative, they are difficult to

identify and typically require manual interpretation. In contrast, the ETD-CID technique allows the two constituent peptides to be sequenced individually and simplifies spectral interpretation.

Collision-induced dissociation of the charge-reduced products arising from electron transfer (but without dissociation) of the cross-linked peptides was also performed to determine if preferential cleavage of the hydrazone bond could be observed from the non-dissociative electron transfer product (**Figure 6.8**). An example of this type of charge-reduced ion (*m/z* 951.6) was noted in **Figure 6.2** upon ETD of [Ac-RFMWMK-NH_2 + BAH + α-MSH]$^{4+}$. Typically, supplemental activation in the form of resonant collisional excitation[44] or IR irradiation[45, 46] of charge-reduced peptides yields c- and $z^{\bullet}$-type fragment ions. It is thought that the c and $z^{\bullet}$ ions are initially held together by non-covalent interactions in the charge-reduced products, and supplemental activation releases them as free fragment ions. In the present study, CID of the charge-reduced [Ac-RFMWMK-NH_2 + BAH + α-MSH]$^{3+\bullet}$ ion resulted in a broad array of c- and $z^{\bullet}$-type ions, in addition to even electron b- and y-type fragment ions (**Figure 6.8**). The abundances of

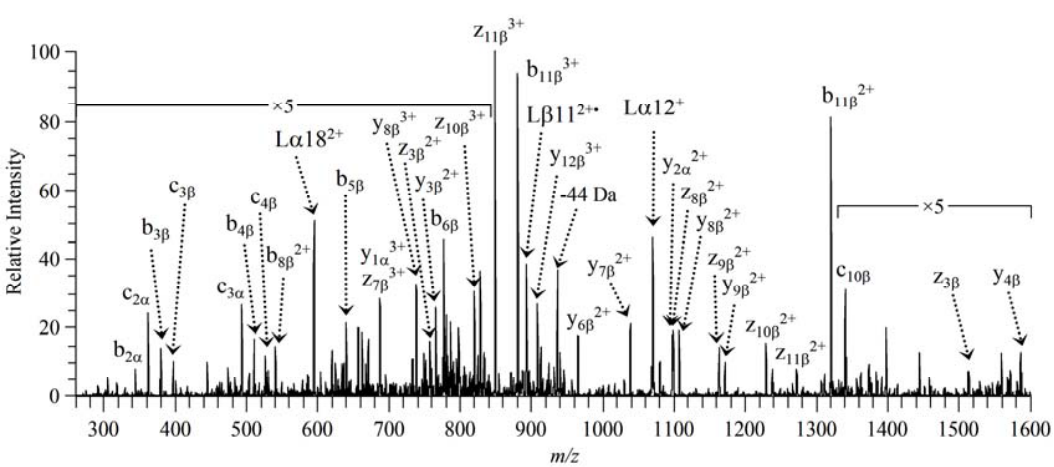

Figure 6.8 ET-CID mass spectrum of [Ac-RFMWMK-NH_2 + BAH + α-MSH + 4H]$^{3+\bullet}$ of *m/z* 951.6 (12.5% NCE). The first peptide listed is referred to as α and the second peptide as β.

Lα12 and Lβ11• ions was low. These results suggest that only a small fraction of the charge-reduced cross-linked peptides are comprised of the Lα12 and Lβ11• ions held together by non-covalent bonds.

The sequence information obtained upon CID of the Lα9 and Lβ9 product ions formed upon ETD of the DSP-cross-linked peptides was compared to the ETD-CID results for the analogous BAH-cross-linked peptides. CID of the Lα9 product ion formed upon ETD of α-MSH + DSP + Ac-RFMWMK-NH_2 produced many unidentifiable product ions in addition to neutral losses stemming from the CO–CH_2–CH_2–SH modification at Lys-11 of α-MSH (data not shown). The Lβ9 product ion (i.e., Ac-RFMWMK-NH_2 + CO–CH_2–CH_2–SH) yielded a complex array of a-, b-, c-, y-, and z-type ions. The amide bond between the cross-linked Lys residue and the CO–CH_2–CH_2–SH tag was also cleaved upon CID of the complementary Lα9 and Lβ9 ions, and thus the tracking information to identify the site of cross-link was lost. In general, lower sequence coverage was obtained using the ETD-CID technique for the DSP-cross-linked peptides compared to the BAH-cross-linked peptides. In addition, upon ETD of these cross-linked peptides greater preferential cleavage of the hydrazone bond compared to disulfide bond cleavage was observed, thus showcasing the compelling advantages of ETD for the analysis of hydrazone-conjugated peptides.

6.5 CONCLUSIONS

Electron transfer dissociation of intermolecularly bis-arylhydrazone cross-linked peptides resulted in preferential dissociation of the N12–N13 hydrazone bond. Cleavage of the hydrazone bond yields the two constituent peptides – one an even-electron product with a 131 Da mass tag (Lα12) and the other an odd-electron product with a 119 Da mass tag (Lβ11•). Greater than 65% of the ion current is comprised of these two key products

for BAH-cross-linked peptides that possess a mobile proton which is presumed to be at least partially localized at the hydrazone functionality. The hydrazone bond cleaves more efficiently than the disulfide bond in analogous DSP-cross-linked peptides. The high propensity for dissociation of the N12–N13 hydrazone bond is presumed to be due to capture of the electron directly at the protonated hydrazone functionality and subsequent rearrangement. This pathway does not require the migration of a hydrogen atom to initiate dissociation as is proposed for the conventional production of c- and $z^{\bullet}$-type fragment ions upon ETD of peptides. Upon subsequent CID, these primary ETD product ions, Lα12 and Lβ11$^{\bullet}$, afford near complete sequence coverage of each constituent peptide. CID of the Lβ11$^{\bullet}$ ion yielded a-, b-, c-, y-, and z-type ions, and CID of the complementary Lα12 ion produced predominantly a-, b-, and y-type ions, with conclusive identification of the cross-linking site. CID of the intact cross-linked peptides did not afford full sequence coverage of each peptide nor identification of the cross-link site. The ETD-CID technique decouples the two constituent peptides and treats the cross-linked peptide instead as two modified peptides which can be sequenced individually, thus allowing the potential use of database search algorithms for peptide sequencing and identification.

6.6 REFERENCES

(1) Borch, J.; Jorgensen, T. J. D.; Roepstorff, P. *Current Opinion in Chemical Biology* **2005**, *9*, 509-516.

(2) Heck, A. J. R.; van den Heuvel, R. H. H. *Mass Spectrometry Reviews* **2004**, *23*, 368-389.

(3) Juan, H.-F.; Liu, H.-L.; Hsu, J.-P. *Current Proteomics* **2004**, *1*, 183-197.

(4) Sinz, A. *Mass Spectrometry Reviews* **2006**, *25*, 663-682.

(5) Back, J. W.; De Jong, L.; Muijsers, A. O.; De Koster, C. G. *Journal of Molecular Biology* **2003**, *331*, 303-313.

(6) Trakselis, M. A.; Alley, S. C.; Ishmael, F. T. *Bioconjugate Chemistry* **2005**, *16*, 741-750.

(7) Young, M. M.; Tang, N.; Hempel, J. C.; Oshiro, C. M.; Taylor, E. W.; Kuntz, I. D.; Gibson, B. W.; Dollinger, G. *Proceedings of the National Academy of Sciences of the United States of America* **2000**, *97*, 5802-5806.

(8) Back, J. W.; Sanz, M. A.; De Jong, L.; De Koning, L. J.; Nijtmans, L. G. J.; De Koster, C. G.; Grivell, L. A.; Van Der Spek, H.; Muijsers, A. O. *Protein Science* **2002**, *11*, 2471-2478.

(9) Chu, F.; Maynard, J. C.; Chiosis, G.; Nicchitta, C. V.; Burlingame, A. L. *Protein Science* **2006**, *15*, 1260-1269.

(10) Lanman, J.; Lam, T. T.; Barnes, S.; Sakalian, M.; Emmett, M. R.; Marshall, A. G.; Prevelige, P. E. *Journal of Molecular Biology* **2003**, *325*, 759-772.

(11) Schulz, D. M.; Ihling, C.; Clore, G. M.; Sinz, A. *Biochemistry* **2004**, *43*, 4703-4715.

(12) Huang, B. X.; Kim, H.-Y. *Molecular and Cellular Proteomics* **2006**, *5*, 1045-1053.

(13) Bovet, C.; Ruff, M.; Eiler, S.; Granger, F.; Wenzel, R.; Nazabal, A.; Moras, D.; Zenobi, R. *Analytical Chemistry* **2008**, *80*, 7833-7839.

(14) Chowdhury, S. M.; Munske, G. R.; Tang, X.; Bruce, J. E. *Analytical Chemistry* **2006**, *78*, 8183-8193.

(15) Chu, F.; Mahrus, S.; Craik, C. S.; Burlingame, A. L. *Journal of the American Chemical Society* **2006**, *128*, 10362-10363.

(16) Hurst, G. B.; Lankford, T. K.; Kennel, S. J. *Journal of the American Society for Mass Spectrometry* **2004**, *15*, 832-839.

(17) Sinz, A.; Kalkhof, S.; Ihling, C. *Journal of the American Society for Mass Spectrometry* **2005**, *16*, 1921-1931.

(18) Back, J. W.; Notenboom, V.; de Koning, L. J.; Muijsers, A. O.; Sixma, T. K.; de Koster, C. G.; de Jong, L. *Analytical Chemistry* **2002**, *74*, 4417-4422.

(19) Ihling, C.; Schmidt, A.; Kalkhof, S.; Schulz, D. M.; Stingl, C.; Mechtler, K.; Haack, M.; Beck-Sickinger, A. G.; Cooper, D. M. F.; Sinz, A. *Journal of the American Society for Mass Spectrometry* **2006**, *17*, 1100-1113.

(20) Mueller, D. R.; Schindler, P.; Towbin, H.; Wirth, U.; Voshol, H.; Hoving, S.; Steinmetz, M. O. *Analytical Chemistry* **2001**, *73*, 1927-1934.

(21) Sinz, A.; Wang, K. *Biochemistry* **2001**, *40*, 7903-7913.

(22) Sinz, A.; Wang, K. *Analytical Biochemistry* **2004**, *331*, 27-32.

(23) Wine, R. N.; Dial, J. M.; Tomer, K. B.; Borchers, C. H. *Analytical Chemistry* **2002**, *74*, 1939-1945.

(24) Yan, F.; Che, F.-Y.; Rykunov, D.; Nieves, E.; Fiser, A.; Weiss, L. M.; Hogue Angeletti, R. *Analytical Chemistry* **2009**, *81*, 7149-7159.

(25) Gardner, M. W.; Vasicek, L. A.; Shabbir, S.; Anslyn, E. V.; Brodbelt, J. S. *Analytical Chemistry* **2008**, *80*, 4807-4819.

(26) Back, J. W.; Hartog, A. F.; Dekker, H. L.; Muijsers, A. O.; de Koning, L. J.; de Jong, L. *Journal of the American Society for Mass Spectrometry* **2001**, *12*, 222-227.

(27) Tang, X.; Munske, G. R.; Siems, W. F.; Bruce, J. E. *Analytical Chemistry* **2005**, *77*, 311-318.

(28) Chowdhury, S. M.; Du, X.; Tolic, N.; Wu, S.; Moore, R. J.; Mayer, M. U.; Smith, R. D.; Adkins, J. N. *Analytical Chemistry* **2009**, *81*, 5524-5532.

(29) Soderblom, E. J.; Goshe, M. B. *Analytical Chemistry* **2006**, *78*, 8059-8068.

(30) Soderblom, E. J.; Bobay, B. G.; Cavanagh, J.; Goshe, M. B. *Rapid Communications in Mass Spectrometry* **2007**, *21*, 3395-3408.

(31) Lu, Y.; Tanasova, M.; Borhan, B.; Reid, G. E. *Analytical Chemistry* **2008**, *80*, 9279-9287.

(32) King, G. J.; Jones, A.; Kobe, B.; Huber, T.; Mouradov, D.; Hume, D. A.; Ross, I. L. *Analytical Chemistry* **2008**, *80*, 5036-5043.

(33) Gaucher, S. P.; Hadi, M. Z.; Young, M. M. *Journal of the American Society for Mass Spectrometry* **2006**, *17*, 395-405.

(34) Gardner, M. W.; Brodbelt, J. S. *Journal of the American Society for Mass Spectrometry* **2008**, *19*, 344-357.

(35) Zubarev, R. A.; Kelleher, N. L.; McLafferty, F. W. *Journal of the American Chemical Society* **1998**, *120*, 3265-3266.

(36) Syka, J. E. P.; Coon, J. J.; Schroeder, M. J.; Shabanowitz, J.; Hunt, D. F. *Proceedings of the National Academy of Sciences of the United States of America* **2004**, *101*, 9528-9533.

(37) McLafferty, F. W.; Horn, D. M.; Breuker, K.; Ge, Y.; Lewis, M. A.; Cerda, B.; Zubarev, R. A.; Carpenter, B. K. *Journal of the American Society for Mass Spectrometry* **2001**, *12*, 245-249.

(38) Zubarev, R. A.; Kruger, N. A.; Fridriksson, E. K.; Lewis, M. A.; Horn, D. M.; Carpenter, B. K.; McLafferty, F. W. *Journal of the American Chemical Society* **1999**, *121*, 2857-2862.

(39) Gunawardena, H. P.; Gorenstein, L.; Erickson, D. E.; Xia, Y.; McLuckey, S. A. *International Journal of Mass Spectrometry* **2007**, *265*, 130-138.

(40) Gardner, M. W.; Brodbelt, J. S. *Analytical Chemistry* **2009**, *81*, 4864-4872.

(41) Schilling, B.; Row, R. H.; Gibson, B. W.; Guo, X.; Young, M. M. *Journal of the American Society for Mass Spectrometry* **2003**, *14*, 834-850.

(42) Eng, J. K.; McCormack, A. L.; Yates, J. R., III *Journal of the American Society for Mass Spectrometry* **1994**, *5*, 976-989.

(43) Perkins, D. N.; Pappin, D. J. C.; Creasy, D. M.; Cottrell, J. S. *Electrophoresis* **1999**, *20*, 3551-3567.

(44) Swaney, D. L.; McAlister, G. C.; Wirtala, M.; Schwartz, J. C.; Syka, J. E. P.; Coon, J. J. *Analytical Chemistry* **2007**, *79*, 477-485.

(45) Tsybin, Y. O.; Witt, M.; Baykut, G.; Kjeldsen, F.; Hakansson, P. *Rapid Communications in Mass Spectrometry* **2003**, *17*, 1759-1768.

(46) Ledvina, A. R.; McAlister, G. C.; Gardner, M. W.; Smith, S. I.; Madsen, J. A.; Schwartz, J. C.; Stafford, G. C., Jr.; Syka, J. E. P.; Brodbelt, J. S.; Coon, J. J. *Angewandte Chemie, International Edition* **2009**, *In Press*.

Chapter 7

Infrared Multiphoton Dissociation of Peptide Cations in a Dual Pressure Linear Ion Trap Mass Spectrometer

7.1 OVERVIEW

A dual pressure linear ion trap mass spectrometer was modified to permit infrared multiphoton dissociation (IRMPD) in each of the two cells – the first a high pressure cell operated at nominally 5×10^{-3} Torr and the second a low pressure cell operated at nominally 3×10^{-4} Torr. When IRMPD was performed in the high pressure cell, most peptide ions did not undergo significant photodissociation; however, in the low pressure cell peptide cations were efficiently dissociated with less than 25 ms of IR irradiation regardless of charge state. IRMPD of peptide cations allowed the detection of low *m/z* product ions including the y_1 fragments and immonium ions which are not typically observed by ion trap collision induced dissociation (CID). Photodissociation efficiencies of ~100% and MS/MS (tandem mass spectrometry) efficiencies of greater than 60% were observed for both multiply and singly protonated peptides. In general, higher sequence coverage of peptides was obtained using IRMPD over CID. Further, greater than 90% of the product ion current in the IRMPD mass spectra of doubly charged peptide ions was composed of singly charged product ions compared to the CID mass spectra in which the abundances of the multiply and singly charged product ions were equally divided. Highly charged primary product ions also underwent efficient photodissociation to yield singly charged secondary product ions, thus simplifying the IRMPD product ion mass spectra.

7.2 INTRODUCTION

As the field of proteomics continues to expand, there has become a growing need for more advanced mass spectrometric techniques for the characterization of biological molecules.[1, 2] Tandem mass spectrometry methods have played a crucial role in the sequencing of proteolytic peptides and identification of proteins.[3, 4] The most common means of fragmenting gas-phase peptide ions is collision-induced dissociation (CID) in which selected ions gain internal energy through collisions with rare gas atoms.[5] However, the amino acid sequence and charge state can greatly influence dissociation; CID is often limited by incomplete backbone fragmentation, preferential backbone cleavage at proline or acidic residues,[6, 7] or dominant loss of labile groups which results in low peptide sequence coverage.[8] These limitations of CID have sparked interest in the development of alternative and more universal ion activation and dissociation methods in recent years.[9, 10] New electron-based activation methods such as electron capture dissociation (ECD)[11] and electron transfer dissociation (ETD)[12] have shown significant promise as each method maintains labile side-chain modifications during ion activation; however, both techniques are limited to the analysis of multiply charged peptides.[13] More recently, electron ionization dissociation (EID) has been developed which utilizes fast electrons to dissociate singly charged peptide cations but the backbone fragment yields obtained were generally less than 5%.[14]

There has also been considerable interest in exploiting photons for ion activation, including infrared multiphoton dissociation (IRMPD),[15-19] ultraviolet photodissociation (UVPD),[20-24] and more recently the use of femtosecond pulsed lasers,[25] and hybrid UVPD-CID methods.[26] One of the primary advantages of performing IRMPD in quadrupole ion traps (QITs)[16-19, 27-29] is the ability to fine-tune the energy deposition by varying the irradiation time or number of laser pulses, the laser power or flux, and

wavelength. In addition, compared to CID, photodissociation is largely independent of the rf trapping voltage during ion activation which provides a broader *m/z* trapping range,[18, 30] an advantage also recognized for ETD. Energy deposition by conventional CID is more efficient at higher rf trapping voltages (i.e., q-values) which prevents storage of product ions of *m/z* below the low-mass cut-off (LMCO), which is approximately the lower 28% of the *m/z* trapping range relative to the precursor ion. CID can be performed at lower q-values but with lower dissociation efficiencies. In addition, pulsed Q-dissociation (PQD)[31] and high amplitude short time excitation (HASTE)[32] have shown promise as alternative collision based fragmentation methods which do not suffer as greatly from the low-mass cut-off problem; however both of these techniques afford modest MS/MS efficiencies. IRMPD can be efficiently performed at low rf trapping voltages because the activation process is not defined by the rf trapping parameters, allowing observation of many informative low-mass fragments including immonium ions and y_1 fragment ions of peptides. Photodissociation is also a non-resonant process in which the precursor ion and all product ions are irradiated and activated simultaneously; thus, dead-end dissociation pathways such as dehydration are largely circumvented as these primary product ions can undergo secondary dissociation to yield more diagnostic fragments. In addition, the photon absorption process does not affect the translational motion of ions and alleviates ion losses due to unstable trajectories that might be encountered in traditional CID.

Infrared multiphoton dissociation has not been widely implemented in quadrupole ion traps due to low fragmentation efficiencies of certain analytes including peptides and proteins. For optimal performance, quadrupole ion trap mass spectrometers are typically operated at a pressure of ~1 – 5 mTorr of He to effectively trap ions and reduce their kinetic energy via collisions with the buffer gas atoms.[33] This high pressure, however,

can cause ion deactivation through collisional cooling at a nearly equivalent or greater rate than that of ion activation by IR photon absorption, ultimately resulting in the observation of low dissociation efficiencies for IRMPD.[10, 34] Several methods have been developed to improve the efficiency of IRMPD in quadrupole ion traps. The pressure in the QIT has been adjusted during the scan function through pulsed gas introduction[35] or dynamic pressure control[36] in which the bath gas is introduced during ion accumulation and then pumped away prior to IR irradiation. Payne et al. utilized thermally-assisted IRMPD[30] and Hashimoto and coworkers collisionally-activated the precursor ions during IR irradiation[37] to increase the internal energy of the ions to provide efficient photodissociation at standard QIT operating pressures. Newsome and Glish recently reported focusing the IR laser to the center of the ion trap as a simple means to improve IRMPD of peptides by increasing the overlap of the ion cloud with the laser beam and exposing the ions to a higher photon flux.[19] Previous work in the Brodbelt group has focused on the development of chemical derivatization techniques that attach chromogenic labels to increase the IR absorption cross sections or reduce the critical energies for dissociation.[38-40] Super-charged peptides can also be efficiently photodissociated in a linear quadrupole ion trap due to a reduction in the dissociation threshold and an increase in the number of mobile protons.[41]

In this chapter, it is demonstrated that unmodified peptides can be efficiently and rapidly dissociated by IR irradiation in the low pressure cell of a dual pressure linear ion trap (LIT). The dual pressure LIT comprises a low pressure cell and high pressure cell to combine the advantages of both pressure regimes.[42] High trapping, isolation, and CID efficiencies are obtained in the high pressure cell (~5×10^{-3} Torr), while the low pressure cell (~3×10^{-4} Torr) offers improved scanning speed and mass resolution. Little photodissociation of peptide ions occurs in the high pressure cell, while highly efficient

IRMPD is observed in the low pressure cell yielding complete dissociation of the precursor ions with less than 25 ms of irradiation. Higher sequence coverage of peptides is obtained by performing IRMPD in the low pressure cell as compared to traditional CID in the high pressure cell.

7.3 EXPERIMENTAL

7.3.1 Chemicals and Reagents

All materials and peptides were used without further purification. The peptides RPKPQQFFGLM-NH_2 (substance P), FSWGAEGQR, YGGFLK, ASHLGLAR, and AGCKNFFWKTFTSC (somatostatin-14) were obtained from Bachem (King of Prussia, PA). DRVYIHPF (angiotensin II), ADSGEGDFLAEGGGVR (fibrinopeptide A), and RPPGFSPFR (bradykinin) were purchased from American Peptide Co. (Sunnyvale, CA). All solvents and other chemicals including melittin (honey bee venom) were from Sigma-Aldrich (St. Louis, MO).

7.3.2 Mass Spectrometry and Infrared Multiphoton Dissociation

All samples were prepared at ~10 μM in 49.5:49.5:1 H_2O/MeOH/acetic acid (v/v/v) and infused at 3 μL/min using the standard electrospray ionization source. Unless indicated otherwise, all mass spectrometry experiments were performed on a modified LTQ Velos dual pressure linear ion trap (Thermo Fisher Scientific, San Jose, CA). A schematic of the instrument is shown in **Figure 7.1**; details of the instrument have been described previously.[42] In brief, the octapole preceding the linear ion trap was reduced in length to accommodate an additional linear ion trap. The two traps are of a symmetrical design and have independent DC power supplies for the six total sections, but have a

single common rf power supply. The pressure of each cell of the dual pressure LIT was regulated by the conductance limits of the front, center, and back lenses. The high pressure cell was maintained at 5 to 6 mTorr He and the low pressure cell at ~0.3 mTorr He. Precursor ions were isolated and cooled in the high pressure cell while mass analysis was performed in the low pressure cell; ion activation and dissociation could be performed in either cell. The ion source optics include a progressively spaced stacked ring ion guide for the improved ion transmission.[43] Photodissociation was implemented on this dual LIT in a manner similar to that described previously.[44] The back flange of the mass spectrometer was modified with a ZnSe window to transmit IR irradiation through a 1.8 mm stainless steel aperture on-axis with the dual pressure LIT. For all IRMPD experiments, the laser power was maintained at 100% (50 W); both the irradiation time (0 – 250 ms) and the q-value (0.05 – 0.25) of the precursor ion were varied. Collision-induced dissociation experiments were conducted solely in the high pressure cell; ions were activated for 30 ms at a q-value of 0.25. IRMPD was performed with a model 48-5 Synrad 50-W CO_2 continuous wave laser (Mukilteo, WA) which emits at 10.6 μm. Other time-resolved IRMPD and MS^3 experiments were performed on a standard LTQ XL mass spectrometer (i.e. single trap) modified for photodissociation operating at ~2.5 mTorr He.

7.3.3 Data Analysis

IRMPD was performed in each of the two cells. Dissociation efficiencies were calculated according to the following formula:

$$Dissociation\ Efficiency = \frac{\sum_i F_i}{\sum_i F_i + P} \times 100\%$$

Equation 7.1

where P is the abundance of the surviving precursor ion after ion activation, and F_i is the abundance of each product ion. The efficiency of the tandem MS experiment (i.e., MS/MS efficiency) is defined below:

$$MS/MS\ Efficiency = \frac{\sum_i F_i}{P_0} \times 100\%$$

Equation 7.2

where P_0 is the abundance of the precursor ion prior to any IR irradiation or collisional activation, and F_i is the abundance of each product ion.[45] The sum of the product ion abundance (i.e., ΣF_i) was determined by subtracting the abundance of any remaining precursor ion from the total ion abundance for the efficiency calculations. Ion abundances were determined by calculating the peak areas using Origin 7.0. Time-resolved IRMPD experiments were performed by incrementally increasing the irradiation time and the abundances of different ion types were plotted against irradiation time. Similarly, q-value resolved IRMPD was performed by sequentially raising the activation q-value and acquiring IRMPD mass spectra at each q-value. All time-resolved and q-value resolved IRMPD experiments were performed in triplicate. The precursor ion abundance was plotted relative to the initial precursor abundance without any ion activation or irradiation (P_0), while the product ion abundances were plotted relative to the total ion current (sum of all fragment ions and precursor, P) in each IRMPD mass spectrum. The abundances and number of product ions in each charge state were also determined by summing the abundances (i.e., peak areas) or counting the number of product ions in each charge state. If a peak's charge state could not be resolved, its area

was not included in the abundance calculation nor was it counted. All spectra are an average of ten scans. Peptide fragment nomenclature includes superscripts "*" and "°" to designate ammonia loss and water loss, respectively. Immonium ions are labeled with the single letter amino acid residue with a subscript *i*.

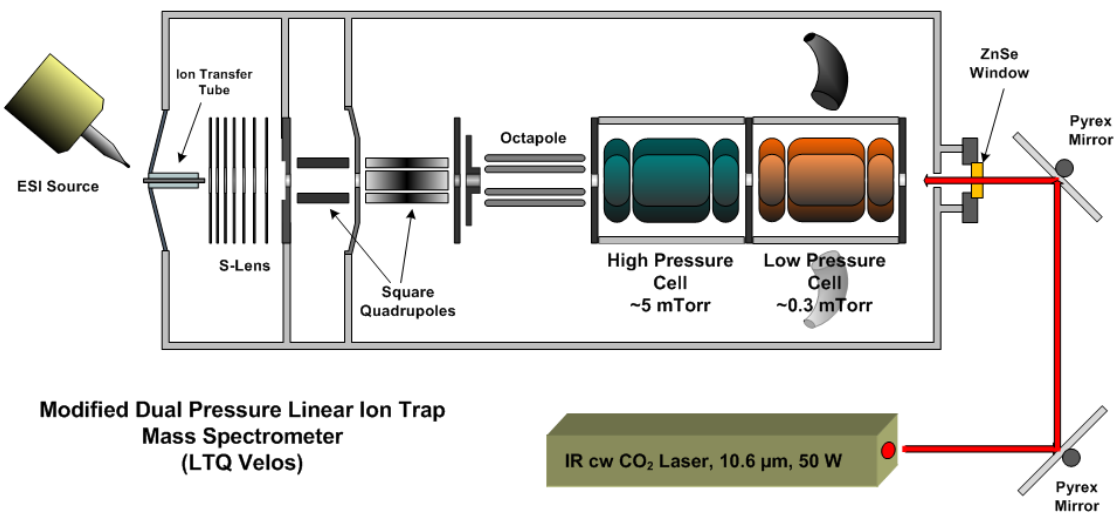

Figure 7.1 Schematic of a dual pressure linear ion trap mass spectrometer modified for infrared multiphoton dissociation.

7.4 RESULTS AND DISCUSSION

7.4.1 IRMPD in the Low Pressure Cell vs. High Pressure Cell

The primary drawback to performing IRMPD in quadrupole ion traps has been low dissociation efficiencies due to competition between ion activation through IR photon absorption and deactivation through collisions with the buffer gas. To evaluate the performance of IRMPD in the low pressure cell of the dual pressure LIT, a series of model peptides was analyzed. Product ion mass spectra of the peptides in various charge states were acquired by performing IRMPD in each of the two cells. IRMPD of doubly

protonated ADSGEGDFLAEGGGVR (fibrinopeptide A) performed in the high pressure cell using 250 ms of irradiation (**Figure 7.2a**) resulted in less than 1.5% dissociation efficiency (precursor to product); in fact, only a single product ion was observed corresponding to dehydration of the precursor ion. The results in the high pressure cell mirror those obtained in a single linear ion trap operated at ~2.5 mTorr He (using the same laser and similar set-up) in which peptides were not observed to photodissociate even with long irradiation times of 250 ms[44] due to the high rate of collisional cooling. In contrast, when IRMPD was performed in the low pressure cell, only 12.5 ms of irradiation was required to dissociate the precursor to less than 6% relative abundance (**Figure 7.2b**). All possible b-type ions and 14 out of 15 possible y-type ions were observed in the IRMPD tandem mass spectrum acquired in the low pressure cell. Low *m/z* products including immonium ions, which can be produced through secondary

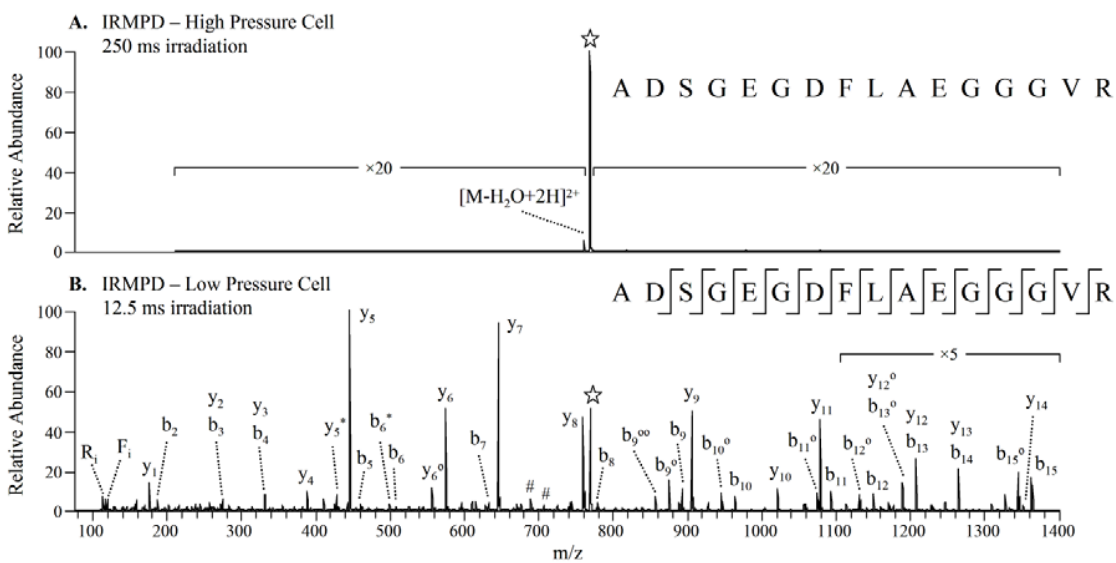

Figure 7.2 IRMPD of $[ADSGEGDFLAEGGGVR + 2H]^{2+}$ of *m/z* 769.2 performed in the (A) high pressure cell (250 ms irradiation, q = 0.25, 50 W) and (B) low pressure cell (12.5 ms irradiation, q = 0.09, 50 W). The precursor ion is indicated with a star (☆) and internal ions are labeled with #.

dissociation of larger b- and y-type ions, are observed. The non-resonant nature of IRMPD also resulted in a high degree of secondary neutral losses from b- and y-type fragment ions, including multiple losses of water (e.g., b_9^{o} and b_9^{oo} in Figure 1B).

The IRMPD efficiencies obtained for each of the model peptides when dissociated in the low pressure and high pressure cell are shown in **Table 7.1**. In the high pressure cell, only three of the peptide ions ([RPPGFSPFR + 3H]$^{3+}$, [RPKPQQFFGLM-NH_2 + 3H]$^{3+}$, and [ADSGEGDFLAEGGGVR + 3H]$^{3+}$) exhibited a photodissociation efficiency of greater than 50%, even using a long irradiation time of 250 ms and a more optimum q-value of 0.25 which should promote better overlap between the ion cloud and the laser beam (discussed in more detail in a later section). The greatest IRMPD efficiencies in the high pressure cell were obtained for three peptides in their highest charge states, an observation consistent with previous work on super-charged peptide cations,[41] while a majority of the lower-charged peptide cations exhibited dissociation efficiencies of less than 5% in the high pressure cell. When performing IRMPD in the low pressure cell, only one of the peptides dissociated with an efficiency less than 70%. All of these IRMPD mass spectra were acquired using less than 25 ms irradiation and using low q-values, the latter factor allowing successful storage and detection of the very lowest *m/z* product ions. In fact, 23 of the 25 peptide precursor ions displayed dissociation efficiencies of greater than 90% at q-values of 0.10 or lower. In general, the more highly charged peptides require shorter irradiation times to yield dissociation efficiencies of ~90%; however, to a lesser extent the q-value of the precursor ion also influences the irradiation time necessary to produce high IRMPD efficiencies.

The time-resolved IRMPD plots in **Figure 7.3** (for DRVYIHPF) and **Figure 7.4** (for ADSGEGDFLAEGGGVR) also show the effect of irradiation time on the photodissociation and MS/MS efficiencies. As shown in **Figure 7.3a**, [DRVYIHPF +

Table 7.1 IRMPD efficiencies of model peptides dissociated in the low pressure and high pressure cells of the dual LIT.

			Low Pressure Cell			High Pressure Cell		
Peptide	MW (Da)	Charge State	Irradiation Time (ms)	q-value	Dissociation Efficiency (%)[a]	Irradiation Time (ms)	q-value	Dissociation Efficiency (%)[a]
YGGFLK	638.4	2+	15	0.1	98	250	0.25	2.6
		1+	25	0.1	94	250	0.25	1.5
		1+	35	0.07	76	---	---	---
		1+	50	0.07	94	---	---	---
ASHLGLAR	823.5	2+	12.5	0.1	93	250	0.25	2.9
		1+	40	0.06	70	250	0.25	3
		1+	50	0.06	82	---	---	---
FSWGAEGQR	1035.5	2+	12.5	0.09	98	250	0.25	6.3
		1+	25	0.06	80	250	0.25	0.8
DRVYIHPF (angiotensin II)	1045.5	3+	7.5	0.1	97	250	0.25	26
		2+	15	0.1	96	250	0.25	1.3
		1+	25	0.1	92	250	0.25	4.3
RPPGFSPFR (bradykinin)	1059.6	3+	7.5	0.1	98	250	0.25	94
		2+	17.5	0.09	92	250	0.25	0.9
		1+	20	0.09	96	250	0.25	4.9
RPKPQQFFGLM-NH_2 (substance P)	1346.7	3+	5	0.1	97	250	0.25	96
		3+	---	---	---	50	0.1	87
		2+	17.5	0.07	93	250	0.25	2.6
		1+	30	0.07	96	250	0.25	2.7
ADSGEGDFLAEGGGVR (fibrinopeptide A)	1535.7	3+	12.5	0.09	99	250	0.25	57
		2+	25	0.06	99	250	0.25	1.3
		2+	12.5	0.09	94	---	---	---
		1+	25	0.06	91	250	0.25	3
AGCKNFFWKTFTSC (somatostatin-14)	1636.7	3+	12.5	0.09	97	250	0.25	5.4
		2+	13.5	0.09	90	250	0.25	0.9
		2+	22.5	0.06	90	---	---	---
		1+	25	0.06	93	250	0.25	22
GIGAVLKVLTTGLPALI SWIKRKRQQ-NH_2 (melittin)	2844.8	5+	9	0.09	96	250	0.25	17
		4+	20	0.07	98	250	0.25	1.3
		3+	15	0.1	96	250	0.25	3
		2+	25	0.07	98	250	0.25	14

[a] Dissociation efficiencies were calculated using equation 7.1 for each individual IRMPD mass spectrum

$2H]^{2+}$ required less than 20 ms of irradiation to yield ~100% photodissociation efficiency and the corresponding triply charged precursor only required ~12 ms of irradiation (Figure 2B). The more highly charged peptides dissociated more readily and this is attributed to higher Coulombic repulsion and greater proton mobility. For

ADSGEGDFLAEGGGVR (fibrinopeptide A), complete dissociation of the singly charged precursor ion required less than 25 ms of irradiation, and the doubly charged analog required ~20 ms of irradiation at a q-value of 0.10 (**Figure 7.4b and 7.4d**, respectively). At lower q-values, longer irradiation times were required to dissociate fibrinopeptide A, indicating a q-value dependence on the photodissociation efficiencies (**Figures 7.4a and 7.4c**). For both of these peptides – fibrinopeptide A and angiotensin II – maximum MS/MS efficiencies between 48% and 78% were obtained using a q-value of 0.10. The maximum MS/MS efficiencies were obtained when the dissociation efficiencies were between 75% and 96%. With longer irradiation times, the MS/MS efficiencies began to steadily decrease which was a result of a decrease in the total product ion abundance. This latter decrease is attributed to the production of low *m/z*

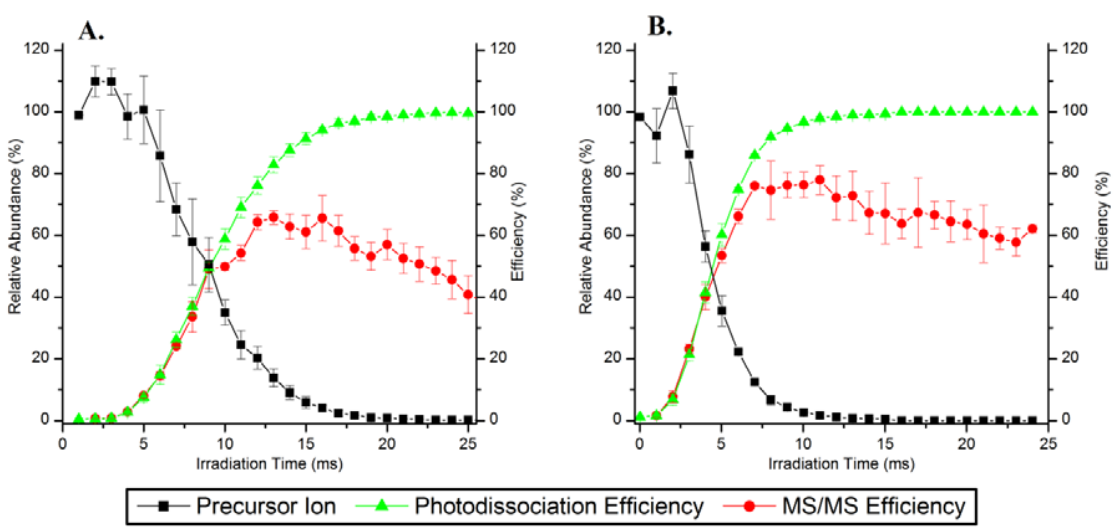

Figure 7.3 Time-resolved IRMPD plots of DRVYIHPF (angiotensin II) activated at a q-value of 0.10. Precursor ion abundances (relative to initial precursor abundance without any irradiation, squares ■), photodissociation efficiencies (triangles ▲) and MS/MS efficiencies (circles ●) of (A) $[M+2H]^{2+}$ and (B) $[M+3H]^{3+}$.

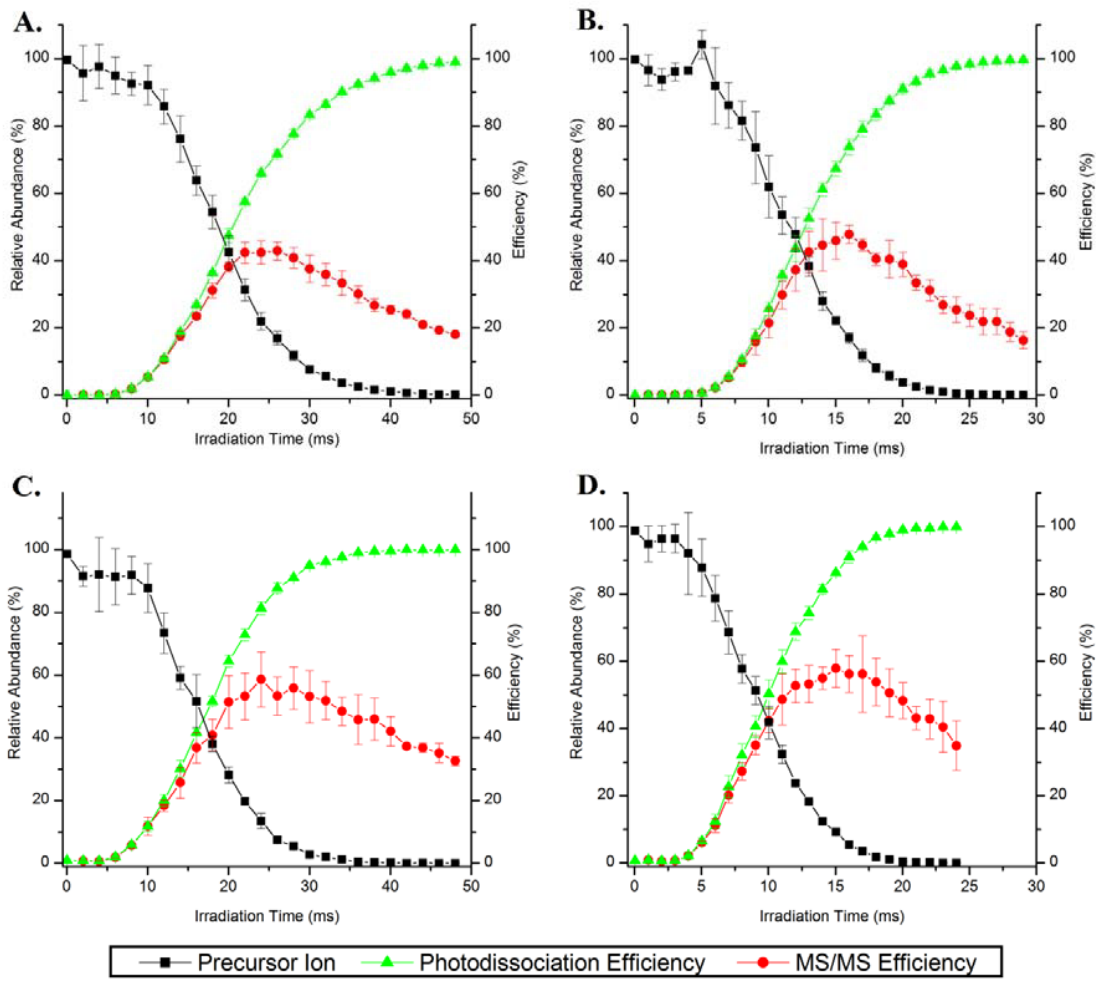

Figure 7.4 Time-resolved IRMPD plots of singly and doubly protonated ADSGEGDFLAEGGGVR (fibrinopeptide A) activated at q-values of 0.06 and 0.10. (A) 1+, q=0.06; (B) 1+, q=0.1; (C) 2+, q=0.06; and (D) 2+, q=0.10 showing relative precursor ion abundance (squares ■), photodissociation efficiencies (triangles ▲) and MS/MS efficiencies (circles ●). The abundances of the precursor ion are relative to the abundance of the precursor ion in the IRMPD mass spectrum of 0.0 ms irradiation.

fragment ions through secondary and higher order dissociation which fall below the LMCO in these spectra (~*m/z* 50 – 100). The MS/MS efficiencies obtained in the dual pressure LIT compare favorably to those measured in a standard three-dimensional

quadrupole ion trap for singly charged peptide ions using a focused IR laser in which a maximum MS/MS efficiency of 43% was obtained.[19]

7.4.2 Comparison of IRMPD to CID

IRMPD performed in the low pressure cell was compared to conventional CID results obtained in the high pressure cell for the series of model peptides. Shown in **Figure 7.5a** is the IRMPD mass spectrum of $[RPPGFSPFR + 3H]^{3+}$, and the complementary CID mass spectrum is shown in **Figure 7.5b**. The CID mass spectrum is dominated by neutral water loss from the precursor ion, whereas the ion current is distributed among a variety of diagnostic product ions in the IRMPD mass spectrum. Immonium ions and several internal fragment ions are observed in the IRMPD mass spectrum that are not detected in the CID mass spectrum. Also, many y-type ions in

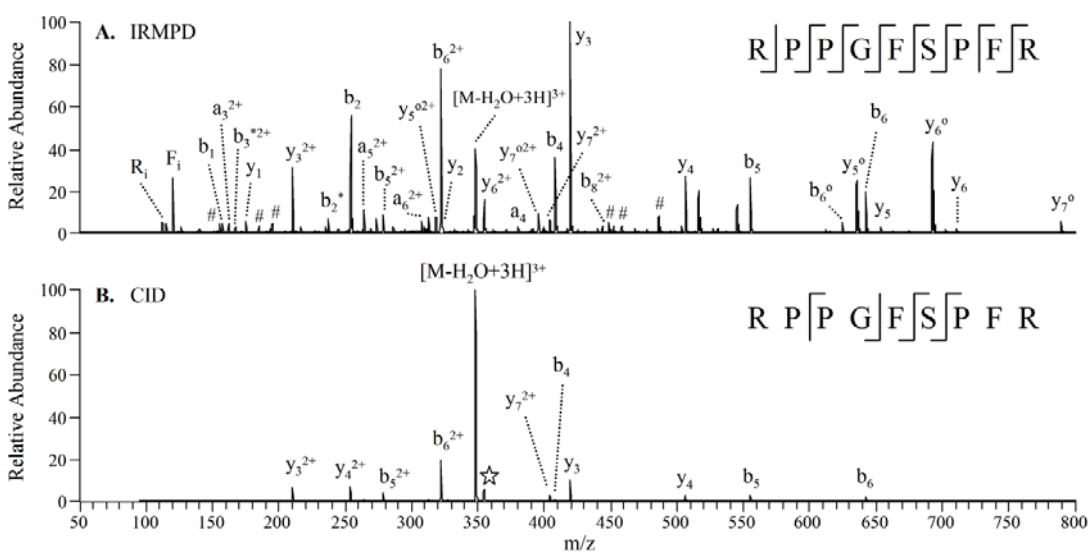

Figure 7.5 (A) IRMPD (7.5 ms irradiation, q = 0.1, 50 W) and (B) CID (30 ms, q = 0.25, 8% normalized collision energy) mass spectra of $[RPPGFSPFR + 3H]^{3+}$ of *m/z* 354.3. The precursor ion is indicated with a star (☆) and internal ions are labeled with #.

conjunction with water losses are detected in the IRMPD spectrum which, presumably arise from secondary dissociation of the initial y-type ions upon absorption of additional IR photons. Experimental evidence suggests that a majority of the product ions observed in the IRMPD mass spectrum are actually produced upon secondary dissociation of $[RPPGFSPFR - H_2O + 3H]^{3+}$ ions. The $[RPPGFSPFR - H_2O + 3H]^{3+}$ ions were isolated and subjected to a discrete second stage of activation via IRMPD or CID, and the resulting MS^3 product ion spectra are shown in the **Figure 7.6**. CID of $[RPPGFSPFR - H_2O + 3H]^{3+}$ yielded three y^o-type ions (i.e., y-type ions with a water loss) as well as the phenylalanine immonium ion (F_i) and the b_2 ion (**Figure 7.6a – 7.6c**). In fact, most of the product ions observed in the MS^3 product ion spectra match those detected in the IRMPD mass spectrum shown in **Figure 7.5a**. These results indicate that triply charged bradykinin (RPPGFSPFR) primarily undergoes dehydration, and then this dehydrated product subsequently dissociates to yield informative sequence ions. Wideband CID of $[RPPGFSPFR + 3H]^{3+}$ was also performed, and it provided higher sequence coverage than CID alone and similar coverage to MS^3 and IRMPD experiments (**Figure 7.6d**). However, as this technique employs a broadband excitation waveform to collisionally activate the m/z region between the precursor ion and neutral loss (e.g. H_2O, NH_3) product ions, no ions were observed between *m/z* 330 and 360 including any diagnostic sequences ions such as y_6^{2+} of *m/z* 355.7 which is detected in the IRMPD mass spectrum (**Figure 7.5a**). For peptide ions which predominantly dissociate through a single pathway (e.g., dehydration), non-resonant ion activation techniques such as photodissociation provide a means to increase the number of diagnostic product ions.

The percentages of b- and y-type fragments, as defined by the number of b- and y-type fragment ions detected divided by the total number of possible b- and y-type fragments, observed in the IRMPD and CID mass spectra of the model peptides are

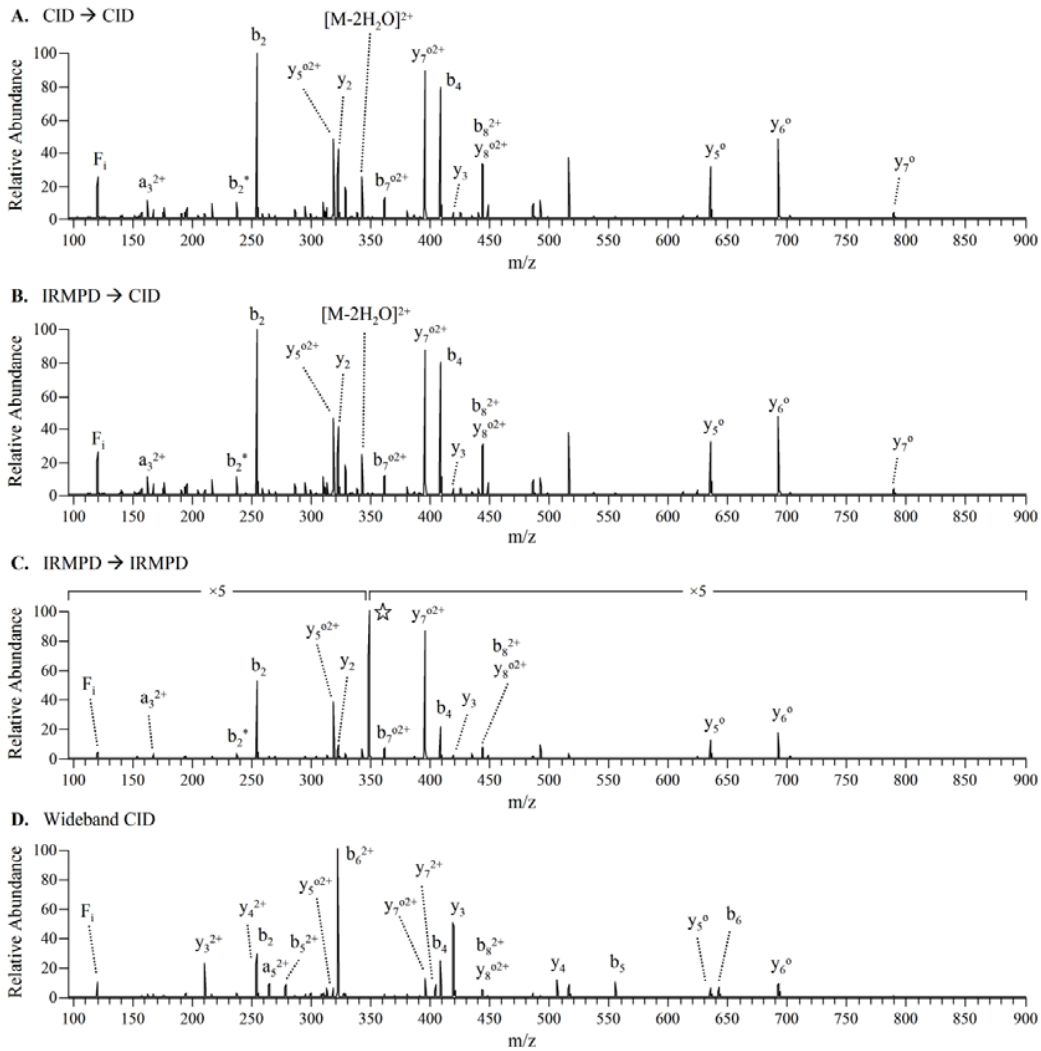

Figure 7.6 MS^3 and wideband CID product ion mass spectra of [RPPGFSPFR – H_2O + 3H]$^{3+}$. (A) CID of [M+3H]$^{3+}$ (30 ms, 15% NCE, q=0.25) and subsequent CID of [M-H_2O+3H]$^{3+}$ (30 ms, 15% NCE, q=0.25). (B) IRMPD of [M+3H]$^{3+}$ (20 ms, 50 W, q=0.1) and subsequent CID of [M-H_2O+3H]$^{3+}$ (30 ms, 15% normalized collision energy, q=0.25). (C) IRMPD of [M+3H]$^{3+}$ (20 ms, 50 W, q=0.1) and subsequent IRMPD of [M-H_2O+3H]$^{3+}$ (100 ms, 50 W, q=0.25). (D) Wideband CID of [M+3H]$^{3+}$ (30 ms, 18% NCE, q=0.25) The precursor ion is indicated with a star (☆) and M represents RPPGFSPFR (bradykinin). These product ion spectra were acquired using a standard LTQ XL mass spectrometer (single linear ion trap instrument) modified for photodissociation (He pressure ~2.5 mTorr).

summarized in **Figure 7.7**. (If a fragment was observed in two or more charge states, it was only counted once to more accurately give an account of the sequence coverage.) For almost every peptide investigated, a higher percentage of b- and y-type ions was observed by IRMPD. IRMPD showed significant increases in the number of b- and y-type fragments observed for all charge states of RPPGFSPFR (bradykinin) and RPKPQQFFGLM-NH_2 (substance P), as well as for singly charged DRVYIHPF (angiotensin II) and ASHLGLAR. For $[RPPGFSPFR + 3H]^{3+}$, the percentage of b- and y-type ions more than doubled for IRMPD in comparison to CID, with fourteen b- and y-type ions observed upon IRMPD but only six b- and y-type ions upon CID. In the two instances that CID outperformed IRMPD (i.e. singly and doubly charged

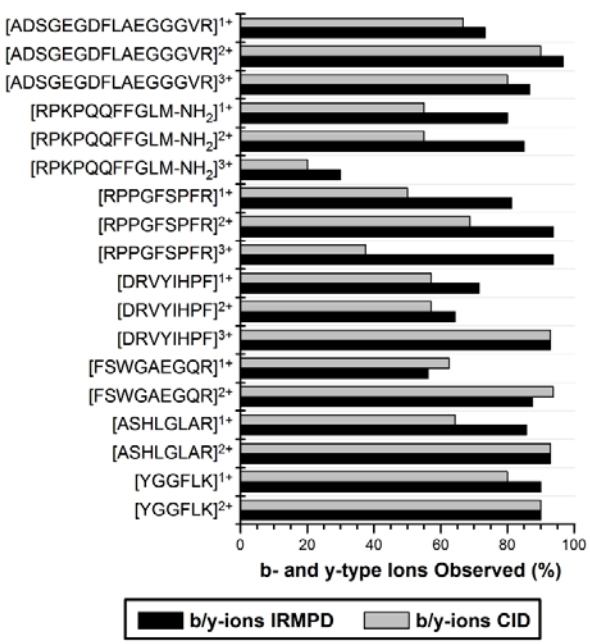

Figure 7.7 Percent of b- and y-type ions of model peptides observed by IRMPD (performed in the low pressure cell; black bars) and CID (performed in the high pressure cell; gray bars). IRMPD mass spectra were acquired using q-values between 0.07 and 0.10 (depending on the precursor *m/z*) to reduce the low-mass cut-off to less than *m/z* 100. A value of 100% would indicate that all b- and y-type ions were detected (including b_1) as all amide bonds were considered to be potential sites of cleavage.

FSWGAEGQR), it was due to formation of a single additional b- or y-type fragment.

Increases in the CID activation time did not yield increased sequence coverage or significant changes in the relative abundances or types of product ions observed. For doubly charged fibrinopeptide A (ADSGEGDFLAEGGGVR), almost identical CID mass spectra were obtained when applying the collisional activation waveforms for between 25 – 100 ms; at shorter activation times, little dissociation was observed (data not shown). Similarly, variation in the normalized collision energy (20 – 100%) did not produce greater secondary dissociation or alter the product ion distribution for ADSGEGDFLAEGGGVR or DRVYIHPF peptide cations once the dissociation threshold (typically less than 20% NCE) was reached (data not shown).

7.4.3 Charge State Distribution of Product Ions

One of the more striking differences observed between the IRMPD and CID mass spectra of multiply protonated peptides is that almost all of the product ions in the IRMPD mass spectra are singly charged as compared to the CID mass spectra in which product ions of multiple charge states are typically observed. The IRMPD and CID mass spectra of $[ADSGEGDFLAEGGGVR + 3H]^{3+}$ illustrate this observation in **Figure 7.8a and 7.8b**, respectively. In the CID mass spectrum, product ions are seen in the 2+ and 1+ charge states, with some sequence ions observed in both charge states (e.g., b_9, b_{10}, b_{11}, and y_{10}). However, in the IRMPD mass spectrum not a single product ion is observed to be multiply charged – all product ions are singly charged. One example of this lack of multiply charged peptide fragment ions is particularly evident in the range between *m/z* 440 and 610 in which more than ten abundant product ions are observed in the CID mass spectrum in the 1+ and 2+ charge states whereas only four fragment ions are detected in the IRMPD mass spectrum, all singly charged.

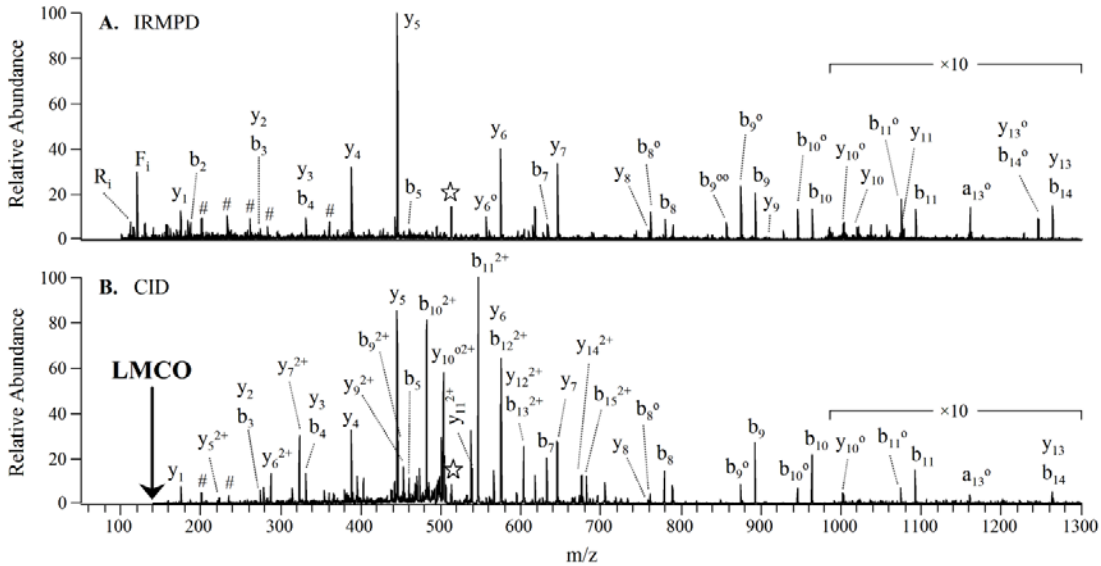

Figure 7.8 (A) IRMPD (12.5 ms irradiation, q = 0.09, 50 W) and (B) CID (30 ms, q = 0.25, 25% normalized collision energy) mass spectra of $[ADSGEGDFLAEGGGVR + 3H]^{3+}$ of *m/z* 512.9. The precursor ion is indicated with a star (☆) and internal ions are labeled with #.

The distributions and numbers of singly, doubly, and triply charged product ions were determined for the IRMPD and CID mass spectra of an array of peptide ions. The distributions (abundances expressed as percentages) of product ions in each charge state are shown in **Figure 7.9a and 7.9b** for fragment ions produced by IRMPD and CID, respectively. Moreover, the number of products ions in each charge state (relative to the total number of fragment ions observed in each spectrum) are shown in **Figure 7.9c and 7.9d** (IRMPD and CID data, respectively). For the doubly charged precursor ions, the singly charged product ions comprise 96.6 ± 3.3% of the product ion current (defined as the total ion current minus the abundance of any surviving precursor) in the IRMPD mass spectra, whereas in the CID mass spectra the average abundance of singly charged fragment ions was 50 ± 23%. Doubly charged and singly charged product ions accounted for 30 ± 27% and 67 ± 30% of the product ion current, respectively, in the IRMPD mass

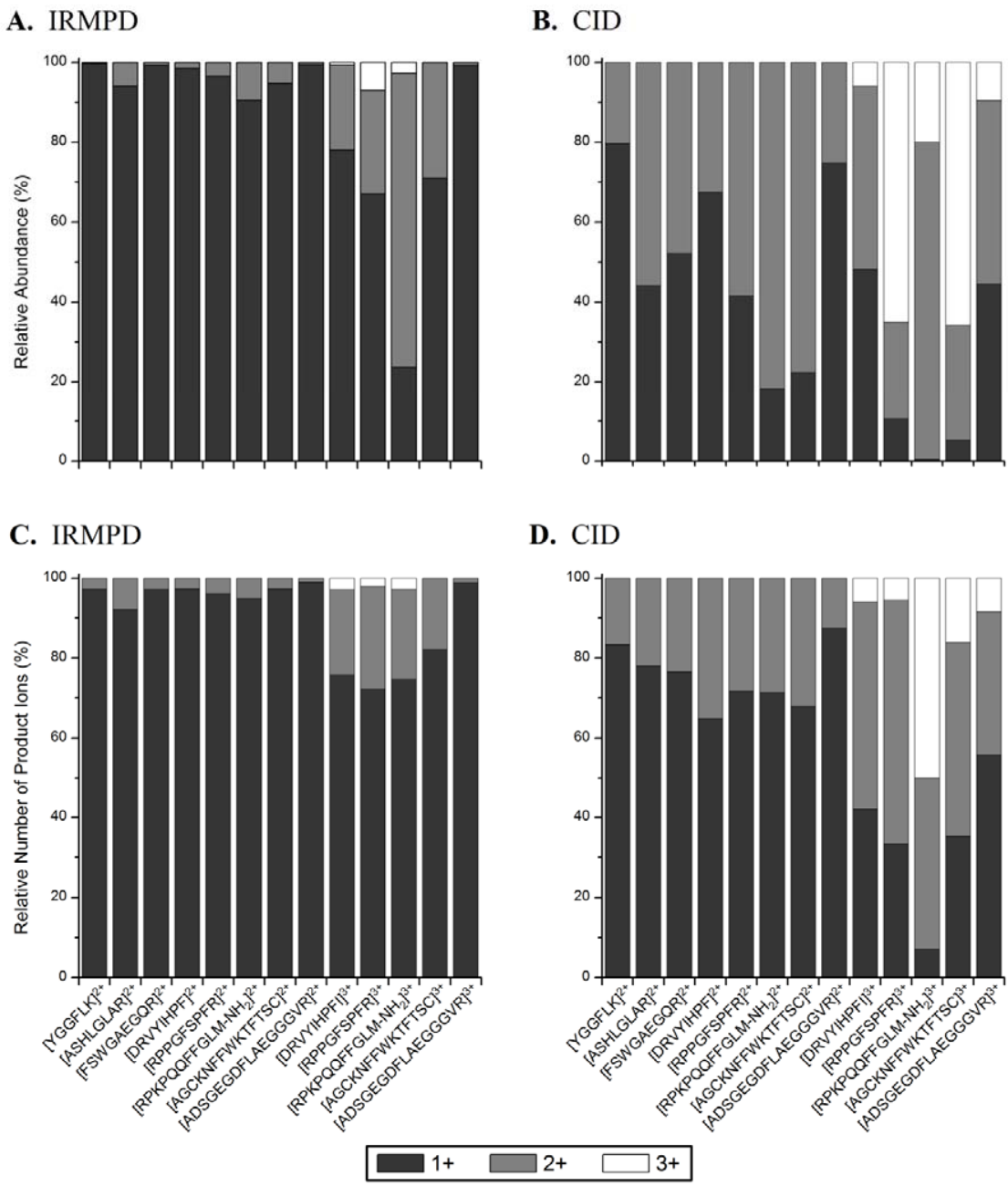

Figure 7.9 Ion abundances of singly (black bars), doubly (gray bars), and triply charged fragment ions (white bars) relative to the total ion abundance (upper panels A and B) and number of fragment ions in each charge relative to the total number of product ions (lower panels C and D) observed in IRMPD (left panels A and C) and CID (right panels B and D) mass spectra.

spectra of the triply charged peptide ions; triply charged product ions accounted for an insignificant abundance. In contrast, the product ion current in the CID mass spectra, on average, was composed of 22 ± 23% of singly charged fragment ions, 45 ± 22% of doubly charged fragment ions, and 33 ± 30% of triply charged fragment ions. The lack of multiply charged product ions in the IRMPD mass spectra was further substantiated when the number of product ions in each charge state was counted and expressed as a percentage of the total number of product ions. Greater than 96% of the product ions were singly charged in the IRMPD mass spectra of doubly charged peptides, and more than 80% were singly charged in the IRMPD mass spectra of the triply charged peptides. In the CID mass spectra of doubly charged peptides, 75% of the product ions were singly charged, and for the triply charged peptides, the distribution of product ions was 35%, 48%, and 17% for singly, doubly, and triply charged product ions. Overall, CID yields product ions in a greater variety of charge states, whereas more than 80% of the fragment ions are singly charged in the IRMPD mass spectra with these ions accounting for over 85% of the product ion current. The lack of multiply charged product ions in the IRMPD mass spectra could be useful for potential *de novo* sequencing or database searches in which only singly charged fragment ions would be considered.

The relative product ion abundances of 1+, 2+, and 3+ charged product ions of $[DRVYIHPF + 2H]^{2+}$ and $[DRVYIHPF + 3H]^{3+}$ are plotted as a function of irradiation time in **Figure 7.10**. As the irradiation time increases from 0 to 4 ms, the abundances of both the 1+ and 2+ product ions of doubly protonated DRVYIHPF (angiotensin II) increase almost linearly; however, for irradiation times longer than 5 ms, the relative abundance of the 2+ charged product ions decreases to less than 1% of the total product ion current at irradiation times exceeding 20 ms (**Figure 7.10a**). For $[DRVYIHPF + 3H]^{3+}$, at short irradiation times, doubly charged product ions are actually observed at a

higher abundance than singly charged fragments (**Figure 7.10b**). At irradiation times longer than 3 ms, however, the abundance of 2+ product ions declines as these species are apparently converted into singly charged product ions via secondary dissociation. The only triply charged product ion observed in the IRMPD mass spectra of $[DRVYIHPF+ 3H]^{3+}$ is the dehydrated precursor ion. By monitoring the abundances of individual product ions in specific charge states as produced upon IRMPD, it is observed that product ions in higher charge states consistently dissociate more readily than those same product ions in lower charge states (e.g. b_{11}^{2+} versus b_{11}^{+} from ADSGEGDFLAEGGGVR, see **Figures 7.11 and 7.12**). The difference in PD efficiencies of doubly vs. singly charged product ions is attributed to a number of factors. In addition to experiencing greater Coulombic repulsion which could reduce the threshold for dissociation, most multiply charged product ions have a greater number of mobile protons which can facilitate their subsequent fragmentation.

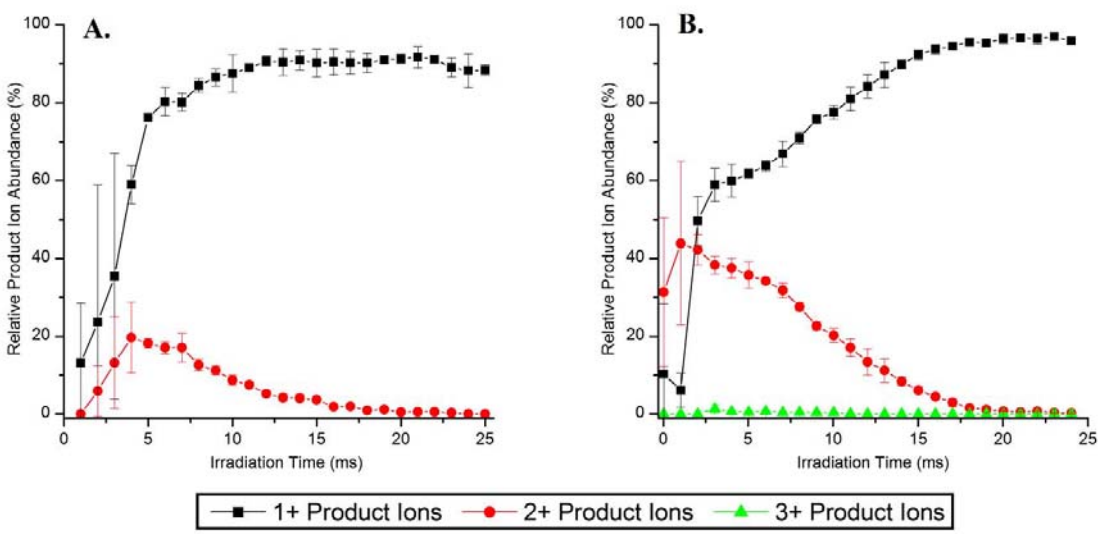

Figure 7.10 Time-resolved IRMPD plots of DRVYIHPF (angiotensin II) activated at a q-value of 0.10. Relative product ion abundances of singly (squares ■), doubly (circles ●), and triply charged product ions (triangles ▲) of (A) $[M+2H]^{2+}$ and (B) $[M+3H]^{3+}$.

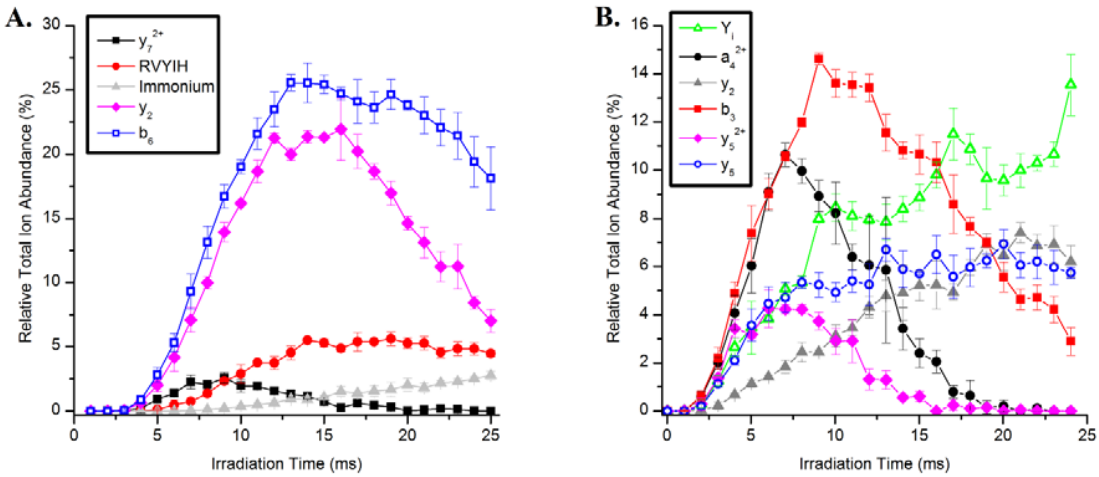

Figure 7.11 Relative abundances of selected product ions of (A) $[DRVYIHPF + 2H]^{2+}$ and (B) $[DRVYIHPF + 3H]^{3+}$ from time-resolved IRMPD experiments. Precursor ions were activated at a q-value of 0.1. The immonium ion abundance in (A) is the sum of the abundances of the immonium ions of isoleucine, histidine, and tyrosine. Abundances are relative to the total ion current in each IRMPD mass spectrum.

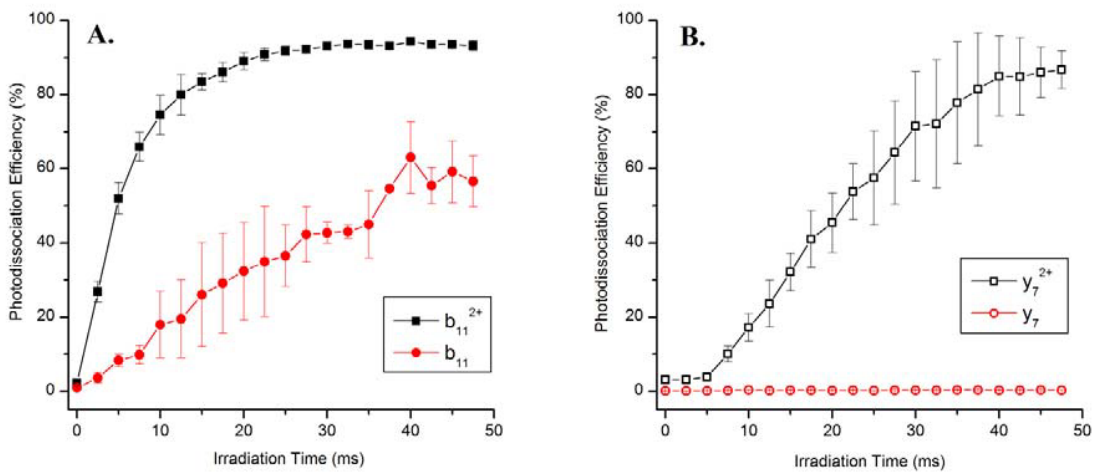

Figure 7.12 Photodissociation efficiencies determined from time-resolved IRMPD experiments of (A) b_{11}^{2+} (filled squares ■) and b_{11} (filled circles ●), and (B) y_7^{2+} (open squares □) and y_7 (open circles ○) of ADSGEGDFLAEGGGVR (fibrinopeptide A). Product ions were activated at a q-value of 0.25 at a laser power of 50 W in a standard LTQ XL (single linear ion trap instrument) modified for photodissociation (He pressure ~2.5 mTorr).

7.4.4 Effect of Q-Value on IRMPD Efficiencies

The photodissociation efficiencies of peptides is dependent on the activation q-value. While it has been widely assumed that photodissociation is completely independent of ion trap operating parameters, recent work by Remes and Glish showed that the q-value (i.e., rf trapping voltage) greatly influences ion position within the ion trap.[45] At higher q-values, which create greater potential well depths, the ions spend more time in the center of the trap where there is better overlap between the ion cloud and the photon beam. While a better overlap and consequently greater photodissociation efficiencies are observed at high q-values, these increases in performance are obtained at the expense of trapping low *m/z* fragment ions (i.e., at higher q-values the low mass cutoff is increased and a narrower range of ions can be effectively trapped and detected). To investigate the effect of the rf trapping level during photodissociation in the dual pressure LIT, IRMPD mass spectra were acquired at q-values between 0.10 and 0.24. The resulting plots for $[DRVYIHPF + 2H]^{2+}$ and $[DRVYIHPF + 3H]^{3+}$ are shown in **Figure 7.13a and 7.13b**, respectively. For these experiments, the MS/MS efficiencies could not be directly calculated as changes in the IRMPD q-value can result in changes in the trapping efficiency of the LIT. However, eq. (2) can be used to calculate MS/MS × trapping efficiencies in which P_0 was determined from the IRMPD mass spectrum acquired at the lowest q-value; these values are plotted as a function of q-value in Figure 8. For $[DRVYIHPF+ 2H]^{2+}$, as the q-value is increased from 0.05 to 0.10, there is a drastic decrease in the relative abundance of the precursor ions and a corresponding increase in photodissociation efficiencies from less than 5% to over 75% (**Figure 7.13a**). At q-values of greater than 0.12, PD efficiencies of ~100% are obtained. IRMPD experiments were not conducted at q-values of greater than 0.24 in these experiments as

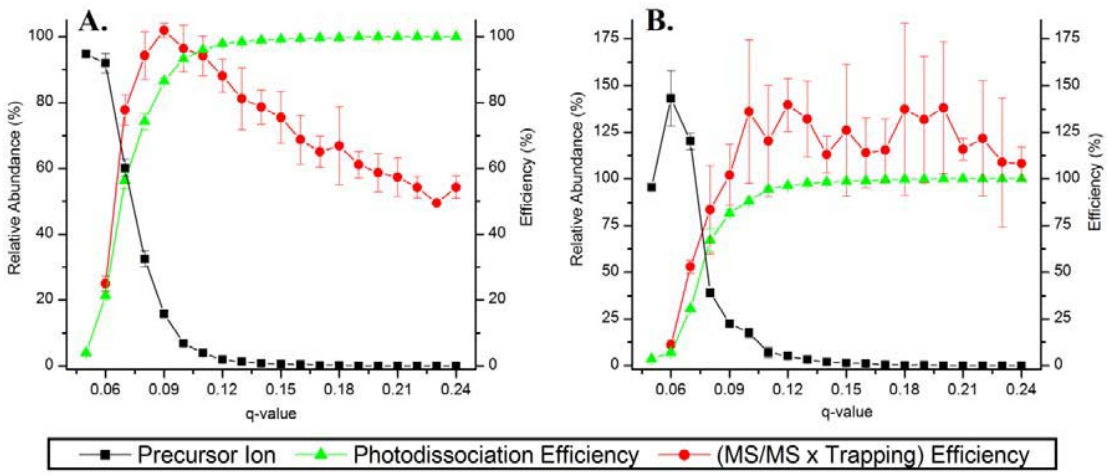

Figure 7.13 Photodissociation efficiencies (triangles ▲), MS/MS × trapping efficiencies (circles ●), and relative precursor ion abundances (squares ■) as a function of q-value of (A) $[DRVYIHPF + 2H]^{2+}$ using 15.0 ms of IR irradiation and (B) $[DRVYIHPF + 3H]^{3+}$ using 7.5 ms of irradiation. Precursor ion abundances are relative to the initial precursor abundance at q = 0.05 without any irradiation.

no increase in photodissociation efficiencies was observed and the MS/MS efficiencies were observed to decrease at greater q-values. In addition, at q-values above 0.25 effects of an increased low mass cutoff would be expected. The MS/MS × trapping efficiencies increase to greater than 95% at q-values between 0.08 and 0.11 for doubly protonated angiotensin II (**Figure 7.13a**). The total abundance of product ions falls at q-values greater than 0.09 as indicated by the decrease in the MS/MS × trapping efficiency. This decrease is attributed to secondary dissociation of product ions resulting in formation of smaller ions of *m/z* below that of the low mass cutoff. However, even at q-values as high as 0.24, the MS/MS × trapping efficiency is greater than 50%. Similar results are obtained for triply protonated DRVYIHPF (angiotensin II) as shown in **Figure 7.13b**. At q-values greater than 0.12, the photodissociation efficiencies are ~100%, and the precursor ion is completely dissociated. The MS/MS × trapping efficiencies varied somewhat more erratically due to larger variations in the total ion current of each mass

spectrum, but the same general trend is observed in which the total abundance of the product ions increases with q-value and then gradually declines as lower *m/z* fragment ions are likely produced (but not detected). (The q-value was also varied for CID experiments conducted in a single linear ion trap mass spectrometer for [DRVYIHPF+ 2H]$^{2+}$ and [DRVYIHPF+ 3H]$^{3+}$, and at low q-values (< 0.15) almost no signal was observed. This is attributed to the low potential well-depth in which the precursor ion resides. Upon collisional activation, the precursor ions are lost due to unstable trajectories. Efficient dissociation (>75%) was observed only at q-values greater than 0.20; data not shown.)

The effect of the q-value on photodissociation is also shown in the time-resolved IRMPD plots of singly and doubly protonated ADSGEGDFLAEGGGVR (fibrinopeptide A) at two different q-values (**Figure 7.4**). Approximately 19 ms of irradiation was required to reduce [ADSGEGDFLAEGGGVR + H]$^{+}$ to 50% relative abundance when activated at a q-value of 0.06 (**Figure 7.4a**), but only 12 ms of IR irradiation was required at a q-value of 0.10 (**Figure 7.4b**). For [ADSGEGDFLAEGGGVR + 2H]$^{2+}$, 16 ms of irradiation was necessary to reduce the precursor to 50% abundance at q = 0.06 and only 9 ms was required at q = 0.10 (**Figure 7.4c and 7.4d**, respectively). These results clearly suggest that at higher q-values there is a greater overlap between the ion cloud and the laser beam, which results in higher photodissociation efficiencies. Thus, upon further comparison of the IRMPD mass spectra in **Figure 7.2a and 7.2b**, the difference is even more striking as almost no dissociation was observed when IRMPD was performed in the high pressure cell even when the q-value was set to 0.25, whereas high sequence coverage and high PD efficiency were obtained in the low pressure cell at a q-value of 0.09 using only 12.5 ms of irradiation.

7.4.5 Further Application and Implementation of IRMPD

While these IRMPD studies were conducted on a small subset of model peptides, the results suggest that IRMPD on the dual pressure LIT would be well suited as a complementary technique to CID and ETD for the analysis of large scale proteomic samples (e.g. enzymatic digests of cell lysates). In general, shorter irradiation times (~5 – 10 ms) were required to completely dissociate triply charged peptide ions with masses of less than 2000 Da. Longer irradiation times and slightly higher q-values were necessary to dissociate doubly charged peptides (~10 – 15 ms) than singly charged peptides (~20 – 25 ms). When peptide ions were irradiated for significantly longer intervals, the product ion mass spectra became cluttered with internal ions and low mass ions which could not be identified. Further experiments need to be performed in order to determine appropriate irradiation conditions based on peptide precursor *m/z* to avoid extensive secondary dissociation for more widespread and commercial implementation of IRMPD, particularly for data-dependent LC-IRMPD-MS experiments. However, a parallel study has shown that intact proteins readily dissociate upon IR irradiation in the low pressure cell indicating the IRMPD is a potentially useful method for top-down protein identification in ion trap mass spectrometers.[46]

7.5 CONCLUSIONS

Infrared multiphoton dissociation has been successfully implemented in a dual pressure LIT mass spectrometer to afford rapid and efficient dissociation of peptides in the low pressure cell. At lower trap pressures the rate of activation through IR photon absorption is greater than the rate of collisional cooling and thus peptides are readily dissociated. Dissociation efficiencies approaching 100% and MS/MS efficiencies of greater than 60% were obtained using irradiation times of less than 25 ms at a q-value of

0.10. The dissociation efficiencies were observed to be dependent on the q-value; at higher q-values the ions spend more time near the center of the trap and the ion cloud has a greater overlap with the photon beam, resulting in more rapid dissociation. Compared to CID, IRMPD allows the observation of low-mass fragment ions such as immonium ions and provides slightly higher sequence coverage of the peptides. The higher sequence coverage was attributed to secondary and higher order dissociation inherent to non-resonant activation methods such as photodissociation. IRMPD predominantly yielded singly charged fragment ions which aids in de-cluttering the product ion spectra and simplifying spectral interpretation. Highly charged product ions were observed to photodissociate more readily than the singly charged species which was attributed to a combination of factors including higher Coulombic repulsion, as well as the influence of a greater number of mobile protons.

7.6 REFERENCES

(1) Winston, R. L.; Fitzgerald, M. C. *Mass Spectrometry Reviews* **1997**, *16*, 165-179.

(2) Godovac-Zimmermann, J.; Brown, L. R. *Mass Spectrometry Reviews* **2001**, *20*, 1-57.

(3) Aebersold, R.; Mann, M. *Nature* **2003**, *422*, 198-207.

(4) Biemann, K. *Methods in Enzymology* **1990**, *193*, 455-479.

(5) Wells, J. M.; McLuckey, S. A. *Methods in Enzymology* **2005**, *402*, 148-185.

(6) Vaisar, T.; Urban, J. *Journal of Mass Spectrometry* **1996**, *31*, 1185-1187.

(7) Tsaprailis, G.; Somogyi, A.; Nikolaev, E. N.; Wysocki, V. H. *International Journal of Mass Spectrometry* **2000**, *195/196*, 467-479.

(8) Kapp, E. A.; Schutz, F.; Reid, G. E.; Eddes, J. S.; Moritz, R. L.; O'Hair, R. A.; Speed, T. P.; Simpson, R. J. *Analytical Chemistry* **2003**, *75*, 6251-6264.

(9) Sleno, L.; Volmer, D. A. *Journal of Mass Spectrometry* **2004**, *39*, 1091-1112.

(10) McLuckey, S. A.; Goeringer, D. E. *Journal of Mass Spectrometry* **1997**, *32*, 461-474.

(11) Zubarev, R. A.; Kelleher, N. L.; McLafferty, F. W. *Journal of the American Chemical Society* **1998**, *120*, 3265-3266.

(12) Syka, J. E. P.; Coon, J. J.; Schroeder, M. J.; Shabanowitz, J.; Hunt, D. F. *Proceedings of the National Academy of Sciences of the United States of America* **2004**, *101*, 9528-9533.

(13) Swaney, D. L.; McAlister, G. C.; Wirtala, M.; Schwartz, J. C.; Syka, J. E. P.; Coon, J. J. *Analytical Chemistry* **2007**, *79*, 477-485.

(14) Fung, Y. M. E.; Adams, C. M.; Zubarev, R. A. *Journal of the American Chemical Society* **2009**, *131*, 9977-9985.

(15) Little, D. P.; Speir, J. P.; Senko, M. W.; O'Connor, P. B.; McLafferty, F. W. *Analytical Chemistry* **1994**, *66*, 2809-2815.

(16) Stephenson, J. L., Jr.; Booth, M. M.; Shalosky, J. A.; Eyler, J. R.; Yost, R. A. *Journal of the American Society for Mass Spectrometry* **1994**, *5*, 886-893.

(17) Brodbelt, J. S.; Wilson, J. J. *Mass Spectrometry Reviews* **2009**, *28*, 390-424.

(18) Colorado, A.; Shen, J. X.; Brodbelt, J. *Analytical Chemistry* **1996**, *68*, 4033-4043.

(19) Newsome, G. A.; Glish, G. L. *Journal of the American Society for Mass Spectrometry* **2009**, *20*, 1127-1131.

(20) Reilly, J. P. *Mass Spectrometry Reviews* **2009**, *28*, 425-447.

(21) Thompson, M. S.; Cui, W.; Reilly, J. P. *Angewandte Chemie, International Edition* **2004**, *43*, 4791-4794.

(22) Moon, J. H.; Yoon, S. H.; Kim, M. S. *Rapid Communications in Mass Spectrometry* **2005**, *19*, 3248-3252.

(23) Joly, L.; Antoine, R.; Broyer, M.; Dugourd, P.; Lemoine, J. *Journal of Mass Spectrometry* **2007**, *42*, 818-824.

(24) Wilson, J. J.; Brodbelt, J. S. *Analytical Chemistry* **2007**, *79*, 7883-7892.

(25) Kalcic, C. L.; Gunaratne, T. C.; Jones, A. D.; Dantus, M.; Reid, G. E. *Journal of the American Chemical Society* **2009**, *131*, 940-942.

(26) Ly, T.; Julian, R. R. *Journal of the American Chemical Society* **2008**, *130*, 351-358.

(27) Gabryelski, W.; Li, L. *Rapid Communications in Mass Spectrometry* **2002**, *16*, 1805-1811.

(28) Goolsby, B. J.; Brodbelt, J. S. *Analytical Chemistry* **2001**, *73*, 1270-1276.

(29) Keller, K. M.; Brodbelt, J. S. *Analytical Biochemistry* **2004**, *326*, 200-210.

(30) Payne, A. H.; Glish, G. L. *Analytical Chemistry* **2001**, *73*, 3542-3548.

(31) Schwartz, J. C.; Syka, J. E. P.; Quarmby, S. T. *Proceedings of the 53th ASMS Conference on Mass Spectrometry and Allied Topics*. San Antonio, TX, June 2005.

(32) Cunningham, C.; Glish, G. L.; Burinsky, D. J. *Journal of the American Society for Mass Spectrometry* **2006**, *17*, 81-84.

(33) Stafford, G. C., Jr.; Kelley, P. E.; Syka, J. E. P.; Reynolds, W. E.; Todd, J. F. J. *International Journal of Mass Spectrometry and Ion Processes* **1984**, *60*, 85-98.

(34) Black, D. M.; Payne, A. H.; Glish, G. L. *Journal of the American Society for Mass Spectrometry* **2006**, *17*, 932-938.

(35) Boue, S. M.; Stephenson, J. L., Jr.; Yost, R. A. *Rapid Communications in Mass Spectrometry* **2000**, *14*, 1391-1397.

(36) Hashimoto, Y.; Hasegawa, H.; Waki, I. *Rapid Communications in Mass Spectrometry* **2004**, *18*, 2255-2259.

(37) Hashimoto, Y.; Hasegawa, H.; Yoshinari, K.; Waki, I. *Analytical Chemistry* **2003**, *75*, 420-425.

(38) Pikulski, M.; Wilson, J. J.; Aguilar, A.; Brodbelt, J. S. *Analytical Chemistry* **2006**, *78*, 8512-8517.

(39) Wilson, J. J.; Brodbelt, J. S. *Analytical Chemistry* **2006**, *78*, 6855-6862.

(40) Vasicek, L. A.; Wilson, J. J.; Brodbelt, J. S. *Journal of the American Society for Mass Spectrometry* **2009**, *20*, 377-384.

(41) Madsen, J. A.; Brodbelt, J. S. *Journal of the American Society for Mass Spectrometry* **2009**, *20*, 349-358.

(42) Schwartz, J. C.; Syka, J. E. P.; Remes, P. M. *Proceedings of the 56th ASMS Conference on Mass Spectrometry and Allied Topics*. Denver, CO, June 2008.

(43) Wouters, E. R.; Splendore, M.; Mullen, C.; Schwartz, J. C.; Senko, M. W.; Dunyach, J. *Proceedings of the 57th ASMS Conference on Mass Spectrometry and Allied Topics*. Philadelphia, PA, June 2009.

(44) Gardner, M. W.; Vasicek, L. A.; Shabbir, S.; Anslyn, E. V.; Brodbelt, J. S. *Analytical Chemistry* **2008**, *80*, 4807-4819.

(45) Remes, P. M.; Glish, G. L. *Journal of Physical Chemistry A* **2009**, *113*, 3447-3454.

(46) Madsen, J. A.; Gardner, M. W.; Smith, S. I.; Ledvina, A. R.; Coon, J. J.; Schwartz, J. C.; Stafford, G. C.; Brodbelt, J. S. *Analytical Chemistry* **2009**, *In Press*.

Chapter 8

Reduction of Chemical Noise in Electrospray Ionization Mass Spectrometry by Supplemental IR Activation

8.1 OVERVIEW

Supplemental infrared (IR) activation was applied to reduce background chemical noise and increase analyte ion signal in a linear ion trap mass spectrometer. Peptides, proteins, and small molecules were all introduced by electrospray ionization, and when regions of chemical noise were isolated and subjected to IR irradiation, protonated analyte molecules were observed in the product ion mass spectra. By isolating the entire mass range (e.g., *m/z* 400 – 2000) and then irradiating all ions in the trap, supplemental IR activation increased the signal of singly protonated peptides by almost 70% and by 40 – 55% for the lower charge states of cytochrome c. This increase in analyte ion signal was less dramatic for the higher charge states of peptides and proteins. The chemical noise present in the mass spectra is attributed to incomplete desolvation of the electrospray, as the abundance of the protonated peptides observed upon supplemental IR activation of the chemical noise decreased with higher inlet capillary temperatures. Collision activation was not as effective for desolvating the ions present in the chemical noise.

8.2 INTRODUCTION

For successful implementation of electrospray ionization (ESI), desolvation of the analyte ions is necessary, and many methods have been developed to afford efficient desolvation including the use of drying gases,[1-3] collisional activation,[2, 3] and heated inlet

capillaries.[4] These techniques are applied to not only aid in desolvation but also reduce the chemical noise in ESI mass spectra which is typically saturated with solvated ion clusters. Other methods have been used to reduce the chemical noise that is due to specific contaminants including using heated shield interfaces[5] and ion-molecule reactions to "filter" selected ions of interest.[6, 7] To further eliminate chemical noise due to solvent clusters in quadrupole ion traps (QITs), broadband waveforms have been applied to gently collisionally activate and dissociate these solvated ions to convert them into free buffer-related ions for subsequent resonance ejection.[8] The nature of the chemical noise background in matrix-assisted laser desorption/ionization (MALDI) has been investigated in some detail and has also been determined to be in part due to matrix and analyte-matrix clusters;[9, 10] in fact, MALDI-TOF-TOF experiments on chemical noise ions of *m/z* greater than that of the analyte ions yielded free analyte ions due to decay and desolvation of analyte-matrix clusters in the flight tube.[10] In ESI mass spectra, background noise is often observed at virtually all *m/z* values and the source of this noise cannot often be determined.[11] While using "soft" ESI conditions (e.g., low inlet capillary temperatures and small potential differences between the capillary and skimmer) enhances the production of very stable hydrated peptide ions with upwards of fifty water adducts, which have been extensively studied by the Williams group,[12, 13] in this work we are investigating chemical noise in ESI mass spectra in which desolvating conditions are employed. In this chapter, supplemental IR activation in a linear ion trap mass spectrometer to reduce the chemical noise background observed in ESI mass spectra is reported. Rather than focusing on eliminating background ions of specific *m/z*, IR irradiation has been applied to activate ions of unresolved *m/z* observed in noise regions of the ESI mass spectra. Upon supplemental IR activation of noise regions, analyte ions of high abundance are detected.

8.3 EXPERIMENTAL

8.3.1 Mass Spectrometry and Materials

All experiments were conducted on a modified LTQ XL linear ion trap mass spectrometer (Thermo Fisher Scientific, San Jose, CA) with the standard ESI source which is directed at an angle to the inlet heated capillary. A ZnSe optical window was mounted to the back plate of the vacuum manifold on axis with the linear ion trap to transmit IR irradiation as previously described.[14] Supplemental IR activation was performed with a model 48-5 Synrad 50-W continuous wave CO_2 laser (Mukilteo, WA) which emits radiation at 10.6 μm. For IR activation experiments, the irradiation time (0 – 50 ms) and power (25 – 50 W) was varied. Wide-range isolation and IR activation experiments were conducted by turning off the isolation waveform through the diagnostics panel of the LTQTune v2.5.0 software. The laser was triggered through the LTQTune software only during the activation step in the scan function and not during ion accumulation, ion cooling, or ion transmission. (It should be noted that the laser beam does interact with all ions along the optical path from the linear ion trap to the skimmer cone but the laser beam does not pass through the inlet heated capillary which is off-axis from the skimmer cone.) The automatic gain control was turned off for all experiments and peak areas calculations were performed in triplicate. All samples were prepared at 10 μM in 50:50:1 H_2O/MeOH/HOAc (v/v/v), unless otherwise noted, and infused at 3 μL/min through a fused silica capillary (194 μm O.D., 98 μm I.D.). The heated capillary temperature was maintained at 180 °C unless otherwise noted. The nitrogen sheath gas flow was set to 20 (arbitrary units, corresponding to ~0.3 L/min) and no auxiliary gas flow was used. The peptides bradykinin (1059.5 Da), angiotensin I (1295.6 Da),

fibrinopeptide A (1535.7 Da), the protein cytochrome c, and reserpine (608.3 Da) were all obtained from Sigma-Aldrich (St. Louis, MO). All solvents and other chemicals were from Fisher Scientific (Fairlawn, NJ).

8.4 RESULTS AND DISCUSSION

In the previous study discussed in Chapter 4, which employed infrared multiphoton dissociation (IRMPD) to differentiate and identify chromogenic cross-linked peptides from other non-cross-linked products, it was observed that the abundances of some of the unmodified peptide cations actually increased upon IR irradiation, particularly when comparing peak areas in the wide-range isolation and IRMPD mass spectra.[14] In a second time-resolved IRMPD study of peptides discussed in Chapter 7, it was also noted that ion abundances of selected precursor ions increased upon exposure to short irradiation times prior to ion dissociation upon longer irradiation times.[15] These increases in ion abundances upon IR irradiation were initially attributed to fluctuations in the ion current between the isolation and the IRMPD scans; however, as this phenomenon was consistently observed, other possible reasons for the increase in ion abundance were investigated.

For this study, peptide samples were introduced by ESI using typical parameters to promote efficient ion desolvation; however, rather than isolating and activating a specific peptide ion, noise regions above the peptide ions or wide *m/z* ranges (including the peptide ions) were subjected to IR irradiation. Typical wide range isolation and supplemental IR activation mass spectra of bradykinin are shown in **Figure 8.1a and 8.1b**, respectively. The wide range isolation mass spectrum is identical to the conventional ESI mass spectrum of bradykinin (Figure 1a), and the range from *m/z* 1000 to 1100 is amplified to showcase the abundance of the protonated peptide. Upon 30 ms

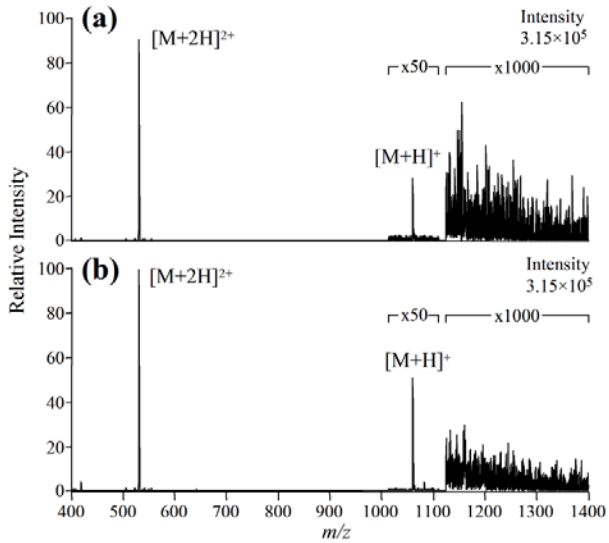

Figure 8.1 (a) Wide range isolation mass spectrum of *m/z* 400 – 2000 (30 ms) and (b) supplemental IR activation mass spectrum (30 ms, 25 W) of bradykinin (M). Both spectra are normalized to the same intensity.

of supplemental IR irradiation at 25 W, a significant increase in the abundance of singly protonated bradykinin is observed (**Figure 8.1b**). The peak area of $[M+H]^+$ increased by 68 ± 17% (~2260 to ~3800 counts), while the abundance of doubly-charged bradykinin increased by 3.8 ± 2.0% (~232000 to ~241000 counts). The total ion current (TIC) in the IR activation mass spectra was on average 4.5 ± 1.2% (~550,000 to ~575,000 counts) greater than that measured in the wide range isolation mass spectra. These increases in peptide ion abundances parallel the decrease in the chemical noise, which is presumed to consist primarily of loosely bound solvated peptide ions of unresolved *m/z*. In the amplified region of *m/z* 1300 – 1400, there is a distinct difference in the noise level between the wide range isolation mass spectrum and the IRMPD mass spectrum (**Figure 8.1a and 8.1b**).

Similar increases in the abundances of the lower charge states of cytochrome c were observed upon supplemental IR irradiation as shown in the wide-range isolation and

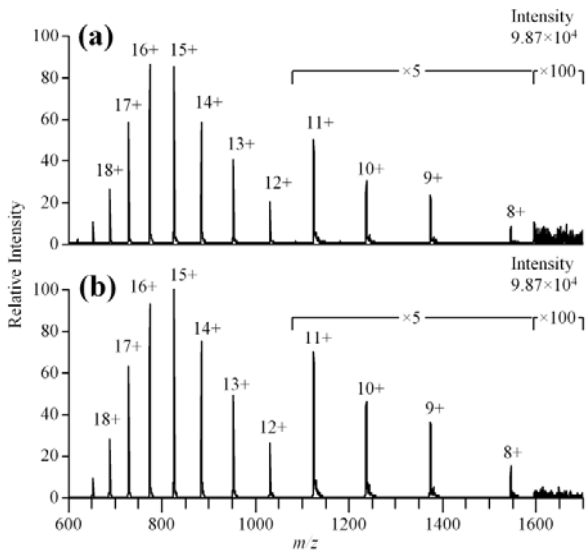

Figure 8.2 (a) Wide range isolation mass spectrum of *m/z* 600 – 2000 (50 ms) and (b) supplemental IR activation mass spectrum (50 ms, 50 W) of cytochrome c. Both spectra are normalized to the same intensity.

IR activation mass spectra in **Figure 8.2a and 8.2b**. The abundances of the 8+ through 10+ charge states of cytochrome c increased by 39 – 55% upon IR irradiation. The peak areas of the 13+ through 15+ charge states only exhibited increases of ~10%, and the peak areas of the more highly charged cytochrome c ions changed by less than 5%. IR irradiation also effectively decreased the noise level above *m/z* 1600. The TIC increased by ~15% between the isolation and the IR activation mass spectra, and this could be due to dissociation of highly solvated ions that have *m/z* values that exceed the detectable mass range of the linear ion trap (maximum *m/z* of 2000) yet still have stable trajectories in the mass analyzer.

The effectiveness of IR activation to dissociate these solvated ions was also compared to collisional activation. The wide-range isolation mass spectrum of angiotensin I is shown in **Figure 8.3a** in which ions of *m/z* 1400 – 2000 were isolated. Upon IR irradiation, the entire noise region was drastically reduced in intensity and

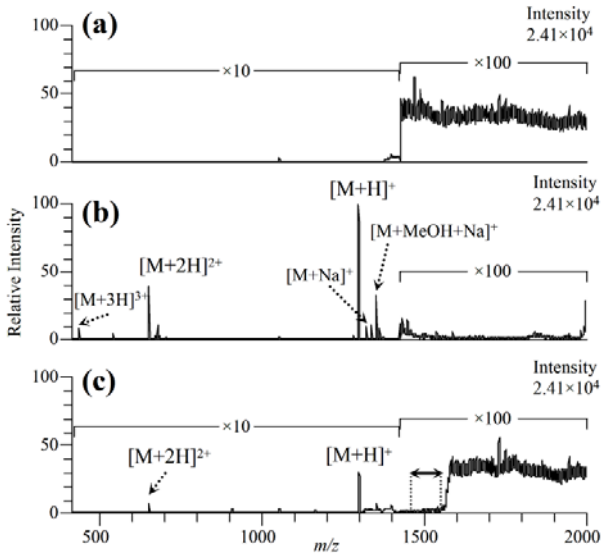

Figure 8.3 (a) Wide range isolation mass spectrum of *m/z* 1400 – 2000 (30 ms), (b) supplemental IR activation mass spectrum (30 ms, 50 W), and (c) collisional activation mass spectrum (30 ms, 100% normalized collision energy) of angiotensin I (M). Only ions of *m/z* 1450 – 1550 were activated in the collisional activation mass spectrum (range indicated with double-headed arrow) while all ions of *m/z* 1400 – 2000 were isolated. All spectra are normalized to the same intensity.

protonated angiotensin in the 1+, 2+ and 3+ charge states were observed (**Figure 8.3b**). In fact, the abundances of the peptide ions were sufficiently high to allow subsequent collision induced dissociation (CID) MS^3 experiments to confirm their identity (data not shown). As shown in **Figure 8.3c**, collisional activation of the range from *m/z* 1450 to 1550 (centered on *m/z* 1500 with an activation window of 100 u) also resulted in a decrease in the chemical noise of ions in resonance with the auxiliary collisional activation waveform, but high levels of noise remained above *m/z* 1575. (Collisional activation waveforms could only be applied to activate ions within a mass window of 100 u due to limitations of the instrument software.) Collisional activation of *m/z* 1450 – 1550 produced low abundances of peptide ions but at signal levels ~30× lower in intensity than obtained by the IR activation process. As a more direct comparison

between the effects of IR irradiation and collisional activation of specific noise regions, the narrow region from *m/z* 1900 to 2000 was isolated after infusion of a solution containing bradykinin (**Figure 8.4a**) and either subsequently irradiated or subjected to collisional activation. IR irradiation yielded an intense signal of singly protonated bradykinin (*m/z* 1060.3) while collisional activation produced the same peptide ions at a 150× lower intensity (**Figure 8.4b and 8.4c**).

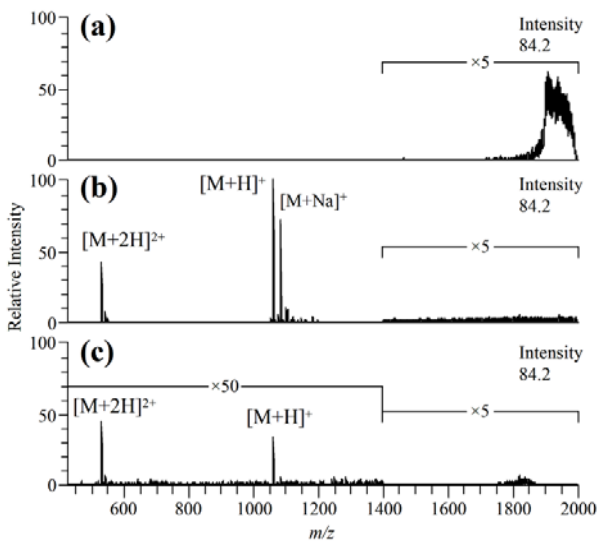

Figure 8.4 (a) Isolation mass spectrum of *m/z* 1900 – 2000 (50 ms), (b) supplemental IR activation mass spectrum (50 ms, 25 W), and (c) collisional activation mass spectrum (30 ms, 100% normalized collision energy corresponding to 348 mV amplitude at *m/z* 1950) of bradykinin (M). All spectra are normalized to the same intensity.

The temperature of the inlet heated capillary was varied to provide more evidence that the source of chemical noise in the ESI mass spectra was solvated ions of unresolved *m/z*. For a solution containing reserpine, the *m/z* region 1900 – 2000 was isolated and subjected to 30 ms of IR irradiation to yield protonated reserpine (*m/z* 609.7), and the peak area of this ion was plotted vs. heated capillary temperature (**Figure 8.5**). As a control, the peak area of protonated reserpine in the ESI mass spectra without isolation or

IR activation was also plotted. At low capillary temperatures, IR activation of *m/z* 1900 – 2000 at 120 °C yielded the highest abundance of protonated reserpine, corresponding to significant IR desolvation of a large population of solvated ions. As the capillary temperature was increased, the abundance of protonated reserpine produced upon IR activation decreased, in accordance with the existence of a smaller population of solvated ions due to more efficient desolvation of the ions exiting the ESI capillary. In the absence of IR activation, the abundance of protonated reserpine in the ESI mass spectra increased with higher inlet capillary temperatures, indicative of the disruption of more of the solvent clusters and their conversion into desolvated reserpine.

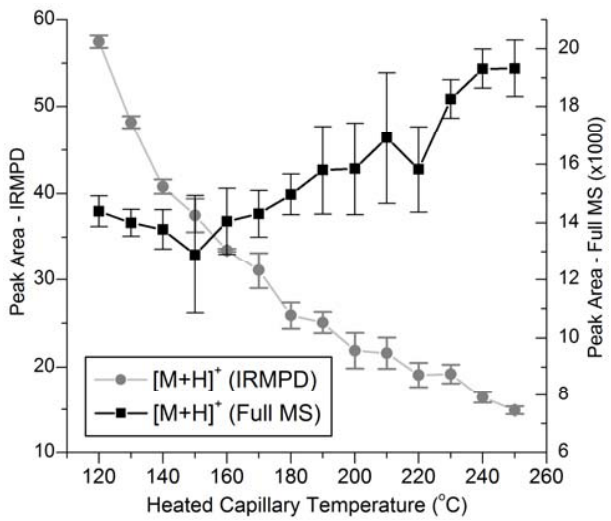

Figure 8.5 Plot of $[M+H]^+$ peak areas in the ESI mass spectra (black squares, ■) and upon IR irradiation (30 ms, 50 W) of *m/z* 1900-2000 (gray circles, ●) as a function of heated inlet capillary temperature when infusing a sample of reserpine (1 μM in MeOH). Ions of *m/z* 1900 – 2000 were subjected to IR irradiation and the abundance of the $[M+H]^+$ product ion was calculated. Data was acquired in triplicate; reserpine is represented by M.

The abundance of various bradykinin peptide ions produced upon IR activation was also monitored as a function of the *m/z* window isolated and irradiated, ranging from *m/z* 1100 – 1200 to *m/z* 1900 – 2000. IR activation of the *m/z* region just above that of

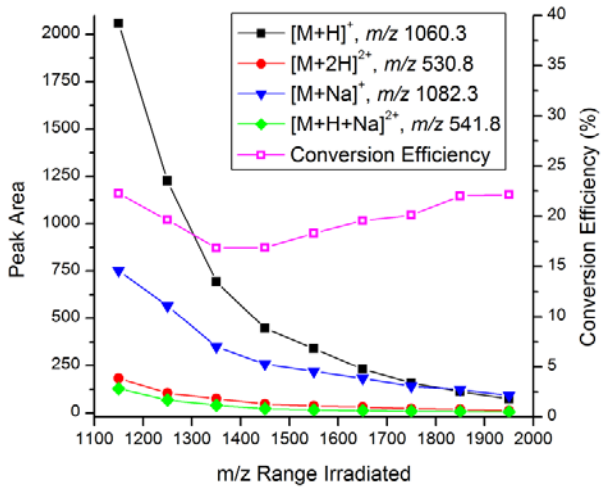

Figure 8.6 Plot of bradykinin (M) cations (protonated and sodium-cationized forms) observed upon IR irradiation of 100 *m/z* range windows. Supplemental IR activation of each window (e.g., *m/z* 1100 – 1200) was performed using 50 ms of irradiation at 25 W and the peak areas of $[M+H]^+$ (filled black squares, ■), $[M+2H]^{2+}$ (filled red circles, ●), $[M+Na]^+$ (filled blue triangles, ▼) and $[M+H+Na]^{2+}$ (filled green diamonds, ♦) were measured. The efficiency of producing bradykinin ions from chemical noise (i.e., conversion efficiency), defined as the sum of the peak areas of bradykinin ions divided by the total area of the noise in the isolation mass spectra, is also plotted (open pink squares, □).

protonated bradykinin (*m/z* 1060.3) yielded the highest abundances of protonated, doubly protonated, and sodium-cationized bradykinin (**Figure 8.6**). As the isolation window increased from *m/z* 1100 – 1200 to *m/z* 1900 – 2000, the abundance of the peptide cations produced upon supplemental IR activation decreased, thus suggesting that the greatest portion of the chemical noise consists of bradykinin ions solvated by only a few solvent molecules with *m/z* values just above that of the protonated peptide, as opposed to large clusters of bradykinin ions surrounded by dozens of solvent molecules resulting in "noise" ions of much higher *m/z*.

IR and collisional activation of an *m/z* region between that of the 1+ and 2+ charge states of fibrinopeptide A produced both the singly and doubly protonated peptide

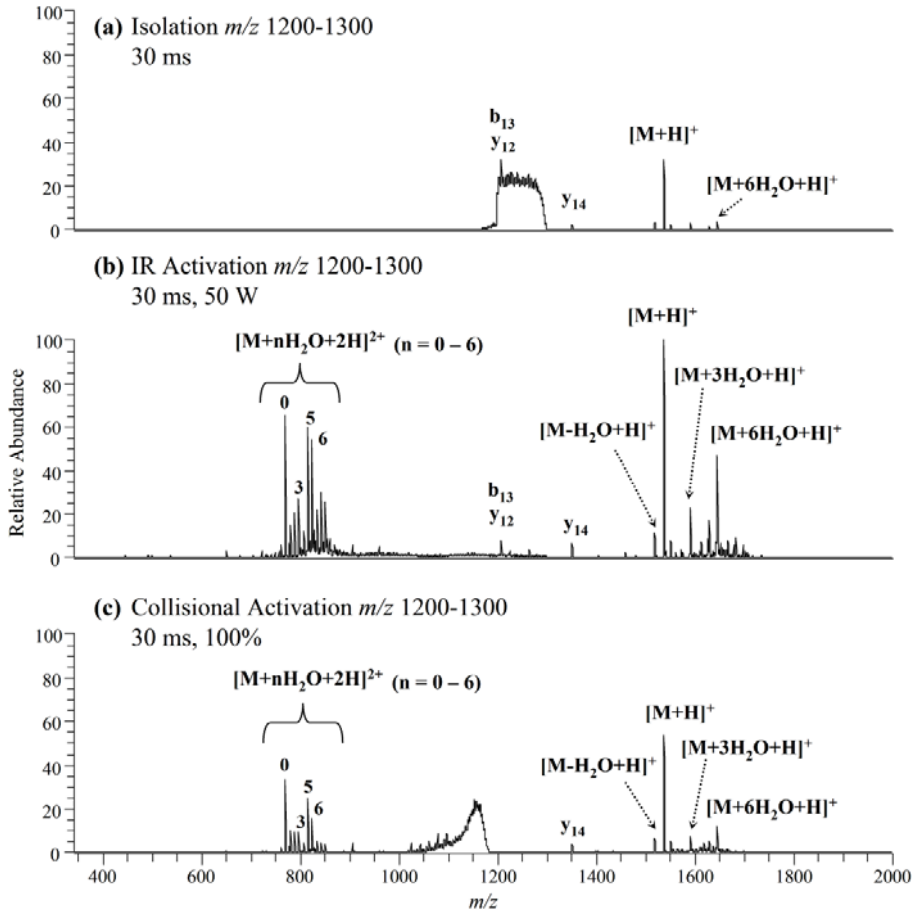

Figure 8.7 (a) Isolation (30 ms), (b) IR activation (30 ms, 50 W), and (c) collisional activation (100% normalized collision energy) mass spectra of *m/z* 1200 – 1300 for a sample of 10 μM fibrinopeptide A in 50:50:1 H_2O/MeOH/HOAc (v/v/v).

which suggests that charged solvent clusters also solvate the peptides (see **Figure 8.7**). Supplemental activation of this noise region also yielded stable hydrated forms of the peptide – up to six water molecule adducts were observed. The observation of protonated fibrinopeptide A in **Figure 8.7a** is attributed to collisional activation of solvated ions during the isolation step (i.e., the application of the low amplitude isolation waveforms and the ramping of the rf amplitude to isolate the specified *m/z* range). Both IR and collisional activation of the noise region of *m/z* 1200 – 1300 (**Figure 8.7b and 8.7c**,

respectively) produced the singly and doubly protonated peptide as well as hydrated forms (up to six water molecule adducts) of the peptide. The observation of the singly protonated peptide upon supplemental activation is attributed to the loss of H_3O^+ or other charged or protonated solvent clusters.

The efficiency of converting noise into analyte ions, defined as the sum of the peak areas of the bradykinin ions produced by supplemental IR activation divided by the total area of the noise region in the isolation mass spectra, was also measured as a function of the *m/z* isolation and irradiation window (**Figure 8.6**). Although the total abundance of bradykinin produced upon IR irradiation decreases with higher *m/z* windows, the conversion of chemical noise into bradykinin ions remains relatively constant at 19.8 ± 2.1% averaged across the m/z isolation and irradiation windows, suggesting that at least ~20% of the chemical noise is composed of solvated analyte ions.

At the high standard operating pressures of QITs, low power IR irradiation does not result in dissociation of covalent bonds of most analyte ions due to a near equivalent rate of ion activation through photon absorption and collisional cooling with the buffer gas.[16] The non-resonant nature of IR activation provides an inherent advantage over collisional activation in that all ions in the trap are simultaneously irradiated by the laser beam and thus effectively desolvated. It has been previously shown that broadband auxiliary waveforms can be used to heat a wider range of ions for successful noise reduction,[8] a procedure that is not feasible on the current generation of commercial quadrupole ion traps.

8.5 CONCLUSIONS

Chemical noise in ESI mass spectra was reduced by low power supplemental IR activation and produced protonated analyte ions. IR irradiation increased the abundances

of protonated peptides and proteins by 30 – 70% upon isolation and irradiation of a wide *m/z* range. Regions of chemical noise were drastically reduced upon IR irradiation and produced higher abundances of protonated analyte ions than collisional activation due to the non-resonant activation nature of photoabsorption. It is speculated that solvated analyte ions and solvent-analyte clusters constitute a large portion of the chemical noise. Further application of supplemental IR activation in linear QITs prior to ion ejection or tandem MS could be used to reduce noise and increase analyte ion signal particularly for LC-MS analyses in which survival of a higher abundance of solvated ions is expected.

8.6 REFERENCES

(1) Fenn, J. B.; Mann, M.; Meng, C. K.; Wong, S. F.; Whitehouse, C. M. *Science* **1989**, *246*, 64-71.

(2) Loo, J. A.; Udseth, H. R.; Smith, R. D. *Rapid Communications in Mass Spectrometry* **1988**, *2*, 207-210.

(3) Light-Wahl, K. J.; Schwartz, B. L.; Smith, R. D. *Journal of the American Chemical Society* **1994**, *116*, 5271-5278.

(4) Chowdhury, S. K.; Katta, V.; Chait, B. T. *Rapid Communications in Mass Spectrometry* **1990**, *4*, 81-87.

(5) Aebi, B.; Henion, J. D. *Rapid Communications in Mass Spectrometry* **1996**, *10*, 947-951.

(6) Jarvis, M. J. Y.; Koyanagi, G. K.; Zhao, X.; Covey, T. R.; Bohme, D. K. *Analytical Chemistry* **2007**, *79*, 4006-4012.

(7) Guo, X.; Bruins, A. P.; Covey, T. R.; Troetzmueller, M.; Lankmayr, E. *Journal of the American Society for Mass Spectrometry* **2009**, *20*, 105-111.

(8) Ramsey, R. S.; Goeringer, D. E.; McLuckey, S. A. *Analytical Chemistry* **1993**, *65*, 3521-3524.

(9) Krutchinsky, A. N.; Chait, B. T. *Journal of the American Society for Mass Spectrometry* **2002**, *13*, 129-134.

(10) Sachon, E.; Clodic, G.; Blasco, T.; Bolbach, G. *Journal of the American Society for Mass Spectrometry* **2007**, *18*, 1880-1890.

(11) Cech, N. B.; Enke, C. G. *Mass Spectrometry Reviews* **2002**, *20*, 362-387.

(12) Rodriguez-Cruz, S. E.; Klassen, J. S.; Williams, E. R. *Journal of the American Society for Mass Spectrometry* **1997**, *8*, 565-568.

(13) Rodriguez-Cruz, S. E.; Klassen, J. S.; Williams, E. R. *Journal of the American Society for Mass Spectrometry* **1999**, *10*, 958-968.

(14) Gardner, M. W.; Vasicek, L. A.; Shabbir, S.; Anslyn, E. V.; Brodbelt, J. S. *Analytical Chemistry* **2008**, *80*, 4807-4819.

(15) Gardner, M. W.; Smith, S. I.; Ledvina, A. R.; Madsen, J. A.; Coon, J. J.; Schwartz, J. C.; Stafford, G. C.; Brodbelt, J. S. *Analytical Chemistry* **2009**, *81*, 8109-8118.

(16) McLuckey, S. A.; Goeringer, D. E. *Journal of Mass Spectrometry* **1997**, *32*, 461-474.

Chapter 9

Infrared Multiphoton Dissociation of Small-Interfering RNA Anions and Cations

9.1 OVERVIEW

Infrared multiphoton dissociation (IRMPD) on a linear ion trap mass spectrometer is applied for the sequencing of small interfering RNA (siRNA). Both single-strand siRNAs and duplex siRNA were characterized by IRMPD, and the results were compared to that obtained by traditional ion trap based collision induced dissociation (CID). The single-strand siRNA anions were observed to dissociate via cleavage of the 5' P–O bonds yielding c- and y-type product ions as well as undergo neutral base loss. Full sequence coverage of the siRNA anions was obtained by both IRMPD and CID. While the CID mass spectra were dominated by base loss ions, accounting for ~25 – 40% of the product ion current, these ions were eliminated through secondary dissociation by increasing the irradiation time in the IRMPD mass spectra to produce higher abundances of informative sequence ions. With longer irradiation times, however, internal ions corresponding to cleavage of two 5' P–O bonds began to populate the product ion mass spectra as well as higher abundances of [a - Base] and w-type ions. IRMPD of siRNA cations predominantly produced c- and y-type ions with minimal contributions of [a - Base] and w-type ions to the product ion current; the presence of only two complementary series of product ions in the IRMPD mass spectra simplified spectral interpretation. In addition, IRMPD produced high abundances of protonated nucleobases – $[G+H]^+$, $[A+H]^+$, and $[C+H]^+$ - which were not detected in the CID mass spectra due to the low-mass cut-off associated with conventional CID in ion traps. CID and IRMPD using short irradiation

times of duplex siRNA resulted in strand separation, similar to the dissociation trends observed for duplex DNA. With longer irradiation times, however, the individual single-strands underwent secondary dissociation to yield informative sequence ions not obtained by CID.

9.2 INTRODUCTION

The identification and determination of the function of small non-coding (i.e., non-messenger) RNA including small interfering RNA (siRNA) and micro-RNA (miRNA) has become an important challenge due to the growing recognition of these RNAs in fundamental cellular processes including gene regulation, RNA processing, translocation of proteins, chromosome maintenance, and cancer and disease development.[1, 2] For example, RNA interference (RNAi) is a biological pathway which down-regulates or silences gene expression and has shown great potential to be harnessed as a therapeutic tool via introduction of siRNA, typically short double stranded RNA consisting of approximately 25 nucleotides (per single strand), to cells.[3, 4] Micro-RNAs, which consist of ~22 nucleotides, have also been shown to effect gene silencing by binding directly to the target mRNA.[5] Several siRNA-based drugs are currently in clinical trials,[6, 7] and recent studies have explored the impact of siRNA on coronary artery disease,[8] Alzheimer's disease,[9] and HIV.[10, 11]

The traditional methods used to identify these non-coding RNAs are wet-lab techniques including over-expression and cloning, and sequencing.[12] Deep sequencing analyses in conjunction with predictive computational approaches have also been utilized to identify miRNAs.[13, 14] Tandem mass spectrometry is well-suited for the characterization of novel miRNAs, as well as synthesized siRNAs, including those that contain chemical modifications to increase their stability, such as deoxynucleotides, 3'-

overhangs, or 2'-O-methyl modifications.[15, 16] While tandem mass spectrometry has been widely used to sequence DNA,[17-22] little effort has been devoted to the analysis of RNA until recently.[23-27] Gas-phase dissociation of DNA anions is initiated by base loss and subsequent dissociation of the 3' C O bond yielding complementary [a - Base] and w-type ions.[18] In contrast, collision-induced dissociation (CID) of RNA typically results in fragmentation of the 5' P O bond producing complementary c- and y-type fragment ions.[23-26] Schürch and co-workers observed that dissociation of RNA was independent of the nucleobase and that cleavage of the 5' P O bond is related to the presence of the 2'-hydroxyl group.[24, 26] That is, upon ion activation, an intramolecular cyclic transition-state involving the 2'-hydroxyl proton and the 5' oxygen of the phosphate is formed, and migration of the 2'-hydroxyl proton and subsequent cleavage yields the c- and y-type fragments.[24, 26] McLuckey's group observed that the dissociation pathways of RNA anions were charge-dependent in which more highly charged species predominantly underwent base loss, and the lower charge states gave higher sequence coverage.[23] More recently, McLuckey et al. obtained full sequence coverage of deprotonated siRNA ions by CID with subsequent proton transfer reactions which effectively "deconvoluted" and simplified interpretation of the product ion mass spectra.[27] The Håkansson group investigated the fragmentation pathways of oligoribonucleotides by both electron capture dissociation (ECD) and electron detachment dissociation (EDD).[28] They observed that the ECD fragmentation patterns were dependent on the nucleobase. Both c/y-type ions and d/w-type ions were produced by ECD; whereas EDD predominantly yielded d- and w-type ions, and full sequence coverage was obtained.

Infrared multiphoton dissociation (IRMPD) has been previously been shown to be a viable alternative and complementary dissociation method to CID for the sequencing of DNA.[19, 20, 29-31] One of the primary advantages of IRMPD in ion traps is that as a non-

resonant method, the precursor ion and all ensuing product ions are activated by IR irradiation. Uninformative product ions due to dead-end dissociation pathways (e.g., neutral base loss) can undergo secondary dissociation to yield diagnostic sequence ions. IRMPD also does not suffer significantly from the low-mass cut-off problem intrinsic to conventional CID in rf ion traps. The energy deposition by conventional CID is dependent on the rf trapping voltage which prevents the storage of ions of *m/z* in the lower 28% of the mass range relative to the precursor ion. Since IRMPD can be performed using far lower rf trapping levels, diagnostic low-mass product ions can be detected. The energy deposition by photon absorption is also not dependent on the rf trapping voltage, but rather on the absorptivity of the ion at the wavelength of the laser. Compared to proteins and peptides which do not undergo efficient photodissociation at normal trap pressures of ~ 1 mTorr, oligonucleotides dissociate rapidly upon exposure to IR irradiation at 10.6 μm due to the high IR absorptivity of the phosphodiester backbone at this wavelength,[32] an effect noted initially by Little et al.[33] IRMPD also affords a high degree of tunability and control with regards to energy deposition, as the irradiation time and power can both be varied.

In the present study, the use of IRMPD to sequence single-strand and duplex siRNA anions and cations as a function of charge state is examined. Time-resolved IRMPD experiments reveal the genealogy of product ion formation. Compared to CID, IRMPD produces a higher abundance of diagnostic sequence ions and favors the formation of shorter product ions in lower charge states. Full sequence coverage was generally obtained by both dissociation techniques; however, the IRMPD product ion mass spectra were often simpler to interpret due to conversion of the neutral base loss product ions into informative sequence ions upon secondary dissociation.

9.3 EXPERIMENTAL

9.3.1 Chemicals and Materials

Imidazole, piperidine, and Amberlite IRN77 resin were purchased from Sigma-Aldrich (St. Louis, MO). Methanol, ammonium acetate, and isopropanol were obtained from Fisher Scientific (Fairlawn, NJ). The siRNAs targeting the glyceraldehydes 3-phosphate dehydrogenase (GAPDH) gene and the Lamin A/C gene were purchased from Integrated DNA Technologies (Coralville, IA). The sequences for anti-GAPDH were 5'OH-GUGGAUAUUGUUGCCAUCAdTdT-3'OH (sense strand, GAPDH.S, 6633.9 Da) and 5'OH-UGAUGGCAACAAUAUCCACdTdT-3'OH (antisense strand, GAPDH.AS, 6644.9 Da). The sequences for anti-Lamin A/C were 5'-biotin-GGAACUGGACUUCCAGAAGAACAUCUA-3'OH (sense strand, Lamin A/C.S, 9053.6 Da) and 5'-UAGAUGUUCUUCUGGAAGUCCAGUUCC (antisense strand, Lamin A/C.AS, 8544.1 Da).

Single-strand siRNA samples were desalted by cation exchange using the Amberlite IRN77 resin as described by McLuckey et al.[27] Duplex siRNA was annealed by combining the sense and antisense siRNA strands (30 μM each) in 150 mM NH_4OAc, pH 7.0. The samples were heated at 90 °C for three minutes and then cooled to room temperature overnight. Duplex siRNA solutions were diluted to 10 μM in 25:75 (v/v) methanol/50 mM NH_4OAc in nano-pure H_2O. Solutions of GAPDH single-strand siRNAs were prepared at 10 μM in either 25:75 (v/v) methanol/25 mM NH_4OAc for negative and positive electrospray mass spectrometry (ESI-MS) or 20:80 (v/v) isopropanol/H_2O with 25 mM imidazole and 25 mM piperidine for negative ESI-MS. The Lamin A/C single strand siRNAs were prepared at 10 μM in 25:75 (v/v) methanol/25 mM NH_4OAc for negative and positive ion ESI-MS.

9.3.2 Mass Spectrometry and Infrared Multiphoton Dissociation

All experiments were conducted on a modified LTQ XL linear ion trap mass spectrometry (Thermo Fisher Scientific, San Jose, CA) with the standard electrospray ionization (ESI) source. Samples were infused at 2.5 μL/min and the ESI voltage was set to either -3.5 or +4.0 kV for negative and positive ion mode analysis, respectively. The inlet heated capillary was maintained at 90 °C. The mass spectrometer was modified to perform infrared multiphoton dissociation as previously described.[34] Briefly, a ZnSe window was mounted to the back plate of the vacuum manifold to transmit 10.6 μm radiation from a model 48-5 Synrad 50 W cw CO2 laser (Mukilteo, WA). The laser was triggered through the LTQTune v.2.5.0 software during the activation step in the scan function. The irradiation time was varied between 0.0 and 20.0 ms and the power was maintained at 10 W (25%). The q-value for all IRMPD experiments was set between 0.055 and 0.100. Collision-induced dissociation was performed at the typical q-value of 0.25, the activation time was set to 30 ms, and the normalized collision energy was adjusted to dissociate the precursor ion to less than 1% relative abundance.

9.3.3 Data Analysis

Time-resolved IRMPD experiments were performed by incrementally increasing the irradiation time and the abundances of the precursor and product ions were plotted against the irradiation time. Ion abundances were determined by measuring the peak areas using Origin 7.0. Product ions were identified using Mongo Oligo Mass Calculator (http://library.med.utah.edu/masspec/mongo.htm) in addition to an oligonucleotide product ion calculator program written in-house using National Instruments LabView 8.5. Only product ions which could be unambiguously identified were included in the product

ion type abundance calculations. Product ions were labeled according to the nomenclature proposed by McLuckey et al.[18]

9.4 RESULTS AND DISCUSSION

9.4.1 Infrared Multiphoton Dissociation vs. Collision-Induced Dissociation of Single-Strand siRNA

In the negative ion mode, ESI of the GAPDH sequences in ammonium acetate buffer produced ions in the 4- to 6- charge states, while ESI of Lamin A/C samples in ammonium acetate yielded ions predominantly in the 5- and 6- charge states (data not shown). Electrospray ionization of the GAPDH sequences in the imidazole/piperidine additive solution produced ions in charge states ranging from 6- to 10-. In the positive mode, both the GAPDH and Lamin A/C sequences produced ions in only two charge states. The single-strand siRNAs were subjected to IRMPD, and the product ion mass spectra were compared to that obtained by conventional ion-trap CID. Examples of the IRMPD and CID mass spectra are shown in **Figures 9.1 and 9.2**. Sannes-Lowery and Hofstadler have previously analyzed an oligoribonucleotide by IRMPD in an external hexapole by FT-ICR-MS,[29] but IRMPD has not been extensively investigated as an alternative dissociation method for RNA. The fragmentation patterns of siRNA anions by IRMPD is dependent on the irradiation time (i.e., photon flux), and thus by varying the time (or laser power), the product ion mass spectra can be effectively tuned by controlling the extent of secondary dissociation. IRMPD of the 5- charge state of GAPDH.S using 6.0 ms irradiation predominantly yielded c- and y-type product ions due to cleavage of the 5' P–O bond (**Figure 9.1a**). Lower abundance [a - Base] and complementary w-type ions were also detected. The abundances of product ions stemming from neutral base loss, which typically dominate CID product ion mass spectra

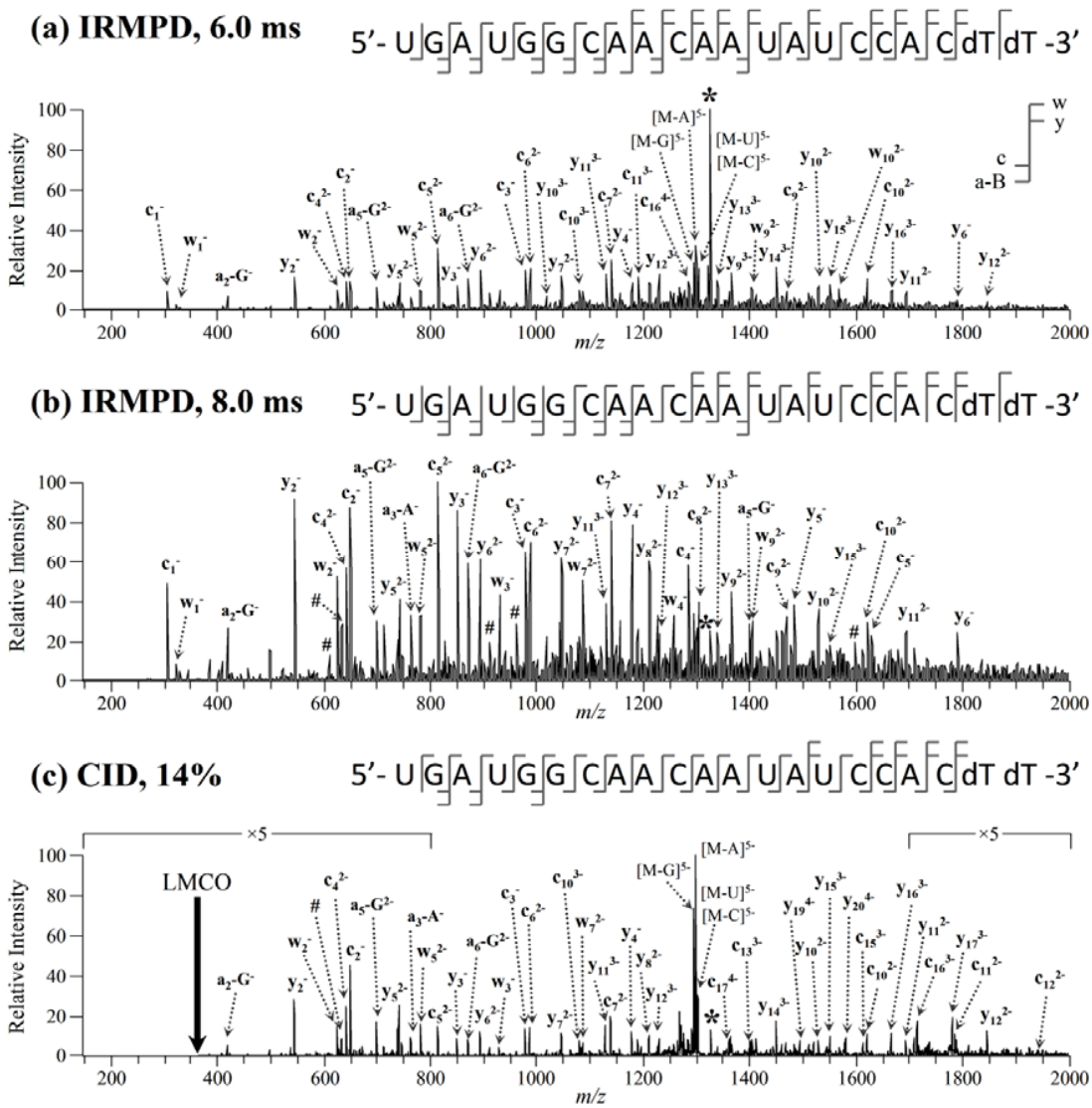

Figure 9.1 IRMPD product ion mass spectra of $[GAPDH.S - 5H]^{5-}$ of *m/z* 1326.0 using (a) 6.0 ms and (b) 8.0 ms of irradiation at 10 W at q-value of 0.10. (c) CID product ion mass spectra of the same siRNA anion (14% normalized collision energy, q = 0.25). The precursor ion is indicated by an asterisk (*) and internal ions by #. Not all peaks were labeled to reduce congestion.

of RNA,[23] were modest. Almost a complete series of c-type (19/20) and y-type (18/20) ions was observed for this siRNA anion. The three c and y product ions which were not observed were y_1, its complementary c_{20} ion, and y_{20}. Cleavage between the two dT

nucleotides would yield the y_1 and c_{20} ions, and these product ions are not likely to be observed due to the lack of the 2'-OH group to facilitate cleavage of the 5' P–O bond. However, the w_1 ion, which corresponds to cleavage of the 3' C–O bond, was detected, and full sequence coverage of this siRNA anion was obtained. The complementary [a_{20} - T] and the y_{20} product ions were most likely not detected due to secondary dissociation of these large product ions. Upon increasing the irradiation time to 8.0 ms, the product ion mass spectra changes significantly (**Figure 9.1b**). The more highly-charged and larger product ions observed in **Figure 9.1a** undergo secondary dissociation into smaller product ions. Both the precursor ion and base loss product ions are almost completely dissociated, and the product ion mass spectrum is dominated by c- and y-type fragment ions. A majority of the [a - Base] ions detected are due to the facile loss of neutral guanine (i.e., [a_n - G] product ions predominant) which has previously been reported to be a significant dissociation pathway for RNA anions in low charge states.[23] The [a - Base] and w-type product ions are likely produced by secondary photodissociation of the neutral base loss product ions (e.g., $[M - G]^{5-}$) and subsequent cleavage of the 3' C–O bond of the ribose from which the base was lost. Full sequence coverage of GAPDH.S was obtained using 8.0 ms of irradiation even though fewer sequence ions were detected ($c_1 - c_{12}$ and $y_2 - y_{15}$). The lack of larger, more highly-charged product ions reduces the spectral complexity while still allowing the siRNA anion to be completely sequenced. A majority of the product ions were singly or doubly charged. Several low mass, singly charged product ions which could be not be identified as sequence (i.e., [a - Base], c-, y-, w-type) ions were also detected. These product ions were determined to be internal ions due to cleavage of two 5' P–O bonds. These internal ions could not be unambiguously identified due to isobaric species (e.g., AUG = GAU). The abundances of the internal ions are low, and the ions likely arise from secondary dissociation of larger c- and y-type

product ions. The CID product ion mass spectrum of $[GAPDH.S - 5H]^{5-}$ was dominated by neutral base loss (**Figure 9.1c**). Product ions were observed in all possible charge states and almost complete sequence coverage was obtained. Due to the low-mass cut-off (LMCO) problem inherent to conventional CID, the low mass c_1 (*m/z* 305) and w_1 (*m/z* 324) sequence ions could not be detected. Fewer [a - Base] and w-type ions were observed upon CID, a result attributed to the fact that only the precursor ion is activated and primary product ions such as [M-G] are not further dissociated into sequence informative species. Small internal ions were also detected by CID; however, these product ions were not as abundant as those in the IRMPD mass spectrum obtained using 8.0 ms of irradiation.

IRMPD mass spectra of the 6+ charge state of the sense strand of Lamin A/C using 4.0 and 6.0 ms of irradiation are shown in **Figures 9.2a and 9.2b**. At short irradiation times, almost complete series of both c-ions ($c_1 - c_{25}$) and y-ions ($y_2 - y_{26}$) were observed. In contrast to dissociation of siRNA anions, the product ions were predominantly composed of c/y-type fragments, and the mass spectrum was almost completely void of [a - Base] and w-type ions. Also, siRNA cations of all charge states dissociated through protonated base loss, and the resulting protonated bases were observed in the low *m/z* range of the IRMPD mass spectrum. The $[Base + H]^+$ ions were the most abundant product ions in the mass spectrum with protonated guanine observed at higher abundance than $[A + H]^+$ and $[C + H]^+$; $[U + H]^+$ and $[T + H]^+$ were not detected in the IRMPD mass spectra of any of the siRNA cations. The relative abundances of the protonated nucleobases are not directly proportional to the relative contribution of each nucleobase to the sequence composition. In fact, the position of the nucleobases and their relative gas-phase basicities influence the abundance of the protonated base product ions as well. Since uracil and thymine have the lowest gas-phase

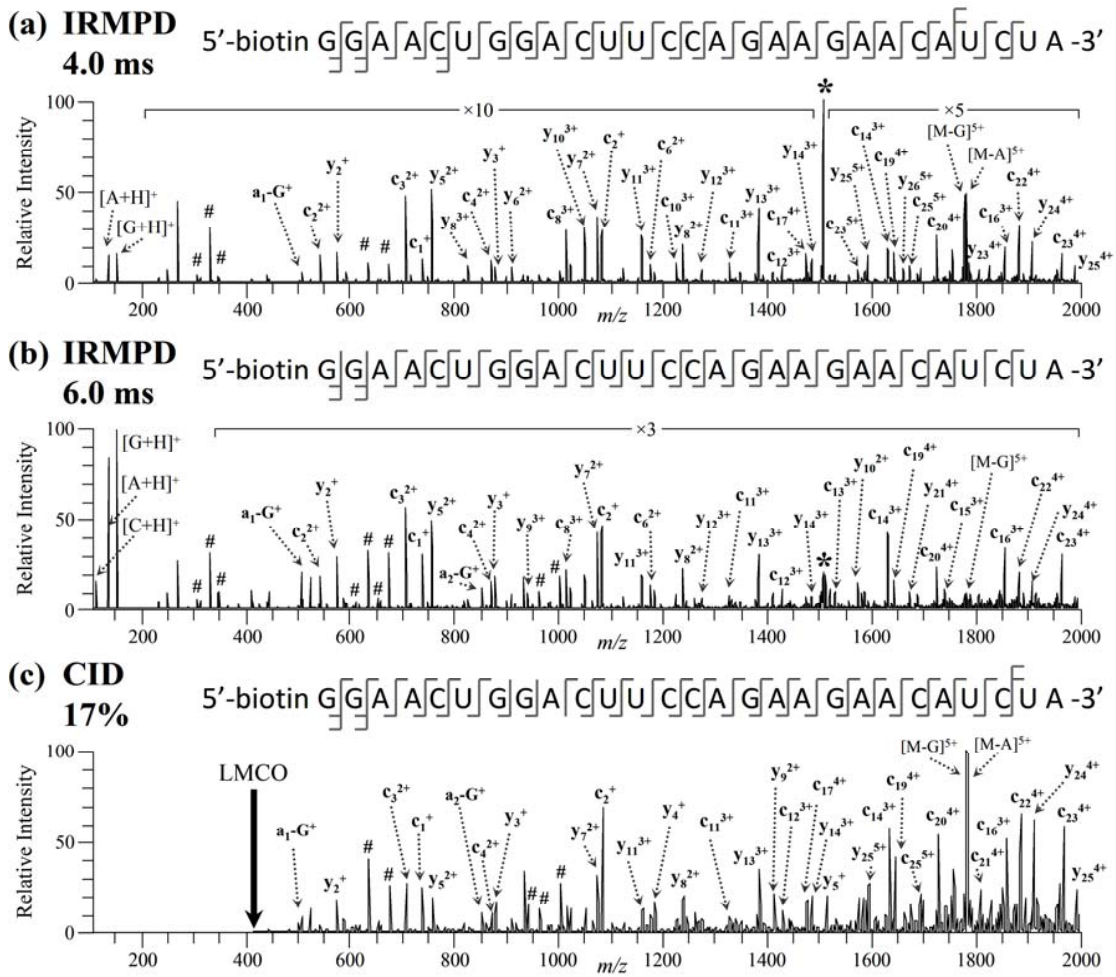

Figure 9.2 IRMPD product ion mass spectra of $[\text{Lamin A/C.S} + 6\text{H}]^{6+}$ of *m/z* 1509.8 using (a) 4.0 ms and (b) 6.0 ms of irradiation at 10 W at q-value of 0.065. (c) CID product ion mass spectra of the same siRNA cation (17% normalized collision energy, q = 0.25). The precursor ion is indicated by an asterisk (*) and internal ions by #. Not all peaks were labeled to reduce congestion.

proton affinities of the five nucleobases[35-37] the absence of these protonated bases in the IRMPD spectra is not surprising. Low mass internal ions were also detected in the IRMPD mass spectrum. Increasing the irradiation time to 6.0 ms led to significantly higher abundances of the three protonated nucleobases, $[\text{G} + \text{H}]^+$, $[\text{A} + \text{H}]^+$, and $[\text{C} + \text{H}]^+$, as shown in **Figure 9.2b**. Identical sequence coverage was obtained using 6.0 ms of

irradiation as 4.0 ms of irradiation, but base loss ions (e.g., $[M - G]^{5+}$ and $[M - A]^{5+}$) were significantly reduced in abundance, and a higher abundance of internal ions were produced. With even longer irradiation times, sequence ions were converted almost exclusively into protonated bases (data not shown). The CID mass spectrum of [Lamin A/C.S + 6H]$^{6+}$ was dominated by protonated base loss, but due to the LMCO problem, the protonated base ions were not detected (**Figure 9.2c**). While the spectrum is more cluttered than the IRMPD mass spectra, full sequence coverage was still obtained. The c/y ions were prominent, but almost no [a - Base] and w-type ions were detected upon CID of siRNA cations. Interestingly, a higher abundance of internal ions was observed upon CID of the siRNA cations than the anions.

The percentages of c/y-type ions and [a - Base]/w-type ions observed by IRMPD and CID arising from IRMPD and CID are summarized for all of the siRNA ions in **Figure 9.3**. In general, both IRMPD and CID yielded similar degrees of sequence coverage based on the number of unique product ions. As the "charge level" (defined as the number of negative charges per phosphate for oligonucleotide anions[38] or the number of positive charges per nucleobase for cations) of the anions increased above 33% (i.e., 7- through 10- charge states of GAPDH.S and GAPDH.AS), the percent of c/y-type ions observed by IRMPD and CID decreased as many product ions could not be unambiguously identified due to isobaric overlaps and the inability to isotopically resolve the peaks to determine the charge state. For charge levels of the siRNA anions below 33% (4- through 6- charge states), near complete series of c/y-ions were detected, and CID generally outperformed IRMPD as the longer c- and y-type ions were often not detected in the IRMPD mass spectra likely due to rapid secondary dissociation. The percent of [a - Base]/w-ions was generally between 20 and 50% for the siRNA anions studied, and a higher number of these product ions were detected in the IRMPD mass

spectra. This trend is attributed to secondary dissociation of base loss product ions by IRMPD as discussed earlier.

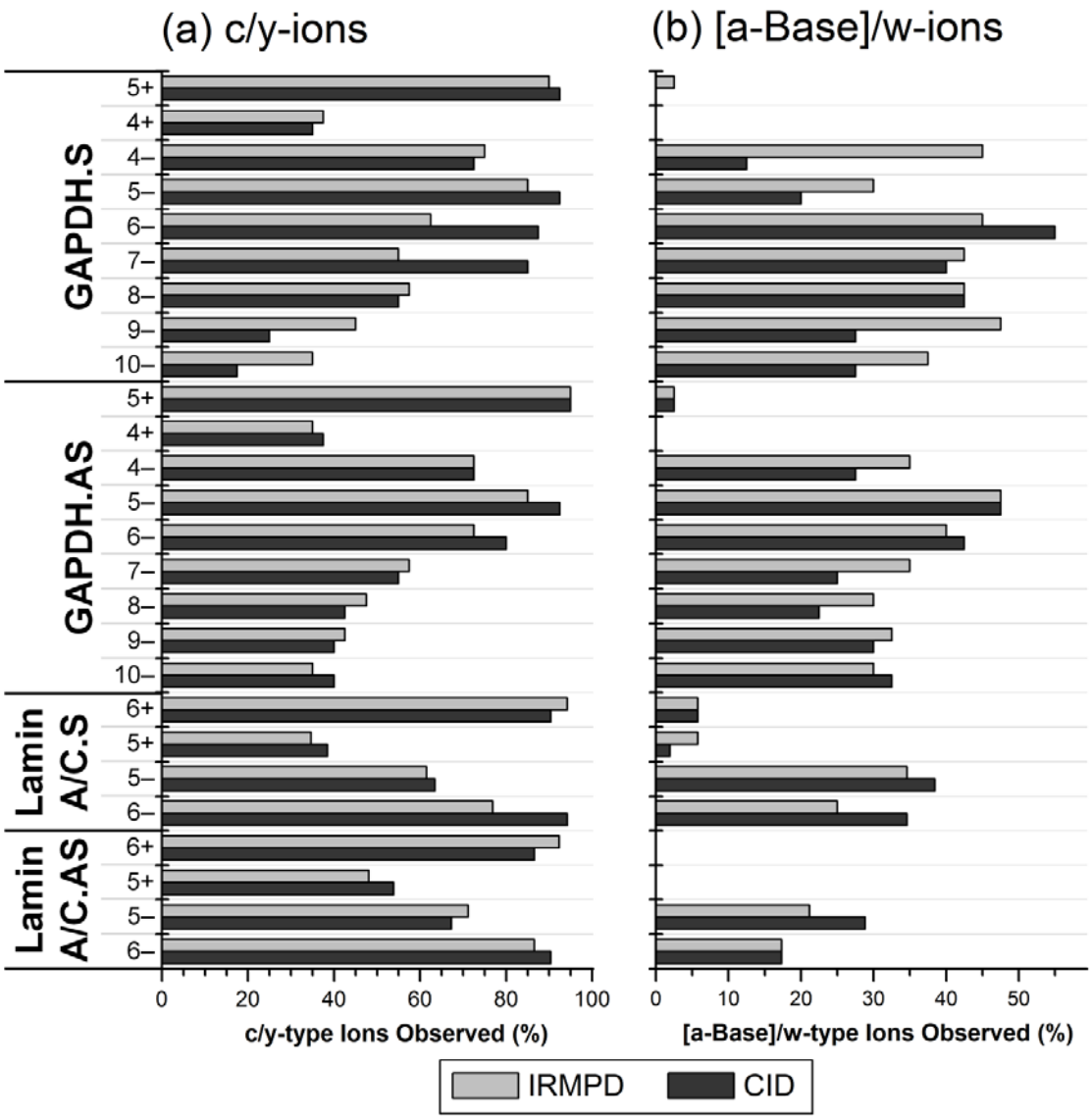

Figure 9.3 (a) Percent of c- and y-type ions and (b) percent of [a - Base] and w-type ions of model single-strand siRNAs in various charge states observed by IRMPD (light gray) and CID (dark gray). The data was compiled from IRMPD mass spectra in which the precursor ion was reduced to ~10% relative abundance (required 5 – 7 ms of irradiation). A value of 100% would indicate that all possible c/y-ions or [a - Base]/w-ions were detected.

In the positive ion mode, only two charge states of each the single-strand siRNAs were observed in the ESI mass spectra. For the siRNA cations in all charge states examined, less than 10% of the possible [a - Base]/w-type ions were detected by both IRMPD and CID (**Figure 9.3**). At charge levels above 20% (5+ charge state of GAPDH and 6+ charge state of Lamin A/C siRNAs), near complete series of c/y-ions were detected by both dissociation methods, but at charge levels below 20% (4+ charge state of GAPDH and 5+ charge state of Lamin A/C siRNAs) less than 40% of the possible c/y-ions were observed. IRMPD mass spectra of $[\text{Lamin A/C.AS} + 5\text{H}]^{5+}$ and $[\text{GAPDH.AS} + 4\text{H}]^{4+}$ are shown in **Figures 9.4a and 9.4b**. Fewer than 30 and 20 product ions were identified in the two product ion mass spectra, respectively, and only the 5' and 3' ends of the siRNAs were sequenced. Between six and ten nucleotides from either terminal were sequenced for the GAPDH and Lamin A/C siRNAs. For all of the siRNA cations in the lowest charge state (5+ for the Lamin A/C sequences and 4+ for the GAPDH sequences), no product ions stemming from cleavage of the phosphate backbone near the middle of the oligonucleotide were detected (typically the middle ten nucleotides). A summary of the product ions observed by CID and IRMPD of these siRNA cations in low charge states is shown in **Scheme 9.1**. Almost identical results were obtained by CID as well (data not shown). The low sequence coverage of these siRNAs may be due in part to the high *m/z* value of the precursor ion. Upon cleavage of the phosphate backbone, some of the expected product ions would have *m/z* values greater than 2000 due to their low charge states. It is also possible that these siRNA cations have adopted an unexpected secondary structure which results in bond cleavage predominantly near the 5' and 3' terminals. The lack of product ions arising from dissociation near the center of the siRNAs does not seem to be nucleobase dependent as this effect was observed for all four of the siRNAs which each have a different composition of nucleobases in this region.

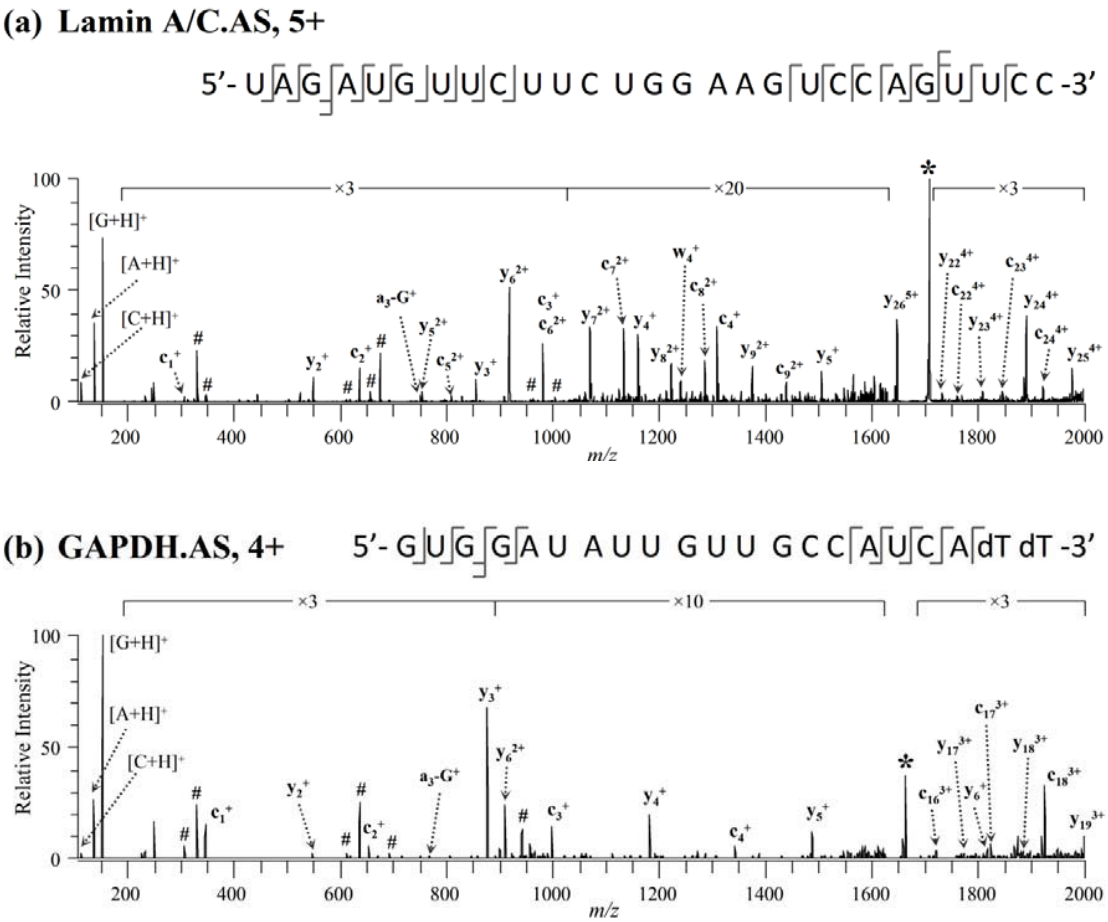

Figure 9.4 IRMPD product ion mass spectra of (a) $[\text{Lamin A/C.AS} + 5\text{H}]^{5+}$ of *m/z* 1710.0 using 5.0 ms of irradiation at 10 W (q-value = 0.058) and (b) $[\text{GAPDH.AS} + 4\text{H}]^{4+}$ of *m/z* 1662.2 using 7.0 ms of irradiation at 10 W (q-value = 0.060). The precursor ion is indicated by an asterisk (*) and internal ions by #.

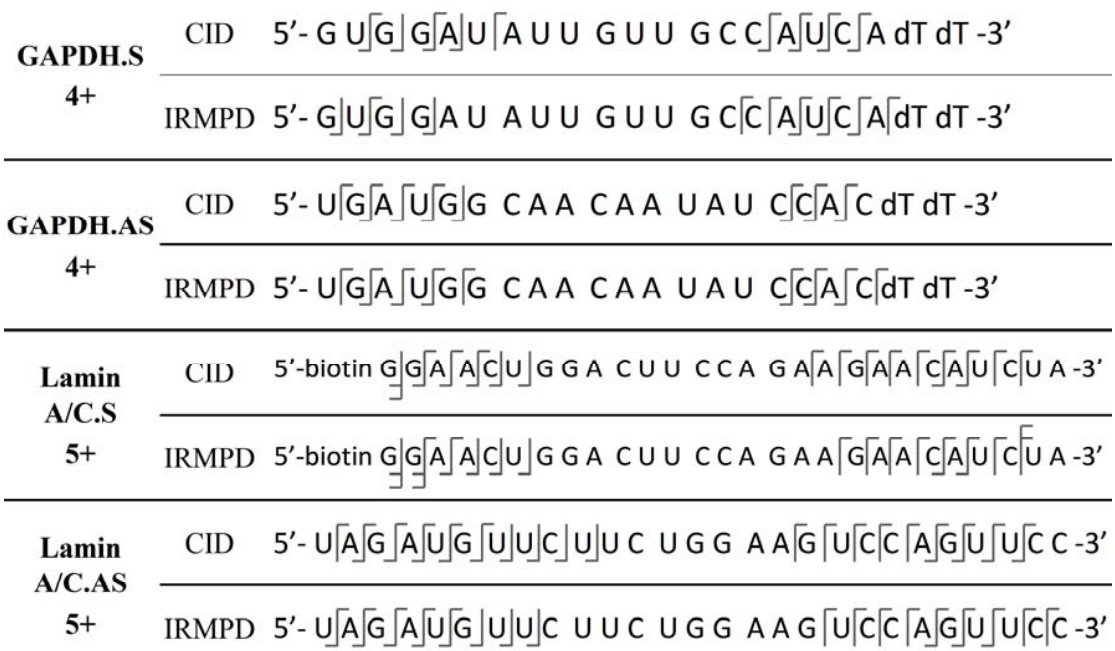

Scheme 9.1 Observed bond cleavages of siRNA cations in the lowest observed charge states.

9.4.2 Product Ion Abundances and Time-resolved IRMPD of Single-Strand siRNA

The contributions of each type of product ion to the total product ion current in IRMPD and CID mass spectra of GAPDH.AS in the 6-, 5-, 4-, 4+ and 5+ charge states were calculated and summarized in **Figure 9.5**. (The more negatively charged GAPDH.AS precursor ions – 7-, 8-, 9- and 10- charge states – were not included in this analysis because many ions could not be unambiguously identified as the isotopic profiles of the more highly charged product ions could not be resolved.) In general, approximately 40 – 50% of the product ion current was composed of c- and y-type ions; the lone exception was the 4- charge state of GAPDH.AS which was dominated by neutral base loss. For the GAPDH.AS anions, [a - Base] and w-type ions comprised ~5 –

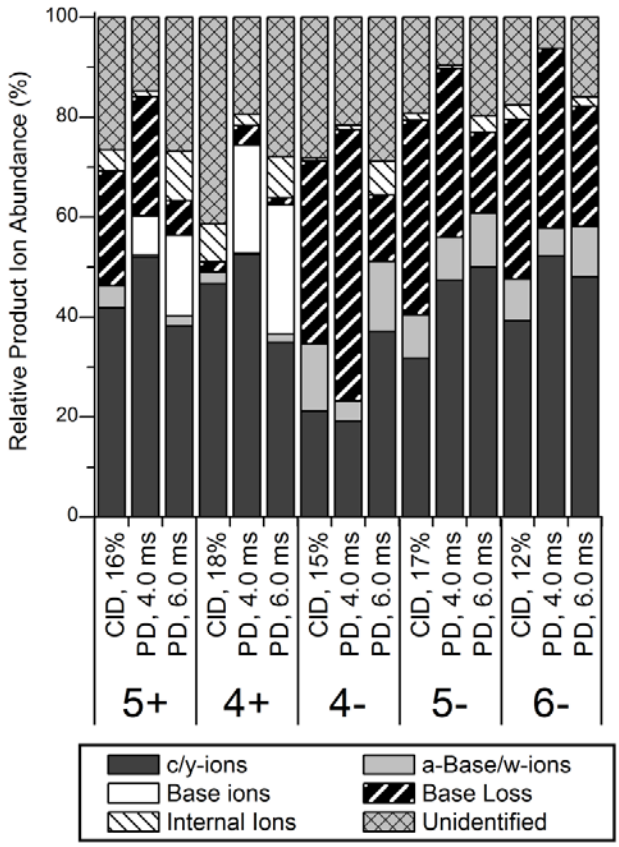

Figure 9.5 Relative abundances of different product ion types of GAPDH.AS in various charge states observed by IRMPD at 4.0 and 6.0 ms of irradiation and by CID. The abundances are relative to the total product ion abundance in the product ion mass spectra.

10% of the product ion current. It should be noted that a majority of the [a - Base] and w-type ions of GAPDH siRNAs and Lamin A/C siRNAs contained fewer than 9 or 12 nucleotides, respectively, suggesting that these fragments are produced by dissociation of base loss fragment ions. Using short irradiation times (4.0 ms), the distribution of product ions in the IRMPD mass spectra were almost identical to that of the CID mass spectra. Longer irradiation times yielded lower abundances of base loss ions and higher abundances of both internal ions and protonated base ions (for the GAPDH.AS cations).

Base loss ions were not observed for GAPDH.AS in the 4+ charge state as these product ions (e.g., $[M\text{-}G]^{3+}$, *m/z* 2165.6), which are due to loss of protonated bases, have *m/z* values greater than that of the mass range of the linear ion trap. Similar results were also observed for the Lamin A/C siRNA single strands – CID yielded more abundant base loss ions than IRMPD using irradiation times of greater than 6 ms (data not shown).

The abundances of each of these product ion types was also monitored as a function of irradiation time as shown in **Figure 9.6** for the 5-, 5+, 4- and 4+ charge states of GAPDH.S. Base loss ions are initially observed at irradiation times of ~2 ms while c- and y-type ions begin to appear at irradiation times of ~3 ms for the GAPDH.S anions (**Figure 9.6a and 9.6c**). However, [a - Base] and w-type ions appear after using longer irradiation times, again providing evidence that a significant abundance of these products ions may be secondary fragment ions of base loss species or larger c/y-type ions. As the irradiation time increased, a maximum relative abundance of base loss ions was observed at ~5 ms at which point the abundance of base loss ions decreased at a similar rate to that of the precursor ion. After 8 ms of IR irradiation, the precursor ion was completely dissociated and base loss ions accounted for less than 3% of the total ion current in the IRMPD mass spectra. Since the precursor ion and the base loss ions contain the same number of chromogenic phosphate groups and, for the GAPDH.S anions, the same charge, it is not unexpected that both of these species would photodissociate at a similar rate. The c- and y-type ions were observed to have similar relative abundances independent of the irradiation time as one would expect for complementary fragment ions. For the GAPDH.S siRNA anions, c- and y-type ions accounted for more than 30 – 40% of the total ion current at irradiation times of ~7 ms at which point their abundances decreased due to secondary dissociation. The complementary [a - Base] and w-type ions comprised between 10 and 15% of the total ion current at their maximum abundance for

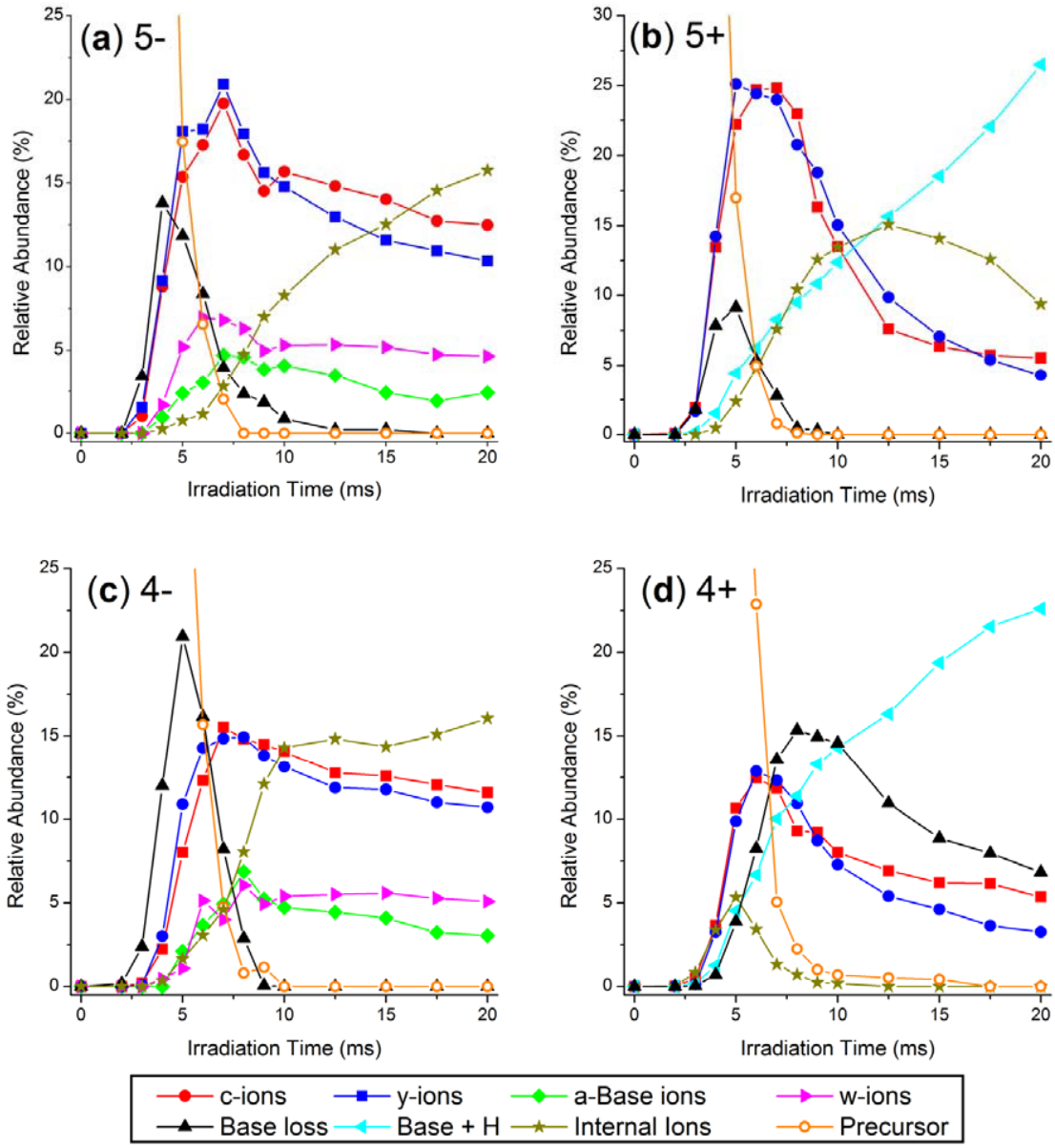

Figure 9.6 Relative abundances of product ions and the precursor ion as a function of irradiation time for the (a) 5-, (b) 5+, (c) 4-, and (d) 4+ charge states of GAPDH.S. Abundances are relative to the total ion current in each IRMPD product ion mass spectrum.

the siRNA anions. In contrast, c/y-type ions accounted for upwards of 50% of the total ion current in the IRMPD mass spectra of $[GAPDH.S + 5H]^{5+}$ and only 25% for

$[GAPDH.S + 4H]^{4+}$ (**Figure 9.6b and 9.6d**). Base loss ions and c/y-type ions for the GAPDH.S cations were initially observed at ~3 ms of irradiation whereas the onset for $[Base + H]^{+}$ ions was at ~4 ms. The abundance of protonated bases increased almost linearly with irradiation time for the GAPDH.S siRNA cations. Internal ions were also observed to increase in abundance with time, but at long irradiation times their abundance tapered off for the 5+ charge state of GAPDH.S as these ions were likely further dissociated into protonated base product ions.

The average charge state and the average length (in number of nucleotides) of the product ions of GAPDH.S were also plotted as a function of irradiation time for the IRMPD mass spectra, in addition to the values obtained from the CID mass spectra in **Figure 9.7**. The complete charge state distribution plots and relative abundances of product ions of varying nucleotide length are shown in **Figures 9.8 and 9.9** for the GAPDH.S anions and cations, respectively. Both the average charge state and the average product ion length decreased exponentially as the irradiation time increased. As the abundance of more highly-charged product ions decreased, the abundance of product ions in lower charge states correspondingly increased due to secondary dissociation of the more highly-charged species (**Figure 9.7a**). At irradiation times less than 4 ms, a majority of product ions of $[GAPDH.S – 5H]^{5-}$ were in the 5-, 4- and 3- charge states, but at 7 ms, doubly charged product ions dominated the IRMPD mass spectra. Singly charged product ions were predominantly observed at irradiation times of greater than 10 ms, with negligible contributions from ions in the 5-, 4-, and 3- charge states were negligible. In fact, greater than 90% of the identified product ions were singly or doubly charged after 10 ms irradiation. At 20 ms of irradiation time, 89% of the identified product ions were singly charged. The same trends were also observed for the Lamin

A/C siRNAs – long irradiation times yielded product ions in lower charge states and with fewer nucleotides (data not shown).

While these trends suggest that more highly charged product ions undergo more rapid secondary dissociation potentially due to a greater charge mobility, other factors are likely in play. In particular, one must note that product ions observed in higher charge states also are generally greater in size (i.e., number of nucleotides) and have a greater number of phosphate chromophores. Upon examination of the relative abundances of products ions of varying length vs. irradiation time, a similar trend is observed (**Figure 9.7b**). Product ions containing all 21 nucleotides (i.e., base loss ions) were initially observed as the most abundant fragment ion at irradiation times less than 5 ms. As the

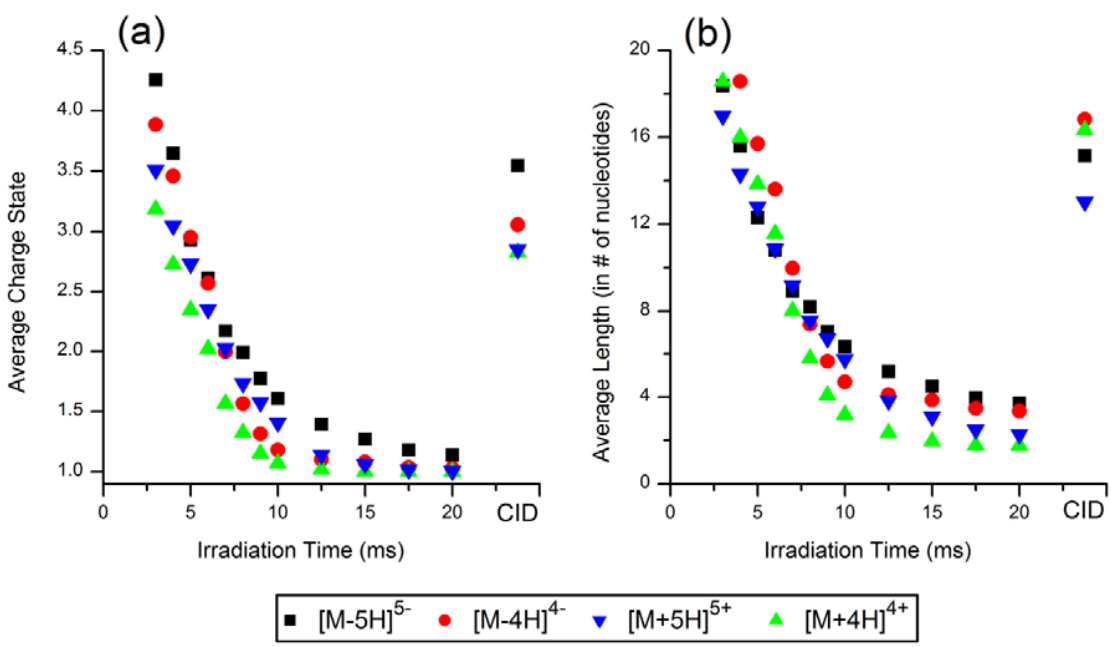

Figure 9.7 (a) Average charge state (absolute value) and (b) average length (in # of nucleotides) of product ions of GAPDH.S in the 5- (squares), 5+ (upside-down triangles), 4- (circles) and 4+ (triangles) charge states as a function of irradiation time. Values from the CID mass spectra are also plotted as the right most points in each panel.

irradiation increased, the abundance of longer product ions decreased and product ions containing fewer nucleotides increased. As the irradiation time increased from 7 to 9 ms, the average length of the product ions of the 5- charge state of GAPDH.S was reduced from ~9 to ~7 nucleotides but at 20 ms of irradiation, less than 8% of the total ion current was composed of product ions of greater than 6 nucleotides. For the GAPDH.S cations, the abundance of product ions with fewer than 6 nucleotides actually decreased at irradiation times greater than 10 – 12 ms as these small product ions were dissociated into protonated base ions. These trends suggest that both the charge state and the number of chromophores (i.e., phosphate groups) influence the rate of IR photodissociation of oligoribonucleotides.

The IRMPD results using a short and a longer irradiation time complement each other in that each provide different levels of sequence confirmation. Short irradiation times predominantly yield large product ions in high charge states and a minimal abundance of [a - Base] and w-type ions which simplifies spectral interpretation as one only has to search for a single ion type. By using longer irradiation times, one can more easily unambiguously identify the product ions as a majority of the species will be singly or doubly charged. Also, the presence of more [a – Base] and w-type ions provides confirmation of the nucleobase and the sequence. For potential *de novo* sequencing algorithms, it may be better to provide a product ion mass spectrum which only contains a single 5'-series and a single 3'-series of product ions (e.g., the c- and y-ions), but for database searching, more product ions (e.g., [a - Base], c-, w-, y-type ions) may yield more confident results. IRMPD of siRNAs can yield product ion mass spectra containing both types of information.

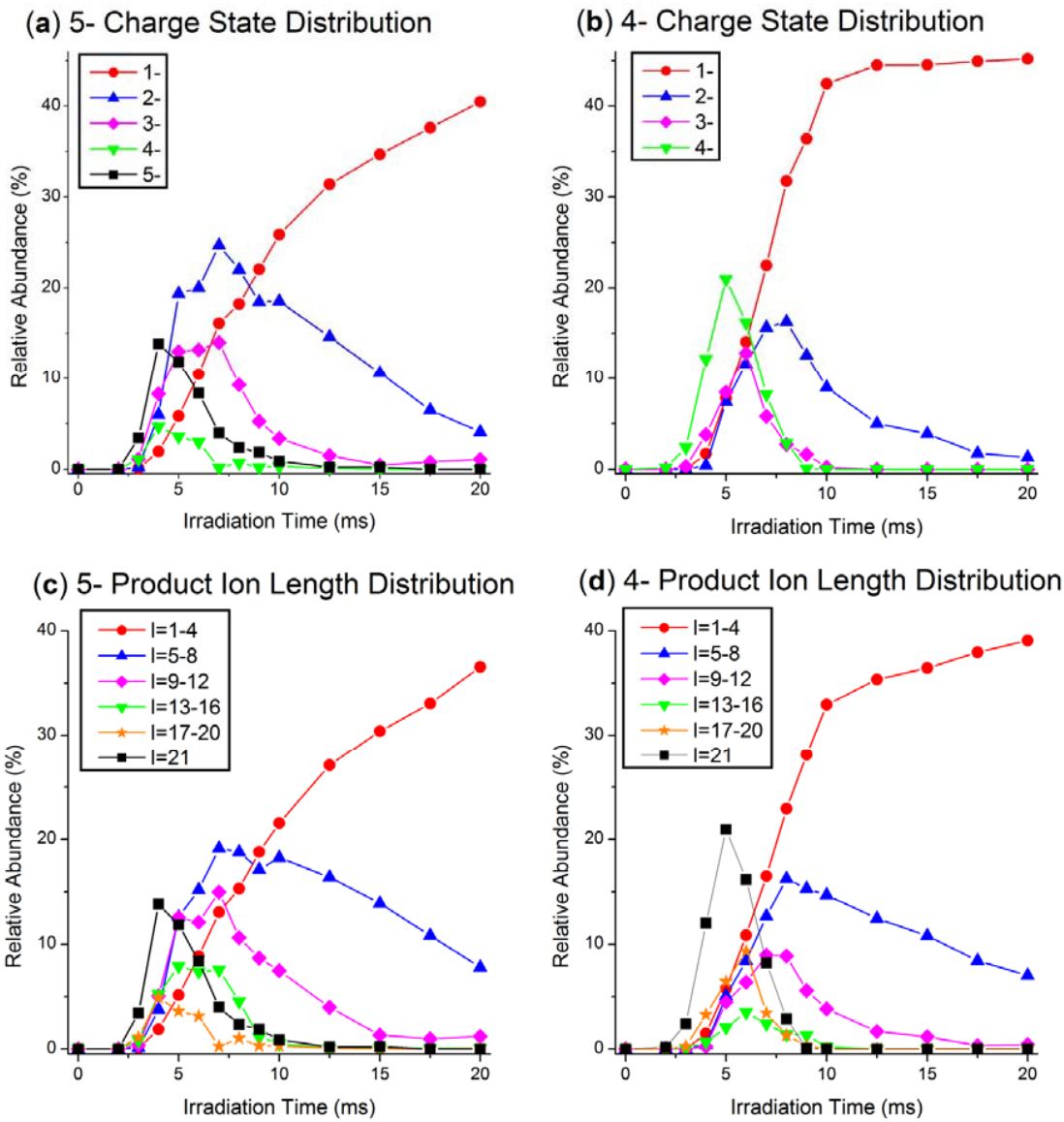

Figure 9.8 Charge state distribution of product ions observed in IRMPD mass spectra of (a) 5- and (b) 4- charge states of GAPDH.S as a function of irradiation time. Relative abundances of product ions containing 1-4, 5-8, 9-12, 13-16, 17-20, and 21 nucleotides as a function of irradiation time in the IRMPD mass spectra of the (c) 5- and (d) 4- charge states of GAPDH.S. Abundances are relative to the total ion current in the IRMPD mass spectra.

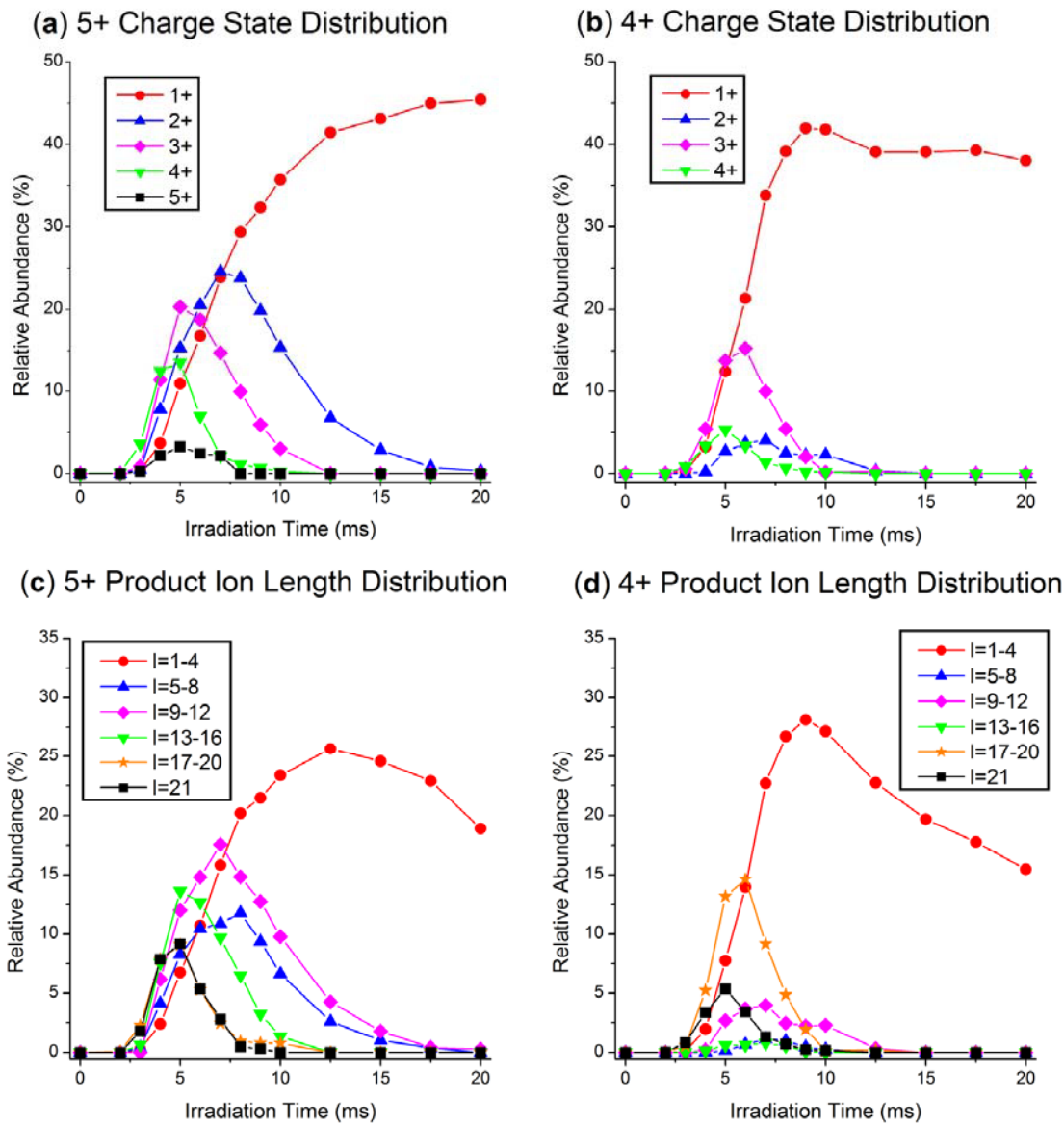

Figure 9.9 Charge state distribution of product ions observed in IRMPD mass spectra of (a) 5+ and (b) 4+ charge states of GAPDH.S as a function of irradiation time. Relative abundances of product ions containing 1-4, 5-8, 9-12, 13-16, 17-20, and 21 nucleotides as a function of irradiation time in the IRMPD mass spectra of the (c) 5+ and (d) 4+ charge states of GAPDH.S. Abundances are relative to the total ion current in the IRMPD mass spectra.

9.4.3 IRMPD vs. CID of Duplex siRNA

For effective down-regulation of target genes, duplex siRNA generally needs to be introduced to the organisms. The annealed duplex GAPDH and duplex Lamin A/C siRNAs were characterized by both CID and IRMPD. Strand separation was observed upon CID of duplex GAPDH in the 9- charge state as shown in **Figure 9.10a**. Similar results were observed for the other charge states of duplex GAPDH and for duplex Lamin A/C (data not shown). Asymmetric charge partitioning of the duplex siRNAs is evident in **Figure 9.10a** in which the two single-strands are observed in the 6- charge state preferentially as opposed to the more symmetric 5- and 4- charge states. (It is presumed that the 3- charge state of the single-strands is also produced, however, these ions are not observed as they have *m/z* values beyond that of the mass analyzer.) The CID results are in line with previous reports on the gas-phase dissociation trends of DNA duplexes.[39-41] Diagnostic sequence ions were observed by CID when the collisional energy was increased as previously reported,[27] but the sequence coverage was limited to less than 5 nucleotides (data not shown). IRMPD using 2.0 ms of irradiation yielded a product ion mass spectrum (**Figure 9.10b**) almost identical to the CID mass spectrum in which the only dissociation channel observed was strand separation. With longer irradiation times, however, these single strands dissociated into diagnostic sequence ions, predominantly c- and y-type product ions, as shown in **Figure 9.10c**. Due to homologous sequences between the two single strands, the origin of many of the product ions could not be unambiguously determined, and the overall sequence coverage of the individual single strands was low. All product ions observed were in the 1- or 2- charge state and none contained greater than eight nucleotides. While IRMPD of siRNA duplexes can yield informative product ions, the sequence information is limited to generally between 5 and 8 nucleotides from either terminal.

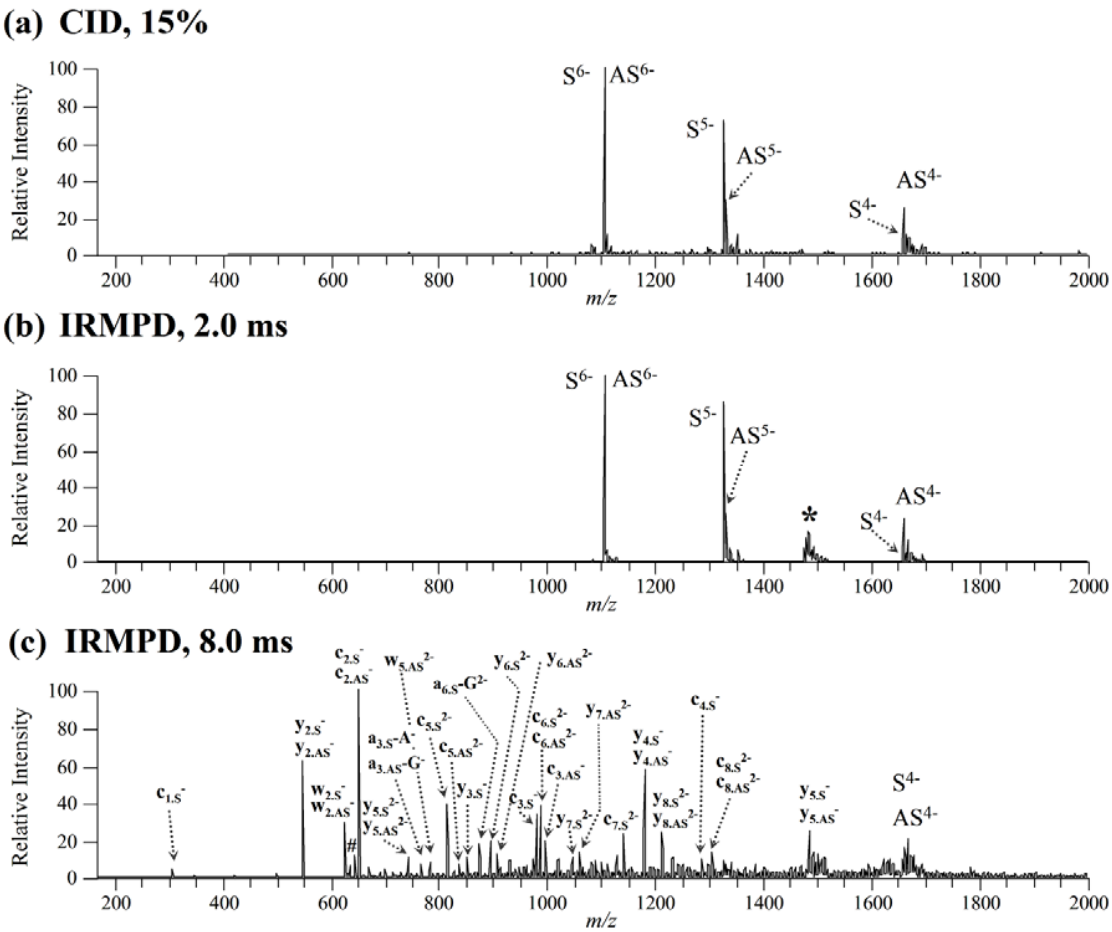

Figure 9.10 (a) CID product ion mass spectra of [duplex GAPDH – 9H]$^{9-}$ of *m/z* 1475 (17% normalized collision energy). IRMPD product ion mass spectra of the same duplex siRNA anion using (b) 2.0 ms and (c) 8.0 ms of irradiation at 10 W (q-value = 0.1). The precursor ion is indicated by an asterisk (*) and internal ions by #. Sense and antisense single strands are indicated by S and AS, respectively.

9.5 CONCLUSIONS

Infrared multiphoton dissociation of model single-strand siRNAs yields complete sequence coverage and has been shown to be a complementary dissociation method to traditional ion-trap based collision-induced dissociation. IRMPD affords rapid and

efficient dissociation of siRNAs in less than 10 ms. The siRNA ions preferentially dissociated through cleavage of the 5' P–O bonds by both IRMPD and CID to produce c/y-type sequence ions. The other dominant dissociation pathway was loss of neutral nucleobases from the siRNA anions or loss of protonated nucleobases from precursor cations. While CID produced high abundances of base loss ions, the irradiation time could be tuned to reduce the abundance of these uninformative product ions through secondary dissociation to yield higher abundances of c- and y-type fragment ions. The large degree of secondary dissociation also produced higher abundances of [a - Base] and w-type ions, as well as internal ions due to cleavage of two 5' P–O bonds. At long irradiation times, larger and more highly charged product ions were also dissociated into shorter products in lower charge states. In fact, at irradiation times of greater than 10 ms, greater than 90% of the identified product ions were singly or doubly charged. While this effect reduced the total number of unique fragment ions in the IRMPD mass spectra, full sequence was still obtained and the product ion mass spectra was simpler to interpret. IRMPD of the siRNA cations produced high abundances of protonated bases with the exceptions of uracil and thymine. The protonated bases were only detected in the IRMPD mass spectra due to the alleviation of the low-mass cut-off. Both CID and IRMPD of the siRNA cations in charge levels above 20% yielded full sequence coverage and only c- and y-type fragment ions were observed; [a - Base] and w-ions were detected at insignificant levels. Near complete sequence coverage was obtained for most of the siRNA anions and cations by both IRMPD and CID. The primary differences between the IRMPD and CID mass spectra were in the total number of product ions observed. With longer irradiation times, larger product ions were eliminated from the IRMPD mass spectra (due to conversion to smaller, diagnostic ions), however full sequence coverage was generally maintained in all cases. Short irradiation times typically yielded near

complete series of c- and y-type ions, similar to results obtained by CID. These results suggest IRMPD analysis of siRNA in the positive ion mode may be a more fruitful means of sequencing oligoribonucleotides as the cations primarily dissociated through a single pathway to yield c- and y-type ions. While duplex siRNA predominantly underwent strand separation by CID, either single strands or sequence ions were produced by IRMPD by varying the irradiation time.

9.6 REFERENCES

(1) Costa, F. F. *Gene* **2005**, *357*, 83-94.

(2) Hüttenhofer, A.; Brosius, J.; Bachellerie, J.-P. *Current Opinion in Chemical Biology* **2002**, *6*, 835-843.

(3) Meister, G.; Tuschl, T. *Nature* **2004**, *431*, 343-349.

(4) Karagiannis, T. C.; El-Osta, A. *Cancer Gene Therapy* **2005**, *12*, 787-795.

(5) Hudder, A.; Novak, R. F. *Toxicological Sciences* **2008**, *103*, 228-240.

(6) Uprichard, S. L. *FEBS Letters* **2005**, *579*, 5996-6007.

(7) Grimm, D. *Advanced Drug Delivery Reviews* **2009**, *61*, 672-703.

(8) Zimmermann, T. S.; Lee, A. C. H.; Akinc, A.; Bramlage, B.; Bumcrot, D.; Fedoruk, M. N.; Harborth, J.; Heyes, J. A.; Jeffs, L. B.; John, M.; Judge, A. D.; Lam, K.; McClintock, K.; Nechev, L. V.; Palmer, L. R.; Racie, T.; Roehl, I.; Seiffert, S.; Shanmugam, S.; Sood, V.; Soutschek, J.; Toudjarska, I.; Wheat, A. J.; Yaworski, E.; Zedalis, W.; Koteliansky, V.; Manoharan, M.; Vornlocher, H.-P.; MacLachlan, I. *Nature* **2006**, *441*, 111-114.

(9) Miller, V. M.; Gouvion, C. M.; Davidson, B. L.; Paulson, H. L. *Nucleic Acids Research* **2004**, *32*, 661-668.

(10) Liu, Y. P.; Haasnoot, J.; Berkhout, B. *Nucleic Acids Research* **2007**, *35*, 5683-5693.

(11) Liu, Y. P.; Haasnoot, J.; ter Brake, O.; Berkhout, B.; Konstantinova, P. *Nucleic Acids Research* **2008**, *36*, 2811-2824.

(12) Hüttenhofer, A.; Vogel, J. *Nucleic Acids Research* **2006**, *34*, 635-646.

(13) Friedlaender, M. R.; Chen, W.; Adamidi, C.; Maaskola, J.; Einspanier, R.; Knespel, S.; Rajewsky, N. *Nature Biotechnology* **2008**, *26*, 407-415.

(14) Landgraf, P.; Rusu, M.; Sheridan, R.; Sewer, A.; Iovino, N.; Aravin, A.; Pfeffer, S.; Rice, A.; Kamphorst, A. O.; Landthaler, M.; Lin, C.; Socci, N. D.; Hermida, L.; Fulci, V.; Chiaretti, S.; Foa, R.; Schliwka, J.; Fuchs, U.; Novosel, A.; Muller, R.-U.; Schermer, B.; Bissels, U.; Inman, J.; Phan, Q.; Chien, M.; Weir, D. B.; Choksi, R.; De Vita, G.; Frezzetti, D.; Trompeter, H.-I.; Hornung, V.; Teng, G.; Hartmann, G.; Palkovits, M.; Di Lauro, R.; Wernet, P.; Macino, G.; Rogler, C. E.; Nagle, J. W.; Ju, J.; Papavasiliou, F. N.; Benzing, T.; Lichter, P.; Tam, W.;

Brownstein, M. J.; Bosio, A.; Borkhardt, A.; Russo, J. J.; Sander, C.; Zavolan, M.; Tuschl, T. *Cell* **2007**, *129*, 1401-1414.

(15) Bramsen, J. B.; Laursen, M. B.; Nielsen, A. F.; Hansen, T. B.; Bus, C.; Langkjaer, N.; Babu, B. R.; Hojland, T.; Abramov, M.; Van Aerschot, A.; Odadzic, D.; Smicius, R.; Haas, J.; Andree, C.; Barman, J.; Wenska, M.; Srivastava, P.; Zhou, C.; Honcharenko, D.; Hess, S.; Mueller, E.; Bobkov, G. V.; Mikhailov, S. N.; Fava, E.; Meyer, T. F.; Chattopadhyaya, J.; Zerial, M.; Engels, J. W.; Herdewijn, P.; Wengel, J.; Kjems, J. *Nucleic Acids Research* **2009**, *37*, 2867-2881.

(16) Koller, E.; Propp, S.; Murray, H.; Lima, W.; Bhat, B.; Prakash, T. P.; Allerson, C. R.; Swayze, E. E.; Marcusson, E. G.; Dean, N. M. *Nucleic Acids Research* **2006**, *34*, 4467-4476.

(17) Wu, J.; McLuckey, S. A. *International Journal of Mass Spectrometry* **2004**, *237*, 197-241.

(18) McLuckey, S. A.; Van Berkel, G. J.; Glish, G. L. *Journal of the American Society for Mass Spectrometry* **1992**, *3*, 60-70.

(19) Little, D. P.; Aaserud, D. J.; Valaskovic, G. A.; McLafferty, F. W. *Journal of the American Chemical Society* **1996**, *118*, 9352-9359.

(20) Keller, K. M.; Brodbelt, J. S. *Analytical Biochemistry* **2004**, *326*, 200-210.

(21) Gabelica, V.; Tabarin, T.; Antoine, R.; Rosu, F.; Compagnon, I.; Broyer, M.; De Pauw, E.; Dugourd, P. *Analytical Chemistry* **2006**, *78*, 6564-6572.

(22) Smith, S. I.; Brodbelt, J. S. *International Journal of Mass Spectrometry* **2009**, *283*, 85-93.

(23) Huang, T.; Kharlamova, A.; Liu, J.; McLuckey, S. A. *Journal of the American Society for Mass Spectrometry* **2008**, *19*, 1832-1840.

(24) Schürch, S.; Bernal-Mendez, E.; Leumann, C. J. *Journal of the American Society for Mass Spectrometry* **2002**, *13*, 936-945.

(25) Kirpekar, F.; Krogh, T. N. *Rapid Communications in Mass Spectrometry* **2001**, *15*, 8-14.

(26) Tromp, J. M.; Schürch, S. *Journal of the American Society for Mass Spectrometry* **2005**, *16*, 1262-1268.

(27) Huang, T.; Liu, J.; Liang, X.; Hodges, B. D. M.; McLuckey, S. A. *Analytical Chemistry* **2008**, *80*, 8501-8508.

(28) Yang, J.; Håkansson, K. *Journal of the American Society for Mass Spectrometry* **2006**, *17*, 1369-1375.

(29) Sannes-Lowery, K. A.; Hofstadler, S. A. *Journal of the American Society for Mass Spectrometry* **2003**, *14*, 825-833.

(30) Yang, J.; Håkansson, K. *European Journal of Mass Spectrometry* **2009**, *15*, 293-304.

(31) Hofstadler, S. A.; Griffey, R. H.; Pasa-Tolic, L.; Smith, R. D. *Rapid Communications in Mass Spectrometry* **1998**, *12*, 1400-1404.

(32) Silverstein, R. M.; Webster, F. X.; Kiemle, D. J. *Spectrometric Identification of Organic Compounds*, 7th ed.; John Wiley & Sons: Hoboken, NJ, 2005.

(33) Little, D. P.; Speir, J. P.; Senko, M. W.; O'Connor, P. B.; McLafferty, F. W. *Analytical Chemistry* **1994**, *66*, 2809-2815.

(34) Gardner, M. W.; Vasicek, L. A.; Shabbir, S.; Anslyn, E. V.; Brodbelt, J. S. *Analytical Chemistry* **2008**, *80*, 4807-4819.

(35) Lee, J. K. *International Journal of Mass Spectrometry* **2005**, *240*, 261-272.

(36) Liu, M.; Li, T.; Amegayibor, F. S.; Cardoso, D. S.; Fu, Y.; Lee, J. K. *Journal of Organic Chemistry* **2008**, *73*, 9283-9291.

(37) Zhachkina, A.; Liu, M.; Sun, X.; Amegayibor, F. S.; Lee, J. K. *Journal of Organic Chemistry* **2009**, *74*, 7429-7440.

(38) Pan, S.; Verhoeven, K.; Lee, J. K. *Journal of the American Society for Mass Spectrometry* **2005**, *16*, 1853-1865.

(39) Gabelica, V.; De Pauw, E. *Journal of Mass Spectrometry* **2001**, *36*, 397-402.

(40) Gabelica, V.; De Pauw, E. *Journal of the American Society for Mass Spectrometry* **2002**, *13*, 91-98.

(41) Wan, K. X.; Gross, M. L.; Shibue, T. *Journal of the American Society for Mass Spectrometry* **2000**, *11*, 450-457.

Chapter 10

Conclusions

Mass spectrometry has continued to play a greater role in the field of proteomics, particularly for the structural characterization of biological complexes. Chemical cross-linking of proteins along with mass spectrometric analysis has shown to be an effective tool to obtain low resolution distance constraint information and for three-dimensional structural determination of proteins as well as to map interfaces of protein-protein interactions. As this field continues to expand, there is a growing need to develop analytical tools to more readily and confidently identify chemical cross-links. In this dissertation, selective dissociation methods coupled with chromogenic cross-linkers were developed, and systematic studies focusing on the gas-phase dissociation trends of cross-linked peptides and RNA were examined.

Intermolecularly cross-linked peptides were observed to have similar dissociation trends to linear peptides, as discussed in Chapter 3. Both prolyl and aspartyl residues influenced the dissociation of cross-linked peptides identically to that observed for unmodified peptides. For cross-linked peptides containing prolyl residues, cleavage N-terminal to the proline was dominant, and in particular for cross-linked peptide ions without a mobile proton, a high degree of internal ion formation was observed with Pro as the N-terminal residue. Cleavage C-terminal to aspartyl residues was dominant also for cross-linked peptide ions with all protons sequestered. Collision-induced dissociation of cross-linked peptides possessing mobile protons predominantly yielded single cleavage product ions due to dissociation of a single amide bond of one of the two constituent peptides. A high abundance of double cleavage product ions were detected for cross-linked peptides without mobile protons. In addition, cross-linker specific

product ions were detected for all species. Incorporation of these dissociation trends into database search algorithms should improve sequencing of cross-linked peptides and facilitate more accurate protein identification for in vivo cross-linking experiments in which the proteins cross-linked are unknown a priori.

An IR chromogenic cross-linker (IRCX) possessing a phosphate was utilized to provide rapid differentiation of cross-linked peptides in enzymatic digests and to simplify the product ion spectra of cross-linked peptides by selective IRMPD, as reported in Chapter 4. Only peptides containing the chromogenic cross-linker were observed to undergo efficient and complete dissociation by IR irradiation. All primary product ions which possessed the cross-linker underwent secondary photodissociation resulting in IRMPD mass spectra which predominantly contained y-type product ions originating from each peptide C-terminal to the cross-linked lysines. These series of y-ions could potentially be used to de novo sequence the cross-linked peptides for identification of the site of cross-link and to identify the proteins. Research in the Brodbelt group is currently aimed at applying widely used database search algorithms to more confidently identify and sequence cross-linked peptides.

As discussed in Chapter 5, selective photodissociation methods were further applied to conjugated peptides, in which a bis-arylhydrazone (BAH) UV-chromophore was formed only upon cross-linked, allowing the use of UVPD for rapid differentiation of cross-linked and un-cross-linked products. UVPD also provided greater sequence ion coverage than CID alone for the BAH-conjugated peptides. The UVPD efficiencies were charge-dependent – protonation of the hydrazone bond was necessary for successful UVPD which mirrored the solution phase behavior of the chromophore. BAH-conjugated peptides were further analyzed by ETD and preferential dissociation of the hydrazone bond was observed (Chapter 6). Preferential cleavage of the hydrazone bond

yielded the two constituent peptides – one with a 131 Da mass tag (even-electron) and the other with a 119 Da mass tag (odd-electron). These modified peptides were subsequently characterized by CID to sequence the peptides and locate the original site of cross-linking. Greater sequence coverage of the peptides was obtained by the ETD-CID method than CID of the intact cross-linked peptides. This preferential dissociation of BAH-cross-linked has great potential for not only the characterization of protein-protein complexes but as a complement or substitute to MS-based applications utilizing gas-phase labile bonds. As an ergodic dissociation method in which the internal energy is re-distributed amongst all vibrational modes of the ion, CID may not predominantly result in cleavage of the desired bond due to competing low-energy dissociation pathways. However, ETD should generally result in preferential cleavage of the hydrazone bond regardless of the presence of labile functional groups on the peptide. Further investigation and research into the hydrazone bond functionality as it relates to ETD including molecular modeling studies is ongoing.

IRMPD of peptide cations was explored on a dual pressure linear ion trap (LIT) mass spectrometer (Chapter 7). Peptide cations were observed to undergo efficient and rapid photodissociation exclusively in the low pressure cell due to the lower rate of collisional deactivation. No dissociation was detected when peptide ions were irradiated in the high pressure cell or in similar experiments on a single cell LIT. Greater sequence coverage of the peptides was obtained by IRMPD performed in the low pressure cell than CID. In fact, IRMPD generally produced singly-charged product ions due to secondary dissociation of the more-highly charged primary product ions, which resulted in product ion mass spectra that were more easily interpreted. As the necessary instrument modifications to interface lasers to quadrupole ion trap mass spectrometers become less arduous and the shortcomings of IRMPD are circumvented, IRMPD will likely be

presented as an option on commercial instruments similar to that already available for FT-ICR mass spectrometers.

In Chapter 8, supplemental IR irradiation was applied to reduce the chemical noise in ESI mass spectra and to increase the abundance of protonated analyte ions. The chemical noise was determined to predominantly consist of highly solvated analyte ions of unresolved *m/z*, and IR irradiation of the noise regions effectively "desolvated" these ions. IR irradiation was observed to more effectively reduce chemical noise than collisional activation. Due to the high bath gas pressure in the linear ion trap, supplemental IR irradiation selectively dissociates only species with low dissociation energies such as non-covalent complexes of solvated ions and does not result in covalent bond dissociation. To improve sensitivity, one could envision irradiating ions of a wide range of *m/z* values in the high pressure cell of the dual pressure LIT to increase analyte ion abundance and then transfer this greater ion population to the low pressure cell for IRMPD and peptide sequencing.

Complete sequence coverage of siRNA anions and cations was obtained by IRMPD (Chapter 9). RNA is well-suited for sequence analysis by IRMPD because of its IR chromogenic phosphodiester backbone which allows for it to be rapidly dissociated by IR irradiation. IRMPD of siRNA anions predominantly yielded c- and y-ions and [a-Base]/w-ions to a lesser degree. In contrast, IRMPD mass spectra of siRNA cations were dominated by c- and y-type ions with [a-Base]/w-ions contributing insignificantly to the product ion current. IRMPD of duplex siRNA yielded sequence ions originated from both single strands whereas CID resulted in strand separation providing no sequence coverage. The IRMPD mass spectra could be "tuned" to predominantly consist of singly and doubly charged product ions or of larger, more highly charged species by adjusting the IR irradiation time.

The work presented in this dissertation helps pave the way for the analysis of larger macromolecular complexes whose functions or structure have yet to be determined. Ribonucleoproteins are a prime example of biologically relevant complexes which the techniques described herein could be applied. RNA-protein complexes could be covalently chemically or photo-cross-linked for analysis by selective photodissociation mass spectrometry. As unmodified peptides are not observed to undergo efficient IRMPD, only peptides bound to the RNA, which is inherently IR chromogenic due to its phosphodiester backbone, would photodissociate allowing ready differentiation between RNA-peptide cross-links from free RNA or peptide ions. Furthermore, ETD could be applied to these cross-linked species which would selectively cleave the peptide backbone and allow the sites of cross-links to be pinpointed. Ongoing work in the Brodbelt group is focusing on using IRCX with selective IRMPD for the characterization of eukaryotic translation initiation factor-4E (eIF4E) with its protein binding partners as well as its mRNA target. The structure eIF4E protein and its complexes are of interest as protein synthesis in eukaryotic cells begins with the binding of eIF4E with mRNA.

As the complexity of the biological macromolecules increases, there is a growing need for higher resolution and higher mass accuracy mass spectrometers. This research has led to the design, development, and current construction of a quadrupole – rectilinear ion trap – time-of-flight (Q-RIT-TOF) mass spectrometer in the Brodbelt group. The Q-RIT-TOF will be able to analyze ions of a larger mass range (> *m/z* 50,000) while providing higher mass resolution than that available on quadrupole ion trap mass spectrometers. This instrument will have dual sources – one for electrospray ionization of the macromolecular complex and the second for reagent anions – and have an IR laser or UV laser interfaced to allow for multiple types of ion activation and dissociation to be

performed simultaneously or sequentially during a single experiment. Intact macromolecular complexes will be subjected to IR or UV irradiation and then the primary product ions which will exist in multiple charge states, will undergo proton transfer reactions with a reagent anion to reduce the product ions to lower charge states for TOF-MS analysis. It is the goal that a combination of selective dissociation methods along with higher resolution MS analysis will allow for more rapid and definitive structural characterization of biological macromolecular complexes.

Vita

Myles Winston Gardner was born in New Jersey in January 1982 to Win and Rebecca Gardner. He was raised in Doylestown, Pennsylvania and Clifton, Virginia, a suburb of Washington, D.C. He attended Thomas Jefferson High School for Science and Technology in Alexandria, VA and graduated in 2000. In the fall of 2000, Myles began attending Duke University where he completed the academic requirements for a Bachelor's of Science degree in chemistry in May 2004. As an undergraduate student, he performed research in Prof. Michael C. Fitzgerald's lab studying protein-ligand interactions by MALDI mass spectrometry. Upon graduation from Duke University, he began his graduate studies at the University of Texas at Austin under the supervision and guidance of Prof. Jennifer S. Brodbelt in the field of analytical chemistry. While in Dr. Brodbelt's group, he has focused his research on mass spectrometry, both in the development of selective gas-phase dissociation methods but also in instrumentation.

Permanent Address: 6402 Noble Rock Ct., Clifton, VA 20124

This dissertation was typed by the author.